Multiple-Description

Lattice Vector Quantization

Proefschrift

ter verkrijging van de graad van doctor
aan de Technische Universiteit Delft,
op gezag van de Rector Magnificus prof.dr.ir. J. T. Fokkema,
voorzitter van het College voor Promoties,
in het openbaar te verdedigen op maandag 18 juni 2007 om 12:30 uur
door Jan ØSTERGAARD
Civilingeniør van Aalborg Universitet, Denemarken
geboren te Frederikshavn.

Multiple-Description

Lattice Vector Quantization

Preface

The research for this thesis was conducted within the STW project DET.5851, *Adaptive Sound Coding (ASC)*. One of the main objectives of the ASC project was to develop a universal audio codec capable of adapting to time-varying characteristics of the input signal, user preferences, and application-imposed constraints or time-varying network-imposed constraints such as bit rate, quality, latency, bandwidth, and bit-error rate (or packet-loss rate).

This research was carried out during the period February 2003 – February 2007 in the Information and Communication Theory group at Delft University of Technology, Delft, The Netherlands. During the period June 2006 – September 2006 the research was conducted in the department of Electrical Engineering-Systems at Tel Aviv University, Tel Aviv, Israel.

I would like to take this opportunity to thank my supervisor Richard Heusdens and cosupervisor Jesper Jensen, without whose support, encouragement, and splendid supervision this thesis would not have been possible.

I owe a lot to my office mates Omar Niamut and Pim Korten. Omar, your knowledge of audio coding is impressive. On top of that you are also a gifted musician. A truly marvelous cocktail. Pim, you have an extensive mathematical knowledge, which one can only envy. I thank you for the many insightful and delightful discussions we have had over the years.

I am grateful to Ram Zamir for hosting my stay at Tel Aviv University. I had such a great time and sincerely appreciate the warm welcoming that I received from you, your family and the students at the university. It goes without saying that I will definitely be visiting Tel Aviv again.

I would also like to thank Inald Lagendijk for accepting being my Promotor and of course cheers go out to the former and current audio cluster fellows; Christoffer Rødbro, Ivo Shterev, Ivo Batina, Richard Hendriks, and Jan Erkelens for the many insightful discussions we have had. In addition I would like to acknowledge all

Summary

Internet services such as voice over Internet protocol (VoIP) and audio/video streaming (e.g. video on demand and video conferencing) are becoming more and more popular with the recent spread of broadband networks. These kind of "real-time" services often demand low delay, high bandwidth and low packet-loss rates in order to deliver tolerable quality for the end users. However, the heterogeneous communication infrastructure of today's packet-switched networks does not provide a guaranteed performance in terms of bandwidth or delay and therefore the desired quality of service is generally not achieved.

To achieve a certain degree of robustness on errorprone channels one can make use of multiple-description (MD) coding, which is a discipline that recently has received a lot of attention. The MD problem is basically a joint source-channel coding problem. It is about (lossy) encoding of information for transmission over an unreliable K-channel communication system. The channels may break down resulting in erasures and a loss of information at the receiving side. Which of the $2^K - 1$ non-trivial subsets of the K channels that are working is assumed known at the receiving side but not at the encoder. The problem is then to design an MD scheme which, for given channel rates (or a given sum rate), minimizes the distortions due to reconstruction of the source using information from any subsets of the channels.

While this thesis focuses mainly on the information theoretic aspects of MD coding, we will also show how the proposed MD coding scheme can be used to construct a perceptually robust audio coder suitable for audio streaming on packet-switched networks.

We attack the MD problem from a source coding point of view and consider the general case involving K descriptions. We make extensive use of lattice vector quantization (LVQ) theory, which turns out to be instrumental in the sense that the proposed MD-LVQ scheme serves as a bridge between theory and practice. In asymptotic cases of high resolution and large lattice vector quantizer dimension,

we show that the best known information theoretic rate-distortion MD bounds can be achieved, whereas in non-asymptotic cases of finite-dimensional lattice vector quantizers (but still under high resolution assumptions) we construct practical MD-LVQ schemes, which are comparable and often superior to existing state-of-the-art schemes.

In the two-channel symmetric case it has previously been established that the side descriptions of an MD-LVQ scheme admit side distortions, which (at high resolution conditions) are identical to that of L-dimensional quantizers having spherical Voronoi cells. In this case we say that the side quantizers achieve the L-sphere bound. Such a result has not been established for the two-channel asymmetric case before. However, the proposed MD-LVQ scheme is able to achieve the L-sphere bound for two descriptions, at high resolution conditions, in both the symmetric and asymmetric cases.

The proposed MD-LVQ scheme appears to be among the first schemes in the literature that achieves the largest known high-resolution three-channel MD region in the quadratic Gaussian case. While optimality is only proven for $K \leq 3$ descriptions we conjecture it to be optimal for any K descriptions.

We present closed-form expressions for the rate and distortion performance for general smooth stationary sources and squared error distortion criterion and at high resolution conditions (also for finite-dimensional lattice vector quantizers). It is shown that the side distortions in the three-channel case is expressed through the dimension-less normalized second moment of an L-sphere independent of the type of lattice used for the side quantizers. This is in line with previous results for the two-description case.

The rate loss when using finite-dimensional lattice vector quantizers is lattice independent and given by the rate loss of an L-sphere and an additional term describing the ratio of two dimensionless expansion factors. The overall rate loss is shown to be superior to existing three-channel schemes.

Contents

Chapter 1

Introduction

1.1 Motivation

Internet services such as voice over Internet protocol (VoIP) and audio/video streaming (e.g. video on demand and video conferencing) are becoming more and more popular with the recent spread of broadband networks. These kinds of "real-time" services often demand low delay, high bandwidth and low packet-loss rates in order to deliver tolerable quality for the end users. However, the heterogeneous communication infrastructure of today's packet-switched networks does not provide a guaranteed performance in terms of bandwidth or delay and therefore the desired quality of service is (at least in the authors experience) generally not achieved.

Clearly, many consumers enjoy the Internet telephony services provided for free through e.g. Skype™. This trend seems to be steadily growing, and more and more people are replacing their traditional landline phones with VoIP compatible systems. On the wireless side it is likely that cell phones soon are to be replaced by VoIP compatible wireless (mobile) phones. A driving impetus is consumer demand for cheaper calls, which sometimes may compromise quality.

The structure of packet-switched networks makes it possible to exploit diversity in order to achieve robustness towards delay and packet losses and thereby improve the quality of existing VoIP services. For example, at the cost of increased bandwidth (or bit rate), every packet may be duplicated and transmitted over two different paths (or channels) throughout the network. If one of the channels fails, there will be no reduction in quality at the receiving side. Thus, we have a great degree of robustness. On the other hand, if none of the channels fail so that both packets are received, there will be no improvement in quality over that of using a single packet. Hence, robustness via diversity comes with a price.

However, if we can tolerate a small quality degradation on reception of a single

1

packet, we can reduce the bit rates of the individual packets, while still maintaining the good quality on reception of both packets by making sure that the two packets improve upon each other. This idea of trading off bit rate vs. quality between a number of packets (or descriptions) is usually referred to as the multiple-description (MD) problem and is the topic of this thesis.

While this thesis focuses mainly on the information theoretic aspects of MD coding, we will also show how the proposed MD coding scheme can be used to construct a perceptually robust audio coder suitable for audio streaming on packet-switched networks. To the best of the author's knowledge the use of MD coding in current state-of-the-art VoIP systems or audio streaming applications is virtually non-existent. We expect, however, that future schemes will employ MD coding to achieve a certain degree of robustness towards packet losses. The research presented in this thesis is a step in that direction.

1.2   Introduction to MD Lattice Vector Quantization

The MD problem is basically a joint source-channel coding problem. It is about (lossy) encoding of information for transmission over an unreliable K-channel communication system. The channels may break down resulting in erasures and a loss of information at the receiving side. Which of the $2^K - 1$ non-trivial subsets of the K channels that are working is assumed known at the receiving side but not at the encoder. The problem is then to design an MD scheme which, for given channel rates (or a given sum rate), minimizes the distortions on the receiver side due to reconstruction of the source using information from any subsets of the channels.

1.2.1   Two Descriptions

The traditional case involves two descriptions as shown in Fig. 1.1. The total bit rate R_T, also known as the sum rate, is split between the two descriptions, i.e. $R_T = R_0 + R_1$, and the distortion observed at the receiver depends on which descriptions arrive. If both descriptions are received, the resulting distortion (D_c) is smaller than if only a single description is received (D_0 or D_1). It may be noticed from Fig. 1.1 that Decoder 0 and Decoder 1 are located on the sides of Decoder c and it is therefore customary to refer to Decoder 0 and Decoder 1 as the side decoders and Decoder c as the central decoder. In a similar manner we often refer to $D_i, i = 0, 1$, as the side distortions and D_c as the central distortion. The situation where $D_0 = D_1$ and $R_0 = R_1$ is called symmetric MD coding and is a special case of asymmetric MD coding, where we allow unequal side rates and unequal side distortions.

One of the fundamental problems of MD coding is that if two descriptions both represent the source well, then, intuitively, they must be very similar to the source and therefore also similar to each other. Thus, their joint description is not much better
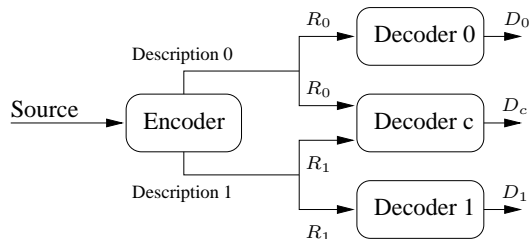
Figure 1.1: *The traditional two-channel MD system.*

than a single one of them. Informally, we may therefore say that the MD problem is about how good one can make the simultaneous representations of the individual descriptions as well as their joint description.

The two-description MD problem was formalized and presented by Wyner, Witsenhausen, Wolf and Ziv at an information theory workshop in September 1979 [50].[1] Formally, the traditional two-description MD problem asks what is the largest possible set of distortions (D_0, D_1, D_c) given the bit rate constraints (R_0, R_1) or alternatively the largest set of bit rates (R_0, R_1) given the distortion constraints (D_0, D_1, D_c)? Both these questions were partially answered by El Gamal and Cover who presented an achievable rate-distortion region [42], which Ozarow [107] proved was tight in the case of a memoryless Gaussian source and the squared error distortion measure. Currently, this is the only case where the solution to the MD problem is completely known.

1.2.2   Many Descriptions

Recently, the information theoretic aspects of the general case of $K > 2$ descriptions have received a lot of attention [111, 114, 141, 142, 146]. This case is the natural extension of the two-description case. Given the rate tuple $(R_0, \ldots, R_{K-1})$, we seek the largest set of simultaneously achievable distortions over all subsets of descriptions. The general K-channel MD problem will be treated in greater detail in Chapter 4.

With this thesis we show that, at least for the case of audio streaming for lossy packet-switched networks, there seems to be a lot to be gained by using more than two descriptions. It is likely that this result carries over to VoIP and video streaming applications.

---

[1]At that time the problem was already known to several people including Gersho, Ozarow, Jayant, Miller, and Boyle who all made contributions towards its solution, see [50] for more information.

1.2.3   Scalar vs. Vector Quantization

In the single-description (SD) case it is known that the scalar rate loss (i.e. the bit rate increase due to using a scalar quantizer instead of an optimal infinite-dimensional vector quantizer) is approximately 0.2546 bit/dim. [47]. For many applications this rate loss is discouraging small and it is tempting to quote Uri Erez:[2]

> *"The problem of vector quantization is that scalar quantization works so well."*

However, in the MD case, the sum (or accumulative) rate loss over many descriptions can be severe. For example, in the two-description case, it is known that the scalar rate loss is about twice that of the SD scalar rate loss [136]. Therefore, when constructing MD schemes for many descriptions, it is important that the rate loss is kept small. To achieve this, we show in this thesis, that one can, for example, use lattice vector quantizers combined with an index-assignment algorithm.

1.3   Contributions

The MD problem is a joint source-channel coding problem. However, in this work we mainly attack the MD problem from a source coding point of view, where we consider the general case involving K descriptions. We make extensive use of lattice vector quantization (LVQ) theory, which turns out to be instrumental in the sense that the proposed MD-LVQ scheme serves as a bridge between theory and practice. In asymptotic cases of high resolution and large lattice vector quantizer dimension, we show that the best known information theoretic rate-distortion MD bounds can be achieved, whereas in non-asymptotic cases of finite-dimensional lattice vector quantizers (but still under high resolution assumptions) we construct practical MD-LVQ schemes, which are comparable and often superior to existing state-of-the-art schemes.

The main contributions of this thesis are the following:

1. L-**sphere bound for two descriptions**

   In the two-channel symmetric case it has previously been established that the side descriptions of an MD-LVQ scheme admit side distortions, which (at high resolution conditions) are identical to that of L-dimensional quantizers having spherical Voronoi cells [120, 139]. In this case we say that the side quantizers achieve the L-sphere bound. Such a result has not been established for the two-channel asymmetric case before. However, the proposed MD-LVQ scheme is able to achieve the L-sphere bound for two descriptions, at high resolution conditions, in both the symmetric and asymmetric cases.

---

[2]Said during a break at the International Symposium on Information Theory in Seattle, July 2006.

2. **MD high-resolution region for three descriptions**

   The proposed MD-LVQ scheme appears to be among the first schemes in the literature that achieves the largest known high-resolution three-channel MD region in the quadratic Gaussian case.[3] We prove optimality for $K \leq 3$ descriptions, but conjecture optimality for any K descriptions.

3. **Exact rate-distortion results for L-dimensional LVQ**

   We present closed-form expressions for the rate and distortion performance when using L-dimensional lattice vector quantizers. These results are valid for smooth stationary sources and squared-error distortion criterion and at high resolution conditions.

4. **Rate loss for finite-dimensional LVQ**

   The rate loss of the proposed MD-LVQ scheme when using finite-dimensional lattice vector quantizers is lattice independent and given by the rate loss of an L-sphere and an additional term describing the ratio of two dimensionless expansion factors. The overall rate loss is shown to be superior to existing three-channel schemes, a result that appears to hold for any number of descriptions.

5. **K-channel asymmetric MD-LVQ**

   In the asymmetric two-description case it has previously been shown that by introducing weights, the distortion profile of the system can range from successive refinement to complete symmetric MD coding [27, 28]. We show a similar result for the general case of K descriptions. Furthermore, for any set of weights, we find the optimal number of descriptions and show that the redundancy in the scheme is independent of the target rate, source distribution and choice of lattices for the side quantizers. Finally, we show how to optimally distribute a given bit budget among the descriptions, which is a topic that has not been addressed in previous asymmetric designs.

6. **Lattice construction using algebraic $\mathscr{J}$-modules**

   For the two-description case it has previously been shown that algebraic tools can be exploited to simplify the construction of MD-LVQ schemes [27, 28, 120, 139]. We extend these results to K-channel MD-LVQ and show that algebraic $\mathscr{J}$-modules provide simple solutions to the problem of constructing the lattices used in MD-LVQ.

---

[3]A conference version of the proposed symmetric K-channel MD-LVQ scheme appeared in [104] and the full version in [105]. The asymmetric K-channel MD-LVQ scheme appeared in [99]. Independently, Chen et al. [16–18] presented a different design of K-channel asymmetric MD coding.

7. K-**channel MD-LVQ based audio coding**

   We present a perceptually robust audio coder based on the modified discrete cosine transform and K-channel MD-LVQ. This appears to be the first scheme to consider more than two descriptions for audio coding. Furthermore, we show that using more than two descriptions is advantageous in packet-switched network environments with excessive packet losses.

1.4   Structure of Thesis

The main contributions of this thesis are presented in Chapters 5–8 and the corresponding appendices, i.e. Appendices E–K.

The general structure of the thesis is as follows:

Chapter 2 The theory of LVQ is a fundamental part of this thesis and in this chapter we describe in detail the construction of lattices and show how they can be used as vector quantizers. A majority of the material in this chapter is known, but the use of $\mathscr{J}$-modules for constructing product lattices based on more than two sublattices is new.

Chapter 3 We consider the MD problem from a source-coding perspective and in this chapter we cover aspects of SD rate-distortion theory, which are also relevant for the MD case.

Chapter 4 In this chapter we present and discuss the existing MD rate-distortion results, which are needed in order to better understand (and to be able to compare to) the new MD results to be presented in the forthcoming chapters.

Chapter 5 Here we present the proposed entropy-constrained K-channel symmetric MD-LVQ scheme. We derive closed-form expressions for the rate and distortion performance of MD-LVQ at high resolution and find the optimal lattice parameters, which minimize the expected distortion given the packet-loss probabilities. We further show how to construct practical MD-LVQ schemes and evaluate their numerical performance. This work was presented in part in [104, 105].

Chapter 6 We extend the results of the previous chapter to the asymmetric case. In addition we present closed-form expressions for the distortion due to reconstructing using arbitrary subsets of descriptions. We also describe how to distribute a fixed target bit rate across the descriptions so that the expected distortion is minimized. This work was presented in part in [98, 99].

Chapter 7 In this chapter we compare the rate-distortion performance of the proposed MD-LVQ scheme to that of existing state-of-the-art MD schemes as well as to known information theoretic high-resolution K-channel MD rate-distortion bounds. This work was presented in part in [98, 102].

Chapter 8 In this chapter we propose to combine the modified discrete cosine transform with MD-LVQ in order to construct a perceptually robust audio coder. Part of the research presented in this chapter represents joint work with O. Niamut. This work was presented in part in [106].

Chapter 9 A summary of results and future research directions are given here.

Appendices The appendices contain supporting material including proofs of lemmas, propositions, and theorems.

1.5   List of Papers

The following papers have been published by the author of this thesis during his Ph.D. studies or are currently under peer review.

1. J. Østergaard and R. Zamir, "Multiple-Description Coding by Dithered Delta Sigma Quantization", IEEE Proc. Data Compression Conference (DCC), pp. 63 – 72. March 2007. (Reference [127]).

2. J. Østergaard, R. Heusdens, and J. Jensen, "Source-Channel Erasure Codes With Lattice Codebooks for Multiple Description Coding", IEEE Int. Symposium on Information Theory (ISIT), pp. 2324 – 2328, July 2006. (Reference [102]).

3. J. Østergaard, R. Heusdens and J. Jensen "n-Channel Asymmetric Entropy-Constrained Multiple-Description Lattice Vector Quantization", Submitted to IEEE Trans. Information Theory, June 2006. (Reference [98]).

4. J. Østergaard, J. Jensen and R. Heusdens,"n-Channel Entropy-Constrained Multiple-Description Lattice Vector Quantization", IEEE Trans. Information Theory, vol. 52, no. 5, pp. 1956 – 1973, May 2006. (Reference [105]).

5. J. Østergaard, O. A. Niamut, J. Jensen and R. Heusdens, "Perceptual Audio Coding using n-Channel Lattice Vector Quantization", Proc. IEEE Int. Conference on Audio, Speech and Signal Processing (ICASSP), vol. V, pp. 197 – 200, May 2006. (Reference [106]).

6. J. Østergaard, R. Heusdens, and J. Jensen, "On the Rate Loss in Perceptual Audio Coding", IEEE Benelux/DSP Valley Signal Processing Symposium, pp. 27 – 30, March 2006. (Reference [101]).

7. J. Østergaard, R. Heusdens, J. Jensen, "n-Channel Asymmetric Multiple-Description Lattice Vector Quantization", IEEE Int. Symposium on Information Theory (ISIT), pp. 1793 – 1797. September 2005. (Reference [99]).

8. J. Østergaard, R. Heusdens, J. Jensen, "On the Bit Distribution in Asymmetric Multiple-Description Coding", 26th Symposium on Information Theory in the Benelux, pp. 81 – 88, May 2005. (Reference [100]).

9. J. Østergaard, J. Jensen and R. Heusdens, "n-Channel Symmetric Multiple-Description Lattice Vector Quantization", IEEE Proc. Data Compression Conference (DCC), pp. 378 – 387, March 2005. (Reference [104]).

10. J. Østergaard, J. Jensen and R. Heusdens, "Entropy Constrained Multiple Description Lattice Vector Quantization", Proc. IEEE Int. Conference on Audio, Speech and Signal Processing (ICASSP), vol. 4, pp. 601 – 604, May 2004. (Reference [103]).

Chapter 2

Lattice Theory

In this chapter we introduce the concept of a lattice and show that it can be used as a vector quantizer. We form subsets (called sublattices) of this lattice, and show that these sublattices can also be used as quantizers. In fact, in later chapters, we will use a lattice as a central quantizer and the sublattices will be used as side quantizers for MD-LVQ. We defer the discussion on rate-distortion properties of the lattice vector quantizer to Chapters 3 and 4.

We begin by describing a lattice in simple terms and show how it can be used as a vector quantizer. This is done in Section 2.1 and more details can be found in Appendix C. Then in Section 2.2 we show that lattice theory is intimately connected to algebra and it is therefore possible to use existing algebraic tools to solve lattice related problems. For example it is well known that lattices form groups under ordinary vector addition and it is therefore possible to link fundamental group theory to lattices. In Section 2.3 we then use these algebraic tools to construct lattices and sublattices. It might be a good idea here to consult Appendix A for the definition of Quaternions and Appendix B for a brief introduction to module theory.

We would like to point out that Section 2.1 contains most of the essential lattice theory needed to understand the concept of MD-LVQ. Sections 2.2 and 2.3 are supplementary to Section 2.1. In these sections we construct lattices and sublattices in an algebraic fashion by using the machinery of module theory. This turns out to be a very convenient approach, since it allows simple constructions of lattices. This theory is therefore also very helpful for the practical implementation of MD-LVQ schemes. In addition, we would like to emphasize that by use of module theory we are able to prove the existence of lattices which admit the required sublattices and product lattices. In Chapters 5–7 we will implicitly assume that all lattices, sublattices, and product lattices are constructed as specified in this chapter.

2.1 Lattices

An L-dimensional lattice is a discrete set of equidistantly spaced points in the L-dimensional Euclidean vector space $\mathbb{R}^L$. For example, the set of integers $\mathbb{Z}$ forms a lattice in $\mathbb{R}$ and the Cartesian product $\mathbb{Z} \times \mathbb{Z}$ forms a lattice in $\mathbb{R}^2$. More formally, we have the following definition.

Definition 2.1.1 ([22]). A lattice $\Lambda \subset \mathbb{R}^L$ consists of all possible integral linear combinations of a set of basis vectors, that is

$$\Lambda = \left\{ \lambda \in \mathbb{R}^L : \lambda = \sum_{i=1}^{L} \xi_i \zeta_i, \ \forall \xi_i \in \mathbb{Z} \right\}, \tag{2.1}$$

where $\zeta_i \in \mathbb{R}^L$ are the basis vectors also known as generator vectors of the lattice.

The generator vectors $\zeta_i, i = 1, \ldots, L$, (or more correctly their transposes) form the rows of the generator matrix M. Usually there exists several generator matrices which all lead to the same lattice. In Appendix D we present some possible generator matrices for the lattices considered in this thesis.

Definition 2.1.2. Given a discrete set of points $S \subset \mathbb{R}^L$, the nearest neighbor region of $s \in S$ is called a Voronoi cell, Voronoi region or Dirichlet region, and is defined by

$$V(s) \triangleq \{x \in \mathbb{R}^L : \|x - s\|^2 \leq \|x - s'\|^2, \ \forall \, s' \in S\}, \tag{2.2}$$

where $\|x\|$ denotes the usual norm in $\mathbb{R}^L$, i.e. $\|x\|^2 = x^T x$.

As an example, Fig. 2.1(a) shows a finite region of the lattice $\Lambda = \mathbb{Z}^2$ consisting of all pairs of integers. For this lattice, the Voronoi cells $V(\lambda), \lambda \in \Lambda$, form squares in the two-dimensional plane. This lattice is also referred to as the Z^2 lattice or the square lattice, cf. Appendix D.2. A lattice Λ and its Voronoi cells $V(\lambda), \forall \lambda \in \Lambda$, actually form a vector quantizer. When Λ is used as a vector quantizer, a point x is mapped (or quantized) to $\lambda \in \Lambda$ if $x \in V(\lambda)$. An example of a non-lattice vector quantizer is shown in Fig. 2.1(b). Here we have randomly picked a set of elements of $\mathbb{R}^2$. Notice that the Voronoi cells are not identical but still their union cover the space. On the other hand, in Fig. 2.1(a), it may be noticed that the Voronoi cells of Λ are all identical, and we say that each one of them describes a fundamental region. A fundamental region of a lattice is a closed region which contains a single lattice point and tessellates the underlying space.

Lemma 2.1.1 ([22]). All fundamental regions have the same volume ν.

Lemma 2.1.2 ([22]). The fundamental volume ν of Λ is given by $\nu = \sqrt{\det(A)}$, where $A = MM^T$ is called the Gram matrix. We sometimes write the volume as $\nu = \det(\Lambda)$.

(a) $\Lambda = \mathbb{Z}^2$ (b) Random point set
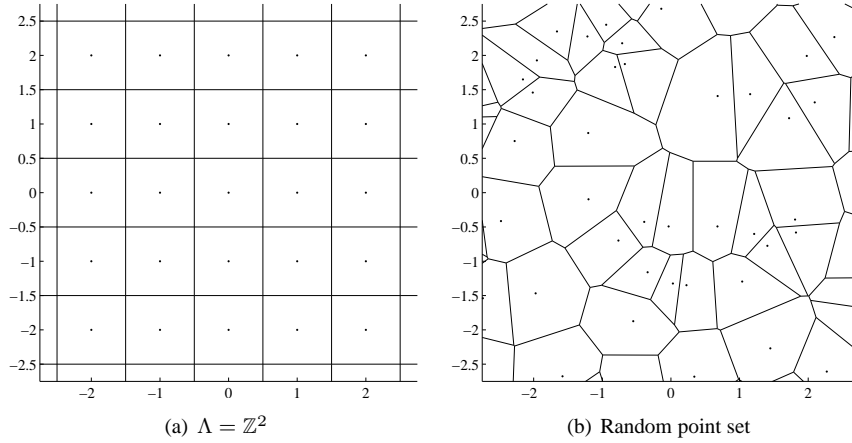
Figure 2.1: *(a) finite region of the lattice $\Lambda = \mathbb{Z}^2$. (b) randomly selected points of $\mathbb{R}^2$. The solid lines describe the boundaries of the Voronoi cells of the points.*

Let us define $V_0 \triangleq V(0)$, i.e. the Voronoi cell around the lattice point located at the origin. This region is called a fundamental region of the lattice since it specifies the complete lattice through translations. We then have the following definition.

Definition 2.1.3 ([22])**.** The dimensionless normalized second moment of inertia $G(\Lambda)$ of a lattice Λ is defined by

$$G(\Lambda) \triangleq \frac{1}{L\nu^{1+2/L}} \int_{V_0} \|x\|^2 dx, \qquad (2.3)$$

where ν is the volume of V_0.

Applying any scaling or orthogonal transform, e.g. rotation or reflection on Λ will not change $G(\Lambda)$, which makes it a good figure of merit when comparing different lattices (quantizers). Furthermore, $G(\Lambda)$ depends only upon the shape of V_0, and in general, the more sphere-like shape, the smaller normalized second moment [22].

2.1.1   Sublattices

If Λ is a lattice then a sublattice $\Lambda' \subseteq \Lambda$ is a subset of the elements of Λ that is itself a lattice. For example if $\Lambda = \mathbb{Z}$ then the set of all even integers is a sublattice of Λ. Geometrically speaking, a sublattice $\Lambda' \subset \Lambda$ is obtained by scaling and rotating (and possibly reflecting) the lattice Λ so that all points of Λ' coincide with points of Λ. A sublattice $\Lambda' \subset \Lambda$ obtained in this manner is referred to as a geometrically-similar sublattice of Λ. Fig. 2.2 shows an example of a lattice $\Lambda \subset \mathbb{R}^2$ and a geometrically-similar sublattice $\Lambda' \subset \Lambda$. In this case Λ is the hexagonal lattice which is described in

Appendix D.3. It may be noticed from Fig. 2.2 that all Voronoi cells of the sublattice Λ' contain exactly seven points of Λ. In general we would like to design a sublattice so that each of its Voronoi cells contains exactly N points of Λ. We call N the index value of the sublattice and usually write it as $N = |\Lambda/\Lambda'|$. Normalizing N by dimension, i.e. $N' = N^{1/L}$, gives what is known as the nesting ratio. We call a sublattice $\Lambda' \subset \Lambda$
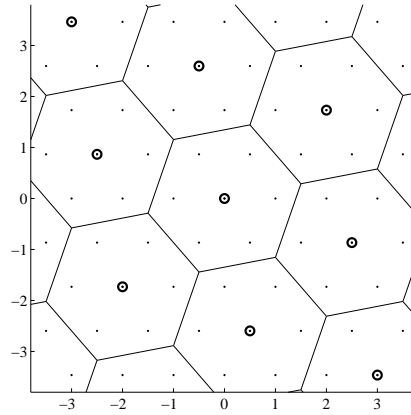
Figure 2.2: *The hexagonal lattice Λ (small dots) and a sublattice $\Lambda' \subset \Lambda$ (circles) of index $N = 7$. The solid lines illustrate the boundaries of the Voronoi cells of Λ'.*

clean if no points of Λ lies on the boundaries of the Voronoi cells of Λ'. For example, the sublattice of Fig. 2.2 is clean. If $\Lambda' \subset \Lambda$ is a clean sublattice we call the index $N = |\Lambda/\Lambda'|$ an admissible index value. In this work we are mainly interested in clean sublattices and we will further discuss the issue of admissible index values in Section 2.3.1.

2.2 $\mathscr{J}$-Lattice

We showed in the previous section that, geometrically speaking, an L-dimensional lattice $\Lambda \subset \mathbb{R}^L$ is a discrete set of regularly spaced points in $\mathbb{R}^L$. From Appendix B it can be deduced that, algebraically speaking, an L-dimensional lattice $\Lambda \subset \mathbb{R}^L$ is a free (torsion-free) discrete $\mathscr{J}$-module of rank L with compact quotient $\mathbb{R}^L/\Lambda$. In this section we will consider the latter definition of a lattice and construct lattices and sublattices by use of the theory of modules.

A lattice $\Lambda \subset \mathbb{R}^L$ as defined in (2.1) forms an additive group $(\Lambda, +)$ under ordinary vector addition with the zero-vector being the identity element. If the group further admits left or right multiplication by the ring $\mathscr{J}$ then we call Λ a $\mathscr{J}$-module. In other words, Λ is a $\mathscr{J}$-module if it is closed under addition and subtraction of members of the group and closed under scalar multiplication by members of the ring,

see Appendix B for details. Since Λ is also a lattice we sometimes prefer the name $\mathscr{J}$-lattice over $\mathscr{J}$-module.

Let $\zeta_i, i = 1, \ldots, L$ be a set of linearly independent vectors in $\mathbb{R}^L$ and let $\mathscr{J} \subset \mathbb{R}$ be a ring. Then a left $\mathscr{J}$-lattice Λ generated by $\zeta_i, i = 1, \ldots, L$ consists of all linear combinations

$$\xi_1 \zeta_1 + \cdots + \xi_L \zeta_L, \tag{2.4}$$

where $\xi_i \in \mathscr{J}, i = 1, \ldots, L$ [22]. A right $\mathscr{J}$-lattice is defined similarly with the multiplication of ζ_i on the right by ξ_i instead.

We have so far assumed that the underlying field is the Cartesian product of the reals, i.e. $\mathbb{R}^L$. However, there are other fields which when combined with well defined rings of integers will lead to $\mathscr{J}$-lattices that are good for quantization. Let the field be the complex field $\mathbb{C}$ and let the ring of integers be the Gaussian integers $\mathscr{G}$, where [22]

$$\mathscr{G} = \{\xi_1 + i\xi_2 : \xi_1, \xi_2 \in \mathbb{Z}\}, \quad i = \sqrt{-1}. \tag{2.5}$$

Then we may form a one-dimensional complex lattice (to which there always exists an isomorphism that will bring it to $\mathbb{R}^2$) by choosing any non-zero element (a basis) $\zeta_1 \in \mathbb{C}$ and insert in (2.4), cf. Fig. 2.3(a) where we have made the arbitrary choice of $\zeta_1 = 11.2 - 2.3i$. The lattice described by the set of Gaussian integers is isomorphic to the square lattice $Z^2 = \mathbb{Z}^2$. The operation $\mathscr{G}\zeta_1$ then simply rotate and scale the Z^2 lattice. To better illustrate the shape of the $\mathscr{J}$-lattice we have in Fig. 2.3(a) also shown the boundaries (solid lines) of the nearest neighbor regions (also called Voronoi cells) between the lattice points. Fig. 2.3(b) shows an example where the basis $\zeta_1 = 11.2 - 2.3i$ has been multiplied by the Eisenstein integers $\mathscr{E}$, where [22]

$$\mathscr{E} = \{\xi_1 + \omega\xi_2 : \xi_1, \xi_2 \in \mathbb{Z}\}, \quad \omega = e^{2\pi i/3}. \tag{2.6}$$

The ring of algebraic integers $\mathscr{Q}$ is defined by [22]

$$\mathscr{Q} = \{\xi_1 + \omega_1\xi_2 : \xi_1, \xi_2 \in \mathbb{Z}\}, \tag{2.7}$$

where ω_1 is, for example, one of

$$\sqrt{-2}, \sqrt{-5}, \frac{-1 + \sqrt{-7}}{2}, \frac{-1 + \sqrt{-11}}{2}. \tag{2.8}$$

Figs. 2.3(c) and 2.3(d) show examples where $\mathscr{J}$ is the ring of algebraic integers and where $\omega_1 = \sqrt{-5}$ and $\omega_1 = (-1 + \sqrt{-7})/2$, respectively. In both cases we have used the basis $\zeta_1 = 11.2 - 2.3i$.

2.2.1   𝒥**-Sublattice**

If Λ' is a submodule of a $\mathscr{J}$-module Λ then Λ' is simply a sublattice of the lattice Λ. More formally we have the following lemma.

(a) $\Lambda = \mathscr{G}\zeta_1$

(b) $\Lambda = \mathscr{E}\zeta_1$

(c) $\Lambda = \mathscr{Q}\zeta_1, \omega_1 = \sqrt{-5}$

(d) $\Lambda = \mathscr{Q}\zeta_1, \omega_1 = (-1 + \sqrt{-7})/2$
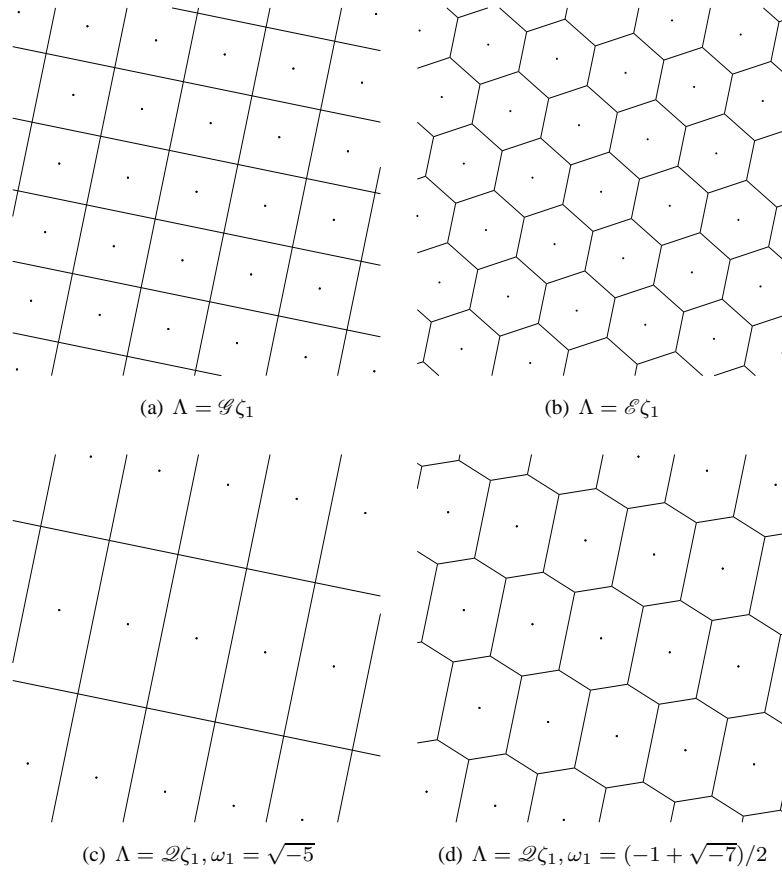
Figure 2.3: *One-dimensional complex $\mathscr{J}$-lattices constructed from different rings of integers by use of the basis $\zeta_1 = 11.2 - 2.3i$. The solid lines illustrate the boundaries of the nearest neighbor regions (Voronoi cells) between lattice points.*

Lemma 2.2.1 ([1]). Let $\mathscr{J}$ be a ring. If Λ is $\mathscr{J}$-module and $\Lambda' \subseteq \Lambda, \Lambda' \neq \emptyset$, then Λ' is a $\mathscr{J}$-submodule of Λ if and only if $\xi_1\lambda_1' + \xi_2\lambda_2' \in \Lambda'$ for all $\lambda_1', \lambda_2' \in \Lambda'$ and $\xi_1, \xi_2 \in \mathscr{J}$.

Let Λ be a $\mathscr{J}$-module. Then we may form the left submodule $\Lambda' = \xi\Lambda$ and the right submodule $\Lambda'' = \Lambda\xi$ by left (or right) multiplication of Λ by $\xi \in \mathscr{J}$. For example let Λ be the $\mathscr{J}$-module given by the Eisenstein integers, i.e. $\Lambda = \mathscr{E}$. This lattice can be regarded as a two-dimensional real lattice in $\mathbb{R}^2$ in which case it is usually referred to as A_2. Then let us form the submodule $\Lambda' = \xi\Lambda$ where $\xi = -3 - 2\omega$ and $\omega = e^{2\pi i/3}$, see Fig. 2.4. When the modules in question are lattices we will usually call Λ a $\mathscr{J}$-lattice and Λ' a $\mathscr{J}$-sublattice. Sometimes when the ring

$\mathscr{J}$ is clear from the context or irrelevant we will use the simpler terms lattice and sublattice for Λ and Λ', respectively.
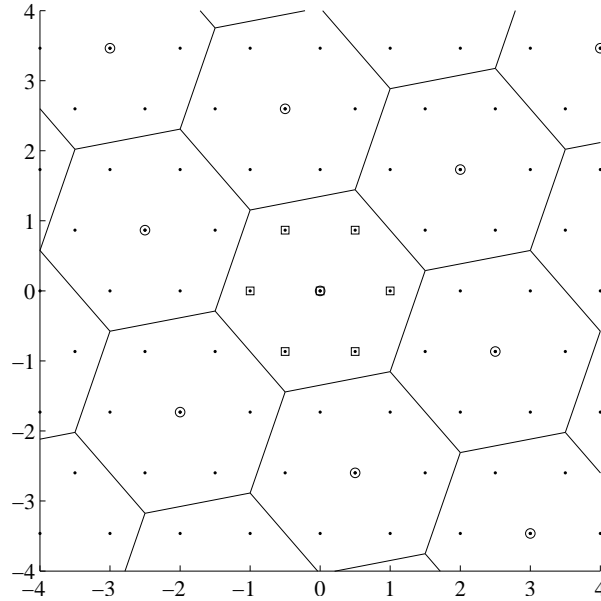
Figure 2.4: *The Eisenstein lattice Λ is here shown with dots and the circles illustrate points of the sublattice $\Lambda' = \xi\Lambda, \xi = -3 - 2\omega, \omega = e^{2\pi i/3}$. The solid lines describe the boundaries between neighboring Voronoi cells of the sublattice points. Notice that there are 7 dots in each Voronoi cell. The points marked with squares are the seven coset representatives of the quotient Λ/Λ'.*

2.2.2   Quotient Modules

In this section we consider quotient modules and the next section is concerned with group actions on these quotient modules. Although perhaps unclear at this point, we show later that these concepts are important in order to identify or associate a set of sublattice points with a given lattice point. This identification process, which we call either the labeling problem or the problem of constructing an index assignment map, focuses on labeling the coset representatives of Λ/Λ', i.e. the quotient module. It then turns out, as first observed in [120, 139], that we actually only need to label the representatives of the orbits of $\Lambda/\Lambda'/\Gamma_m$ instead of all coset representatives of Λ/Λ'. Further details about quotient modules and group actions are given in Appendix B.

Definition 2.2.1. Let Λ be a $\mathscr{J}$-module and Λ' a $\mathscr{J}$-submodule of Λ. Then Λ' induces a partition Λ/Λ' of Λ into equivalence classes (or cosets) modulo Λ'. We call such a partition the quotient module.

The order or index $|\Lambda/\Lambda'|$ of the quotient module Λ/Λ' is finite and each element of Λ/Λ' is a representative for an infinite set called a coset. For any $\lambda \in \Lambda$ the coset of Λ' in Λ determined by λ is the set $\lambda + \Lambda' = \{\lambda + \lambda' : \lambda' \in \Lambda'\}$. In this work we always let the group operation be ordinary vector addition which is a commutative operation so that the left and right cosets coincide. As such there is no ambiguity with respect to left and right cosets when referring to the coset $\lambda + \Lambda'$. We will use the notation $[\lambda]$ when referring to the coset $\lambda + \Lambda'$ and we call λ the coset representative. It should be clear that any member of the coset $[\lambda]$ can be the coset representative. To be consistent we will always let the coset representative be the unique[4] vector of $[\lambda]$ which is in the Voronoi cell of the zero-vector of Λ'. For example if Λ and Λ' are defined as in Fig. 2.4 then the index $|\Lambda/\Lambda'| = 7$ and there is therefore seven distinct cosets in the quotient module Λ/Λ'. The seven cosets representatives are indicated with squares in Fig. 2.4.

2.2.3   Group Actions on Quotient Modules

Let $\Gamma_m \subseteq \mathrm{Aut}(\Lambda)$ be a group of order m of automorphisms of Λ. We then denote the set of orbits under the action of Γ_m on the quotient module Λ/Λ' by $\Lambda/\Lambda'/\Gamma_m$. For example let $\Gamma_2 = \{I_2, -I_2\}$ be a group (closed under matrix multiplication) of order 2, where I_2 is the two-dimensional identity matrix. Let the $\mathscr{J}$-module Λ be identical to $\mathbb{Z}^2$ and let Λ' be a submodule of Λ of index $N = 81$. In other words, there are N coset representatives in the quotient module Λ/Λ' whereas the set of orbits $\Lambda/\Lambda'/\Gamma_2$ has cardinality $|\Lambda/\Lambda'/\Gamma_2| = 41$. This is illustrated in Fig. 2.5(a) where the coset representatives of Λ/Λ' are illustrated with dots and representatives of the orbits of $\Lambda/\Lambda'/\Gamma_2$ are marked with circles.

Next consider the group given by

$$\Gamma_4 = \left\{\pm I_2, \pm \begin{pmatrix} 0 & -1 \\ 1 & 0 \end{pmatrix}\right\}, \tag{2.9}$$

which has order 4 and includes Γ_2 as a subgroup. Fig. 2.5(b) shows coset representatives for Λ/Λ' and representatives for the set of orbits $\Lambda/\Lambda'/\Gamma_4$. Notice that $|\Lambda/\Lambda'/\Gamma_4| = 21$.

2.3   Construction of Lattices

We now show how to construct the lattices and sublattices that later will be used as quantizers in MD-LVQ.

---

[4]We will later require that Λ' is a clean sublattice of Λ from which the uniqueness property is evident. If Λ' is not clean then we make an arbitrary choice amongst the candidate representatives.

(a) $\Lambda/\Lambda'/\Gamma_2$ (b) $\Lambda/\Lambda'/\Gamma_4$
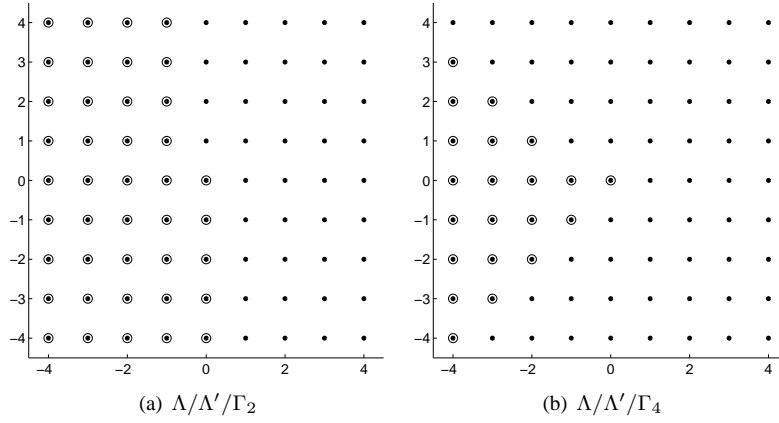
Figure 2.5: *The 81 coset representatives for Λ/Λ' are here shown as dots and representatives for the orbits of (a) $\Lambda/\Lambda'/\Gamma_2$ and (b) $\Lambda/\Lambda'/\Gamma_4$ are shown as circles.*

2.3.1   Admissible Index Values

For any geometrically-similar sublattice Λ' of Λ, a number of lattice points of Λ will be located within each Voronoi cell of Λ' and perhaps on the boundaries between neighboring Voronoi cells. In the latter case ties must be broken in order to have well defined Voronoi cells. To avoid tie breaking it is required that Λ' has no lattice points on the boundary of its Voronoi cells. In this case, Λ' is said to be clean. As previously mentioned, we call an index value of a clean sublattice an admissible index value. In [21] partial answers are given to when Λ contains a sublattice Λ' of index N that is geometrically-similar to Λ, and necessary and sufficient conditions are given for any lattice in two dimensions to contain a geometrically-similar and clean sublattice of index N. These results are extended in [28] to geometrically-similar and clean sublattices in four dimensions for the Z^4 and D_4 lattice. In addition, results are given for any Z^L lattice where $L = 4k, k \geq 1$. Table 2.1 briefly summarizes admissible index values for the known cases. In general Z^L has a geometrically-similar and clean sublattice if and only if N is odd and

a) L odd and N an Lth power, or

b) $L = 2$ and N of the form $a^2 + b^2$, or

c) $L = 4k$, $k \geq 1$ and N of the form $m^{L/2}$ for some integer m,

see [28] for details.

It can be shown that squaring an admissible index value yields another admissible index value for all lattices considered in this work. We can generalize this even

Lattice	Dim.	Admissible index values
Z	1	1,3,5,7,9,...
Z^2	2	1,5,9,13,17,25,29,37,41,45,49,...
A_2	2	1,7,13,19,31,37,43,49,...
D_4	4	1,25,49,169,289,625,...
Z^4	4	1,25,49,81,121,169,225,289,361,...

Table 2.1: *Admissible index values for geometrically-similar and clean sublattices in one, two and four dimensions. See Appendix D for more information about these sets of index values.*

further and show that the product of any number of admissible index values leads to an admissible index value.

Lemma 2.3.1. For the lattices A_2, D_4 and Z^L where $L = 1, 2$ or $L = 4k$, where $k \geq 1$, the product of two or more admissible index values yields another admissible index value.

Proof. See Appendix E. $\qquad\qquad\qquad\qquad\qquad\qquad\qquad\qquad\qquad\qquad\qquad\square$

As noted in [21] it is always possible by e.g. exhaustive search to see if a lattice Λ contains a sublattice Λ' with an index value of $N = c^{L/2}, c \in \mathbb{R}^+$. Let the Gram matrix of Λ be A. Then search through Λ to see if it contains a set of generator vectors with Gram matrix cA. In large lattice dimensions this approach easily becomes infeasible. However, for known lattices the admissible index values can be found off-line and then tabulated for later use.

If two lattices $\Lambda \subset \mathbb{R}^L$ and $\Lambda' \subset \mathbb{R}^{L'}$ are concatenated (i.e. their Cartesian product is formed) then the resulting lattice Λ'' is of dimension $L'' = L + L'$, cf. Definition C.1.7. The set of admissible index values of Λ'' (when normalized by dimension) might be different than that of Λ or Λ'. For example let $\Lambda = Z^1$ where the admissible index values are the odd integers. Then notice that the four-dimensional Z^4 lattice is simply a cascade of four Z^1 lattices. However, the admissible index values (normalized per dimension) of Z^4 are given by (see Appendix D.4)

$$N' = \{\mathbf{1}, 2.24, 2.65, \mathbf{3}, 3.32, 3.61, 3.87, 4.12, 4.36, 4.58, 4.8, \mathbf{5}, \dots\}, \qquad (2.10)$$

where we have shown the index values of Z^1 in boldface. Thus, by forming a higher dimensional lattice by cascading smaller dimensional lattices it is possible to achieve more (or at least different) index values.

A different strategy is to change the underlying ring $\mathscr{J}$ as shown in Fig. 2.3 which results in a different lattice of the same dimension that might lead to new index values. In this thesis, however, we will be using the known admissible index values of Table 2.1.

2.3.2   Sublattices

In this section we construct sublattices and primarily focus on a special type of sublattices called product lattices. In [28] the following definition of a product lattice was presented.

Definition 2.3.1 ([28])**.** Let $\mathscr{J}$ be an arbitrary ring, let $\Lambda = \mathscr{J}$ and form the two sublattices $\Lambda_0 = \xi_0 \Lambda$ and $\Lambda_1 = \Lambda \xi_1$, $\xi_i \in \Lambda, i = 0, 1$. Then the lattice $\Lambda_\pi = \xi_0 \Lambda \xi_1$ is called a product lattice and it satisfies $\Lambda_\pi \subseteq \Lambda_i, i = 0, 1$.

In this work, however, we will make use of a more general notion of a product lattice which includes Definition 2.3.1 as a special case.

Definition 2.3.2. A product lattice Λ_π is any sublattice satisfying $\Lambda_\pi \subseteq \Lambda_i$ where $\Lambda_i = \xi_i \Lambda$ or $\Lambda_i = \Lambda \xi_i, i = 0, \ldots, K - 1$.

The construction of product lattices based on two sublattices as described in Definition 2.3.1 was treated in detail in [28]. In this section we extend the existing results of [28] and construct product lattices based on more than two sublattices for $L = 1, 2$ and 4 dimensions for the root lattices Z^1, Z^2, A_2, Z^4 and D_4, which are described in Appendix D. Along the same lines as in [28] we construct sublattices and product lattices by use of the ordinary rational integers $\mathbb{Z}$ as well as the Gaussian integers $\mathscr{G}$, Eisenstein integers $\mathscr{E}$, Lipschitz integral Quaternions $\mathscr{H}_0$ and the Hurwitz integral Quaternions $\mathscr{H}_1$, where $\mathscr{G}$ and $\mathscr{E}$ are given by (2.5) and (2.6), respectively, and [22]

$$\mathscr{H}_0 = \{\xi_1 + i\xi_2 + j\xi_3 + k\xi_4 : \xi_1, \xi_2, \xi_3, \xi_4 \in \mathbb{Z}\}, \tag{2.11}$$

$$\mathscr{H}_1 = \{\xi_1 + i\xi_2 + j\xi_3 + k\xi_4 : \xi_1, \xi_2, \xi_3, \xi_4 \text{ all in } \mathbb{Z} \text{ or all in } \mathbb{Z} + 1/2\}, \tag{2.12}$$

where i, j and k are unit Quaternions, see Appendix A for more information. For example a sublattice Λ_1 of $\Lambda = \mathbb{Z}$ is easily constructed, simply by multiplying all points $\lambda \in \Lambda$ by ξ where $\xi \in \mathbb{Z} \backslash \{0\}$.[5] This gives a geometrically-similar sublattice $\Lambda_1 = \xi \mathbb{Z}$ of index $|\xi|$. This way of constructing sublattices may be generalized by considering different rings of integers. For example, for the square lattice $\Lambda = \mathscr{G}$ whose points lie in the complex plane, a geometrically-similar sublattice of index 2 may be obtained by multiplying all elements of Λ by the Gaussian integer $\xi = 1 + i$.

Sublattices and product lattices of Z^1, Z^2 and A_2

The construction of product lattices based on the sublattices Z^1, Z^2 and A_2 is a straight forward generalization of the approach taken in [28]. Let the lattice Λ be any one of $Z^1 = \mathbb{Z}, Z^2 = \mathscr{G}$ or $A_2 = \mathscr{E}$ and let the geometrically-similar sublattices Λ_i be given by $\xi_i \Lambda$ where ξ_i is an element of the rational integers $\mathbb{Z}$, the Gaussian integers $\mathscr{G}$ or the Eisenstein integers $\mathscr{E}$, respectively.

---

[5]Since Λ is a torsion free $\mathscr{J}$-module the submodule $\Lambda' = \xi \Lambda$ is a non-trivial cyclic submodule whenever $0 \neq \xi \in \Lambda$.

Lemma 2.3.2. $\Lambda_\pi = \xi_0\xi_1\cdots\xi_{K-1}\Lambda$ is a product lattice.

Proof. See Appendix E. □

Also, as remarked in [28], since the three rings considered are unique factorization rings, the notion of least common multiple (lcm) is well defined. Let us define $\xi_\cap \triangleq \mathrm{lcm}(\xi_0,\ldots,\xi_{K-1})$ so that $\xi_i|\xi_\cap$, i.e. ξ_i divides $\xi_\cap$. This leads to the following lemma.

Lemma 2.3.3. $\Lambda'_\pi = \xi_\cap\Lambda$ is a product lattice.

Proof. See Appendix E. □

The relations between $\Lambda, \Lambda_i, \Lambda'_\pi$ and Λ_π as addressed by Lemmas 2.3.2 and 2.3.3 are shown in Fig. 2.6. For example, let $\Lambda = \mathscr{G}(\equiv Z^2)$ and let $N_0 = 45$ and $N_1 = 81$. Then we have that $\mathrm{lcm}(45, 81) = 405$ and $45 \cdot 81 = 3645$. We may choose $\xi_0 = 3 + 6i, \xi_1 = 9$ and $\xi_\cap = 9 + 18i$, so that $|\xi_0|^2 = 45, |\xi_1|^2 = 81$ and $|\xi_\cap|^2 = 405$. Notice that $\xi_0|\xi_\cap$ and $\xi_1|\xi_\cap$, i.e. $\frac{\xi_\cap}{\xi_0} = 3 \in \mathscr{G}$ and $\frac{\xi_\cap}{\xi_1} = 1 + 2i \in \mathscr{G}$. Since both ξ_0 and ξ_1 divides $\xi_\cap$, the lattice $\Lambda_\cap = \xi_\cap\Lambda$ will be a sublattice of $\Lambda_0 = \xi_0\Lambda$ as well as $\Lambda_1 = \xi_1\Lambda$, see Fig. 2.7.
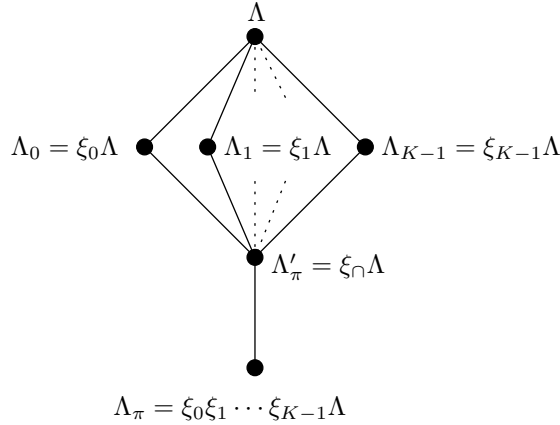
Figure 2.6: *The intersection (meet) of K arbitrary sublattices form a product lattice for Z^1, Z^2 and A_2.*

Sublattices and product lattices of Z^4

As was done in [28] we will use the Quaternions [71, 150] for the construction of sublattices and product lattices for Z^4. The Quaternions form a non-commutative ring and it is therefore necessary to distinguish between left and right multiplication [71, 150]. For the case of two sublattices we adopt the approach of [28] and construct the sublattice Λ_0 by multiplying Λ on the left, i.e. $\Lambda_0 = \xi_0\Lambda$ and Λ_1 is obtained by right
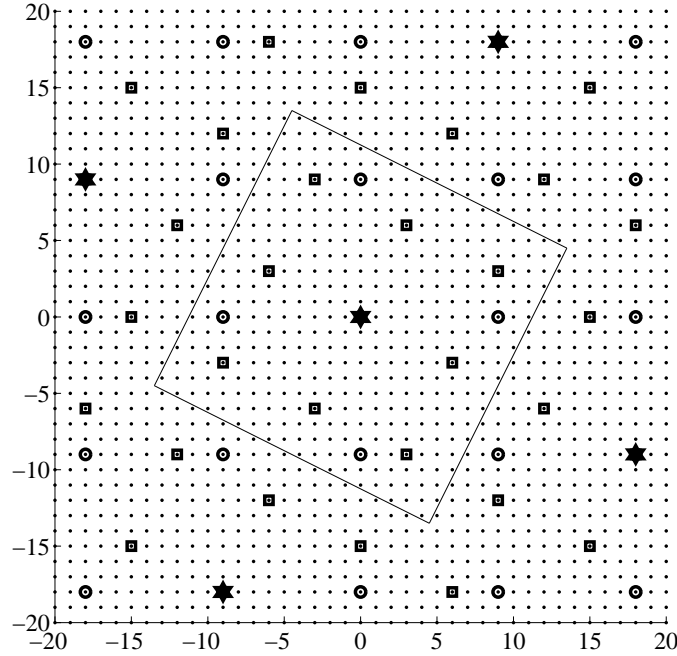
Figure 2.7: *The lattice $\Lambda = \mathscr{G}$ is here shown as dots. The two lattices $\Lambda_0 = (3 + 6i)\Lambda$ (squares) and $\Lambda_1 = 9\Lambda$ (circles) are sublattices of Λ and the lattice $\Lambda_\cap = (9 + 18i)\Lambda$ (stars) is a sublattice of all the lattices Λ_0, Λ_1 and Λ. The solid lines describe the boundary of the Voronoi cell V_0 of the product lattice point located at the origin.*

multiplication $\Lambda_1 = \Lambda\xi_1$, see Fig. 2.8. More than two descriptions was not considered in [28]. Let the K sublattices be of index $N_0, \ldots, N_{K-1}$ respectively. Then we may form $\Lambda_0 = \xi_0\Lambda$ and $\Lambda_1 = \Lambda\xi_1$ as above. However, by letting $\Lambda_2 = \Lambda\xi_2$ we run into trouble when creating the product lattice. For example, if we define $\Lambda_\pi = \xi_0\Lambda\xi_1\xi_2$ it is clear that $\Lambda_\pi \subseteq \Lambda_0$ and $\Lambda_\pi \subseteq \Lambda_2$. The problem is that in general $\Lambda_\pi \not\subseteq \Lambda_1$ since $\xi_1\xi_2 \neq \xi_2\xi_1$ and we therefore have to restrict the set of admissible index values.

Lemma 2.3.4. Let N_0 and N_1 be admissible index values for Z^2. Then N_0^2 and N_1^2 (which are admissible index values for Z^4), can be associated with a pair of Lipschitz integers (ξ_0, ξ_1) that commute, i.e. $\xi_0\xi_1 = \xi_1\xi_0$.

Proof. See Appendix E.   □

From Lemma 2.3.4 it follows that there exist an infinite number of pairs of admissible index values (N_0, N_1) where $N_0 \neq N_1$ such that the Lipschitz integers ξ_0 and ξ_1 commute. For example, let $N_0 = 7^2, N_1 = 13^2, N_2 = 5^2$ and define $\Lambda_0 = \xi_0\Lambda, \Lambda_1 = \Lambda\xi_1$ and $\Lambda_2 = \Lambda\xi_2$ where $\xi_0 = -2-i-j-k, \xi_1 = -2-i+0j+0k$
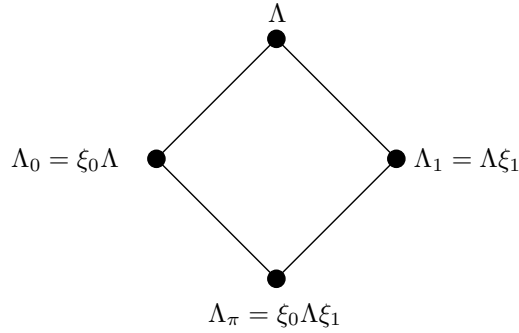
Figure 2.8: *Two arbitrary sublattices form a product lattice.*

and $\xi_2 = -3 - 2i + 0j + 0k$. For this example we have $\xi_0 \xi_1 \neq \xi_1 \xi_0$ and $\xi_0 \xi_2 \neq \xi_2 \xi_0$ but $\xi_1 \xi_2 = \xi_2 \xi_1$. Letting $\Lambda_\pi = \xi_0 \Lambda \xi_1 \xi_2$ makes sure that $\Lambda_\pi \subseteq \Lambda_i$ for $i = 0, 1, 2$, since $\Lambda_\pi = (\xi_0 \Lambda \xi_1) \xi_2 = (\xi_0 \Lambda \xi_2) \xi_1$. In general it is possible to construct the product lattice Λ_π such that $\Lambda_\pi \subseteq \Lambda_i$ for $i = 0, \ldots, K - 1$ as long as any $K - 1$ of the K ξ_i's commute, see Fig. 2.9, where $\xi'_\cap = \text{lcm}(\xi_1, \ldots, \xi_{K-1})$. If all the pairs $(\xi_i, \xi_j), i, j \in \{0, \ldots, K - 1\}$ commute the procedure shown in Fig. 2.6 is also valid.
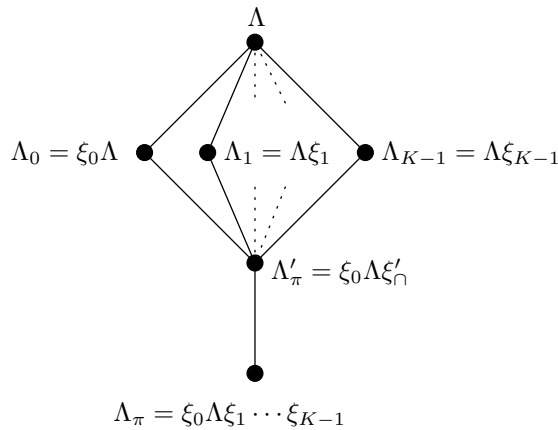
Figure 2.9: *The intersection (meet) of K arbitrary sublattices form a product lattice for Z^4.*

Sublattices and product lattices of D_4

For D_4 we use the ring of Hurwitzian integers, i.e. $\xi_i \in \mathscr{H}_1$. For the case of two sublattices we design the sublattices and product lattices as in [28] and shown in Fig. 2.8. For more than two sublattices we have to make a restriction on the set of allowable admissible index values. The Quaternions leading to admissible index values for D_4 obtained in [28] are of the form[6] $\xi_i = \frac{a}{2}(1+i) + \frac{b}{2}(j+k) \in \mathscr{H}_1$, where a and b are odd positive integers. Quaternions of this form do generally not commute since both a and b are nonzero. In fact two Quaternions commute if and only if their vector parts are proportional [6], i.e. linearly-dependent, which rarely happens for the Quaternions of the form $\xi_i = \frac{a}{2}(1+i) + \frac{b}{2}(j+k) \in \mathscr{H}_1$. For example we did an exhaustive search based on all admissible index values between 25 and 177241 and found only five pairs (up to permutations) of Quaternions that commute. These are shown in Table 2.2.

N_0	N_1	ξ_0	ξ_1
25	15625	$\frac{1}{2} + \frac{1}{2}i + \frac{3}{2}j + \frac{3}{2}k$	$\frac{5}{2} + \frac{5}{2}i + \frac{15}{2}j + \frac{15}{2}k$
169	105625	$\frac{1}{2} + \frac{1}{2}i + \frac{5}{2}j + \frac{5}{2}k$	$\frac{5}{2} + \frac{5}{2}i + \frac{25}{2}j + \frac{25}{2}k$
625	28561	$\frac{5}{2} + \frac{5}{2}i + \frac{5}{2}j + \frac{5}{2}k$	$\frac{13}{2} + \frac{13}{2}i + \frac{13}{2}j + \frac{13}{2}k$
625	83521	$\frac{5}{2} + \frac{5}{2}i + \frac{5}{2}j + \frac{5}{2}k$	$\frac{17}{2} + \frac{17}{2}i + \frac{17}{2}j + \frac{17}{2}k$
28561	83521	$\frac{13}{2} + \frac{13}{2}i + \frac{13}{2}j + \frac{13}{2}k$	$\frac{17}{2} + \frac{17}{2}i + \frac{17}{2}j + \frac{17}{2}k$

Table 2.2: *Each row shows two Quaternions ξ_0 and ξ_1 which commute, i.e. $\xi_0\xi_1 = \xi_1\xi_0$.*

We therefore restrict the set of admissible index values to $N_i \in \{a, b\}$ for $i = 0, \ldots, K-1$ where a and b are any two admissible index values. With this the product lattice, for $K > 2$ sublattices, is based on only two integers e.g. ξ_0 and ξ_1 as shown in Fig. 2.8 and the index of the product lattice is then $N_\pi = ab$. With this approach it is possible to obtain $\Lambda_\pi \subseteq \Lambda_i$ for $i = 0, \ldots, K-1$.

---

[6]With two exceptions being $\xi_i = \frac{1}{2} + \frac{1}{2}i + \frac{1}{2}j + \frac{5}{2}k$ and $\xi_i = \frac{1}{2} + \frac{3}{2}i + \frac{3}{2}j + \frac{3}{2}k$ both leading to an index value of $N = 49$.

Single-Description Rate-Distortion Theory

Source coding with a fidelity criterion, also called rate-distortion theory (or lossy source coding), was introduced by Shannon in his two landmark papers from 1948 [121] and 1959 [122] and has ever since received a lot of attention. For an introduction to rate-distortion theory we refer the reader to the survey papers by Kieffer [74] and Berger and Gibson [9] and the text books by Berger [8], Cziszár and Körner [26] and Cover and Thomas [24].

3.1 Rate-Distortion Function

A fundamental problem of rate-distortion theory is that of describing the rate R required to encode a source X at a prescribed distortion (fidelity) level D. Let $X^L = \{X_i\}, i = 1, \ldots, L$ be a sequence of random variables (or letters) of a stationary[7] random process X. Let $\hat{X}$ be the reproduction of X and let x and $\hat{x}$ be realizations of X and $\hat{X}$, respectively. The alphabets $\mathscr{X}$ and $\hat{\mathscr{X}}$ of X and $\hat{X}$, respectively, can be continuous or discrete and in the latter case we distinguish between discrete alphabets of finite or countably infinite cardinality. When it is clear from context we will often ignore the superscript ^{L} which indicates the dimension of the variable or alphabet so that $x \in \mathscr{X} \subset \mathbb{R}^L$ denotes an L-dimensional vector or element of the alphabet $\mathscr{X}$ which is a subset of $\mathbb{R}^L$.

Definition 3.1.1. A fidelity criterion for the source X is a family $\rho^{(L)}(X, \hat{X}), L \in \mathbb{N}$ of distortion measures of which $\rho^{(L)}$ computes the distortion when representing

---

[7]Throughout this work we will assume all stochastic processes to be discrete-time zero-mean weak-sense stationary processes (unless otherwise stated).

X by $\hat{X}$. If $\rho^{(L)}(X, \hat{X}) \triangleq \frac{1}{L} \sum_{i=1}^{L} \rho(X_i, \hat{X}_i)$ then ρ is said to be a single-letter fidelity criterion and we will then use the notation $\rho(X, \hat{X})$. Distortion measures of the form $\rho(X - \hat{X})$ are called difference distortion measures. For example $\rho(X, \hat{X}) = \frac{1}{L}\|X - \hat{X}\|^2$ is a difference distortion measure (usually referred to as the squared-error distortion measure).

In this work we will be mainly interested in the squared-error single-letter fidelity criterion which is defined by

$$\rho(X, \hat{X}) \triangleq \frac{1}{L} \sum_{i=1}^{L} (X_i - \hat{X}_i)^2. \tag{3.1}$$

With this, formally stated, Shannon's rate-distortion function $R(D)$ (expressed in bit/dim.) for stationary sources with memory and single-letter fidelity criterion, ρ, is defined as [8]

$$R(D) \triangleq \lim_{L \to \infty} R_L(D), \tag{3.2}$$

where the Lth order rate-distortion function is given by

$$R_L(D) = \inf\{\frac{1}{L} I(X; \hat{X}) : E\rho(X, \hat{X}) \leq D\}, \tag{3.3}$$

where $I(X; \hat{X})$ denotes the mutual information[8] between X and $\hat{X}$, E denotes the statistical expectation operator and the infimum is over all conditional distributions $f_{X|\hat{X}}(\hat{x}|x)$ for which the joint distributions $f_{X,\hat{X}}(x, \hat{x}) = f_X(x) f_{\hat{X}|X}(\hat{x}|x)$ satisfy the expected distortion constraint given by

$$\int_{\mathscr{X}} \int_{\hat{\mathscr{X}}} f_X(x) f_{\hat{X}|X}(\hat{x}|x) \rho(x, \hat{x}) d\hat{x} dx \leq D. \tag{3.4}$$

The Lth order rate-distortion function $R_L(D)$ can be seen as the rate-distortion function of an L-dimensional i.i.d. vector source X producing vectors with the distribution of X [82].

Let $h(X)$ denote the differential entropy (or continuous entropy) of X which is given by [24]

$$h(X) = -\int_{\mathscr{X}} f_X(x) \log_2(f_X(x)) \, dx$$

and let the differential entropy rate $\bar{h}(X)$ be defined by $\bar{h}(X) \triangleq \lim_{L \to \infty} \frac{1}{L} h(X)$ where for independently and identically distributed (i.i.d.) scalar processes $\bar{h}(X) =$

---

[8]The mutual information between to continuous-alphabet sources X and $\hat{X}$ with a joint pdf $f_{X,\hat{X}}$ and marginals f_X and $f_{\hat{X}}$, respectively, is defined as [24]

$$I(X; \hat{X}) = \int_{\mathscr{X}} \int_{\hat{\mathscr{X}}} f_{X,\hat{X}}(x, \hat{x}) \log_2 \left(\frac{f_{X,\hat{X}}(x, \hat{x})}{f_X(x) f_{\hat{X}}(\hat{x})} \right) dx d\hat{x}.$$

$\frac{1}{L}h(X)$. With a slight abuse of notation we will also use the notation $\bar{h}(X)$ to indicate the dimension normalized differential entropy of an i.i.d. vector source. If ρ is a difference distortion measure, then (3.2) and (3.3) can be lower bounded by the Shannon lower bound [8]. Specifically, if $E\rho$ is the mean squared error (MSE) fidelity criterion, then [8, 82]

$$R(D) \geq \bar{h}(X) - \frac{1}{2}\log_2(2\pi e D), \tag{3.5}$$

where equality holds at almost all distortion levels D for a (stationary) Gaussian source [8].[9] In addition it has been shown that (3.5) becomes asymptotically tight at high resolution, i.e. as $D \rightarrow 0$, for sources with finite differential entropies and finite second moments for general difference distortion measures, cf. [82].

Recall that the differential entropy of a jointly Gaussian vector is given by [24]

$$h(X) = \frac{1}{2}\log_2((2\pi e)^L |\Phi|), \tag{3.6}$$

where $|\Phi|$ is the determinant of $\Phi = EXX^T$, i.e. the covariance matrix of X. It follows from (3.5) that the rate-distortion function of a memoryless scalar Gaussian process of variance σ_X^2 is given by

$$R(D) = \frac{1}{2}\log_2\left(\frac{\sigma_X^2}{D}\right), \tag{3.7}$$

whenever $D \leq \sigma_X^2$ and $R(D) = 0$ for $D > \sigma_X^2$ since $R(D)$ is everywhere non-negative.

The inverse of $R(D)$ is called the distortion-rate function $D(R)$ and it basically says that if a source sequence is encoded at a rate R the distortion is at least $D(R)$. From (3.7) we see that the distortion-rate function of the memoryless Gaussian process is given by

$$D(R) = \sigma_X^2 2^{-2R}, \tag{3.8}$$

which is shown in Fig. 3.1 for the case of $\sigma_X^2 = 1$.

Remark 3.1.1. From (3.8) and also from Fig. 3.1 it may be seen that each extra bit reduces the distortion by a factor of four — a phenomena often referred to as the "6 dB per bit rule" [60]. In fact, the "6 dB per bit rule" is approximately true not just for the Gaussian source but for arbitrary sources.

The rate-distortion function of a memoryless scalar source and squared-error distortion measure may be upper and lower bounded by use of the entropy-power inequality, that is [8]

$$\frac{1}{2}\log_2\left(\frac{\sigma_X^2}{D}\right) \geq R(D) \geq \frac{1}{2}\log_2\left(\frac{P_X}{D}\right), \tag{3.9}$$

---

[9]Eq. (3.5) is tight for all $D \leq \operatorname{ess\,inf} S_X$, where S_X is the power spectrum of a stationary Gaussian process X [8].
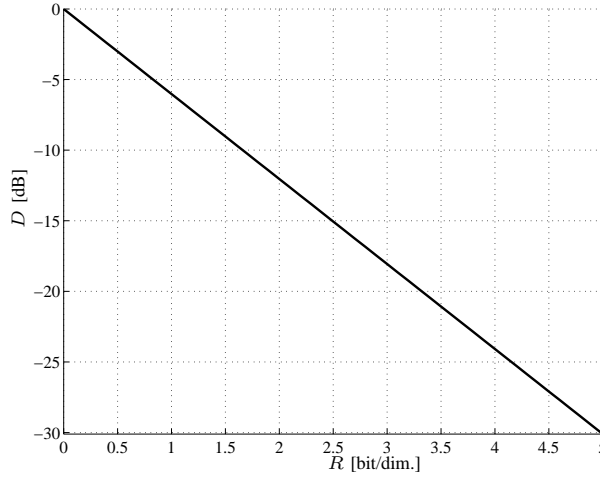
Figure 3.1: $D(R)$ *for the unit-variance memoryless Gaussian source.*

where P_X is the entropy power.[10] Similarly, the distortion-rate function is bounded as

$$P_X 2^{-2R} \leq D(R) \leq \sigma_X^2 2^{-2R}, \tag{3.10}$$

with equalities all the way in both (3.9) and (3.10) if X is Gaussian.

Remark 3.1.2. Inequalities (3.9) and (3.10) show that, of all sources, the Gaussian source is the hardest to compress.

3.2   Quantization Theory

A quantizer Q consists of a set of decision cells $\mathscr{S} = \{S_i : i \in \mathscr{I}\}$ where $\mathscr{I} \subseteq \mathbb{N}$ together with a set of reproduction values $\mathscr{C} = \{c_i : i \in \mathscr{I}\}$ [60]. The operation of quantization is defined as $Q(x) \triangleq c_i$ if $x \in S_i$. We require that $\mathscr{S}$ cover the input space $\mathscr{X}$ which implies that $\bigcup_{i \in \mathscr{I}} S_i \supset \mathscr{X}$ and often we need $\mathscr{S}$ to partition $\mathscr{X}$ so that sets of $\mathscr{S}$ are pairwise disjoint, i.e. $S_i \cap S_j = \emptyset, i \neq j$ so that $\bigcup_{i \in \mathscr{I}} S_i = \mathscr{X}$.

Definition 3.2.1. The decision cells of a nearest neighbor quantizer are called Voronoi cells, Voronoi regions or Dirichlet regions [22]. Given the ith reproduction value c_i the Voronoi cell $V(c_i)$ is defined by

$$V(c_i) \triangleq \{x \in \mathscr{X} : \rho(x, c_i) \leq \rho(x, c_j), \ \forall j \in \mathscr{I}\}, \tag{3.11}$$

---

[10]The entropy power $P_X \triangleq (2\pi e)^{-1} 2^{2h(X)}$ of a source X is defined as the variance of a Gaussian density that has the same differential entropy as X [8].

where ties (if any) can be arbitrarily broken.[11]

It follows that the expected distortion of a quantizer is given by

$$D_Q = \sum_{i \in \mathscr{I}} \int_{x \in S_i} f_X(x) \rho(x, c_i) \, dx. \tag{3.12}$$

Let us for the moment assume that $\mathscr{X} = \mathbb{R}^L$ and $\mathscr{C} = \hat{\mathscr{X}} \subset \mathbb{R}^L$. Then, for the squared error distortion measure, the Voronoi cells of an L-dimensional nearest neighbor quantizer (vector quantizer) are defined as

$$V(\hat{x}_i) \triangleq \{x \in \mathbb{R}^L : \|x - \hat{x}_i\|^2 \le \|x - \hat{x}_j\|^2, \, \forall x_j \in \hat{\mathscr{X}}\}, \quad \hat{x}_i \in \hat{\mathscr{X}}, \tag{3.13}$$

where $\| \cdot \|$ denotes the ℓ_2-norm, i.e. $\|x\|^2 = \sum_{n=1}^L x_n^2$.

Vector quantizers are often classified as either entropy-constrained quantizers or resolution-constrained quantizers or as a mixed class where for example the output of a resolution-constrained quantizer is further entropy coded.[12] When designing an entropy-constrained quantizer one seeks to form the Voronoi regions $V(\hat{x}_i), \hat{x}_i \in \hat{\mathscr{X}}$, and the reproduction alphabet $\hat{\mathscr{X}}$ such that the distortion D_Q is minimized subject to an entropy constraint R on the discrete entropy $H(\hat{X})$. Recall that the discrete entropy of a random variable is given by [24]

$$H(\hat{X}) = -\sum_{i \in \mathscr{I}} P(\hat{x}_i) \log_2(P(\hat{x}_i)), \tag{3.14}$$

where P denotes probability and $P(\hat{x}_i) = P(x \in V(\hat{x}_i))$. On the other hand, in resolution-constrained quantization the distortion is minimized subject to a constraint on the cardinality of the reproduction alphabet. In this case the elements of $\hat{\mathscr{X}}$ are coded with a fixed rate of $R = \log_2(|\hat{\mathscr{X}}|)/L$. For large vector dimensions, i.e. when $L \gg 1$, it is very likely that randomly chosen source vectors belong to a typical set $\mathscr{A}^{(L)}$ in which the elements are approximately uniformly distributed [24]. As a consequence, in this situation there is not much difference between entropy-constrained and resolution-constrained quantization.

There exists several iterative algorithms for designing vector quantizers. One of the earliest such algorithms is the Lloyd algorithm which is used to construct resolution-constrained scalar quantizers [87], see also [88]. The Lloyd algorithm is basically a cyclic minimizer that alternates between two phases:

1. Given a codebook $\mathscr{C} = \hat{\mathscr{X}}$ find the optimal partition of the input space, i.e. form the Voronoi cells $V(\hat{x}_i), \forall \hat{x}_i \in \hat{\mathscr{X}}$.

---

[11]Two neighboring L-dimensional Voronoi cells for continuous-alphabet sources share a common L'-dimensional face where $L' \le L - 1$. For discrete-alphabet sources it is also possible that a point is equally spaced between two or more centroids of the codebook, in which case tie breaking is necessary in order to make sure that the point is not assigned to more than one Voronoi cell.

[12]Entropy-constrained quantizers (resp. resolution-constrained quantizers) are also called variable-rate quantizers (resp. fixed-rate quantizers).

2. Given the partition, form an optimal codebook, i.e. let $\hat{x}_i \in \hat{\mathscr{X}}$ be the centroid of the set $x \in V(\hat{x}_i)$.

If an analytical description of the pdf is unavailable it is possible to estimate the pdf by use of empirical observations [45]. Furthermore, Lloyd's algorithm has been extended to the vector case [45, 81] but has not been explicitly extended to the case of entropy-constrained vector quantization. Towards that end Chou et al. [19] presented an iterative algorithm based on a Lagrangian formulation of the optimization problem. In general these empirically designed quantizers are only locally optimal and unless some structure is enforced on the codebooks, the search complexity easily becomes overwhelming (the computational complexity of an unconstrained quantizer increases exponentially with dimension) [45]. There exists a great deal of different design algorithms and we refer the reader to the text books [22, 45, 57] as well as the in-depth article by Gray and Neuhoff [60] for more information about the theory and practice of vector quantization.

3.3 Lattice Vector Quantization

In this work we will focus on structured vector quantization and more specifically on lattice vector quantization (LVQ) [22, 46, 57]. A family of highly structured quantizers is the tesselating quantizers which includes lattice vector quantizers as a sub family. In a tesselating quantizer all decision cells are translated and possibly rotated and reflected versions of a prototype cell, say V_0. In a lattice vector quantizer all Voronoi cells are translations of V_0 which is then taken to be $V_0 \triangleq V(0)$, i.e. the Voronoi cell of the reproduction point located at the origin (the zero vector) so that $V(\hat{x}_i) = V_0 + \hat{x}_i$.[13] In a high-resolution lattice vector quantizer the reproduction alphabet $\hat{\mathscr{X}}$ is usually given by an L-dimensional lattice $\Lambda \subset \mathbb{R}^L$, see Appendices C and D for more details about lattices.

In order to describe the performance of a lattice vector quantizer it is convenient to make use of high resolution (or high rate) assumptions which for a stationary source can be summarized as follows [45, 57]:

1. The rate or entropy of the codebook is large, which means that the variance of the quantization error is small compared to the variance of the source. Thus, the pdf of the source can be considered constant within a Voronoi cell, i.e. $f_X(x) \approx f_X(\hat{x}_i)$ if $x \in V(\hat{x}_i)$. Hence, the geometric centroids of the Voronoi cells are approximately the midpoints of the cells

2. The quantization noise process tends to be uncorrelated even when the source is correlated

---

[13]Notice that not all tesselating quantizers are lattice quantizers. For example, a tesselating quantizer having triangular shaped decision cells is not a lattice vector quantizer.

3. The quantization error is approximately uncorrelated with the source

Notice that 1) is always true if the source distribution is uniform. Furthermore, all the above assumptions have been justified rigorously in the limit as the variance of the quantization error tends to zero for the case of smooth sources (i.e. continuous-alphabet sources having finite differential entropies) [86, 145, 161]. If subtractive dither is used, as is the case of entropy-constrained dithered (lattice) quantization (ECDQ), the above assumptions are valid at any resolution and furthermore the quantization errors are independent of the source [159, 160, 165]. A nice property of ECDQ is that the additive noise model is accurate at any resolution, so that the quantization operation can be modeled as an additive noise process [160]. The dither signal of an ECDQ is an i.i.d. random[14] process which is uniformly distributed over a Voronoi cell of the quantizer so that for a scalar quantizer the distribution of the quantization errors is uniform. Asymptotically, as the dimension of the ECDQ grows unboundedly, any finite-dimensional marginal of the noise process becomes jointly Gaussian distributed and the noise process becomes Gaussian distributed in the divergence[15] sense [161]. These properties of the noise process are also valid for entropy-constrained LVQ (without dither) under high resolution assumptions [161]. It is interesting to see that at very low resolution, i.e. as the variance of the quantization error tends to the variance of the source, the performance of an entropy-constrained scalar quantizer is asymptotically as good as any vector quantizer [91].

3.3.1   LVQ Rate-Distortion Theory

Let H denote the discrete entropy $H(\hat{\mathscr{X}})$ of the codebook of an entropy-constrained vector quantizer and let the dimension-normalized MSE distortion measure D_L be defined as

$$D_L \triangleq \frac{1}{L} E\|X - \hat{X}\|^2. \tag{3.15}$$

Then by extending previous results of Bennett [7] for high resolution scalar quantization to the vector case it was shown by Zador [156] that if X has a probability density then[16]

$$\lim_{H \to \infty} D_L 2^{2H/L} = a_L 2^{2h(X)/L}, \tag{3.16}$$

where $h(X)$ is the differential entropy of X and a_L is a constant that depends only on L. In the scalar case where $L = 1$ it was shown by Gish and Pierce [47] that $a_1 = 1/12$

---

[14]The dither signal is assumed known at the decoder so it is in fact a pseudo-random process.

[15]The information divergence (also called Kullback-Leibler distance or relative entropy) between two pdfs f_X and g_X is defined as [24]

$$\mathbb{D}(f\|g) = \int_{\mathscr{X}} f_X(x) \log_2(f_X(x)/g_X(x))\, dx.$$

[16]Later on the precise requirements on the source for (3.16) to be valid was formalized by Linder and Zeger [86].

and that the quantizer that achieves this value is the unbounded uniform scalar (lattice) quantizer. For the case of $1 < L < \infty$ the value of a_L is unknown [86].[17] It was conjectured by Gersho in 1979 [44] that if the source distribution is uniform over a bounded convex set in $\mathbb{R}^L$ then the optimal quantizer will have a partition whose regions are all congruent to some polytope. Today, more than 25 years after, this conjecture remains open. But if indeed it is true then, at high resolution, the optimal entropy-constrained quantizer is a tessellating quantizer independent of the source distribution (as long as it is smooth).

The distortion at high resolution of an entropy-constrained lattice vector quantizer is given by [44, 86]

$$D_L \approx G(\Lambda)\nu^{2/L}, \tag{3.17}$$

where ν (the volume of a fundamental region of the lattice) is given by

$$\nu^{2/L} = 2^{2(h(X)-H)/L}. \tag{3.18}$$

Thus, if we assume that Gersho's conjecture is true and furthermore assume that a lattice vector quantizer is optimal then (3.17) implies that $a_L = G(\Lambda)$. By inserting (3.18) in (3.17) the discrete entropy (again at high resolution) is found to be given by

$$H(\hat{\mathscr{X}}) \approx h(X) - \frac{L}{2} \log_2 \left(\frac{D_L}{G(\Lambda)} \right) \text{ [bit]}. \tag{3.19}$$

The Shannon lower bound is the most widely used tool to relate the performance of lattice quantizers to the rate-distortion function of a source. For example, at high resolution, the Shannon lower bound is tight for all smooth sources, thus

$$R(D) \approx \bar{h}(X) - \frac{1}{2} \log_2(2\pi eD) \text{ [bit/dim.]}, \tag{3.20}$$

so that the asymptotic rate-redundancy R_{red} of a lattice vector quantizer over the rate-distortion function of a smooth source under the MSE distortion measure is[18]

$$R_{\text{red}} = \frac{1}{2} \log_2(2\pi eG(\Lambda)) \text{ [bit/dim.]} \tag{3.21}$$

From (3.17) it may be noticed that the distortion of a lattice vector quantizer is source independent and in fact, for fixed ν, the distortion only depends upon $G(\Lambda)$. Furthermore, $G(\Lambda)$ is scale and rotation invariant and depends only upon the shape of the fundamental region V_0 of the lattice Λ [22]. In general the more sphere-like shape of V_0 the smaller $G(\Lambda)$ [22]. It follows that $G(\Lambda)$ is lower bounded by $G(S_L)$ the dimensionless normalized second moment of an L-sphere where [22]

$$G(S_L) = \frac{1}{(L+2)\pi}\Gamma\left(\frac{L}{2}+1\right)^{2/L}, \tag{3.22}$$

---

[17]For the case of resolution-constrained quantization both a_1 and a_2 are known [58].

[18]R_{red} is in fact the divergence of the quantization noise from Gaussianity in high resolution lattice vector quantization.

and where $\Gamma(\cdot)$ is the Gamma function. For $L \to \infty$ we have $G(S_\infty) = 1/2\pi e$. The L-fold Cartesian product of the integers form an L-dimensional lattice $Z^L = \mathbb{Z}^L$ which has a hypercubic fundamental region. It can easily be computed that $G(Z^L) = 1/12$ which is in fact the largest dimensionless normalized second moment over all admissible fundamental regions [22]. Thus,

$$1/12 \geq G(\Lambda) \geq G(S_L) \geq \frac{1}{2\pi e}, \qquad (3.23)$$

where the first two inequalities become equalities for $L = 1$ since in one dimension the only possible lattice is Z^1, the scalar uniform lattice, and $G(Z^1) = G(S_1) = 1/12$. For $1 < L < \infty$ L-spheres do not pack the Euclidean space and are therefore not admissible fundamental regions [22]. However, for $L \to \infty$ and with a proper choice of lattice it is known that $G(\Lambda) \to G(S_\infty)$ [161]. Table 3.1 shows $G(\Lambda)$ for the best known L-dimensional lattices with respect to quantization.

Lattice name	Dimension	Notation	$G(\Lambda)$	$G(S_L)$
Scalar	1	Z^1	0.0833	0.0833
Hexagonal	2	A_2	0.0802	0.0796
BCC	3	$\tilde{A}_3$	0.0787	0.0770
Schläfli	4	D_4	0.0766	0.0750
—	5	$\tilde{D}_5$	0.0756	0.0735
—	6	E_6	0.0743	0.0723
—	7	$\tilde{E}_7$	0.0731	0.0713
Gosset	8	E_8	0.0717	0.0705
Coxeter-Todd	12	K_{12}	0.0701	0.0681
Barnes-Walls	16	BW_{16}	0.0683	0.0666
Leech	24	Λ_{24}	0.0658	0.0647
Poltyrev[19]	∞	Λ_∞	0.0585	0.0585

Table 3.1: *The dimensionless normalized second moments of the lattice Λ and the L-sphere are denoted $G(\Lambda)$ and $G(S_L)$, respectively. All figures are obtained from [22].*

While all the lattices in Table 3.1 are the best known lattices for quantization in their dimensions it is in fact only $Z^1, A_2, \tilde{A}_3$ and Λ_∞ which are known to be optimal among all lattices [22] and furthermore, only Z^1 and Λ_∞ are known to be optimal among all entropy-constrained vector quantizers.

It is interesting to compare the optimal performance of an entropy-constrained scalar quantizer Z^1 to that of an optimal entropy-constrained infinite-dimensional lattice vector quantizer Λ_∞. From Table 3.1 it can be seen that the rate loss R_{Loss}

---

[19]The fact that there actually exist lattices in infinite dimensions which are capable of achieving the dimensionless normalized second moment of a sphere was proven in [161], a proof which was contributed by G. Poltyrev.

(at high resolution or at any resolution for the uniform density) when using Z^1 instead of Λ_∞ is given by

$$R_{\text{Loss}} = \frac{1}{2} \log_2 \left(\frac{G(Z^1)}{G(\Lambda_\infty)} \right) = 0.2546 \text{ bit/dim.} \tag{3.24}$$

or equivalently the increase in distortion (also known as the space-filling loss or space-filling gain when reversed) for using Z^1 instead of Λ_∞ is given by

$$D_{\text{Loss}} = 10 \log_{10} \left(\frac{G(Z^1)}{G(\Lambda_\infty)} \right) = 1.5329 \text{ dB.} \tag{3.25}$$

Fig. 3.2 illustrates the space-filling loss for the lattices of Table 3.1. For comparison we also show the space-filling loss of L-dimensional "quantizers" having spherical Voronoi cells which is given by $D_{\text{Loss}} = 10 \log_{10}(G(S_L)/G(\Lambda_\infty))$.

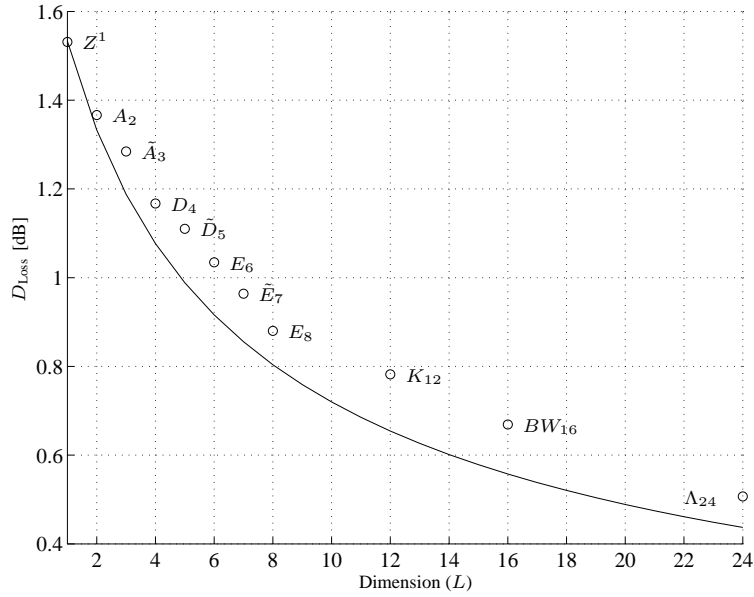**Figure 3.2:** *Space-filling loss for the lattices of Table 3.1. The solid line describes the space-filling loss of L-spheres.*

3.4   Entropy Coding

In the previous section we saw that for stationary sources one achieves space-filling gains if vector quantizers are used instead of scalar quantizers. The space-filling gain is independent of the statistical properties of the source. In other words, whether

the source is i.i.d. or has memory the space-filling gain remains the same. However, for this to be true, we implicitly assume that any statistical redundancy (correlation) which might be present in the quantized signal is removed by a (lossless) entropy coder. Recall that the discrete entropy $H(\hat{\mathscr{X}})$ of the quantizer is given by (3.19) and that $P(\hat{x}_i)$ denotes the probability of the symbol $\hat{x}_i$ where $\hat{x}_i \in \hat{\mathscr{X}}$. Assume now that a codeword (of the entropy coder) of length l_i is assigned to the symbol $\hat{x}_i$. Then the average codeword length $\bar{s}$ is given by

$$\bar{s} = \sum_{i \in \mathscr{I}} P(\hat{x}_i) l_i. \tag{3.26}$$

The idea of an entropy coder is to assign short codewords to very probable symbols and long codewords to less probable symbols in order to drive $\bar{s}$ towards its minimum. Since we require the (entropy) code to be lossless it means that the code should be a uniquely decodable code. Due to a result of Shannon we can lower bound $\bar{s}$ by the following theorem.

Theorem 3.4.1. [121] The average codeword length $\bar{s}$ of a uniquely decodable binary code satisfies

$$\bar{s} \geq H(\hat{\mathscr{X}}). \tag{3.27}$$

In the same paper Shannon also gave an upper bound on $\bar{s}$, i.e. $\bar{s} < H(\hat{\mathscr{X}}) + 1$ and he furthermore showed that if a sequence of, say s, symbols is jointly coded then the average number of bits per symbol satisfy

$$H(\hat{\mathscr{X}}) \leq \bar{s} < H(\hat{\mathscr{X}}) + \frac{1}{s}, \tag{3.28}$$

which shows that the entropy $H(\hat{\mathscr{X}})$ can be approximated arbitrarily closely by encoding sufficiently long sequences [121].

In (3.26) we have $|\mathscr{I}| = |\hat{\mathscr{X}}|$ and we thereby implicitly restrict $\hat{\mathscr{X}}$ to be a discrete alphabet be it finite or countably finite, but we do in fact not always require that $|\hat{\mathscr{X}}| < \infty$. For example it is known that an entropy-constrained vector quantizer (ECVQ) may be recast in a Lagrangian sense [19, 59, 63] and that a Lagrangian-optimal[20] ECVQ always exists under general conditions on the source and distortion measure [63]. Furthermore, György et al. [64] showed that, for the squared error distortion measure, a Lagrangian-optimal ECVQ has only a finite number of codewords if the tail of the source distribution is lighter than the tail of the Gaussian distribution (of equal variance), while if the tail is heavier than that of the Gaussian distribution the Lagrangian-optimal ECVQ has an infinite number of codewords [64]. If the source distribution is Gaussian then the finiteness of the codebook depends upon the rate of

---

[20]The operational distortion-rate function is the infimum of the set of distortion-rate functions that can be obtained by use of any vector quantizer which satisfies the given entropy constraints. A Lagrangian-optimal ECVQ achieves points on the lower convex hull of the operational distortion-rate function and in general any point can be achieved by use of time-sharing [63].

the codebook. In addition they also showed that for source distributions with bounded support the Lagrangian-optimal ECVQ has a finite number of codewords.[21] [22]

In this work we will not delve into the theory of entropy coding but merely assume that there exist entropy coders which are complex enough so that (at least in theory) the discrete entropies of the quantizers can be reached. For more information about entropy coding we refer the reader to Chapter 9 of the text book by Gersho and Gray [45] as well as the references cited in this section.

---

[21]These quantizers are not unique. For example it was shown by Gray et al. [58] that for the uniform density on the unit cube there exists Lagrangian-optimal ECVQs with codebooks of infinite cardinality.

[22]In Chapter 7 we will show that, in certain important cases, the cardinality of lattice codebooks is finite.

Chapter 4

Multiple-Description Rate-Distortion Theory

The MD problem is concerned with lossy encoding of information for transmission over an unreliable K-channel communication system. The channels may break down resulting in erasures and a potential loss of information at the receiving side. Which of the $2^K - 1$ non-trivial subsets of the K channels that are working is assumed known at the receiving side but not at the encoder. The problem is then to design an MD system which, for given channel rates or a given sum rate, minimizes the distortions due to reconstruction of the source using information from any subsets of the channels. The compound channel (or composite channel) containing the K subchannels is often described as a packet-switched network where individual packets are either received errorless or not at all. In such situations the entire system is identified as a multiple-description system having K descriptions.

The classical case involves two descriptions as shown in Fig. 4.1. The total rate R_T, also known as the sum rate, is split between the two descriptions, i.e. $R_T = R_0 + R_1$, and the distortion observed at the receiver depends on which descriptions arrive. If both descriptions are received, the distortion (D_c) is lower than if only a single description is received (D_0 or D_1). The general K-channel MD problem involves K descriptions and is depicted in Fig. 4.2.

4.1   Information Theoretic MD Bounds

From an information theoretic perspective the MD problem is partly about describing the achievable MD rate-distortion region and partly about designing good practical codes whose performance is (in some sense) near optimum. Before presenting the known information theoretic bounds we need the following definitions.
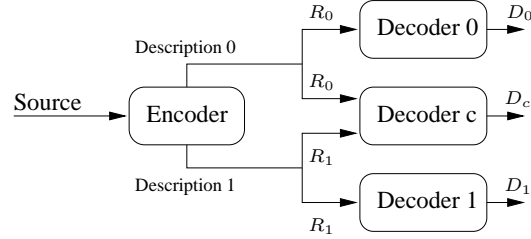
Figure 4.1: *The traditional two-channel MD system.*
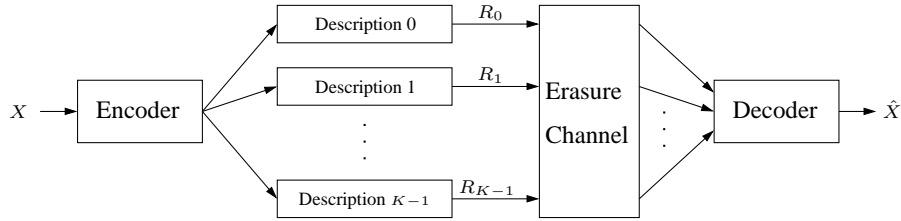
Figure 4.2: *General K-channel MD system. Descriptions are encoded at an entropy of R_i, $i = 0, \ldots, K - 1$. The erasure channel either transmits the ith description errorlessly or not at all.*

Definition 4.1.1. The *MD rate-distortion region* given a source and a fidelity criterion is the closure of the set of simultaneously achievable rates and distortions.

Example 4.1.1. In the two-channel case the MD rate-distortion region is the closure of the set of achievable quintuples $(R_0, R_1, D_c, D_0, D_1)$.

Definition 4.1.2. An *inner bound* to the MD problem is a set of achievable rate-distortion points for a specific source and fidelity criterion.

Definition 4.1.3. An *outer bound* to the MD problem is a set of rate-distortion points, for a specific source and fidelity criterion, for which it is known that no points outside this bound can be reached.

Definition 4.1.4. If the inner and outer bounds coincide they are called *tight*.

Example 4.1.2. An example of inner and outer bounds for the set of achievable rate pairs (R_0, R_1) given some fixed distortion triple (D_c, D_0, D_1) is shown in Fig. 4.3. In this example there exists a region where the inner and outer bounds meet (coincide) and the bounds are said to be tight within that region.

Remark 4.1.1. The SD rate-distortion bounds form simple outer bounds to the MD problem. For example $R_i \geq R(D_i), i = 0, \ldots, K - 1$ and $\sum_{i=0}^{K-1} R_i \geq R(D_c)$ where $R(\cdot)$ describes the SD rate-distortion function.
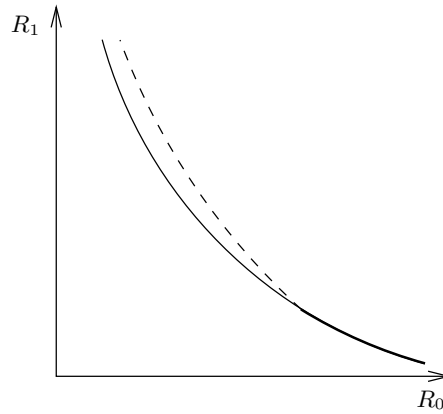
Figure 4.3: *The solid thin curve show an example of an outer bound and the dashed curve illustrates an inner bound. In the region where the bounds coincide (thick line), the bounds are tight.*

Definition 4.1.5. The term *no excess marginal rates* refers to the situation where, for fixed side distortions D_i, the side description rates of an MD system meet the SD rate-distortion bounds, i.e. $R_i = R(D_i)$. At the other extreme we have the situation of *no excess sum rate* where for a given sum rate the the central distortion D_c achieves its minimum so that $\sum_{i=0}^{K-1} R_i = R(D_c)$.

An interesting subset of the MD rate-distortion region is the symmetric MD rate-distortion region.[23] The term symmetric relates to the situation where all channel rates (description rates) are equal and the distortion depends only upon the number of working channels (received descriptions) and as such not on which of the channels are working. This is in contrast to the asymmetric case where the description rates as well as side distortions are allowed to be unequal.

Another important subset of the MD rate-distortion region is the high resolution region which refers to an MD rate-distortion region that becomes achievable asymptotically as the description rates of the system become large relative to the variance of the source (or equivalently, asymptotically as the distortions tend to zero).

4.1.1   Two-Channel Rate-Distortion Results

El Gamal and Cover [42] obtained inner bounds to the two-channel MD problem (known as the EGC region) and Ozarow [107] showed that these inner bounds are

---

[23]The lower bound of this symmetric region is the symmetric MD rate-distortion function of the source. With a slight abuse of notation we sometimes call the MD rate-distortion function a region.

tight for the memoryless Gaussian source under the squared-error fidelity criterion.[24]
Ahlswede [2] and Zhang and Berger [163] showed that the EGC region is also tight for
general sources and distortion measures in the no excess sum rate case. However, in
the excess sum rate case it was shown by Zhang and Berger [163] that the EGC region
is not always tight for the binary memoryless source under the Hamming distortion
measure. Outer bounds for the binary symmetric source and Hamming distortion have
also been obtained by Wolf, Wyner and Ziv [153], Witsenhausen [152] and Zhang and
Berger [164]. Zamir [157, 158] obtained inner and outer bounds for smooth stationary
sources and the squared-error fidelity criterion and further showed that the bounds
become tight at high resolution. High resolution bounds for smooth sources and
locally quadratic distortion measures have been obtained by Linder et al. [84]. Outer
bounds for arbitrary memoryless sources and squared-error distortion measure were
obtained by Feng and Effros [35] and Lastras-Montaño and Castelli [79].

To summarize, the achievable MD rate-distortion region is only completely known
for the case of two channels, squared-error fidelity criterion and the memoryless
Gaussian source [42, 107]. This region consists of the convex hull of the set of
achievable quintuples $(R_0, R_1, D_0, D_1, D_c)$ where the rates satisfy [18, 107]

$$R_0 \geq R(D_0) = \frac{1}{2} \log_2 \left(\frac{\sigma_X^2}{D_0} \right) \tag{4.1}$$

$$R_1 \geq R(D_1) = \frac{1}{2} \log_2 \left(\frac{\sigma_X^2}{D_1} \right) \tag{4.2}$$

$$R_0 + R_1 \geq R(D_c) + \frac{1}{2} \log_2 \delta(D_0, D_1, D_c) \tag{4.3}$$

$$= \frac{1}{2} \log_2 \left(\frac{\sigma_X^2}{D_c} \right) + \frac{1}{2} \log_2 \delta(D_0, D_1, D_c), \tag{4.4}$$

where σ_X^2 denotes the source variance and $\delta(\cdot)$ is given by [18]

$$\delta(D_0, D_1, D_c) = \begin{cases} 1, & D_c < D_0 + D_1 - \sigma_X^2 \\ \frac{\sigma_X^2 D_c}{D_0 D_1}, & D_c > \left(\frac{1}{D_0} + \frac{1}{D_1} - \frac{1}{\sigma_X^2} \right)^{-1} \\ \frac{(\sigma_X^2 - D_c)^2}{(\sigma_X^2 - D_c)^2 - \left(\sqrt{(\sigma_X^2 - D_0)(\sigma_X^2 - D_1)} - \sqrt{(D_0 - D_c)(D_1 - D_c)} \right)^2}, & \text{o.w.,} \end{cases} \tag{4.5}$$

and the distortions satisfy [107]

$$D_0 \geq \sigma_X^2 2^{-2R_0} \tag{4.6}$$

$$D_1 \geq \sigma_X^2 2^{-2R_1} \tag{4.7}$$

$$D_c \geq \frac{\sigma_X^2 2^{-2(R_0 + R_1)}}{1 - \left(\sqrt{\Pi} - \sqrt{\triangle} \right)^2}, \tag{4.8}$$

---

[24]It is customary in the literature to refer to the case of a memoryless Gaussian source and squared-error
fidelity criterion as the quadratic Gaussian case.

where $\Pi = (1 - D_0/\sigma_X^2)(1 - D_1/\sigma_X^2)$ and $\triangle = (D_0 D_1/\sigma_X^4) - 2^{-2(R_0+R_1)}$. In general it is only possible to simultaneously achieve equality in two of the three rate inequalities given by (4.1) – (4.3). However, in the high side distortion case, i.e. when $\delta(\cdot) = 1$, it is in fact possible to have equality in all three [42].

Fig. 4.4 shows the central distortion (4.8) as a function of the side distortion (4.6) in a symmetric setup where $D_0 = D_1$ and $R_0 = R_1 = 1$ bit/dim. for the unit-variance Gaussian source. Notice that at one extreme we have optimal side distortion, i.e. $D_0 = D(R_0) = -6.02$ dB, which is on the single-channel rate-distortion function of a unit-variance Gaussian source at 1 bit/dim. At the other extreme we have optimal central distortion, i.e. $D_c = D(2R_0) = -12.04$ dB, which is on the single-channel rate-distortion function of the Gaussian source at 2 bit/dim. Thus, in this example, the single-channel rate-distortion bounds become effective for the two-channel MD problem only at two extreme points.
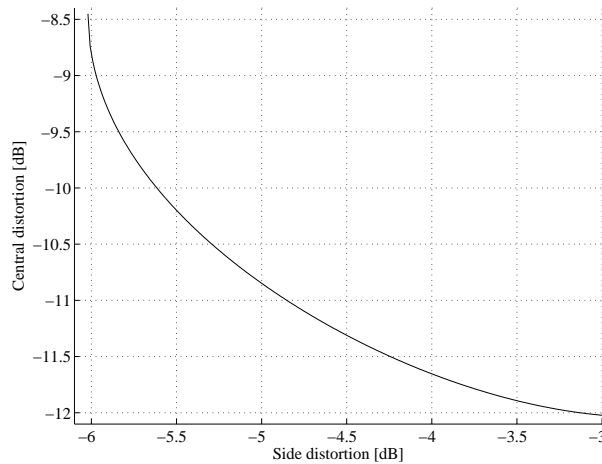
Figure 4.4: *Central distortion (D_c) as a function of side distortion $(D_0 = D_1)$ in a symmetric setup where $R_0 = R_1 = 1$ bit/dim. for the unit-variance Gaussian source and MSE.*

The rate region comprising the set of achievable rate pairs (R_0, R_1) which satisfy (4.1), (4.2) and (4.3) is illustrated in Fig. 4.5. In this example we assume a unit-variance Gaussian source and choose distortions $D_0 = \frac{1}{2}, D_1 = \frac{1}{4}$ and $D_c = \frac{1}{13.9}$. Notice that R_0 and R_1 are lower bounded by 0.5 and 1 bit/dim., respectively, and the sum rate is lower bounded by $R_0 + R_1 \geq 2$ bit/dim.

Ozarow's Double-Branch Test Channel

Ozarow [107] showed that the double-branch test channel depicted in Fig. 4.6 achieves the complete two-channel MD rate-distortion region in the quadratic Gaussian case. This channel has two additive noise branches $Y_0 = X + N_0$ and $Y_1 = X + N_1$,
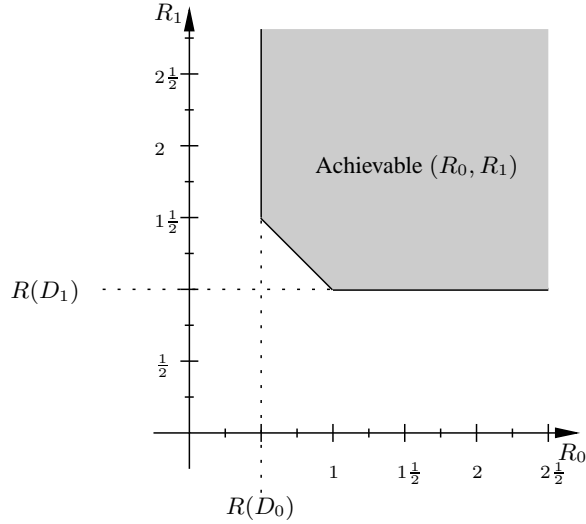
Figure 4.5: *Achievable rate pairs (R_0, R_1) for the distortion triplet $(D_c, D_0, D_1) = (\frac{1}{13.9}, \frac{1}{2}, \frac{1}{4})$ in the quadratic Gaussian case.*

where all variables are Gaussian distributed and the noise pair (N_0, N_1) is independent of X but jointly Gaussian and *negatively* correlated (except from the case of no-excess marginal rates, in which case the noises are independent). In the symmetric case and when the correlation between N_0 and N_1 is high, i.e. near -1, the central distortion is close to optimum but the side distortions are then generally poor. On the other hand, when the side distortions are optimal, the noise pair becomes independent and the central distortion is not much better than either of the side distortions. The post filters (Wiener filters) a_i and $b_i, i = 0, 1$ describe the scalar weights which are required for minimum MSE (MMSE) estimation of X based on either Y_0, Y_1 or both. At high resolution this test channel is particularly simple since the filters degenerate. Specifically, in the symmetric case, where the noise variances are equal, the side reconstructions $\hat{X}_0$ and $\hat{X}_1$ become $\hat{X}_0 = Y_0$ and $\hat{X}_1 = Y_1$, while the central reconstruction $\hat{X}_c$ becomes a simple average, i.e. $\hat{X}_c = (\hat{X}_0 + \hat{X}_1)/2$.

Rate-Redundancy Region

The redundancy rate-distortion function (RRD) introduced in [97] for the symmetric case and further developed in [52, 149] describes how fast the side distortion decays with increasing rate redundancy R_{red}^* when the central distortion D_c is fixed.[25] Let $R_c = R(D_c)$ be the rate needed for an SD system to achieve the (central) distortion

---

[25]The rate redundancy R_{Red}^* is sometimes referred to as the excess sum rate.
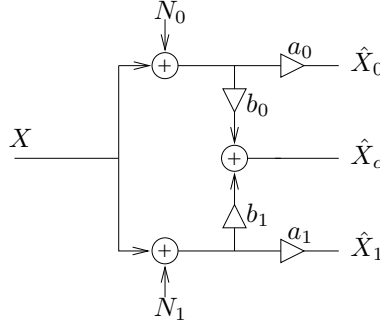
Figure 4.6: *The MD optimum test channel of Ozarow [107]. At high resolution the filters degenerate so in the symmetric case we have $a_i = 1$ and $b_i = 1/2, i = 1, 2$ so that $\hat{X}_0 = Y_0, \hat{X}_1 = Y_1$ and $\hat{X}_c = \frac{1}{2}(\hat{X}_0 + \hat{X}_1)$.*

D_c. Then consider a symmetric setup where $D_0 = D_1$ and $R_0 = R_1$ and define $R^*_{\text{red}} \triangleq 2R_0 - R_c$, i.e. R^*_{red} describes the additional rate needed for an MD system over that of an SD system to achieve the central distortion D_c. In order to reduce the side distortion D_0 while keeping D_c fixed it is necessary to introduce redundancy such that $2R_0 \geq R_c$. For a given R_c (or equivalently a given D_c) and a given R^*_{red} the side distortion for the unit-variance Gaussian source is lower bounded by [52]

$$D_0 \geq \begin{cases} \frac{1}{2}(1 + 2^{-2R_c} - (1 - 2^{-2R_c})\sqrt{1 - 2^{-2R^*_{\text{red}}}}), & R^*_{\text{red}} \leq \bar{R}^*_{\text{red}} \\ 2^{-(R_c + R^*_{\text{red}})}, & R^*_{\text{red}} > \bar{R}^*_{\text{red}} \end{cases} \qquad (4.9)$$

where $\bar{R}^*_{\text{red}} = R_c - 1 + \log_2(1 + 2^{-2R_c})$. If $R^*_{\text{red}} = 0$ we have optimum central distortion, i.e. no excess sum rate, but the side distortions will then generally be high. As we increase the rate while keeping the central distortion fixed we are able to lower the side distortions. Fig. 4.7 shows the side distortion $D_0 = D_1$ as a function of the rate redundancy R^*_{red} when the central distortion is fixed at $D_c = 2^{-2R_c}, R_c \in \{0.5, 1, 1.5, 2, 2.5\}$. It is interesting to observe that when D_c is optimal, i.e. when $R^*_{\text{red}} = 0$, then the gap from D_1 to $D(R_0)$ increases with increasing R_c. To see this, notice that when $R^*_{\text{red}} = 0$ it follows from the first bound of (4.9) that $D_0 \geq (1 + 2^{-2R_c})/2$. The second bound of (4.9) is actually the SD rate-distortion bound, i.e. $2^{-(R_c + R^*_{\text{red}})} = 2^{-2R_0}$, and the gap between these two bounds is shown in Table 4.1.

Two-Channel High-Resolution Results

Based on the results for the Gaussian source of Ozarow [107] it was shown by Vaishampayan et al. [136, 137] that at high resolution and for the symmetric case,
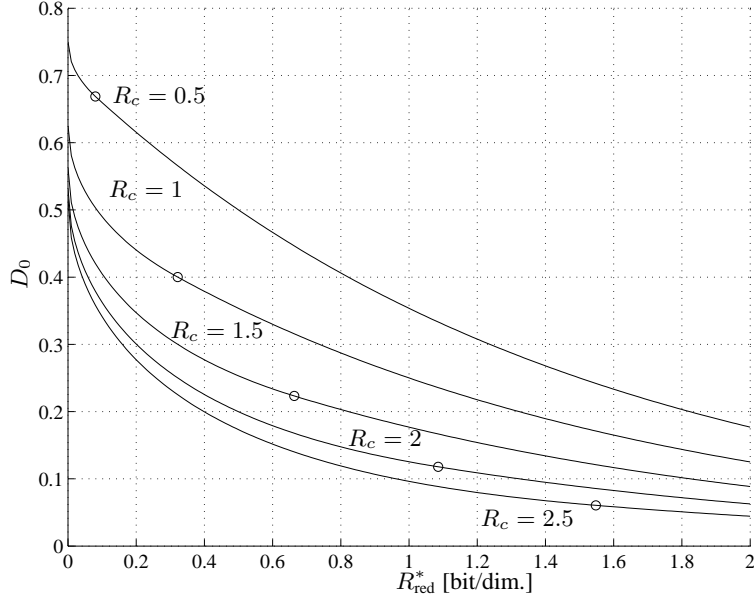
Figure 4.7: *Side distortions $D_0 = D_1$ as a function of rate redundancy R_{red}^*. For each curve the central distortion is held fixed at $D_c = 2^{-2R_c}$. The circles mark the points beyond which the second bound of (4.9) becomes effective. This example is from [52].*

if the side distortions satisfy

$$D_0 = \sigma_X^2 b 2^{-2R_0(1-a)}, \tag{4.10}$$

for $0 < a < 1$ and $b \geq 1$ then the central distortion is lower bounded by

$$D_c \geq \frac{\sigma_X^2}{4b} 2^{-2R_0(1+a)}, \tag{4.11}$$

which leads to a simple bound on the distortion product $D_c D_0$, that is

$$D_c D_0 \geq \frac{\sigma_X^4}{4} 2^{-4R_0}. \tag{4.12}$$

It was further shown that an optimal two-channel scheme achieves equality in (4.11) and therefore also in (4.12) at high resolution and when $D_c \ll D_0$. Since (4.12) is independent of a it serves as a simple means of relating the performance of MD schemes to the information theoretic rate-distortion bounds of [107]. It is therefore a standard figure of merit when assessing the performance of two-channel MD schemes at high resolution. For small ratios of D_0/D_c it is not possible to achieve equality in (4.12). However, at high resolution the more general but less used distortion product

R_c	R_0	$(1 + 2^{-2R_c})/2$	$D(R_0)$	Gap
0.5	0.25	0.75	0.707	0.043
1	0.5	0.625	0.5	0.125
1.5	0.75	0.563	0.354	0.209
2	1	0.531	0.25	0.281
2.5	1.25	0.516	0.177	0.339

Table 4.1: *The gap between the two bounds of (4.9) when $R_{red}^* = 0$. In this case $R_0 = R_c/2$.*

is also achievable [137]

$$D_c D_0 = \frac{\sigma_X^4}{4} \frac{1}{1 - D_c/D_0} 2^{-4R_0}, \tag{4.13}$$

which meets the lower bound of (4.12) if $D_c/D_0 \rightarrow 0$. If D_0 is optimal, i.e. if $D_0 = D(R_0)$, then it follows from [107] that $D_c \geq D_0/2$. Using the ratio $D_c/D_0 = 1/2$ in (4.13) yields $D_c D_0 = \frac{\sigma_X^4}{2} 2^{-4R_0}$ which is twice as large as the lower bound of (4.12).

Fig. 4.8 compares the high resolution approximations given by (4.10) and (4.11) (solid lines) to the true bounds given by (4.6) and (4.8) (dashed lines) for the case of a unit-variance memoryless Gaussian source and $b = 1$. Notice that the asymptotic expressions meet the true bounds within a growing interval as the rate increases. Since a is positively bounded away from zero and always less than one, the interval where they meet will never include the entire high resolution region. For example only large distortion ratios D_0/D_c are achievable.[26]

The asymmetric situation is often neglected but it is in fact fairly simple to come up with a distortion product in the spirit of (4.12). Let us first rewrite the central and side distortions in Ozarow's solution by use of the entropy power P_X as was done by Zamir [157, 158], that is

$$D_i \geq P_X 2^{-2R_i}, \quad i = 0, 1, \tag{4.14}$$

and

$$D_c \geq \frac{P_X 2^{-2(R_0 + R_1)}}{1 - (|\sqrt{\Pi} - \sqrt{\triangle}|^+)^2}, \tag{4.15}$$

where

$$\Pi = (1 - D_0/P_X)(1 - D_1/P_X) \tag{4.16}$$

and

$$\triangle = D_0 D_1/P_X^2 - 2^{-2(R_0 + R_1)}, \tag{4.17}$$

---

[26]In Section 7.1 Remark 7.1.1 we explain in more detail why the asymptotic curves never meet the true curves at the extreme points.
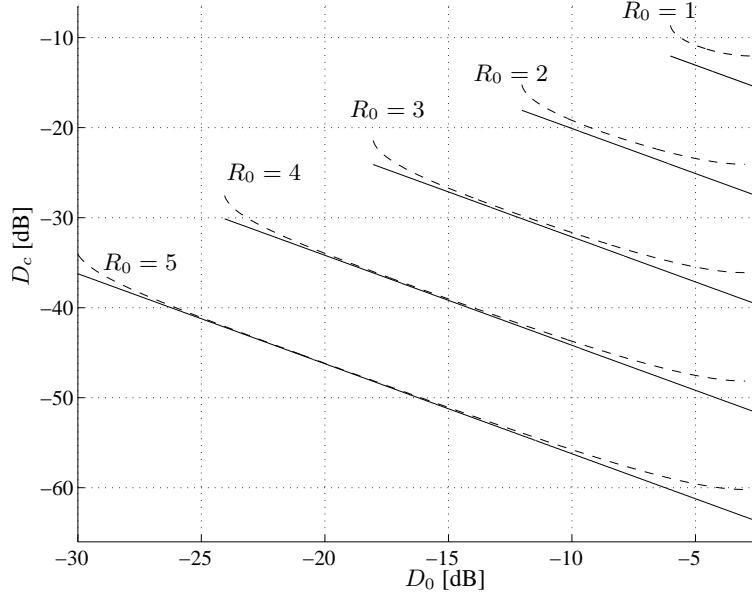
Figure 4.8: *The central distortion D_c as a function of side distortions $D_0 = D_1$ at different rates $R_0 = R_1 \in \{1, \ldots, 5\}$. The dashed lines illustrate the true distortion bounds given by (4.6) and (4.8) and the solid lines represent the high resolution asymptotic bounds given by (4.10) and (4.11).*

and where[27]

$$|x|^+ \triangleq \begin{cases} x, & \text{if } x > 0 \\ 0, & \text{otherwise.} \end{cases} \tag{4.18}$$

An advantage of Zamir's solution is that it acts as an outer bound to the MD problem for general sources under the squared-error distortion measure. For the memoryless Gaussian source it becomes tight at any resolution, i.e. it becomes identical to Ozarow's solution, and for arbitrary smooth stationary sources it becomes asymptotically tight at high resolution.

Lemma 4.1.1. If $2^{-2(R_0 + R_1)} \ll D_0 D_1 \ll D_i, i = 0, 1$ then

$$D_c(D_0 + D_1 + 2\sqrt{D_0 D_1}) \geq \left(\frac{2^{2h(X)}}{2\pi e}\right)^2 2^{-2(R_0 + R_1)}. \tag{4.19}$$

Proof. Let us expand the denominator in (4.15) as[28]

$$1 - \left(\sqrt{\Pi} - \sqrt{\triangle}\right)^2 = 1 - \left(\sqrt{(1 - D_0/P_X)(1 - D_1/P_X)}\right.$$

---

[27] $| \cdot |^+$ becomes effective only in the high side distortion case, i.e. when $D_0 + D_1 > \sigma_X^2(1 + 2^{-2(R_0 + R_1)})$ [158].

[28] Here we neglect the high side distortion case.

$$
\left. - \sqrt{D_0 D_1/P_X^2 - 2^{-2(R_0+R_1)}} \right)^2
$$

$$
= 1 - \Big((1 - D_0/P_X)(1 - D_1/P_X) + D_0 D_1/P_X^2 - 2^{-2(R_0+R_1)}
$$

$$
- 2\sqrt{(1 - D_0/P_X)(1 - D_1/P_X)(D_0 D_1/P_X^2 - 2^{-2(R_0+R_1)})} \Big)
$$

$$
= D_0/P_X + D_1/P_X - 2 D_0 D_1/P_X^2 + 2^{-2(R_0+R_1)}
$$

$$
+ 2 \Big(D_0 D_1/P_X^2 - D_0^2 D_1/P_X^3 - D_0 D_1^2/P_X^3 + (D_0 D_1/P_X^2)^2
$$

$$
- (1 - D_0/P_X - D_1/P_X + D_0 D_1/P_X^2) 2^{-2(R_0+R_1)} \Big)^{\frac{1}{2}}
$$

$$
\approx \frac{D_0 + D_1 + 2\sqrt{D_0 D_1}}{P_X}, \tag{4.20}
$$

where the approximation follows from the assumption of high resolution, i.e. $R_i \to \infty, i = 0, 1$, so that we have $2^{-2(R_0+R_1)} \ll D_0 D_1 \ll D_i$. The inequality $2^{-2(R_0+R_1)} \ll D_0 D_1$ is valid when we have excess marginal rates, i.e. when at least one of the side decoders is not operating on its lower bound. As such we assume that D_i grows as $\mathscr{O}(2^{-2\tilde{R}_i})$ where $\tilde{R}_i \leq R_i$ and $\tilde{R}_0 + \tilde{R}_1 < R_0 + R_1$ and it follows that the entire expression is dominated by terms that grow as $\mathscr{O}(2^{-2\tilde{R}_i})$ or $\mathscr{O}(2^{-(\tilde{R}_0+\tilde{R}_1)})$. Inserting (4.20) into (4.15) leads to

$$
D_c \geq \frac{P_X 2^{-2(R_0+R_1)}}{1 - \left(\sqrt{\Pi} - \sqrt{\triangle} \right)^2}
$$

$$
\approx \frac{P_X^2}{D_0 + D_1 + 2\sqrt{D_0 D_1}} 2^{-2(R_0+R_1)}, \tag{4.21}
$$

which completes the proof since $P_X = 2^{2h(X)}/(2\pi e)$. $\qquad\square$

Remark 4.1.2. It follows that an optimal asymmetric (or symmetric) MD system achieves equality in (4.19) at high resolution for arbitrary (smooth) sources. Notice that the bound (4.19) holds for arbitrary bit distributions of R_0 and R_1 as long as their sum remains constant and the inequalities (4.14) and (4.15) are satisfied (or more correctly that the corresponding lower bounds on the individual side rates and their sum rate are satisfied).

4.1.2 K-Channel Rate-Distortion Results

Recently, an achievable K-channel MD rate-distortion region was obtained by Venkataramani, Kramer and Goyal [141, 142] for arbitrary memoryless sources and single-letter distortion measures. This region generally takes a complicated form but in the quadratic Gaussian case it becomes simpler. The region presented in [142] describes an asymmetric MD rate-distortion region and includes as a special case the symmetric MD rate-distortion region. The construction of this region relies upon forming layers

of conditional random codebooks. It was, however, observed by Pradhan, Puri and Ramchandran in a series of papers [109–114] that by exploiting recent results on distributed source coding it is possible to replace the conditional codebooks with universal codebooks whereby the codebook rate can be reduced through random binning. While Pradhan et al. limited their interests to the symmetric case it can be shown that their results carry over to the asymmetric case as well. This has recently been done by Wang and Viswanath [146] who further extended the results to the case of vector Gaussian sources and covariance distortion measure constraints.

The largest known achievable rate-distortion region for the K-channel MD problem is that of Pradhan et al. [111, 114].[29] Common for all the achievable rate-distortion regions is that they represent inner bounds and it is currently not known whether they can be further improved. However, for the quadratic Gaussian case it was conjectured in [114] that their bound is in fact tight. That conjecture remains open.

The key ideas behind the achievable region obtained by Pradhan et al. are well explained in [111, 114] and we will here repeat some of their insights and results before presenting the largest known K-channel achievable rate-distortion region.

Consider a packet-erasure channel with parameters K and k, i.e. at least k out of K descriptions are received. For the moment being, we assume $k = 1$. Generate K independent random codebooks, say $\mathscr{C}_0, \ldots, \mathscr{C}_{K-1}$ each of rate R. The source is now separately and independently quantized using each of the codebooks. The index of the nearest codeword in the ith codebook is transmitted on the ith channel. A code constructed in this way was dubbed a source-channel erasure code in [111] which we, for notational convenience, abridge to (K, k) SCEC. Notice that since each of the individual codebooks are optimal for the source then if only a single index is received the source is reconstructed with a distortion that is on the distortion-rate function $D(R)$ of the source. However, if more than one index is received, the quality of the reconstructed signal can be strictly improved due to multiple versions of the quantized source. The above scheme is generalized to (K, k) SCEC for $k > 1$ by making use of random binning. This is possible since the quantized variables are assumed (symmetrically) correlated so that general results of distributed source coding are applicable. Specifically, due to celebrated results of Slepian and Wolf [124] and Wyner and Ziv [154], if it is assumed that some k out of the set of K correlated variables are received then (by e.g. use of random binning) it is possible to encode at a rate close to the joint entropy of any k variables, in a distributed fashion, so that the encoder does not need to know which k variables that are received. It is usually then not possible to decode on reception of fewer than k variables.

Before presenting the main theorem of [111] which describes the achievable rate-distortion regions of (K, k) SCECs in the general case of $1 \leq k \leq K$, we need some definitions.

---

[29] Outer bounds for the K-channel quadratic Gaussian problem were presented in [142].

Definition 4.1.6. $D^{(K,k)}$ denotes the distortion when receiving k out of K descriptions.

Definition 4.1.7. A tuple $(R, D^{(K,k)}, D^{(K,k+1)}, \ldots, D^{(K,K)})$ is said to be achievable if for arbitrary $\delta > 0$, there exists, for sufficiently large block length L, a (K,k) SCEC with parameters $(L, \Theta, \Delta_k, \Delta_{k+1}, \ldots, \Delta_K)$ with

$$\Theta \leq 2^{L(R+\delta)} \text{ and } \Delta_h \leq D^{(K,h)} + \delta, \; h = k, k+1, \ldots, K. \tag{4.22}$$

Let $\mathscr{I}_k = \{I : I \subseteq \{0, \ldots, K-1\}, |I| \geq k\}$. A (K,k) SCEC with parameters $(L, \Theta, \Delta_k, \Delta_{k+1}, \ldots, \Delta_K)$ is defined by a set of K encoding functions [111]

$$F_i \colon \mathscr{X} \to \{1, 2, \ldots, \Theta\}, \qquad i = 0, \ldots, K-1, \tag{4.23}$$

and a set of $|\mathscr{I}_k|$ decoding functions

$$G_I \colon \bigotimes_I \{1, 2, \ldots, \Theta\} \to \hat{\mathscr{X}}, \qquad \forall I \in \mathscr{I}_k \tag{4.24}$$

where $\bigotimes$ denotes the Cartesian product and for all $h \in \{k, k+1, \ldots, K\}$ and $X \in \mathscr{X}$ we have

$$\begin{aligned} \Delta_h &= E\rho(X, G_I(F_{i_1}(X), \ldots, F_{i_h}(X))) \\ I &= \{i_1, \ldots, i_h\}, \quad \forall I \in \mathscr{I}_k, |I| = h. \end{aligned} \tag{4.25}$$

Theorem 4.1.1 ([111], Th. 1)**.** For a probability distribution[30]

$$p(x, y_0, \ldots, y_{K-1}) = q(x)p(y_0, \ldots, y_{K-1}|x) \tag{4.26}$$

defined over $\mathscr{X} \bigoplus \mathscr{Y}^K$ where $\mathscr{Y}$ is some finite alphabet, $p(y_0, \ldots, y_{K-1}|x)$ is symmetric, and a set of decoding functions $\forall I \in \mathscr{I}_k, g_I : \mathscr{Y}^{|I|} \to \hat{\mathscr{X}}$, if

$$E\rho(X, g_I(Y_I)) \leq D^{(K,|I|)}, \qquad \forall I \in \mathscr{I}_k \tag{4.27}$$

and

$$R > \frac{1}{k}H(Y_0, \ldots, Y_{k-1}) - \frac{1}{K}H(Y_0, \ldots, Y_{K-1}|X) \tag{4.28}$$

then $(R, D^{(K,k)}, D^{(K,k+1)}, \ldots, D^{(K,K)})$ is an achievable rate-distortion tuple.

In [114] an achievable rate-distortion region for the K-channel MD problem was presented. The region was obtained by constructing a number of layers within each description where the set of all j^{th} layers across the K descriptions corresponds to a (K,j) SCEC. Assume that it is desired to achieve some distortion triplet $(D^{(3,1)}, D^{(3,2)}, D^{(3,3)})$ for a three-channel system. Then first a $(3,1)$ SCEC is constructed using a rate of $R^{(0)}$ bit/dim. per description. We use the superscript to distinguish

---

[30]To avoid clutter we omit the subscripts on the probability distributions in this section.

between the rate R_0 of encoder 0 in an asymmetric setup and the rate $R^{(0)}$ of layer 0 in a symmetric setup. The rate $R^{(0)}$ is chosen such that $D^{(3,1)}$ can be achieved with the reception of any single description. If two descriptions are received the distortion is further decreased. However if $D^{(3,2)}$ is not achieved on the reception of any two descriptions, then a (3,2) SCEC is constructed at a rate $R^{(1)}$ bit/dim. per description. The rate $R^{(1)}$ is chosen such that $D^{(3,2)}$ can be achieved on the reception of any two descriptions. If $D^{(3,3)}$ is not achieved on the reception of all three descriptions, a refinement layer is constructed at a rate of $R^{(2)}$ bit/dim. per description, see Fig. 4.9. Each description contains three layers, e.g. description i consists of a concatenation of L_{0i}, L_{1i} and L_{2i}. It is important to see that the first layer, i.e. the (3,1) SCEC is constructed exactly as described by Theorem 4.1.1. The second layer, i.e. the (3,2) SCEC differs from the construction in that of the binning rate. Since, on reception of any two descriptions (say description 0 and 1), we have not only the two second layers (L_{10} and L_{11}) but also two base layers (L_{00} and L_{01}). This makes it possible to decrease the binning rate $R^{(1)}$ by exploiting correlation across descriptions as well as across layers. The final layer can be a simple refinement layer where bits are evenly split among the three descriptions or for example a (3,3) SCEC. The rate of each description is then given by $R = R^{(0)} + R^{(1)} + R^{(2)}$ and the total rate is $3R$.
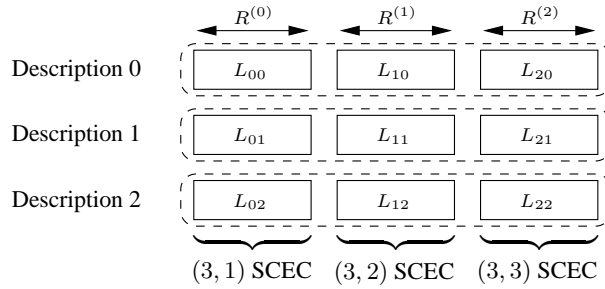
Figure 4.9: *Concatenation of (3,1), (3,2) and (3,3) SCECs to achieve the distortion triplet* $(D^{(3,1)}, D^{(3,2)}, D^{(3,3)})$. *Each description contains three layers and the rate of each description is* $R = R^{(0)} + R^{(1)} + R^{(2)}$.

We are now in a position to introduce the main theorem of [114] which describes an achievable rate-distortion region for the concatenations of (K, k) SCECs. Let Y_{ij} be a random variable in the ith layer and j^{th} description and let $I_0^{K-1} = \{0, \dots, K-1\}$. For $i \in I_0^{K-2}$, let $Y_{iI_0^{K-1}} = (Y_{i0}, Y_{i1}, \dots, Y_{iK-1})$ represent K random variables in the ith layer taking values in alphabet $\mathcal{Y}_i$. Let Y_{K-1} be the last layer refinement variable taking values in the alphabet $\mathcal{Y}_{K-1}$ and

$$Y_{I_0^{K-2}I_0^{K-1}} = (Y_{0I_0^{K-1}}, Y_{1I_0^{K-1}}, \dots, Y_{(K-2)I_0^{K-1}}). \tag{4.29}$$

A joint distribution $p(y_{I_0^{K-2}I_0^{K-1}}, y_{K-1}|x)$ is called symmetric if for all $1 \le r_i \le$

K where $i \in I_0^{K-2}$, the following is true: the joint distribution of Y_{K-1} and all $(r_0 + r_1 + \cdots + r_{K-2})$ random variables where any r_i are chosen from the ith layer, conditioned on x, is the same.

Theorem 4.1.2 ([114], Th. 2)**.** For any probability distribution

$$p(x, y_{I_0^{K-2} I_0^{K-1}}, y_{K-1}) = p(x)p(y_{I_0^{K-2} I_0^{K-1}}, y_{K-1}|x) \tag{4.30}$$

where $p(y_{I_0^{K-2} I_0^{K-1}}, y_{K-1}|x)$ is symmetric, defined over $\mathscr{X} \times \mathscr{Y}_0^K \times \mathscr{Y}_1^K \times \cdots \times \mathscr{Y}_{K-2}^K \times \mathscr{Y}_{K-1}$, and a set of decoding functions given by[31]

$$
\begin{aligned}
g_I &: \mathscr{Y}_0^{|I|} \times \cdots \times \mathscr{Y}_{|I|-1}^{|I|} \to \hat{\mathscr{X}} \quad \forall I \subset I_0^{K-1} \\
g_{I_0^{K-1}} &: \mathscr{Y}_0^K \times \mathscr{Y}_1^K \times \cdots \times \mathscr{Y}_{K-2}^K \times \mathscr{Y}_{K-1} \to \hat{\mathscr{X}}
\end{aligned}
\tag{4.31}
$$

the convex closure of $(R, D^{(K,1)}, D^{(K,2)}, \ldots, D^{(K,K)})$ is achievable where

$$E\rho_I(X, g_I(Y_{I_0^{|I|-1} I})) \leq D^{(K,|I|)} \quad \forall I \subset I_0^{K-1}, \tag{4.32}$$

$$E\rho_{I_0^{K-1}}(X, g_{I_0^{K-1}}(Y_{I_0^{K-2} I_0^{K-1}}, Y_{K-1})) \leq D^{(K,K)}, \tag{4.33}$$

and

$$
\begin{aligned}
R \geq {}& H(Y_{00}) + \sum_{k=2}^{K-1} \frac{1}{k} H(Y_{k-1 I_0^{k-1}}|Y_{I_0^{k-2} I_0^{k-1}}) \\
&+ \frac{1}{K} H(Y_{K-1}|Y_{I_0^{K-2} I_0^{K-1}}) - \frac{1}{K} H(Y_{I_0^{K-2} I_0^{K-1}}, Y_{K-1}|X).
\end{aligned}
\tag{4.34}
$$

The main difference between Theorem 4.1.1 and Theorem 4.1.2 is that the latter theorem considers the complete K-tuple of distortions $(D^{(K,1)}, D^{(K,2)}, \ldots, D^{(K,K)})$ whereas the former theorem considers the $(K - k + 1)$-tuple of distortions $(D^{(K,k)}, D^{(K,k+1)}, \ldots, D^{(K,K)})$. Hence, an SCEC based on the construction presented in [111] is specifically tailored to networks where it is known that at least k channels out K channels are always working. With the construction presented in [114] it is possible to concatenate several SCECs and obtain a code that works for networks where the number of working channels is not known a priori.

4.1.3   Quadratic Gaussian K-Channel Rate-Distortion Region

We will now describe the achievable K-channel rate-distortion region for the quadratic Gaussian case. This appears to be the only case where explicit (and relatively simple) closed-form expressions for rate and distortion have been found.

---

[31] $\mathscr{Y}_i^j$ denotes the j times Cartesian product of the alphabet $\mathscr{Y}_i$.

Consider a unit-variance Gaussian source X and define the random variables $Y_i, i = 0, \ldots, K - 1$, given by

$$Y_i = X + Q_i, \tag{4.35}$$

where the Q_i's are identically distributed jointly Gaussian random variables (independent of X) with variance σ_q^2 and covariance matrix Q given by

$$Q = \sigma_q^2 \begin{bmatrix} 1 & \rho_q & \rho_q & \cdots & \rho_q \\ \rho_q & 1 & \rho_q & \cdots & \rho_q \\ \rho_q & \rho_q & 1 & \cdots & \rho_q \\ \vdots & \vdots & \vdots & \ddots & \vdots \\ \rho_q & \rho_q & \rho_q & \cdots & 1 \end{bmatrix}, \tag{4.36}$$

where, for $K > 1$, it is required that the correlation coefficient satisfies $-1/(K-1) < \rho_q \leq 1$ to ensure that Q is positive semidefinite [142]. In the case of Ozarow's double branch test channel for $K = 2$ descriptions, we only need to consider non positive ρ_q's. This is, in fact, also the case for $K > 2$ descriptions [142].

It is easy to show that the MMSE when estimating X from any set of m Y_i's is given by [111, 142]

$$D^{(K,m)} = \frac{\sigma_q^2(1 + (m-1)\rho_q)}{m + \sigma_q^2(1 + (m-1)\rho_q)}. \tag{4.37}$$

We now focus on the (K, k) SCEC as presented in Theorem 4.1.1. The rate of each description is given by [111]

$$R = \frac{1}{2} \log_2 \left(\frac{k + \sigma_q^2(1 + (k-1)\rho_q)}{\sigma_q^2(1 - \rho_q)} \right)^{1/k} \left(\frac{1 - \rho_q}{1 + (K-1)\rho_q} \right)^{1/K}. \tag{4.38}$$

The quantization error variance σ_q^2 can now be obtained from (4.38)

$$\sigma_q^2 = k \left((1 - \rho_q)2^{2kR} \left(\frac{1 + (K-1)\rho_q}{1 - \rho_q} \right)^{k/K} - (1 + (k-1)\rho_q) \right)^{-1}. \tag{4.39}$$

We will follow [111] and look at the performance of a (K, k) SCEC in three different situations distinguished by the amount of correlation ρ_q introduced in the quantization noise.

Independent quantization noise: $\rho_q = 0$

The quantization noise is i.i.d., i.e. $\rho_q = 0$, hence Q is diagonal. Assuming that the quantization noise is normalized such that $\sigma_q^2 = k/(2^{2kR} - 1)$, we get the following expressions for the distortion

$$D^{(K,k+r)} = \frac{\sigma_q^2}{\sigma_q^2 + (k+r)} = \frac{k}{2^{2kR}(k+r) - r} \quad \text{for } 0 \leq r \leq K - k, \tag{4.40}$$

and

$$D^{(K,m)} = 1 \quad \text{for } 0 \le m < k. \tag{4.41}$$

The distortion when receiving k descriptions is optimal, i.e. $D^{(K,k)} = 2^{-2kR}$.

Correlated quantization noise: $\rho_q = \rho_q^*$

The amount of correlation ρ_q^* needed in order to be on the distortion-rate function on the reception of $k = K$ descriptions is given by

$$\rho_q^* = -\frac{2^{2KR} - 1}{(K-1)2^{2KR} + 1} \approx -\frac{1}{K-1}. \tag{4.42}$$

This leads to the following performance

$$D^{(K,r)} = 1 - \frac{r}{K}(1 - 2^{-2KR}) \quad \text{for } 0 \le r \le K. \tag{4.43}$$

Notice that the distortion when receiving K descriptions is optimal, i.e. $D^{(K,K)} = 2^{-2KR}$.

Correlated quantization noise: $\rho_q^* < \rho_q < 0$

Here a varying degree of correlation is introduced and the performance is given by

$$D^{(K,r)} = \frac{\sigma_q^2(1 + (r-1)\rho_q)}{\sigma_q^2(1 + (r-1)\rho_q) + r} \quad \text{for } k \le r \le K, \tag{4.44}$$

and

$$D^{(K,m)} = 1 \quad \text{for } 0 \le m < k. \tag{4.45}$$

Fig. 4.10 shows the three-channel distortion $D^{(3,3)}$ as a function of the two-channel distortion $D^{(3,2)}$ when varying ρ_q and keeping the rate constant by use of (4.39). In this example we use a $(3,2)$ SCEC with $R = 1$ bit/dim. At one end we have $D^{(3,2)} = -12.0412$ dB which is on the distortion-rate function of the source and at the other end we have $D^{(3,3)} = -18.0618$ dB which is also on the distortion-rate function.

In Fig. 4.11 we show the simultaneously achievable one-channel $D^{(3,1)}$, two-channel $D^{(3,2)}$ and three-channel $D^{(3,3)}$ distortions for the unit-variance memoryless Gaussian source at 1 bit/dim. when using a $(3,1)$ SCEC. It is interesting to observe that while it is possible to achieve optimum one-channel distortion ($\rho_q = 0 \Rightarrow D^{(3,1)} \approx -6$ dB) and optimum three-channel distortion ($\rho_q \rightarrow -1/2 \Rightarrow D^{(3,3)} \approx -18$ dB) it is not possible to drive the two-channel distortion towards its optimum ($\forall \rho_q, D^{(3,2)} < -12$ dB). In other words, a $(3,1)$ SCEC can achieve optimal one-channel and three-channel performance and a $(3,2)$ SCEC can achieve optimal two-channel and three-channel performance.
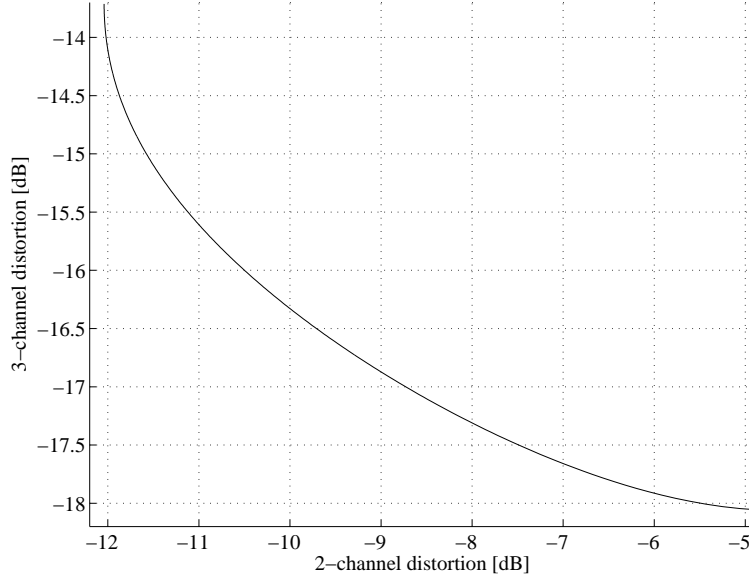
Figure 4.10: *Three-channel versus two-channel distortions for a (3,2) SCEC at $R = 1$ bit/dim. for the unit-variance Gaussian source. This example is from [111].*

Let us now look at the achievable three-channel region presented in [114] for the the memoryless Gaussian source. Let R bit/dim. per description be the rate of transmission. Let the random variables in the three layers be defined as

$$Y_{0j} = X + Q_{0j}, Y_{1j} = X + Q_{1j}, \text{ and } Y_2 = X + Q_2 \quad \text{for } j \in I_0^2, \qquad (4.46)$$

where for $i \in I_0^1, Q_{iI_0^2}$ are symmetrically distributed Gaussian random variables with variance $\sigma_{q_i}^2$ and correlation coefficient ρ_{q_i} and Q_2 is a Gaussian random variable with variance $\sigma_{q_2}^2$. $Q_{0I_0^2}, Q_{1I_0^2}$ and Q_2 are independent of each other and X. By changing the four independent variables $R^{(0)}, R^{(1)}, \rho_{q_0}$ and ρ_{q_1} different trade-offs between $D^{(3,1)}, D^{(3,2)}$ and $D^{(3,3)}$ can be made. The correlation coefficients are lower bounded by [114]

$$\rho_{q_i} \geq -\frac{2^{6R^{(i)}} - 1}{2 \cdot 2^{6R^{(i)}} + 1}. \qquad (4.47)$$

The variance $\sigma_{q_0}^2$ of the base layer follows from (4.39) by letting $k = 1$, that is

$$\sigma_{q_0}^{-2} = 2^{2R^{(0)}} (1 + 2\rho_{q_0})^{\frac{1}{3}} (1 - \rho_{q_0})^{\frac{2}{3}} - 1 \qquad (4.48)$$

and it can be shown that [114]

$$\sigma_{q_1}^{-2} = -\frac{1 + \rho_{q_1}}{(1 + \rho_{q_0})\sigma_{q_0}^2} - \frac{1 + \rho_{q_1}}{2} + \frac{2^{4R^{(1)}}(1 + \rho_{q_0} + 2/\sigma_{q_0}^2)(1 + \rho_{q_1} - 2\rho_{q_1}^2)^{\frac{2}{3}}}{2(1 + \rho_{q_0})(1 - \rho_{q_1})^{\frac{1}{3}}}. \qquad (4.49)$$
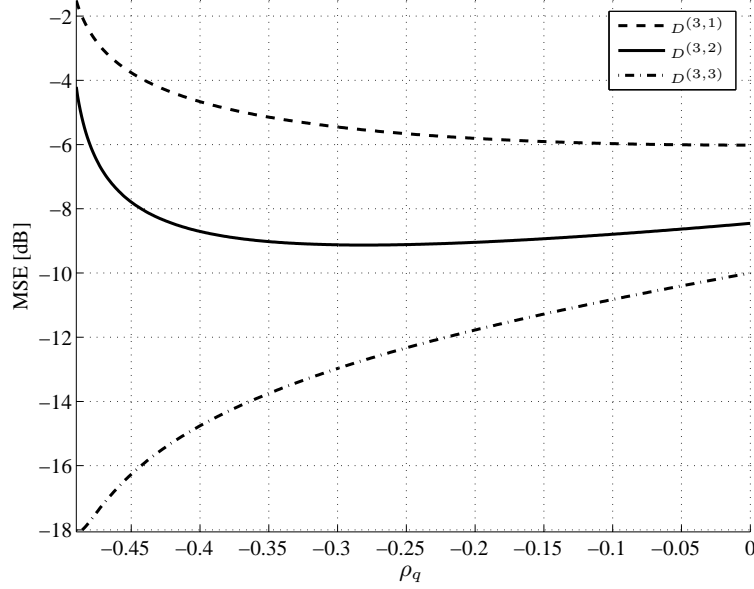
Figure 4.11: *The simultaneously achievable one-channel, two-channel and three-channel distortions for the unit-variance Gaussian source at 1 bit/dim. for a (3,1) SCEC.*

Let MSE_2 denote the distortion given by any two base-layer random variables, and MSE_3 denote the distortion given by all the random variables in the base and the second layer. Hence, MSE_2 denotes the MMSE obtained in estimating the source X using either (Y_{00}, Y_{01}), (Y_{00}, Y_{02}) or (Y_{01}, Y_{02}). Similarly MSE_3 denotes the MMSE in estimating X from $(Y_{00}, Y_{01}, Y_{02}, Y_{10}, Y_{11}, Y_{12})$. From (4.37) it follows that

$$\text{MSE}_2 = \frac{\sigma_{q_0}^2 (1 + \rho_{q_0})}{\sigma_{q_0}^2 (1 + \rho_{q_0}) + 2}, \tag{4.50}$$

and it can also be shown that [114]

$$\text{MSE}_3 = \frac{\sigma_{q_0}^2 \sigma_{q_1}^2 (1 + 2\rho_{q_0} + 2\rho_{q_1} + 4\rho_{q_0}\rho_{q_1})}{3\sigma_{q_0}^2 (1 + 2\rho_{q_0}) + 3\sigma_{q_1}^2 (1 + 2\rho_{q_1}) + \sigma_{q_0}^2 \sigma_{q_1}^2 (1 + 2\rho_{q_0} + 2\rho_{q_1} + 4\rho_{q_0}\rho_{q_1})}, \tag{4.51}$$

and

$$\sigma_{q_2}^2 = \frac{\text{MSE}_3}{2^{6(R - R^{(0)} - R^{(1)})} - 1}. \tag{4.52}$$

Finally, we have [114]

$$D'^{(3,1)} = \frac{\sigma_{q_0}^2}{1 + \sigma_{q_0}^2}, \tag{4.53}$$

$$D'^{(3,2)} = \frac{\sigma_{q_1}^2(1 + \rho_{q_1})\text{MSE}_2}{\sigma_{q_1}^2(1 + \rho_{q_1}) + 2\text{MSE}_2}, \tag{4.54}$$

$$D'^{(3,3)} = \frac{\sigma_{q_2}^2\text{MSE}_3}{\text{MSE}_3 + \sigma_{q_2}^2}. \tag{4.55}$$

The lower convex hull of $(D'^{(3,1)}, D'^{(3,2)}, D'^{(3,3)})$ corresponds to an achievable distortion tuple $(D^{(3,1)}, D^{(3,2)}, D^{(3,3)})$. See Fig. 4.12 for an example of an achievable distortion region for the unit-variance memoryless Gaussian source for $R^{(0)} = R^{(1)} = 0.5$ bit/dim. per description and a description rate of $R = R^{(0)} + R^{(1)} = 1$ bit/dim. In this plot the correlation values are varied throughout the range given by (4.47).
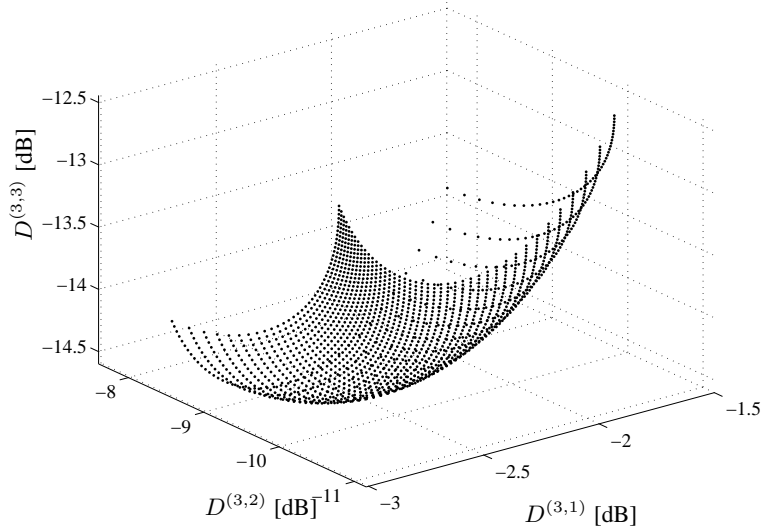
Figure 4.12: *Achievable distortion region for $R^{(0)} = R^{(1)} = 0.5$ bit/dim. per description. The description rate is $R = R^{(0)} + R^{(1)} = 1$ bit/dim. The dense peak is in the front.*

4.2 Multiple-Description Quantization

The previous section described known information theoretic bounds. These bounds were shown to be achievable by use of random codebooks. Unfortunately random codebooks are usually not very practical due to e.g. high search complexity and large

memory requirements. From a practical point of view it is therefore desirable to avoid random codebooks, which is the case for the MD schemes we present in this section.

Existing MD schemes can roughly be divided into three categories: quantizer-based, transform-based and source-channel erasure codes based. Quantizer-based schemes include scalar quantization [5, 10, 39, 68, 130, 131, 135, 138], trellis coded quantization [67, 137, 147] and vector quantization [15, 17, 18, 27, 28, 36, 37, 48, 51, 73, 75, 98, 99, 103–105, 120, 127, 129, 139, 155]. Transform-based approaches include correlating transforms [49, 52, 53, 97, 148], overcomplete expansions and filterbanks [4, 20, 29, 54, 55, 76]. Schemes based on source-channel erasure codes were presented in [109–114]. For further details on many existing MD techniques we refer the reader to the excellent survey article by Goyal [50].

The work in this thesis is based on lattice vector quantization and belongs therefore to the first of the catagories mentioned above to which we will also restrict attention.

4.2.1   Scalar Two-Channel Quantization with Index Assignments

In some of the earliest MD schemes it was recognized that two separate low-resolution quantizers may be combined to form a high-resolution quantizer. The cells of the high-resolution quantizer are formed as the intersections of the cells of the low-resolution quantizers [50]. The two low-resolution quantizers are traditionally called the side quantizers and their joint quantizer, the high-resolution quantizer, is called the central quantizer. If the side quantizers are regular quantizers, i.e. their cells form connected regions, then the central quantizer is not much better than the best of the two side quantizers. However, if disjoint cells are allowed in the side quantizers, then a much better central quantizer can be formed. According to Goyal's survey article [50], the idea of using disjoint cells in the side quantizers seems to originate from some unpublished work of Reudink [116]. Fig 4.13(a) shows an example where two regular side quantizers Q_0 and Q_1 each having 3 cells are combined to form a central quantizer Q_c having 5 cells. Hence, the resolution of the central quantizer is only about twice that of either one of the two side quantizers. Fig. 4.13(b) shows an example where one of the side quantizers have disjoint cells which makes it possible to achieve a very good joint quantizer. In this case both side quantizers have three cells but Q_1 has disjoint cells. The central quantizer has 9 cells which is equal to the product of the number of cells of the side quantizers. Hence, the resolution of the central quantizer is comparable to an optimal single description scalar quantizer operating at the sum rate of the two side quantizers. The price, however, is relatively poor performance of side quantizer Q_1.

The idea of using two quantizers with disjoint cells as side quantizers and their intersections as a central quantizer was independently discovered by Vaishampayan [135] some years after Reudink. Vaishampayan proposed a systematic way to control the redundancy in the two side quantizers by use of an index assignment matrix [135]. The idea is to first partition the real line into intervals in order to obtain the central

(a) Regular side quantizers   (b) Irregular side quantizers
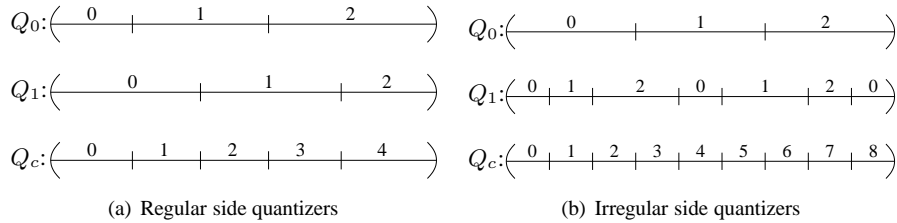
Figure 4.13: *Two quantizers are able to refine each other if their cell bounderies do not coincide. In (a) both Q_0 and Q_1 are good quantizers but Q_c is poor. In (b) quantizer Q_1 is poor whereas Q_0 and Q_c are both good.*

quantizer and then assign a set of central cells to each cell in the side quantizers. For example let us partition the real line into 7 intervals as shown in Fig. 4.14(a) (the bottom quantizer is the central quantizer). We then construct the index assignment matrix as shown in Fig. 4.14(b). Each column of the matrix represent a cell of the side quantizer shown in the top of Fig. 4.14(a). Since there are four columns the side quantizer has four cells. Similarly, the four rows of the matrix represent the four cells of the second side quantizer (the middle quantizer of Fig. 4.14(a)). The central quantizer in this design, which is based on the two main diagonals and where the side quantizers have connected cells, is known as a staggered quantizer.[32] If we only use the main diagonal of the index assignment matrix we get a repetition code. In this case the side quantizers are identical and they are therefore not able to refine each other, which means that the central distortion will be equal to the side distortions.

By placing more elements (numbers) in the index assignment matrix the central quantizer will have more cells and the central distortion can therefore be reduced. There is a trade-off here, since placing more elements in the matrix will usually cause the cells of the side quantizers to be disjoint and the side distortion will then increase. Fig. 4.15(b) shows an example where the index assignment matrix is full and the central quantizer therefore has 16 cells. Hence, the central distortion is minimized. From Fig. 4.15(a) it is clear that the cells of the side quantizers are disjoint and since each cell is spread over a large region of the central quantizer the side distortion will be large.

The main difficulty of the design proposed by Vaishampayan lies in finding good index assignments, i.e. constructing the index assignment matrix. In [135] several heuristic designs were proposed for the case of symmetric resolution-constrained MD

---

[32]It is often possible to make the second side quantizer a translation of the first side quantizer and use their intersection as the central quantizer. The quality improvement of a central quantizer constructed this way over that of the side quantizers is known as the staggering gain. However, as first observed in [39] and further analyzed in [132] the staggering gain dissappears when good high dimensional lattice vector quantizers are used.

(a) Side and central quantizers   (b) Index assignment matrix

Figure 4.14: *(a) The two side quantizers each having four cells are offset from each other. Their intersection forms the central quantizer having 7 cells. (b) shows the corresponding index assignment matrix for the quantizers. The columns of the matrix form a side quantizer and the rows also form a side quantizer.*

(a) Side and central quantizers   (b) Index assignment matrix

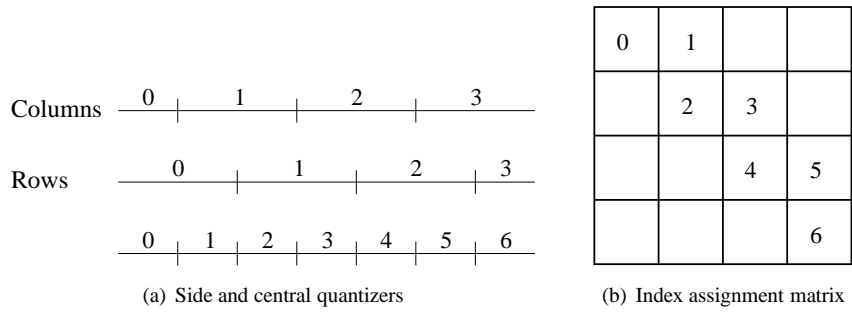**Figure 4.15:** *(a) The two side quantizers each having four cells are not identical. Their intersection forms the central quantizer having 16 cells. (b) shows the corresponding index assignment matrix for the quantizers. The columns of the matrix form a side quantizer and the rows also form a side quantizer.*
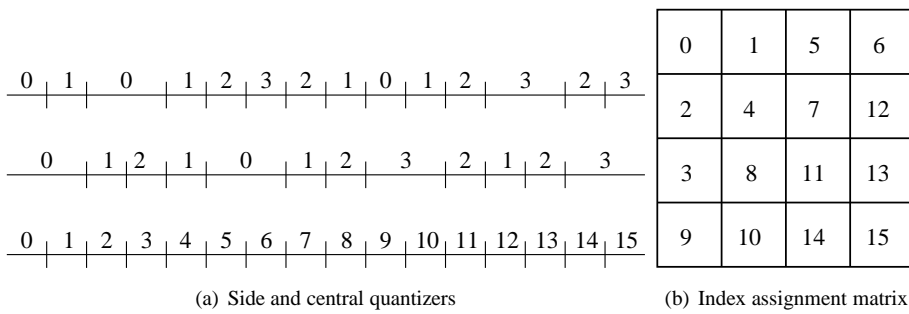
scalar quantization. Their performance at high resolution was evaluated in [136] and it was shown that in the quadratic Gaussian case, the distortion product $D_c D_0$ was 8.69 dB away from the optimal high resolution distortion product (4.12). Vaishampayan and Domaszewicz [138] then proposed an entropy-constrained MD scalar quantizer where the index-assignment matrix was optimized using a generalized Lloyd algorithm. The distortion product of this design was shown to be only 3.06 dB away the theoretical optimum [136]. Recall that the space-filling loss of an SD scalar quantizer is 1.53 dB so that, quite surprisingly, the gap to the optimal distortion product of a two-description scalar quantizer is twice the scalar space-filling loss. The design of good index assignments for the scalar case is further considered in [10].

It is known that the entropy-constrained scalar uniform quantizer is optimal in the SD case, see Chapter 3. This result, however, does not carry over to the MD case. Goyal et al. [51, 73] were the first to recognize that by slightly modifying the central quantizer in a way so that it no longer forms a lattice, it is possible to reduce the distortion product not only in the scalar case but also in the two-dimensional case. This phenomenon was further investigated by Tian et al. [129–131] who showed that the scalar distortion product can be further improved by 0.4 dB by modifying the central quantizer.

4.2.2   Lattice Vector Quantization for Multiple Descriptions

Recently, Servetto, Vaishampayan and Sloane [120, 139] presented a clever construction based on lattices, which at high resolution and asymptotically in vector dimension is able to achieve the symmetric two-channel MD rate-distortion region. The design of [120, 139] is again based on index assignments which are non-linear mappings that lead to a curious result. Let $R_s = R_0 = R_1$ denote the rate of each of the side quantizers and let $0 < a < 1$. Then, at high resolution, the central distortion D_c satisfies [139]

$$\lim_{R \to \infty} D_c 2^{2R_s(1+a)} = \frac{1}{4} G(\Lambda) 2^{2h(X)}, \tag{4.56}$$

whereas the side distortions $D_0 = D_1$ satisfy

$$\lim_{R \to \infty} D_0 2^{2R_s(1-a)} = G(S_L) 2^{2h(X)}, \tag{4.57}$$

where $G(\Lambda)$ and $G(S_L)$ are the dimensionless normalized second moments of the central lattice Λ and an L-sphere, respectively. Thus, remarkably, the performance of the side quantizers is identical to that of quantizers having spherical Voronoi cells; note that in the SD case this is not possible for $1 < L < \infty$.

The design presented in [120, 139] is based on a central lattice Λ and a single sublattice Λ_s of index $N = |\Lambda/\Lambda_s|$. Each central lattice point $\lambda \in \Lambda$ is mapped to a pair of sublattice points $(\lambda_0, \lambda_1) \in \Lambda_s \times \Lambda_s$ using an index assignment function. A pair of sublattice points is called an edge. The edges are constructed by pairing

closely spaced (in the Euclidean sense) sublattice points. By exploiting the direction of an edge (i.e. the pair (λ_0, λ_1) is distinguishable from (λ_1, λ_0)) it is possible to use an edge twice. In order to construct the edges as well as the assignment of edges to central lattice points, geometric properties of the lattices are exploited. Specifically, the edges (λ_0, λ_1) and (λ_1, λ_0) are mapped to the central lattice points $\lambda \in \Lambda$ and $\lambda' \in \Lambda$ which satisfy $\lambda + \lambda' = \lambda_0 + \lambda_1$ and furthermore, the distance from the midpoint of an edge and the associated central lattice point should be as small as possible (when averaged over all edges and the corresponding assigned central lattice points). Only a small number of edges and assignments needs to be found, whereafter the symmetry of the lattices can be exploited in order to cover the entire lattice. Examples of edge constructions and assignments are presented in [120, 139].

The asymmetric case was considered by Diggavi, Sloane and Vaishampayan [27, 28] who constructed a two-channel scheme also based on index assignments and which, at high resolution and asymptotically in vector dimension, is able to reach the entire two-channel MD rate-distortion region. Specifically, at high resolution, the central distortion satisfies [28]

$$D_c = G(\Lambda)2^{2(h(X) - R_c)}, \tag{4.58}$$

where R_c is the rate of the central quantizer and the side distortions satisfy

$$D_0 = \frac{\gamma_1^2}{(\gamma_0 + \gamma_1)^2}G(\Lambda_s)2^{2h(X)}2^{-2(R_0 + R_1 - R_c)}, \tag{4.59}$$

and

$$D_1 = \frac{\gamma_0^2}{(\gamma_0 + \gamma_1)^2}G(\Lambda_s)2^{2h(X)}2^{-2(R_0 + R_1 - R_c)}, \tag{4.60}$$

where $G(\Lambda_s)$ is the dimensionless normalized second moment of a sublattice Λ_s, which is geometrically-similar to both side lattices $\Lambda_i, i = 0, 1$, and $\gamma_0, \gamma_1 \in \mathbb{R}^+$ are weights which are introduced to control the asymmetry in the side distortions. Notice that in the distortion-balanced case we have $\gamma_0 = \gamma_1$ so that $\frac{\gamma_0^2}{(\gamma_0 + \gamma_1)^2} = \frac{1}{4}$ and if $\gamma_0 = 0$ or $\gamma_1 = 0$ then the design degenerates to a successive refinement scheme [28, 32]. It is worth emphasizing that the side quantizers in the asymmetric design do generally not achieve the sphere bound in finite dimensions as was the case of the symmetric design.

The design presented in [27, 28] is based on a central lattice Λ, two sublattices $\Lambda_0 \subset \Lambda$ and $\Lambda_1 \subset \Lambda$ of index $N_0 = |\Lambda/\Lambda_0|$ and $N_1 = |\Lambda/\Lambda_1|$, respectively, and a product lattice $\Lambda_\pi \subset \Lambda_i, i = 0, 1$, of index $N_\pi = N_0 N_1$. The Voronoi cell $V_\pi(\lambda_\pi)$ of the product lattice point $\lambda_\pi \in \Lambda_\pi$ contains N_1 sublattice points of Λ_0 and N_0 sublattice points of Λ_1, see Fig. 4.16 for an example where $N_0 = 5$ and $N_1 = 9$. In this example, only the 45 central lattice points located within $V_\pi(0)$ need to have edges assigned. The remaining assignments are done simply by shifting these assignments by $\lambda_\pi \in \Lambda_\pi$. In other words, if the edge (λ_0, λ_1) is assigned to λ then the edge

$(\lambda_0 + \lambda_\pi, \lambda_1 + \lambda_\pi)$ is assigned to $\lambda + \lambda_\pi$. We say that the assignments are shift invariant with respect to the product lattice.

The 45 edges are constructed in the following way. First, create the set E_{Λ_0} containing the nine sublattice points of Λ_0 which are located within $V_\pi(0)$, i.e.

$$E_{\Lambda_0} = \{(0,0), (-3,1), (-2,-1), (-1,2), (-1,-3), (1,-2), (1,3), (2,1), (3,1)\}.$$

Let λ_0 be the first element of E_{Λ_0}, i.e. $\lambda_0 = (0,0)$. Pair λ_0 with the five λ_1 points located within $V_\pi(0)$. Thus, at this point we have five edges; $\{(0,0),(0,0)\}, \{(0,0),(0,3)\}, \{(0,0),(0,-3)\}, \{(0,0),(3,0)\}$ and $\{(0,0),(-3,0)\}$. Consider now the second element of E_{Λ_0}, i.e. $\lambda_0 = (-3,1)$. Shift $V_\pi(0)$ so that it is centered at λ_0 (illustrated by the dashed square in Fig. 4.16). For notational convenience we denote $V_\pi(0) + \lambda_0$ by $V_\pi(\lambda_0)$. We now pair $\lambda_0 = (-3,1)$ with the five sublattice points of Λ_1 which are contained within $V_\pi(\lambda_0)$, i.e. $\Lambda_1 \cap V_\pi(\lambda_0) = \{(0,0), (-3,0), (-3,3), (-6,0), (-6,3)\}$. This procedure should be repeated for the remaining points of E_{Λ_0} leading to a total of 45 distinct edges. These 45 edges combined with the 45 central lattice points within $V_\pi(0)$ form a bipartite matching problem where the cost of assigning an edge to a central lattice point is given by the Euclidean distance between the mid point (or weighted mid point) of the edge and the central lattice point.

Notice that for large index values, the sublattice point $\lambda_0 \in \Lambda_0$ is paired with points of Λ_1 which are evenly distributed within a region V_π centered at λ_0. If the product lattice Λ_π is based on the hypercubic lattice Z^L then V_π forms a hypercube. In Chapters 5 and 6 we show that it is possible to change the design so that the sublattice points of Λ_1 which are paired with a given $\lambda_0 \in \Lambda_0$ are evenly distributed within an L-dimensional hypersphere regardless of the choice of product lattice Λ_π. The purpose of having the points spherically distributed is twofold; first, the side distortion is reduced and second, it allows a simple extension to more than two descriptions.

Non Index-Assignment Based Designs

To avoid the difficulty of designing efficient index-assignment maps it was suggested in [39] that the index assignments of a two-description system can be replaced by successive quantization and linear estimation. More specifically, the two side descriptions can be linearly combined and further enhanced by a refinement layer to yield the central reconstruction. The design of [39] suffers from a rate loss of 0.5 bit/dim. at high resolution and is therefore not able to achieve the MD rate-distortion bound. Recently, however, this gap was closed by Chen et al. [17, 18] who showed that by use of successive quantization and source splitting[33] it is indeed possible to achieve the two-channel MD rate-distortion bound, at any resolution, without the use of index

---

[33]Source splitting denotes the process of splitting a source X into two or more source variables, e.g. $X \to (X_1, X_2)$ where $X \to X_1 \to X_2$ forms a Markov chain (in that order) [18].
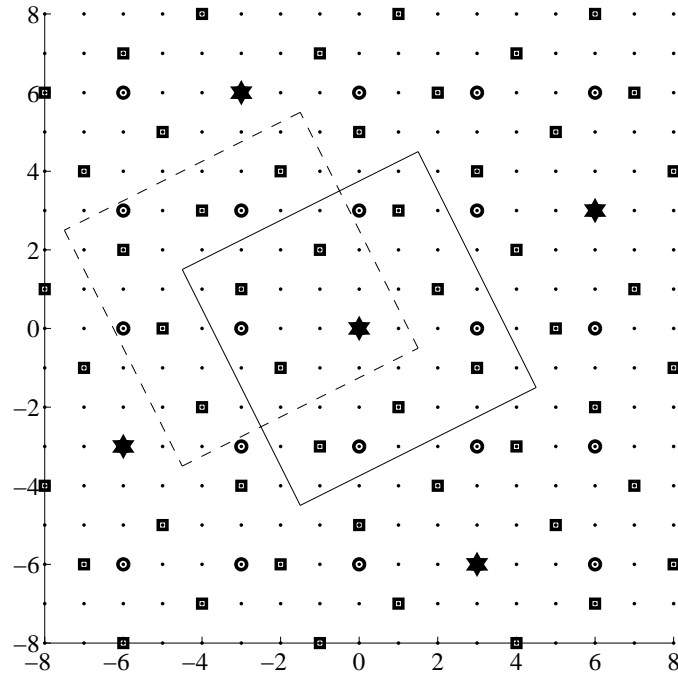
Figure 4.16: *A central lattice Λ (dots), a sublattice Λ_0 (squares) of index 5, a sublattice (circles) of index 9, and a product lattice (stars) of index 45. The solid lines denote the Voronoi cell $V_\pi(0)$ of the product lattice point located at the origin. Notice that $V_\pi(0)$ contains 45 central lattice points. The dashed lines denotes $V_\pi(0)$ shifted so it is centered at $(-3, 1)$.*

assignments. Chen et al. recognized that the rate region of the MD problem forms a polymatroid and showed that corner points of this rate region can be achieved by successive estimation and quantization. This design is inherently asymmetric in the description rate since any corner point of a non-trivial rate region will lead to asymmetric rates. It is therefore necessary to perform source splitting in order to achieve symmetry in the description rate. When finite-dimensional quantizers are employed there is a space-filling loss due to the fact that the quantizer's Voronoi cells are not completely spherical and each description therefore suffers a rate loss. The rate loss of the design given in [17, 18] is that of $2K - 1$ quantizers because source splitting is performed by using an additional $K - 1$ quantizers besides the conventional K side quantizers. In comparison, the designs of the two-channel schemes based on index assignments [27, 28, 120, 139] suffer from a rate loss of only that of two quantizers and furthermore, in the symmetric case, they suffer from a rate loss of only that of two spherical quantizers. That it indeed is possible to avoid source splitting in the symmetric case without the use of index assignments was recently shown by

Østergaard and Zamir [127] who constructed a K-channel symmetric MD scheme based on dithered Delta-Sigma quantization. The design of [127] is able to achieve the entire symmetric two-channel MD rate-distortion region at any resolution and the rate loss when finite-dimensional quantizers are used is that of two lattice quantizers. Hence, in the two-channel case the rate loss when using index assignments is less than or equal to that of the designs which are not using index assignments [17, 18, 127].

Chapter 5

K-**Channel Symmetric Lattice Vector Quantization**

In this chapter we consider a special case of the general K-channel symmetric MD problem where only a single parameter controls the redundancy tradeoffs between the central and the side distortions. With a single controlling parameter it is possible to describe the entire symmetric rate-distortion region for two descriptions and at high resolution, as shown in [120, 139], but it is not enough to describe the symmetric achievable K-channel rate-distortion region. As such the proposed scheme offers a partial solution to the problem of designing balanced MD-LVQ systems. In Chapter 7 we include more controlling parameters in the design and show that the three-channel MD region given by Theorem 4.1.1 can be reached at high resolution.

We derive analytical expressions for the central and side quantizers which, under high-resolution assumptions, minimize the expected distortion at the receiving side subject to entropy constraints on the side descriptions for given packet-loss probabilities. The central and side quantizers we use are lattice vector quantizers. The central distortion depends upon the lattice type in question whereas the side distortions only depend on the scaling of the lattices but are independent of the specific types of lattices. In the case of three descriptions we show that the side distortions can be expressed through the dimensionless normalized second moment of a sphere as was the case for the two descriptions system presented in [120, 139]. Furthermore, we conjecture that this is true in the general case of an arbitrary number of descriptions.

In the presented approach the expected distortion observed at the receiving side depends only upon the number of received descriptions, hence the descriptions are mutually refinable and reception of any κ out of K descriptions yields equivalent expected distortion. This is different from successive refinement schemes [32] where the individual descriptions often must be received in a prescribed order to be able to

refine each other, i.e. description number l will not do any good unless descriptions $0, \ldots, l-1$ have already been received. We construct a scheme which for given packet-loss probabilities and a maximum bit budget (target entropy) determines the optimal number of descriptions and specifies the corresponding quantizers that minimize the expected distortion.

5.1 Preliminaries

We consider a central quantizer and $K \geq 2$ side quantizers. The central quantizer is (based on) a lattice $\Lambda_c \subset \mathbb{R}^L$ with a fundamental region of volume $\nu = \det(\Lambda_c)$. The side quantizers are based on a geometrically-similar and clean sublattice $\Lambda_s \subseteq \Lambda_c$ of index $N = |\Lambda_c/\Lambda_s|$ and fundamental regions of volume $\nu_s = \nu N$. The trivial case $K = 1$ leads to a single-description system, where we would simply use one central quantizer and no side quantizers.

We will consider the balanced situation, where the entropy R is the same for each description. Furthermore, we consider the case where the contribution $D_i, i = 0, \ldots, K-1$ of each description to the total distortion is the same. Our design makes sure[34] that the distortion observed at the receiving side depends only on the number of descriptions received; hence reception of any κ out of K descriptions yields equivalent expected distortion.

5.1.1 Index Assignments

A source vector x is quantized to a reconstruction point λ_c in the central lattice Λ_c. Hereafter follows index assignments (mappings), which uniquely map λ_c to one vector (reconstruction point) in each of the side quantizers. This mapping is done through a labeling function α, and we denote the individual component functions of α by α_i, where $i = 0, \ldots, K - 1$. In other words, the injective map α that maps Λ_c into $\Lambda_s \times \cdots \times \Lambda_s$, is given by

$$\alpha(\lambda_c) = (\alpha_0(\lambda_c), \alpha_1(\lambda_c), \ldots, \alpha_{K-1}(\lambda_c)) \tag{5.1}$$

$$= (\lambda_0, \lambda_1, \ldots, \lambda_{K-1}), \tag{5.2}$$

where $\alpha_i(\lambda_c) = \lambda_i \in \Lambda_s$ and $i = 0, \ldots, K-1$. Each K-tuple $(\lambda_0, \ldots, \lambda_{K-1})$ is used only once when labeling points in Λ_c in order to make sure that λ_c can be recovered unambiguously when all K descriptions are received. At this point we also define the inverse component map, α_i^{-1}, which gives the set of distinct central lattice points a specific sublattice point is mapped to. This is given by

$$\alpha_i^{-1}(\lambda_i) = \{\lambda_c \in \Lambda_c : \alpha_i(\lambda_c) = \lambda_i\}, \qquad \lambda_i \in \Lambda_s, \tag{5.3}$$

---

[34]We prove this symmetry property for the asymptotic case of $N \to \infty$ and $\nu_s \to 0$. For finite N we cannot guarantee the existence of an exact symmetric solution. However, by use of time-sharing arguments, it is always possible to achieve symmetry.

where $|\alpha_i^{-1}(\lambda_i)| \approx N$, since there are N times as many central lattice points as sublattice points within a bounded region of $\mathbb{R}^L$.

Since lattices are infinite arrays of points, we construct a shift invariant labeling function, so we only need to label a finite number of points as is done in [28, 139]. Following the approach outlined in Chapter 2 we construct a product lattice Λ_π which has N^2 central lattice points and N sublattice points in each of its Voronoi cells. The Voronoi cells V_π of the product lattice Λ_π are all similar so by concentrating on labeling only central lattice points within one Voronoi cell of the product lattice, the rest of the central lattice points may be labeled simply by translating this Voronoi cell throughout $\mathbb{R}^L$. Other choices of product lattices are possible, but this choice has a particular simple construction. With this choice of product lattice, we only label central lattice points within $V_\pi(0)$, which is the Voronoi cell of Λ_π around the origin. With this we get

$$\alpha(\lambda_c + \lambda_\pi) = \alpha(\lambda_c) + \lambda_\pi, \tag{5.4}$$

for all $\lambda_\pi \in \Lambda_\pi$ and all $\lambda_c \in \Lambda_c$.

5.2   Rate and Distortion Results

Central Distortion

Let us consider a scalar process that generates i.i.d. random variables with probability density function (pdf) f. Let $X \in \mathbb{R}^L$ be a random vector made by blocking outputs of the scalar process into vectors of length L, and let $x \in \mathbb{R}^L$ denote a realization of X. The L-fold pdf of X is denoted f_X and given by[35]

$$f_X(x) = \prod_{j=0}^{L-1} f(x_j). \tag{5.5}$$

The expected distortion (per dimension) D_c occuring when all packets are received is called the central distortion and is defined as

$$D_c \triangleq \frac{1}{L} \sum_{\lambda_c \in \Lambda_c} \int_{V_c(\lambda_c)} \|x - \lambda_c\|^2 f_X(x)dx, \tag{5.6}$$

where $V_c(\lambda_c)$ is the Voronoi cell of a single reconstruction point $\lambda_c \in \Lambda_c$. Using standard high resolution assumptions, cf. Chapter 3, we may assume that each Voronoi cell is sufficiently small and $f_X(x)$ is smooth and hence approximately constant within each cell. In this case λ_c is approximately the centroid (conditional mean) of the corresponding cell, that is

$$\lambda_c \approx \frac{\int_{V_c(\lambda_c)} x f_X(x)dx}{\int_{V_c(\lambda_c)} f_X(x)dx}. \tag{5.7}$$

---

[35]It is worth pointing out that we actually only require the individual vectors to be i.i.d. and as such correlation within vectors is allowed.

Since the pdf is approximately constant within a small region we also have that

$$f_X(x) \approx f_X(\lambda_c), \quad \forall x \in V_c(\lambda_c), \tag{5.8}$$

and we can therefore express the probability, P, of a cell as

$$P(V_c(\lambda_c)) = \int_{V_c(\lambda_c)} f_X(x)dx \approx f_X(\lambda_c) \int_{V_c(\lambda_c)} dx = \nu f_X(\lambda_c), \tag{5.9}$$

where ν is the volume of a Voronoi cell. With this, we get

$$f_X(\lambda_c) \approx \frac{P(V_c(\lambda_c))}{\nu}. \tag{5.10}$$

Inserting (5.10) into (5.6) gives

$$D_c \approx \frac{1}{L} \sum_{\lambda_c \in \Lambda_c} P(V_c(\lambda_c)) \int_{V_c(\lambda_c)} \frac{\|x - \lambda_c\|^2}{\nu} dx, \tag{5.11}$$

where Λ_c is a lattice so all Voronoi cells are congruent and the integral is similar for all λ_c's. Hence, without loss of generality, we let $\lambda_c = 0$ and simplify (5.11) as

$$D_c \approx \frac{1}{L} \int_{V_c(0)} \frac{\|x\|^2}{\nu} dx, \tag{5.12}$$

where we used the fact that $\sum_{\lambda_c \in \Lambda_c} P(V_c(\lambda_c)) = 1$. We can express the average central distortion (5.12) in terms of the dimensionless normalized second moment of inertia $G(\Lambda_c)$ by

$$D_c \approx G(\Lambda_c) \nu^{2/L}. \tag{5.13}$$

Side Distortions

The side distortion for the ith description, i.e. the distortion when reconstructing using only the ith description, is given by [139]

$$
\begin{aligned}
D_i &= \frac{1}{L} \sum_{\lambda_c \in \Lambda_c} \int_{V_c(\lambda_c)} \|x - \alpha_i(\lambda_c)\|^2 f_X(x)dx, \quad i = 0, \dots, K-1, \\
&= \frac{1}{L} \sum_{\lambda_c \in \Lambda_c} \int_{V_c(\lambda_c)} \|x - \lambda_c + \lambda_c - \alpha_i(\lambda_c)\|^2 f_X(x)dx \\
&= \frac{1}{L} \sum_{\lambda_c \in \Lambda_c} \int_{V_c(\lambda_c)} \|x - \lambda_c\|^2 f_X(x)dx + \frac{1}{L} \sum_{\lambda_c \in \Lambda_c} \int_{V_c(\lambda_c)} \|\lambda_c - \alpha_i(\lambda_c)\|^2 f_X(x)dx \\
&\quad + \frac{2}{L} \sum_{\lambda_c \in \Lambda_c} \int_{V_c(\lambda_c)} \langle x - \lambda_c, \lambda_c - \alpha_i(\lambda_c) \rangle f_X(x)dx \\
&\approx D_c + \frac{1}{L} \sum_{\lambda_c \in \Lambda_c} \|\lambda_c - \alpha_i(\lambda_c)\|^2 P(\lambda_c)
\end{aligned}
$$

$$+ \frac{2}{L} \sum_{\lambda_c \in \Lambda_c} \left\langle \int_{V_c(\lambda_c)} x f_X(x) dx - \int_{V_c(\lambda_c)} \lambda_c f_X(x) dx, \lambda_c - \alpha_i(\lambda_c) \right\rangle$$

$$= D_c + \frac{1}{L} \sum_{\lambda_c \in \Lambda_c} \|\lambda_c - \alpha_i(\lambda_c)\|^2 P(\lambda_c), \tag{5.14}$$

where $P(\lambda_c)$ is the probability that X will be mapped to λ_c, i.e. $Q(X) = \lambda_c$, and the last equality follows since by use of (5.7) we have that

$$\int_{V_c(\lambda_c)} x f_X(x) dx - \int_{V_c(\lambda_c)} \lambda_c f_X(x) dx = 0. \tag{5.15}$$

We notice from (5.14) that independent of which labeling function we use, the distortion introduced by the central quantizer is orthogonal (under high-resolution assumptions) to the distortion introduced by the side quantizers.

Exploiting the shift-invariance property of the labeling function (5.4) makes it possible to simplify (5.14) as

$$D_i \approx D_c + \frac{1}{L} \sum_{\lambda_\pi \in \Lambda_\pi} \frac{P(\lambda_\pi)}{N^2} \sum_{\lambda_c \in V_\pi(0)} \|\lambda_c - \alpha_i(\lambda_c)\|^2$$

$$= D_c + \frac{1}{N^2} \frac{1}{L} \sum_{\lambda_c \in V_\pi(0)} \|\lambda_c - \alpha_i(\lambda_c)\|^2, \quad i = 0, \dots, K-1, \tag{5.16}$$

where we assume the region $V_\pi(0)$ is sufficiently small so $P(\lambda_c) \approx P(\lambda_\pi)/N^2$, for $\lambda_c \in V_\pi(\lambda_\pi)$. Notice that we assume $P(\lambda_\pi)$ to be constant only within each region $V_\pi(\lambda_\pi)$, hence it may take on different values for each $\lambda_\pi \in \Lambda_\pi$.

Central Rate

Let $R_c = H(Q(X))/L$ denote the minimum entropy (per dimension) needed for a single-description system to achieve an expected distortion of D_c, the central distortion of the multiple-description system as given by (5.13).

The single-description rate R_c is given by

$$R_c = -\frac{1}{L} \sum_{\lambda_c \in \Lambda_c} \int_{V_c(\lambda_c)} f_X(x) dx \, \log_2 \left(\int_{V_c(\lambda_c)} f_X(x) dx \right). \tag{5.17}$$

Using that each quantizer cell has identical volume ν and assuming that $f_X(x)$ is

approximately constant within Voronoi cells of the central lattice Λ_c, it follows that

$$
\begin{aligned}
R_c &\approx -\frac{1}{L} \sum_{\lambda_c \in \Lambda_c} \int_{V_c(\lambda_c)} f_X(x)dx \, \log_2 \left(f_X(\lambda_c)\nu \right) \\
&= -\frac{1}{L} \sum_{\lambda_c \in \Lambda_c} \int_{V_c(\lambda_c)} f_X(x)dx \, \log_2 \left(f_X(\lambda_c) \right) \\
&\quad -\frac{1}{L} \sum_{\lambda_c \in \Lambda_c} \int_{V_c(\lambda_c)} f_X(x)dx \, \log_2(\nu) \\
&= -\frac{1}{L} \sum_{\lambda_c \in \Lambda_c} \int_{V_c(\lambda_c)} f_X(x)dx \, \log_2 \left(f_X(\lambda_c) \right) - \frac{1}{L} \log_2(\nu) \\
&= \bar{h}(X) - \frac{1}{L} \log_2(\nu).
\end{aligned}
\tag{5.18}
$$

Side Rates

Let $R_i = H(\alpha_i(Q(X)))/L$ denote the entropy (per dimension) of the ith description, where $i = 0, \ldots, K-1$. Notice that in the symmetric situation we have $R_s = R_i, i \in \{0, \ldots, K-1\}$.

The side descriptions are based on a coarser lattice obtained by scaling (and possibly rotating) the Voronoi cells of the central lattice by a factor of N. Assuming the pdf of X is roughly constant within a sublattice cell, the entropy of the ith side description is given by

$$
\begin{aligned}
R_i &= -\frac{1}{L} \sum_{\lambda_i \in \Lambda_s} \left(\sum_{\lambda_c \in \alpha_i^{-1}(\lambda_i)} \int_{V_c(\lambda_c)} f_X(x)dx \, \log_2 \left(\sum_{\lambda_c \in \alpha_i^{-1}(\lambda_i)} \int_{V_c(\lambda_c)} f_X(x)dx \right) \right) \\
&= -\frac{1}{L} \sum_{\lambda_i \in \Lambda_s} \left(\sum_{\lambda_c \in \alpha_i^{-1}(\lambda_i)} \int_{V_c(\lambda_c)} f_X(x)dx \, \log_2 \left(\nu f_X(\lambda_i) N \right) \right) \\
&= -\frac{1}{L} \sum_{\lambda_i \in \Lambda_s} \left(\sum_{\lambda_c \in \alpha_i^{-1}(\lambda_i)} \int_{V_c(\lambda_c)} f_X(x)dx \, \log_2 \left(f_X(\lambda_i) \right) \right) \\
&\quad -\frac{1}{L} \sum_{\lambda_i \in \Lambda_s} \left(\sum_{\lambda_c \in \alpha_i^{-1}(\lambda_i)} \int_{V_c(\lambda_c)} f_X(x)dx \, \log_2(\nu N) \right) \\
&= \bar{h}(X) - \frac{1}{L} \log_2(N\nu).
\end{aligned}
$$

$$
\tag{5.19}
$$

The entropy of the side descriptions is related to the entropy of the single-description system by

$$
R_i = R_c - \frac{1}{L} \log_2(N).
\tag{5.20}
$$

5.3   Construction of Labeling Function

The index assignment is done by a labeling function α, that maps central lattice points to sublattice points. An optimal index assignment minimizes a cost functional when $0 < \kappa < K$ descriptions are received. In addition, the index assignment should be invertible so the central quantizer can be used when all descriptions are received. Before defining the labeling function we have to define the cost functional to be minimized. To do so, we first describe how to approximate the source sequence when receiving only κ descriptions and how to determine the expected distortion in that case. Then we define the cost functional to be minimized by the labeling function α and describe how to minimize it.

5.3.1   Expected Distortion

At the receiving side, $X \in \mathbb{R}^L$ is reconstructed to a quality that is determined only by the number of received descriptions. If no descriptions are received we reconstruct using the expected value, EX, and if all K descriptions are received we reconstruct using the inverse map $\alpha^{-1}(\lambda_0, \dots, \lambda_{K-1})$, hence obtaining the quality of the central quantizer.

In this work we use a simple reconstruction rule which applies for arbitrary sources.[36] When receiving $1 \leq \kappa < K$ descriptions we reconstruct using the average of the κ descriptions. We show later (Theorem 5.3.1) that using the average of received descriptions as reconstruction rule makes it possible to split the distortion due to reception of any number of descriptions into a sum of squared norms between pairs of lattice points. Moreover, this lead to the fact that the side quantizers' performances approach those of quantizers having spherical Voronoi cells. There are in general several ways of receiving κ out of K descriptions. Let $\mathscr{L}^{(K,\kappa)}$ denote an index set consisting of all possible κ combinations out of $\{0, \dots, K-1\}$. Hence $|\mathscr{L}^{(K,\kappa)}| = \binom{K}{\kappa}$. We denote an element of $\mathscr{L}^{(K,\kappa)}$ by $l = \{l_0, \dots, l_{\kappa-1}\} \in \mathscr{L}^{(K,\kappa)}$. Upon reception of any κ descriptions we reconstruct $\hat{X}$ using

$$\hat{X} = \frac{1}{\kappa} \sum_{j=0}^{\kappa-1} \lambda_{l_j}. \tag{5.21}$$

Our objective is to minimize some cost functional subject to entropy constraints on the description rates. We can, for example, choose to minimize the distortion when receiving any two out of three descriptions. Another choice is to minimize the weighted distortion over all possible description losses. In the following we will assume that the cost functional to be minimized is the expected weighted distortion

---

[36]We show in Chapter 7 that this simple reconstruction rule is, at high resolution, optimal in the quadratic Gaussian case, i.e. we show that the largest known three-channel MD region can be achieved in that case. This is in line with Ozarow's double-branch test-channel, where the optimum post filters are trivial at high resolution.

over all description losses and we further assume that the weights are given by the packet-loss probabilities. We discuss the case where the weights are allowed to be chosen almost arbitrarily in Chapter 6.

Assuming the packet-loss probabilities, say p, are independent and are the same for all descriptions, we may use (5.16) and write the expected distortion when receiving κ out K descriptions as

$$
D_a^{(K,\kappa)} \approx (1-p)^{\kappa} p^{K-\kappa} \times \left(\binom{K}{\kappa} D_c + \frac{1}{N^2} \frac{1}{L} \sum_{l \in \mathscr{L}^{(K,\kappa)}} \sum_{\lambda_c \in V_{\pi}(0)} \left\| \lambda_c - \frac{1}{\kappa} \sum_{j=0}^{\kappa-1} \lambda_{l_j} \right\|^2 \right),
$$
(5.22)

where $\lambda_{l_j} = \alpha_{l_j}(\lambda_c)$ and the two cases $\kappa \in \{0, K\}$, which do not involve the index-assignment map, are given by $D_a^{(K,0)} \approx p^K E \|X\|^2 / L$ and $D_a^{(K,K)} \approx (1-p)^K D_c$.

5.3.2   Cost Functional

From (5.22) we see that the distortion expression may be split into two terms, one describing the distortion occurring when the central quantizer is used on the source, and one that describes the distortion due to the index assignment. An optimal index assignment jointly minimizes the second term in (5.22) over all $1 \leq \kappa \leq K - 1$ possible descriptions. The cost functional $J^{(K)}$ to be minimized by the index assignment algorithm is then given by

$$
J^{(K)} = \sum_{\kappa=1}^{K-1} J^{(K,\kappa)},
$$
(5.23)

where

$$
J^{(K,\kappa)} = \frac{(1-p)^{\kappa} p^{K-\kappa}}{LN^2} \sum_{l \in \mathscr{L}^{(K,\kappa)}} \sum_{\lambda_c \in V_{\pi}(0)} \left\| \lambda_c - \frac{1}{\kappa} \sum_{j=0}^{\kappa-1} \lambda_{l_j} \right\|^2.
$$
(5.24)

The cost functional should be minimized subject to an entropy constraint on the side descriptions. We remark here that the side entropies depend solely on ν and N and as such not on the particular choice of K-tuples. In other words, for fixed N and ν the index assignment problem is solved if (5.23) is minimized. The problem of choosing ν and N such that the entropy constraint is satisfied is independent of the assignment problem and deferred to Section 5.4.2.

The following theorem makes it possible to rewrite the cost functional in a way that brings more insight into which K-tuples to use.[37]

---

[37]Notice that Theorem 5.3.1 is very general. We do not even require Λ_c or Λ_s to be lattices, in fact, they can be arbitrary sets of points.

Theorem 5.3.1. For $1 \leq \kappa \leq K$ we have

$$\sum_{l \in \mathscr{L}^{(K,\kappa)}} \sum_{\lambda_c} \left\| \lambda_c - \frac{1}{\kappa} \sum_{j=0}^{\kappa-1} \lambda_{l_j} \right\|^2 = \sum_{\lambda_c} \binom{K}{\kappa} \left(\left\| \lambda_c - \frac{1}{K} \sum_{i=0}^{K-1} \lambda_i \right\|^2 \right.$$
$$\left. + \left(\frac{K-\kappa}{K^2\kappa(K-1)} \right) \sum_{i=0}^{K-2} \sum_{j=i+1}^{K-1} \| \lambda_i - \lambda_j \|^2 \right).$$

Proof. See Appendix H.1.   □

From Theorem 5.3.1 it is clear that (5.24) can be written as

$$J^{(K,\kappa)} = \frac{(1-p)^\kappa p^{K-\kappa}}{LN^2} \binom{K}{\kappa} \left(\sum_{\lambda_c \in V_\pi(0)} \left\| \lambda_c - \frac{1}{K} \sum_{i=0}^{K-1} \lambda_i \right\|^2 \right.$$
$$\left. + \sum_{\lambda_c \in V_\pi(0)} \left(\frac{K-\kappa}{K^2\kappa(K-1)} \right) \sum_{i=0}^{K-2} \sum_{j=i+1}^{K-1} \| \lambda_i - \lambda_j \|^2 \right). \tag{5.25}$$

The first term in (5.25) describes the distance from a central lattice point to the centroid of its associated K-tuple. The second term describes the sum of pairwise squared distances (SPSD) between elements of the K-tuples. In Section 5.4 (by Proposition 5.4.2) we show that, under a high-resolution assumption, the second term in (5.25) is dominant, from which we conclude that in order to minimize (5.23) we have to choose the K-tuples with the lowest SPSD. These K-tuples are then assigned to central lattice points in such a way, that the first term in (5.25) is minimized.

Independent of the packet-loss probability, we always minimize the second term in (5.25) by using those K-tuples that have the smallest SPSD. This means that, at high resolution, the optimal K-tuples are independent of packet-loss probabilities and, consequently, the optimal assignment is independent[38] of the packet-loss probability.

5.3.3   Minimizing Cost Functional

In order to make sure that α is shift-invariant, a given K-tuple of sublattice reconstruction points is assigned to only one central lattice point $\lambda_c \in \Lambda_c$. Notice that two K-tuples which are translates of each other by some $\lambda_\pi \in \Lambda_\pi$ must not both be assigned to central lattice points located within the same region $V_\pi(\lambda_\pi)$, since this causes assignment of the same K-tuples to multiple central lattice points. The region $V_\pi(0)$ will be translated throughout $\mathbb{R}^L$ and centered at $\lambda_\pi \in \Lambda_\pi$, so there will be no overlap between neighboring regions, i.e. $V_\pi(\lambda'_\xi) \cap V_\pi(\lambda''_\xi) = \emptyset$, for $\lambda'_\xi, \lambda''_\xi \in \Lambda_\pi$ and $\lambda'_\xi \neq \lambda''_\xi$. One obvious way of avoiding assigning K-tuples to multiple central lattice points is

---

[38]Given the central lattice and the sublattice, the optimal assignment is independent of p. However, we show later that the optimal sublattice index N depends on p.

then to exclusively use sublattice points located within $V_\pi(0)$. However, sublattice points located close to but outside $V_\pi(0)$, might be better candidates than sublattice points within $V_\pi(0)$ when labeling central lattice points close to the boundary. A consistent way of constructing K-tuples, is to center a region $\tilde{V}$ at all sublattice points $\lambda_0 \in \Lambda_s \cap V_\pi(0)$, and construct K-tuples by combining sublattice points $\lambda_i \in \Lambda_s, i = 1, \ldots, K - 1$ within $\tilde{V}(\lambda_0)$ in all possible ways and select the ones that minimize (5.25). This is illustrated in Fig. 5.1. For a fixed $\lambda_i \in \Lambda_s$, the expression $\sum_{\lambda_j \in \Lambda_s \cap \tilde{V}(\lambda_i)} \|\lambda_i - \lambda_j\|^2$ is minimized when $\tilde{V}$ forms a sphere centered at λ_i. Our construction allows for $\tilde{V}$ to have an arbitrary shape, e.g. the shape of V_π which is the shape used for the two-description system presented in [28]. However, if $\tilde{V}$ is not chosen to be a sphere, the SPSD is in general not minimized.

For each $\lambda_0 \in \Lambda_s \cap V_\pi(0)$ it is possible to construct $\tilde{N}^{K-1}$ K-tuples, where $\tilde{N}$ is the number of sublattice points within the region $\tilde{V}$. This gives a total of $N\tilde{N}^{K-1}$ K-tuples when all $\lambda_0 \in \Lambda_s \cap V_\pi(0)$ are used. However, only N^2 central lattice points need to be labeled ($V_\pi(0)$ only contains N^2 central lattice points). When $K = 2$, we let $\tilde{N} = N$, so the number of possible K-tuples is equal to N^2, which is exactly the number of central lattice points in $V_\pi(0)$. In general, for $K > 2$, the volume $\tilde{\nu}$ of $\tilde{V}$ is smaller than the volume of $V_\pi(0)$ and as such $\tilde{N} < N$. We can approximate $\tilde{N}$ through the volumes ν_s and $\tilde{\nu}$, i.e. $\tilde{N} \approx \tilde{\nu}/\nu_s$. To justify this approximation let $\Lambda \subset \mathbb{R}^L$ be a real lattice and let $\nu = \det(\Lambda)$ be the volume of a fundamental region. Let $S(c, r)$ be a sphere in $\mathbb{R}^L$ of radius r and center $c \in \mathbb{R}^L$. According to Gauss' counting principle, the number $A_\mathbb{Z}$ of integer lattice points in a convex body $\mathscr{C}$ in $\mathbb{R}^L$ equals the volume $\text{Vol}(\mathscr{C})$ of $\mathscr{C}$ with a small error term [92]. In fact if $\mathscr{C} = S(c, r)$ then by use of a theorem due to Minkowski it can be shown that, for any $c \in \mathbb{R}^L$ and asymptotically as $r \to \infty$, $A_\mathbb{Z}(r) = \text{Vol}(S(c, r)) = \omega_L r^L$, where ω_L is the volume of the L-dimensional unit sphere [40], see also [11, 33, 62, 77, 144]. It is also known that the number of lattice points $A_\Lambda(n)$ in the first n shells of the lattice Λ satisfies, asymptotically as $n \to \infty$, $A_\Lambda(n) = \omega_L n^{L/2}/\nu$ [139]. Hence, based on the above we approximate the number of lattice points in $\tilde{V}$ by $\tilde{\nu}/\nu_s$, which is an approximation that becomes exact as the number of shells n within $\tilde{V}$ goes to infinity[39] (which corresponds to $N \to \infty$). Our analysis is therefore only exact in the limiting case of $N \to \infty$. With this we can lower bound $\tilde{\nu}$ by

$$\lim_{N \to \infty} \tilde{\nu} \geq \nu_s N^{1/(K-1)}. \tag{5.26}$$

Hence, $\tilde{V}$ contains $\tilde{N} \geq N^{1/(K-1)}$ sublattice points so that the total number of possible K-tuples is $N\tilde{N}^{K-1} \geq N^2$.

In Fig. 5.1 is shown an example of $\tilde{V}$ and V_π regions for the two-dimensional Z^2 lattice. In the example we used $K = 3$ and $N = 25$, hence there are 25 sublattice

---

[39]For the high-resolution analysis given in Section 5.4 it is important that $\tilde{\nu}$ is kept small as the number of lattice points within $\tilde{V}$ goes to infinity. This is easily done by proper scaling of the lattices, i.e. making sure that $\nu_s \to 0$ as $N \to \infty$.

points within V_π. There are $\tilde{N} = N^{1/(K-1)} = 5$ sublattice points in $\tilde{V}$ which is exactly the minimum number of points required, according to (5.26).
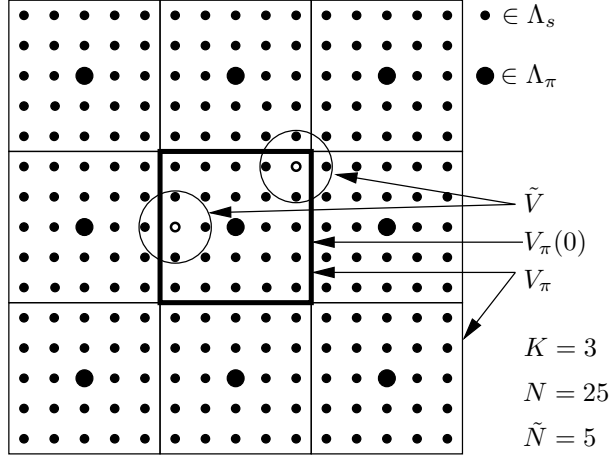

Figure 5.1: *The region $\tilde{V}$ (big circles) is here shown centered at two different sublattice points within $V_\pi(0)$. Small dots represents sublattice points of Λ_s and large dots represents product lattice points $\lambda_\pi \in \Lambda_\pi$. Central lattice points are not shown here. V_π (shown as squares) contains 25 sublattice points centered at product lattice points. In this example $\tilde{V}$ contains 5 sublattice points.*

With equality in (5.26) we obtain a region that contains the exact number of sublattice points required to construct N tuples for each of the N λ_0 points in $V_\pi(0)$. According to (5.25), a central lattice point should be assigned that K-tuple where a weighted average of any subset of the elements of the K-tuple is as close as possible to the central lattice point. The optimal assignment of K-tuples to central lattice points can be formulated and solved as a linear assignment problem [151].

Shift-Invariance by use of Cosets

By centering $\tilde{V}$ around each $\lambda_0 \in \Lambda_s \cap V_\pi(0)$, we make sure that the map α is shift-invariant. However, this also means that all K-tuples have their first coordinate (i.e. λ_0) inside $V_\pi(0)$. To be optimal this restriction must be removed which is easily done by considering all cosets of each K-tuple. The coset of a fixed K-tuple, say $t = (\lambda_0, \lambda_1, \ldots, \lambda_{K-1})$ where $\lambda_0 \in \Lambda_s \cap V_\pi(0)$ and $(\lambda_1, \ldots, \lambda_{K-1}) \in \Lambda_s^{K-1}$, is given by $\text{Coset}(t) = \{t + \lambda_\pi : \forall \lambda_\pi \in \Lambda_\pi\}$. K-tuples in a coset are distinct modulo Λ_π and by making sure that only one member from each coset is used, the shift-invariance property is preserved. In general it is sufficient to consider only those λ_π product lattice points that are close to $V_\pi(0)$, e.g. those points whose Voronoi cell touches $V_\pi(0)$. The number of such points is given by the kissing-number $\mathfrak{K}(\Lambda_\pi)$ of

the particular lattice [22].

Dimensionless Expansion Factor ψ_L

Centering $\tilde{V}$ around λ_0 points causes a certain asymmetry in the pairwise distances of the elements within a K-tuple. Since the region is centered around λ_0 the maximum pairwise distances between λ_0 and any other sublattice point will always be smaller than the maximum pairwise distance between any two sublattice points not including λ_0. This can be seen more clearly in Fig. 5.2. Notice that the distance between the pair of points labeled (λ_1, λ_2) is twice the distance of that of the pair (λ_0, λ_1) or (λ_0, λ_2). However, by slightly increasing the region $\tilde{V}$ to also include λ_2' other tuples may be made, which actually have a lower pairwise distance than the pair (λ_1, λ_2). For this particular example, it is easy to see that the 3-tuple $t = (\lambda_0, \lambda_1, \lambda_2)$ has a greater SPSD than the 3-tuple $t' = (\lambda_0, \lambda_1, \lambda_2')$.
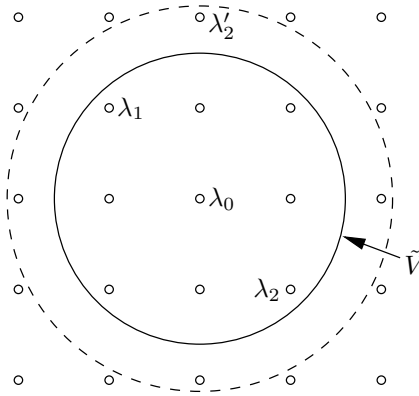
Figure 5.2: *The region $\tilde{V}$ is here centered at the point λ_0. Notice that the distance between λ_1 and λ_2 is about twice the maximum distance from λ_0 to any point in $\Lambda_s \cap \tilde{V}$. The dashed circle illustrates an enlargement of $\tilde{V}$.*

For each $\lambda_0 \in V_\pi(0)$ we center a region $\tilde{V}$ around the point, and choose those N K-tuples, that give the smallest SPSD. By expanding $\tilde{V}$ new K-tuples can be constructed that might have a lower SPSD than the SPSD of the original N K-tuples. However, the distance from λ_0 to the points farthest away increases as $\tilde{V}$ increases. Since we only need N K-tuples, it can be seen that $\tilde{V}$ should never be larger than twice the lower bound in (5.26) because then the distance from the center to the boundary of the enlarged $\tilde{V}$ region is greater than the maximum distance between any two points in the $\tilde{V}$ region that reaches the lower bound. In order to theoretically describe the performance of the quantizers, we introduce a dimensionless expansion factor $1 \leq \psi_L < 2$ which describes how much $\tilde{V}$ must be expanded from the theoretical lower

bound (5.26), to make sure that N optimal K-tuples can be constructed by combining sublattice points within a region $\tilde{V}$.

For the case of $K = 2$ we always have $\psi_L = 1$ independent of the dimension L so it is only in the case $K \geq 3$ that we need to find expressions for ψ_L.

Theorem 5.3.2. For the case of $K = 3$ and any odd L, the dimensionless expansion factor is given by

$$\psi_L = \left(\frac{\omega_L}{\omega_{L-1}} \right)^{1/2L} \left(\frac{L+1}{2L} \right)^{1/2L} \beta_L^{-1/2L}, \tag{5.27}$$

where ω_L is the volume of an L-dimensional unit sphere and β_L is given by

$$
\begin{aligned}
\beta_L = \sum_{n=0}^{\frac{L+1}{2}} \binom{\frac{L+1}{2}}{n} 2^{\frac{L+1}{2}-n}(-1)^n \sum_{k=0}^{\frac{L-1}{2}} \frac{\left(\frac{L+1}{2}\right)_k \left(\frac{1-L}{2}\right)_k}{\left(\frac{L+3}{2}\right)_k k!} \\
\times \sum_{j=0}^{k} \binom{k}{j} \left(\frac{1}{2}\right)^{k-j} (-1)^j \left(\frac{1}{4}\right)^j \frac{1}{L+n+j}.
\end{aligned}
\tag{5.28}
$$

Proof. See Appendix H.2.   □

For the interesting case of $L \to \infty$ we have the following theorem.

Theorem 5.3.3. For $K = 3$ and $L \to \infty$ the dimensionless expansion factor ψ_L is given by

$$\psi_\infty = \left(\frac{4}{3} \right)^{1/4}. \tag{5.29}$$

Proof. See Appendix H.3.   □

Table 5.1 lists[40] ψ_L for $K = 3$ and different values of L and it may be noticed that $\psi_\infty = \sqrt{\psi_1}$.

Remark 5.3.1. In order to extend these results to $K > 3$ it follows from the proof of Theorem 5.3.2 that we need closed-form expressions for the volumes of all the different convex regions that can be obtained by $K - 1$ overlapping spheres. With such expressions it should be straightforward to find ψ_L for any K. However, the analysis of ψ_L for the case of $K = 3$ (as given in the proof of Theorem 5.3.2) is constructive in the sense that it reveals how ψ_L can be numerically estimated for any K and L, see Appendix F.

Remark 5.3.2. In order to achieve the shift-invariance property of the index-assignment algorithm, we impose a restriction upon λ_0 points. Specifically, we require that $\lambda_0 \in V_\pi(0)$ so that the first coordinate of any K-tuple is within the region $V_\pi(0)$.

---

[40]Theorem 5.3.2 is only valid for L odd. However, in the proof of Theorem 5.3.2 it is straightforward to replace the volume of spherical caps by standard expressions for circle cuts in order to obtain ψ_2.

L	ψ_L	L	ψ_L
1	$1.1547005\cdots$	15	$1.1036412\cdots$
2	$1.1480804\cdots$	17	$1.1016878\cdots$
3	$1.1346009\cdots$	19	$1.1000271\cdots$
5	$1.1240543\cdots$	21	$1.0985938\cdots$
7	$1.1172933\cdots$	51	$1.0883640\cdots$
9	$1.1124896\cdots$	71	$1.0855988\cdots$
11	$1.1088540\cdots$	101	$1.0831849\cdots$
13	$1.1059819\cdots$	∞	$1.0745699\ldots$

Table 5.1: ψ_L *values obtained by use of Theorems 5.3.2 and 5.3.3 for $K = 3$.*

To avoid excluding K-tuples that have their first coordinate outside $V_\pi(0)$ we form cosets of each K-tuple and allow only one member from each coset to be assigned to a central lattice point within $V_\pi(0)$. This restriction, which is only put on $\lambda_0 \in \Lambda_s$, might cause a bias towards λ_0 points. However, it is easy to show that, asymptotically as $N \to \infty$, any such bias can be removed. For the case of $K = 2$ we can use similar arguments as used in [28], and for $K > 2$, as shown in Chapter 6, the number of K-tuples affected by this restriction is small compared to the number of K-tuples not affected. So for example this means that we can enforce similar restrictions on all sublattice points, which, asymptotically as $N \to \infty$, will only reduce the number of K-tuples by a neglectable amount. And as such, any possible bias towards the set of points $\lambda_0 \in \Lambda_s$ is removed.

As mentioned above, the K-tuples need to be assigned to central lattice points within $V_\pi(0)$. This is a standard linear assignment problem where a cost measure is minimized. However, solutions to linear assignment problems are generally not unique. Therefore, there might exist several labelings, which all yield the same cost, but exhibit a different amount of asymmetry. Theoretically, exact symmetry may then be obtained by e.g. time sharing through a suitable mixing of labelings. In practice, however, any scheme would use a finite N (and finite rates). In addition, for many applications, time sharing is inconvenient. In these non-asymptotic cases we cannot guarantee exact symmetry. To this end, we have provided a few examples that assess the distortions obtained from practical experiments, see Section 5.6 (Tables 5.3 and 5.4).

5.4   High-Resolution Analysis

In this section we derive high-resolution approximations for the expected distortion. For this high-resolution analysis we let $N \to \infty$ and $\nu_s \to 0$. Thus, the index N of the sublattices increases, but the actual volumes of the Voronoi cells shrink.

5.4.1   Total Expected Distortion

We wish to obtain an analytical expression for the expected distortion given by (5.22). In order to achieve this we first relate the sum of distances between pairs of sublattice points to $G(S_L)$, the dimensionless normalized second moment of an L-sphere. This is done by Proposition 5.4.1.

Proposition 5.4.1. For $K = 2$ and asymptotically as $N \to \infty$ and $\nu_s \to 0$, as well as for $K = 3$ and asymptotically as $N, L \to \infty$ and $\nu_s \to 0$, we have for any pair (λ_i, λ_j), $i, j = 0, \ldots, K - 1$, $i \neq j$,

$$\frac{1}{L} \sum_{\lambda_c \in V_\pi(0)} \|\alpha_i(\lambda_c) - \alpha_j(\lambda_c)\|^2 = G(S_L)\psi_L^2 N^2 N^{2K/L(K-1)}\nu^{2/L}.$$

Proof. See Appendix H.4.   □

Conjecture 5.4.1. Proposition 5.4.1 is true also for $K > 3$ asymptotically as $N, L \to \infty$ and $\nu_s \to 0$.

Remark 5.4.1. Arguments supporting conjecture 5.4.1 are given in Appendix H.4.

Remark 5.4.2. In Appendix H.4 we also present an exact expression for Proposition 5.4.1 for $K = 3$ and finite L.

   Recall that we previously showed that by use of Theorem 5.3.1 it is possible to split (5.22) into two terms; one that describes the distance from a central lattice point to the centroid of its associated K-tuple and another which describes the sum of pairwise squared distances (SPSD) between elements of the K-tuples. To determine which of the two terms that are dominating we present the following proposition:

Proposition 5.4.2. For $N \to \infty$ and $2 \leq K < \infty$ we have

$$\frac{\sum_{\lambda_c \in V_\pi(0)} \left\| \lambda_c - \frac{1}{K} \sum_{i=0}^{K-1} \lambda_i \right\|^2}{\sum_{\lambda_c \in V_\pi(0)} \sum_{i=0}^{K-2} \sum_{j=i+1}^{K-1} \|\lambda_i - \lambda_j\|^2} \to 0. \tag{5.30}$$

Proof. See Appendix H.5.   □

   The expected distortion (5.22) can by use of Theorem 5.3.1 be written as

$$D_a^{(K,\kappa)} \approx (1-p)^\kappa p^{K-\kappa} \times \left(\binom{K}{\kappa} D_c + \frac{1}{L}\frac{1}{N^2} \sum_{l \in \mathscr{L}^{(K,\kappa)}} \sum_{\lambda_c \in V_\pi(0)} \left\| \lambda_c - \frac{1}{\kappa} \sum_{j=0}^{\kappa-1} \lambda_{l_j} \right\|^2 \right)$$

$$= (1-p)^\kappa p^{K-\kappa} \binom{K}{\kappa} \times \left(D_c + \frac{1}{L}\frac{1}{N^2} \sum_{\lambda_c \in V_\pi(0)} \left(\left\| \lambda_c - \frac{1}{K} \sum_{i=0}^{K-1} \lambda_i \right\|^2 \right. \right.$$

$$\left. \left. + \left(\frac{K-\kappa}{K^2\kappa(K-1)} \right) \sum_{i=0}^{K-2} \sum_{j=i+1}^{K-1} \|\lambda_i - \lambda_j\|^2 \right) \right).$$

$$\tag{5.31}$$

By use of Proposition 5.4.1 (as an approximation that becomes exact for $L \to \infty$), Proposition 5.4.2 and Eq. (5.13) it follows that (5.31) can be written as

$$
D_a^{(K,\kappa)} \approx (1-p)^\kappa p^{K-\kappa} \binom{K}{\kappa}
$$

$$
\times \left(D_c + \frac{1}{L}\frac{1}{N^2} \sum_{\lambda_c \in V_\pi(0)} \left(\frac{K-\kappa}{K^2 \kappa (K-1)} \right) \sum_{i=0}^{K-2} \sum_{j=i+1}^{K-1} \|\lambda_i - \lambda_j\|^2 \right) \quad (5.32)
$$

$$
\approx (1-p)^\kappa p^{K-\kappa} \binom{K}{\kappa}
$$

$$
\times \left(G(\Lambda_c)\nu^{2/L} + \left(\frac{K-\kappa}{2K\kappa} \right) G(S_L)\psi_L^2 N^{2K/L(K-1)}\nu^{2/L} \right). \quad (5.33)
$$

The second term in (5.33), that is

$$
\left(\frac{K-\kappa}{2K\kappa} \right) G(S_L)\psi_L^2 N^{2K/L(K-1)}\nu^{2/L} \quad (5.34)
$$

is the dominating term for $\kappa < K$ and $N \to \infty$ and describes the side distortion due to reception of any $\kappa < K$ descriptions. Observe that this term is only dependent upon κ through the coefficient $\frac{K-\kappa}{2K\kappa}$.

The total expected distortion $D_a^{(K)}$ is obtained from (5.33) by summing over κ including the cases where $\kappa = 0$ and $\kappa = K$, which leads to

$$
D_a^{(K)} \approx \hat{K}_1 G(\Lambda_c)\nu^{2/L} + \hat{K}_2 G(S_L)\psi_L^2 N^{2K/L(K-1)}\nu^{2/L} + p^K E\|X\|^2/L, \quad (5.35)
$$

where $\hat{K}_1$ is given by

$$
\hat{K}_1 = \sum_{\kappa=1}^K \binom{K}{\kappa} p^{K-\kappa}(1-p)^\kappa
$$

$$
= 1 - p^K, \quad (5.36)
$$

and $\hat{K}_2$ is given by

$$
\hat{K}_2 = \sum_{\kappa=1}^K \binom{K}{\kappa} p^{K-\kappa}(1-p)^\kappa \frac{K-\kappa}{2\kappa K}. \quad (5.37)
$$

Using (5.18) and (5.19) we can write ν and N as a function of differential entropy and side entropies, that is

$$
\nu^{2/L} = 2^{2(\bar{h}(X)-R_c)}, \quad (5.38)
$$

and

$$
N^{2K/L(K-1)} = 2^{\frac{2K}{K-1}(R_c-R_s)}, \quad (5.39)
$$

where $R_s = R_i, i = 0, \ldots, K - 1$ denotes the side description rate. Inserting (5.38) and (5.39) in (5.35) makes it possible to write the expected distortion as a function of entropies

$$
\begin{aligned}
D_a^{(K)} \approx{} & \hat{K}_1 G(\Lambda_c) 2^{2(\bar{h}(X) - R_c)} \\
& + \hat{K}_2 \psi_L^2 G(S_L) 2^{2(\bar{h}(X) - R_c)} 2^{\frac{2K}{K-1}(R_c - R_s)} + p^K E\|X\|^2 / L,
\end{aligned}
\tag{5.40}
$$

where we see that the distortion due to the side quantizers depends only upon the scaling (and dimension) of the sublattice but not upon which sublattice is used. Thus, the side distortions can be expressed through the dimensionless normalized second moment of a sphere.

5.4.2   Optimal ν, N and K

We now derive expressions for the optimal ν, N and K. Using these values we are able to construct the lattices Λ_c and Λ_s. The optimal index assignment is hereafter found by using the approach outlined in Section 5.3. These lattices combined with their index assignment completely specify an optimal entropy-constrained MD-LVQ system.

In order for the entropies of the side descriptions to be equal to the target entropy R_T/K, we rewrite (5.19) and get

$$
N\nu = 2^{L(\bar{h}(X) - R_T/K)} \triangleq \tau,
\tag{5.41}
$$

where τ is constant. The expected distortion $D_a^{(K)}$ (5.40) may now be expressed as a function of ν,

$$
\begin{aligned}
D_a^{(K)} ={} & \hat{K}_1 G(\Lambda_c) \nu^{2/L} \\
& + \hat{K}_2 \psi_L^2 G(S_L) \nu^{2/L} \nu^{-\frac{2K}{L(K-1)}} \tau^{\frac{2K}{L(K-1)}} + p^K E\|X\|^2 / L.
\end{aligned}
\tag{5.42}
$$

Differentiating w.r.t. ν and equating to zero gives,

$$
\begin{aligned}
0 ={} & \frac{\partial D_a^{(K)}}{\partial \nu} \\
={} & \frac{2}{L} \hat{K}_1 G(\Lambda_c) \frac{\nu^{2/L}}{\nu} + \left(\frac{2}{L} - \frac{2}{L} \frac{K}{K-1} \right) \hat{K}_2 \psi_L^2 G(S_L) \frac{\nu^{2/L}}{\nu} \nu^{-\frac{2K}{L(K-1)}} \tau^{\frac{2K}{L(K-1)}},
\end{aligned}
\tag{5.43}
$$

from which we obtain the optimal value of ν

$$
\nu = \tau \left(\frac{1}{K-1} \frac{\hat{K}_2}{\hat{K}_1} \frac{G(S_L)}{G(\Lambda_c)} \psi_L^2 \right)^{\frac{L(K-1)}{2K}}.
\tag{5.44}
$$

The optimal N follows easily by use of (5.41)

$$N = \left((K-1)\frac{\hat{K}_1}{\hat{K}_2}\frac{G(\Lambda_c)}{G(S_L)}\frac{1}{\psi_L^2} \right)^{\frac{L(K-1)}{2K}}. \tag{5.45}$$

Eq. (5.45) shows that the optimal redundancy N is, for fixed K, independent of the sublattice as well as the target entropy.

For a fixed K the optimal ν and N are given by (5.44) and (5.45), respectively, and the optimal K can then easily be found by evaluating (5.35) for various values of K, and choosing the one that yields the lowest expected distortion. The optimal K is then given by

$$K_{\text{opt}} = \arg \min_K D_a^{(K)}, \quad K = 1, \ldots, K_{\text{max}}, \tag{5.46}$$

where K_{max} is a suitable chosen positive integer. In practice K will always be finite and furthermore limited to a narrow range of integers, which makes the complexity of the minimization approach, given by (5.46), negligible.

5.5   Construction of Practical Quantizers

5.5.1   Index Values

Eqs. (5.44) and (5.45) suggest that we are able to continuously trade off central versus side-distortions by adjusting N and ν according to the packet-loss probability. This is, however, not the case, since certain constraints must be imposed on N. First of all, since N denotes the number of central lattice points within each Voronoi cell of the sublattice, it must be integer and positive. Second, we require the sublattice to be geometrically similar to the central lattice. Finally, we require the sublattice to be a clean sublattice, so that no central lattice points are located on boundaries of Voronoi cells of the sublattice. This restricts the amount of admissible index values for a particular lattice to a discrete set, cf. Section 2.3.1.

Fig. 5.3 shows the theoretically optimal index values (i.e. ignoring the fact that N belongs to a discrete set) for the A_2 quantizer, given by (5.45) for $\psi_L = 1, 1.1481$ and 1.1762 corresponding to $K = 2, 3$ and 4, respectively.[41] Also shown are the theoretical optimal index values when restricted to admissible index values. Notice that the optimal index value N increases for increasing number of descriptions. This is to be expected since a higher index value leads to less redundancy; this redundancy reduction, however, is balanced out by the redundancy increase resulting from the added number of descriptions. In [103] we observed that for a two-description system, usually only very few index values would be used (assuming a certain minimum packet-loss probability). Specifically, for the two-dimensional A_2 quantizer, only

---

[41]The value $\psi_L = 1.1762$ for $K = 4$ is estimated numerically by using the method outlined in Appendix F.
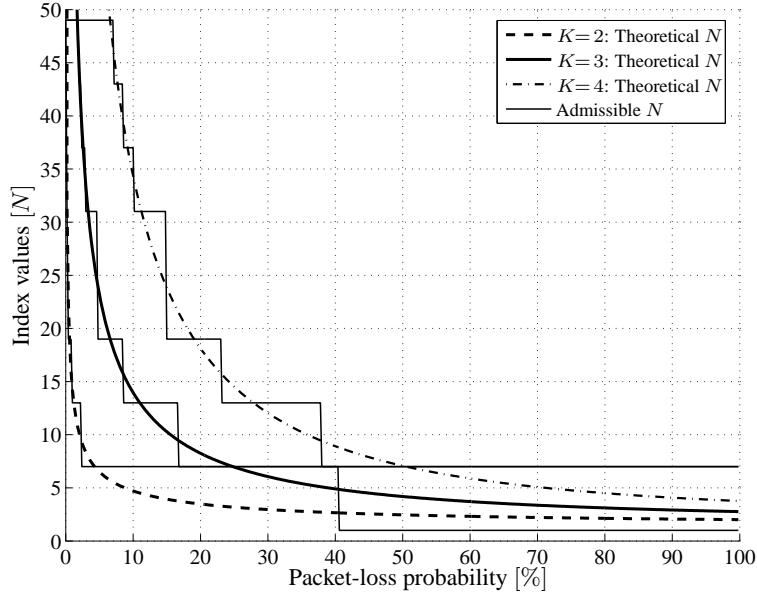
Figure 5.3: *Theoretical optimal index values for the A_2 quantizer as a function of the packet-loss probability. The thin solid lines are obtained by restricting the theoretical optimal index values given by (5.45) to be (optimal) admissible values given by the set $N = \{1, 7, 13, 19, 31, 37, 43, 49, \dots\}$. The optimal admissible index values are those that minimize (5.35) for a given p.*

$N \in \{1, 7, 13\}$ was used, while for higher dimensional quantizers greater index values would be used. However, here we see that by increasing the number of descriptions beyond $K = 2$, it is optimal to use greater index values which adds more flexibility to the scheme.

From Fig. 5.3 it can be seen that when the continuous optimal index value is rounded to the optimal admissible index value it is always the closest one from either below or above. This means that, at least for the A_2 lattice, the optimal admissible index value is found by considering only the two values closest to the continuous index value, and using the one that minimizes (5.35).

5.5.2   Constructing K-tuples

The design procedure for constructing K-tuples as described in Section 5.3.3 can be summarized as follows:

1. Center a sphere $\tilde{V}$ at each $\lambda_0 \in \Lambda_s \cap V_\pi(0)$ and construct all possible K-tuples $(\lambda_0, \dots, \lambda_{K-1})$ where $\lambda_i \in \Lambda_s, i = 1, \dots, K - 1$. This makes sure that all K-tuples have their first coordinate (λ_0) inside $V_\pi(0)$ and they are therefore

shift invariant. We will only use K-tuples whose elements satisfy $\|\lambda_i - \lambda_j\| \leq r, \forall i, j \in \{0, \ldots, K - 1\}$, where r is the radius of $\tilde{V}$. Make $\tilde{V}$ large enough so that at least N distinct K-tuples are found for each λ_0.

2. Construct cosets of each K-tuple.

3. The N^2 central lattice points in $\Lambda_c \cap V_\pi(0)$ must now be matched to distinct K-tuples. This is a standard linear assignment problem where only one member from each coset is (allowed to be) matched to a central lattice point in $V_\pi(0)$.

The restriction $\|\lambda_i - \lambda_j\| \leq r$ from step 1) which is used to avoid bias towards any of the sublattices, reduces the number of K-tuples that can be constructed within the sphere $\tilde{V}$. To be able to form N K-tuples it is therefore necessary to use a sphere $\tilde{V}$ with a volume larger than the lower bound (5.26). This enlargement is exactly given by ψ_L. As such, for each λ_0, we form (at least) N K-tuples and these K-tuples are the ones having minimum norm. We show later (see Lemma 6.2.3 and its proof) that we actually form all such K-tuples of minimal norm which implies that no other K-tuples can improve the SPSD.

5.5.3   Assigning K-Tuples to Central Lattice Points

In order to assign the set of K-tuples to the N^2 central lattice points we solve a linear assignment problem. However, for large N, the problem becomes difficult to solve in practice. To solve a linear assignment problem or more specifically a bipartite matching problem, one can make use of the Hungarian method [78], which has complexity of cubic order. Hence, if the Hungarian method is used to solve the assignment problem the complexity is of order $O(N^6)$. We would like point out that letting $N_\pi = N^2$ is a convenient choice, which is valid for any lattice. However, it is possible to let $N_\pi = N\xi$, where both N and ξ are admissible index values. In this case N_π is also guaranteed to be an admissible index value by Lemma 2.3.1. If $\xi = 1$ then $N_\pi = N$, which is a special case where $V_\pi(0)$ contains a single sublattice point λ_0 of Λ_s.[42] With $N_\pi = N\xi$, the complexity is reduced to $\mathcal{O}(N^3)$.

Vaishampayan et al. observed in [120,139] that the number of central lattice points to be labeled can be reduced by exploiting symmetries in the lattices. For example, one can form the quotient $\mathscr{J}$-module Λ/Λ_π and only label representatives of the orbits of $\Lambda/\Lambda_\pi/\Gamma$, where Γ is a group of automorphisms, cf. Chapter 2. While only two descriptions were considered in [139] it is straight-forward to show that their idea also works in our design for an arbitrary number of descriptions. This is because

---

[42]Practical experiments have shown that having too few sublattice points in $V_\pi(0)$ leads to a poor index assignment. Theoretically, we do not exclude the possibility that $N_\pi = N$, since we only require that $\tilde{V}$ contains a large number of sublattice points but such a contraint is not imposed on $V_\pi(0)$. However, in the following chapter, where we consider the asymmetric case (so there are several index values), the special case is not allowed.

we design the sublattices and product lattices as described in Chapter 2, hence the notion of quotient modules and group action are well defined. Since the order of the group Γ depends on the lattices but is independent of N, the complexity reduction by exploiting the symmetry of the quotient module is a constant multiplicative factor which disappears in the order notation.

Alternatively, Huang and Wu [65] recently showed that for certain low dimensional lattices it is possible to avoid the linear assignment problem by applying a greedy algorithm, without sacrificing optimality. The complexity of the greedy approach is on the order of $\mathcal{O}(N)$, which is a substantial improvement for large N.

In the present work we show that the assignment problem can always be posed and solved as a bipartite matching problem. This holds for any lattice in any dimension and it also holds in the asymmetric case to be discussed in Chapter 6. In a practical situation it might, however, be convenient to compute the assignments offline and tabulate for further use.

5.5.4   Example of an Assignment

In the following we show a simple assignment for the case of $K = 2, N = 7$ and the A_2 lattice. Since $N = 7$ we have $N_\pi = 49$ and as such there is 49 central lattice points within $V_\pi(0)$, see Fig. 5.4. The individual assignments are also shown in Table 5.2.

The assignments shown in Table 5.2 are obtained by using the procedure outlined in Section 5.5.2. Since we have $N_\pi = 49$ and $K = 2$ it follows that we have 7 sublattice points of Λ_s within $V_\pi(0)$ (one of them is the origin). Let us denote this set of sublattice points by E_{Λ_s}.

1. Center a sphere $\tilde{V}$ at the first element of E_{λ_s}, i.e. the origin. Pick the candidate sublattice points of Λ_s, i.e. those which are contained within $\tilde{V} \cap \Lambda_s$. We make sure that the radius of the sphere is so large that it contains $V_\pi(0)$. Thus, we have at least as many sublattice points in $\tilde{V}$ as in $V_\pi(0)$. Then form all possible distinct edges (2-tuples) having the origin (λ_0) as first coordinate and $\lambda_1 \in V_\pi(\lambda_0) \cap \Lambda_s$ as second coordinate. Notice that we have at least N edges. Repeat this for the remaining elements of E_{Λ_s} so that we end up having at least N_π edges in total.

2. Form the coset of each edge. Specifically, construct the following set of edges:

$$\mathrm{Coset}(\lambda_0, \lambda_1) = \{(\lambda_0 + \lambda_\pi, \lambda_1 + \lambda_\pi) : \lambda_\pi \in \Lambda_\pi\}. \qquad (5.47)$$

In practice we restrict each coset to contain a finite number of elements. In fact, we usually only require that the cardinality of the cosets is greater than $\mathfrak{K}(\Lambda_s)$, the kissing number of the lattice. The product lattice points we use when constructing the cosets are then the $\mathfrak{K}(\Lambda_s) + 1$ points of smallest norm.
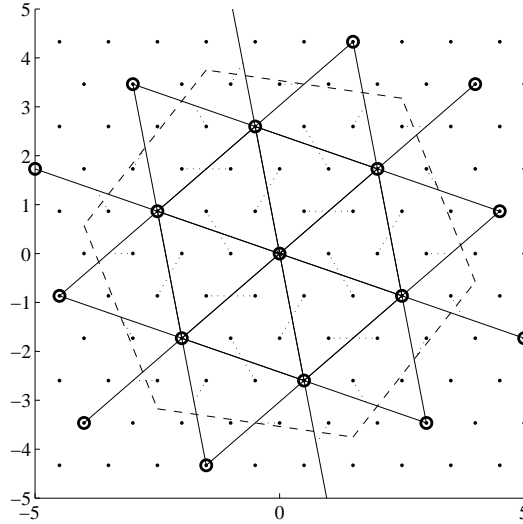
Figure 5.4: *A central lattice Λ_c (dots) based on the A_2 lattice and a sublattice Λ_s (circles) of index 7. The hexagonal region (dashed lines) describes $V_\pi(0)$. The solid lines connect pairs of sublattice points (also called 2-tuples or edges) and the dotted lines connect each edge to a central lattice point. A total of 49 edges (some overlaping each other) are shown and these edges are associated with the 49 central lattice points contained within $V_\pi(0)$.*

3. If we have more edges than central lattice points we introduce "dummy" central lattice points. In this way we have an equal amount of edges and central lattice points. The assignment of edges to central lattice points is now a straight forward bipartite problem, where the costs of the dummy nodes are set to zero, so that the optimal solutions are not affected. We note that only one element of each coset is used. In this way we preserve the shift invariance property of the assignments. We only keep the N_π assignments belonging to *true* central lattice points and as such we discard the assignments (if any) that belong to "dummy" nodes.

In Appendix G we show part of a complete assignment of a more complicated example.

5.6   Numerical Results

In this section we compare the numerical performances of two-dimensional entropy-constrained MD-LVQ (based on the A_2 lattice) to their theoretical prescribed performances.

λ_c	λ_0	λ_1	λ_c	λ_0	λ_1
(-1, 3.46)	(-1, 5.2)	(-0.5, 2.6)	(0, 0)	(0, 0)	(0, 0)
(0, 3.46)	(1.5, 4.33)	(-0.5, 2.6)	(1, 0)	(2.5, -0.87)	(0, 0)
(-1.5, 2.6)	(-3, 3.46)	(-0.5, 2.6)	(2, 0)	(2, 1.73)	(2.5, -0.87)
(-0.5, 2.6)	(-0.5, 2.6)	(-0.5, 2.6)	(3, 0)	(4.5, 0.87)	(2.5, -0.87)
(0.5, 2.6)	(2, 1.73)	(-0.5, 2.6)	(-2.5, -0.87)	(-2.5, 0.87)	(-2, -1.73)
(1.5, 2.6)	(1.5, 4.33)	(2, 1.73)	(-1.5, -0.87)	(-2, -1.73)	(0, 0)
(2.5, 2.6)	(4, 3.46)	(2, 1.73)	(-0.5, -0.87)	(0,0)	(-2, -1.73)
(-3, 1.73)	(-3, 3.46)	(-2.5, 0.87)	(0.5, -0.87)	(0.5, -2.6)	(0, 0)
(-2, 1.73)	(-2.5, 0.87)	(-0.5, 2.6)	(1.5, -0.87)	(0,0)	(2.5, -0.87)
(-1, 1.73)	(-0.5, 2.6)	(-2.5, 0.87)	(2.5, -0.87)	(2.5, -0.87)	(2.5, -0.87)
(0, 1.73)	(0, 0)	(-0.5, 2.6)	(3.5, -0.87)	(5, -1.73)	(2.5, -0.87)
(1, 1.73)	(-0.5, 2.6)	(2, 1.73)	(-3, -1.73)	(-4.5, -0.87)	(-2, -1.73)
(2, 1.73)	(2, 1.73)	(2, 1.73)	(-2, -1.73)	(-2, -1.73)	(-2, -1.73)
(3, 1.73)	(4.5, 0.87)	(2, 1.73)	(-1, -1.73)	(0.5, -2.6)	(-2, -1.73)
(-3.5, 0.87)	(-5, 1.73)	(-2.5, 0.87)	(0, -1.73)	(0, 0)	(0.5, -2.6)
(-2.5, 0.87)	(-2.5, 0.87)	(-2.5, 0.87)	(1, -1.73)	(0.5, -2.6)	(2.5, -0.87)
(-1.5, 0.87)	(0, 0)	(-2.5, 0.87)	(2, -1.73)	(2.5, -0.87)	(0.5, -2.6)
(-0.5, 0.87)	(-0.5, 2.6)	(0, 0)	(3, -1.73)	(3, -3.47)	(2.5, -0.87)
(0.5, 0.87)	(0, 0)	(2, 1.73)	(-2.5, -2.6)	(-4, -3.47)	(-2, -1.73)
(1.5, 0.87)	(2, 1.73)	(0, 0)	(-1.5, -2.6)	(-1.5, -4.33)	(-2, -1.73)
(2.5, 0.87)	(2.5, -0.87)	(2, 1.73)	(-0.5, -2.6)	(-2, -1.73)	(0.5, -2.6)
(-3, 0)	(-4.5, -0.87)	(-2.5, 0.87)	(0.5, -2.6)	(0.5 - 2.6)	(0.5, -2.6)
(-2, 0)	(-2, -1.73)	(-2.5, 0.87)	(1.5, -2.6)	(3, -3.46)	(0.5, -2.6)
(-1, 0)	(-2.5, 0.87)	(0, 0)	(0, -3.46)	(-1.5, -4.33)	(0.5, -2.6)
			(1, -3.46)	(1, -5.2)	(0.5, -2.6)

Table 5.2: *A complete assignment for the 49 central lattice points contained within $V_\pi(0)$ for the case of $K = 2$ and $N = 7$.*

5.6.1   Performance of Individual Descriptions

In the first experiment we design three-channel MD-LVQ based on the A_2 quantizer. We quantize an i.i.d. unit-variance Gaussian source which has been blocked into two-dimensional vectors. The number of vectors used in the experiment is $2 \cdot 10^6$. The entropy of each side description is 5 bit/dim. and we vary the index value in the range $31 - 67$. The dimensionless expansion factor ψ_L is set to 1.14808, see Table 5.1. The numerical and theoretical distortions when receiving only a single description out of three is shown in Table 5.3. Similarly, Table 5.4 shows the distortions of the same system due to reception of two out of three descriptions and Table 5.5 shows the performance of the central quantizer when all three descriptions are received. The column labeled "Avg." illustrates the average distortion of the three numerically measured distortions and the column labeled "Theo." describes the theoretical distortions given by (5.34). It is clear from the tables that the system is symmetric; the

achieved distortion depends on the number of received descriptions but is essentially independent of *which* descriptions are used for reconstruction. The numerically measured discrete entropies of the side descriptions are shown in Table 5.6.

N	λ_0	λ_1	λ_2	Avg.	Theo.
31	-25.6918	-25.6875	-25.6395	-25.6729	-24.8853
37	-24.5835	-24.5324	-24.5404	-24.5521	-24.5011
43	-24.5772	-24.5972	-24.5196	-24.5647	-24.1748
49	-24.2007	-24.2837	-24.2713	-24.2519	-23.8911
61	-23.8616	-23.9011	-23.8643	-23.8757	-23.4155
67	-23.7368	-23.7362	-23.7655	-23.7462	-23.2118

Table 5.3: *Distortion (in dB) due to reception of a single description out of three.*

N	$\frac{1}{2}(\lambda_0 + \lambda_1)$	$\frac{1}{2}(\lambda_0 + \lambda_2)$	$\frac{1}{2}(\lambda_1 + \lambda_2)$	Avg.	Theo.
31	-30.7792	-30.7090	-30.7123	-30.7335	-30.9059
37	-29.8648	-29.8430	-29.9472	-29.8850	-30.5217
43	-29.9087	-29.8749	-29.9641	-29.9159	-30.1954
49	-29.6290	-29.5577	-29.6662	-29.6176	-29.9117
61	-29.3076	-29.2185	-29.3715	-29.2992	-29.4361
67	-29.1752	-29.2128	-29.2151	-29.2010	-29.2324

Table 5.4: *Distortion (in dB) due to reception of two descriptions out of three.*

N	λ_c	Theo.
31	-43.6509	-43.6508
37	-44.4199	-44.4192
43	-45.0705	-45.0719
49	-45.6401	-45.6391
61	-46.5879	-46.5905
67	-46.9992	-46.9979

Table 5.5: *Distortion (in dB) due to reception of all three descriptions.*

The distortions shown in Tables 5.3 to 5.5 correspond to the case where we vary the index value N throughout the range $67 \geq N \geq 31$ for three-channel MD-LVQ operating at $R_s = 5$ bit/dim. per description. To achieve similar performance with a (3,1) SCEC we need to vary the correlation ρ_q within the interval $-0.49 \leq \rho_q \leq -0.45$, as shown in Fig. 5.5.

N	λ_0	λ_1	λ_2
31	5.0011	5.0012	5.0012
37	4.9925	4.9982	4.9988
43	4.9967	5.0006	5.0006
49	4.9993	5.0004	5.0004
61	5.0018	5.0017	5.0017
67	5.0023	5.0022	5.0022

Table 5.6: *Numerically measured discrete entropies [bit/dim.] for the individual descriptions. Here the target description rate is set to 5 bit/dim.*

5.6.2   Distortion as a Function of Packet-Loss Probability

We now show the expected distortion as a function of the packet-loss probability for K-channel MD-LVQ where $K = 1, 2, 3$. We block the i.i.d. unit-variance Gaussian source into $2 \cdot 10^6$ two-dimensional vectors and let the total target entropy be 6 bit/dim. The expansion factor is set to $\psi_2 = 1$ for $K = 1, 2$ and $\psi_2 = 1.14808$ for $K = 3$. We sweep the packet-loss probability p in the range $p \in [0; 1]$ in steps of 1/200 and for each p we measure the distortion for all admissible index values and use that index value which gives the lowest distortion. This gives rise to an operational lower hull (OLH) for each quantizer. This is done for the theoretical curves as well by inserting admissible index values in (5.35) and use that index value that gives the lowest distortion. In other words we compare the numerical OLH with the theoretical OLH and not the "true"[43] lower hull that would be obtained by using the unrestricted index values given by (5.45). The target entropy is evenly distributed over K descriptions. For example, for $K = 2$ each description uses 3 bit/dim., whereas for $K = 3$ each description uses only 2 bit/dim. The performance is shown in Fig. 5.6. The practical performance of the scheme is described by the lower hull of the K-curves. Notice that at higher packet-loss probabilities ($p > 5\%$) it becomes advantageous to use three descriptions instead two.

It is important to see that when the distortion measure is the expected distortion based on the packet-loss probability, then the notion of high resolution is slightly misleading. For example, if we let the rate go to infinity, then for a given fixed packet-loss probability p the only contributing factor to the expected distortion is the distortion due to the estimation of the source when all packets are lost. This term is given by $\frac{1}{L}E\|X\|^2 p^K$ so that for a unit-variance source, in the asymptotic case of $R \to \infty$, the expected distortion is simply given by $K 10 \log_{10}(p)$ dB. In other words, with a packet-loss probability of 10%, if the number of packets is increased by one,

---

[43]A lattice is restricted to a set of admissible index values. This set is generally expanded when the lattice is used as a product quantizer, hence admissible index values closer to the optimal values given by (5.45) can in theory be obtained, cf. Section 2.3.1.
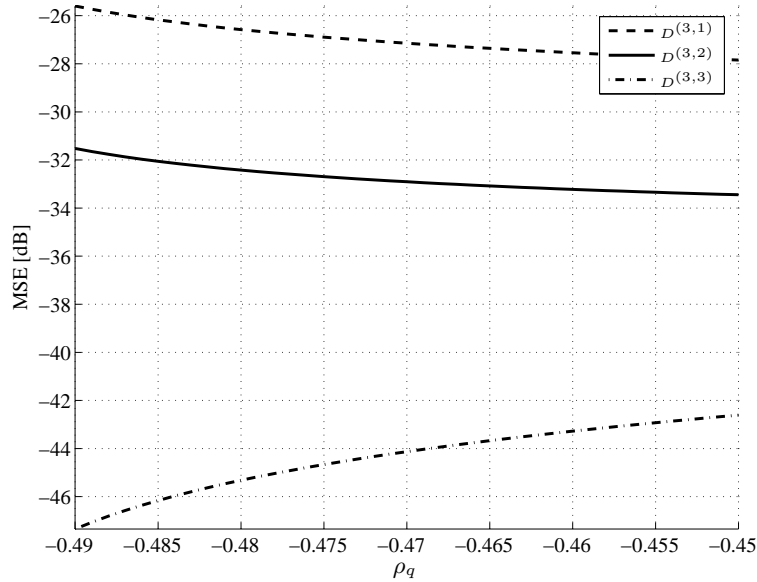
Figure 5.5: *The simultaneously achievable one-channel, two-channel and three-channel distortions for the unit-variance Gaussian source at 5 bit/dim. for* $-0.49 < \rho_q < -0.45$ *for a* $(3, 1)$ *SCEC.*

then the corresponding decrease in distortion is exactly 10 dB. We have illustrated this in Fig. 5.7 for $K = 1, \ldots, 5$.

5.7   Conclusion

We derived closed-form expressions for the central and side quantizers which, at high-resolution conditions, minimize the expected distortion of a symmetric K-channel MD-LVQ scheme subject to entropy constraints on the side descriptions for given packet-loss probabilities. The expected distortion observed at the receiving side depends only upon the number of received descriptions but is independent of which descriptions are received. We focused on a special case of the symmetric MD problem where only a single parameter (i.e. N) controls the redundancy tradeoffs between the central and the side distortions. We showed that the optimal amount of redundancy is in independent of the source distribution, the target rate and the type of lattices used for the side quantizers.

The practical design allows an arbitrary number of descriptions and the optimal number of descriptions depends (among other factors) upon the packet-loss probability. The theoretical rate-distortion results were proven for the case of $K \le 3$ descriptions and conjectured to be true in the general case of arbitrary K descriptions.
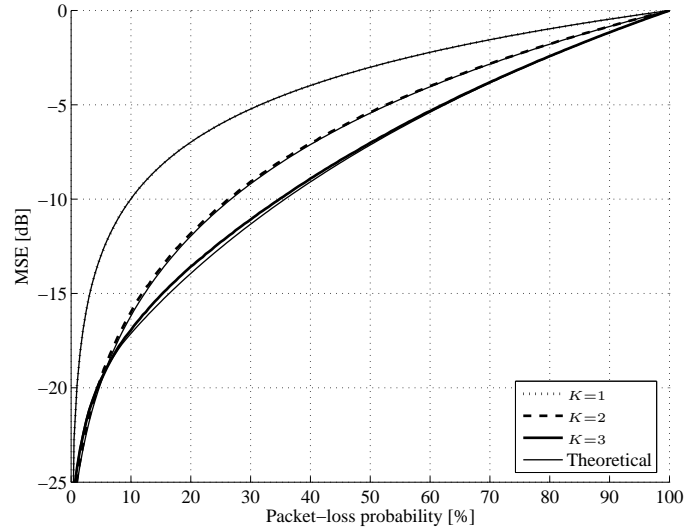
Figure 5.6: *Distortion as a function of the packet-loss probability for the A_2 quantizer. The target entropy is 6 bit/dim., so each description gets 6/K bit/dim. Thick lines show numerical performance and thin solid lines show theoretical performance. The two curves at the top (coinciding) illustrate the case of $K = 1$, the two curves in the middle illustrate the case of $K = 2$, and the bottom two curves illustrate the case of $K = 3$ descriptions.*
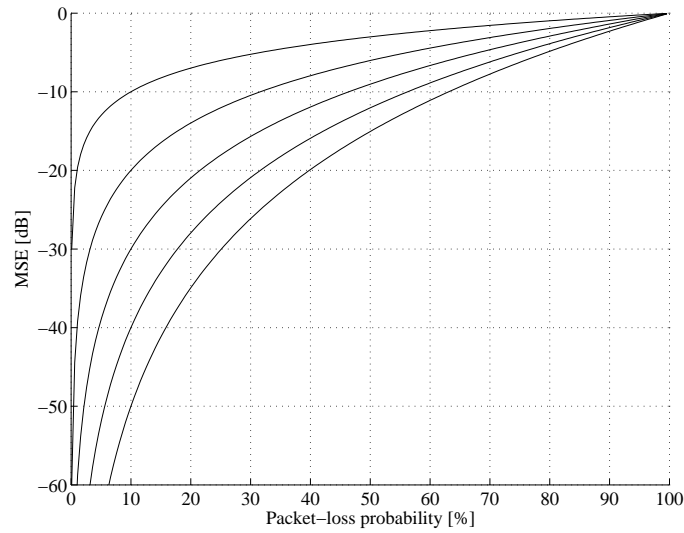

Figure 5.7: *Estimation error $\frac{1}{L}E\|X\|^2 p^K$ as a function of the packet-loss probability for different number of descriptions. The top curve is for $K = 1$, the second from the top is for $K = 2$, and so on. The bottom curve is for $K = 5$.*

K-Channel Asymmetric Lattice Vector Quantization

In this chapter we will focus on asymmetric MD-LVQ for $K \geq 2$ descriptions, see Fig. 6.1. Asymmetric schemes offer additional flexibility over the symmetric schemes, since the bit distribution is also a design parameter and different weights are introduced in order to control the distortions. In fact, symmetric MD-LVQ is a special case of asymmetric MD-LVQ.

In [27, 28] asymmetric two-channel MD-LVQ systems are derived subject to entropy constraints on the individual side entropies. However, since these schemes are subject to individual side entropy constraints and not subject to a single constraint on the sum of the side entropies, the problem of how to distribute a total bit budget among the two descriptions is not addressed. In this chapter we derive MD quantizer parameters subject to individual side entropy constraints and/or subject to a total entropy constraint on the sum of the side entropies. We then show that the optimal bit distribution among the descriptions is not unique but is in fact characterized by a set of solutions, which all lead to minimal expected distortion.

For the case of $K = 2$ our design admits side distortions which are superior to the side distortions of [27, 28] while achieving identical central distortion. Specifically, we show that the side distortions of our design can be expressed through the dimensionless normalized second moment $G(S_L)$ of an L-sphere whereas the side distortions of previous asymmetric designs [27, 28] depend on the dimensionless normalized second moment $G(\Lambda)$ of the L-dimensional lattices. More accurately, the difference in side distortions between the two schemes is given by the difference between $G(S_L)$ and $G(\Lambda)$. Notice that $G(S_L) \leq G(\Lambda)$ with equality for $L = 1$ and for $L \to \infty$ by a proper choice of lattice [161], cf. Section 3.3.1. We also show that, for the case of $K = 3$ and asymptotically in lattice vector dimension, the side

distortions can again be expressed through $G(S_L)$ and we further conjecture this to be true for $K > 3$ descriptions.
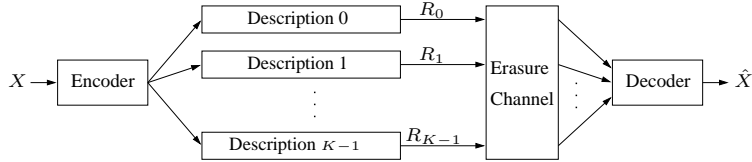

Figure 6.1: *General K-channel system. Descriptions are encoded at an entropy of R_i, $i = 0, \dots, K - 1$. The erasure channel either transmits the ith description errorless or not at all.*

6.1 Preliminaries

To be consistent with the previous chapter we will here introduce the set of lattices required for the asymmetric design and emphasize how they differ from the symmetric design.

Just as in the symmetric case we use a single lattice Λ_c as the central quantizer. However, we will make use of several sublattices $\Lambda_i, i = 0, \dots, K - 1$ for the side quantizers. In fact, we use one side quantizer (sublattice) for each description. We assume that all sublattices are geometrically-similar to Λ_c and clean. The sublattice index of the ith sublattice Λ_i is given by $N_i = |\Lambda_c/\Lambda_i|, N_i \in \mathbb{Z}^+$. The volume ν_i of a sublattice Voronoi cell in the ith sublattice is given by $\nu_i = N_i\nu$, where ν is the volume of a Voronoi cell of Λ_c. As in the symmetric case we will also here make use of a product lattice $\Lambda_\pi \subseteq \Lambda_i \subseteq \Lambda_c$ of index $N_\pi = |\Lambda_c/\Lambda_\pi|$ in the design of the index-assignment map.

The general framework of asymmetric MD-LVQ is similar to the symmetric case. We use a single index-assignment map α, which maps central lattice points to K-tuples of sublattice points. The main difference is that in the asymmetric case the sublattice index values, $N_i, i = 0, \dots, K - 1$, are not necessarily equal, which means that the side descriptions rates R_i are not necessarily equal either. Furthermore, the weights for the case of receiving κ out of K descriptions depend upon which κ descriptions are considered. This was not so in the symmetric case.

6.1.1 Index Assignments

The index assignment map (or labeling function) differs from the symmetric case in that it maps from a single lattice to several distinct sublattices. Specifically, let α denote the labeling function and let the individual component functions of α be denoted by α_i. The injective map α that maps Λ_c into $\Lambda_0 \times \cdots \times \Lambda_{K-1}$, is then given

by

$$\alpha(\lambda_c) = (\alpha_0(\lambda_c), \alpha_1(\lambda_c), \dots, \alpha_{K-1}(\lambda_c)) \tag{6.1}$$

$$= (\lambda_0, \lambda_1, \dots, \lambda_{K-1}), \tag{6.2}$$

where $\alpha_i(\lambda_c) = \lambda_i \in \Lambda_i$ and $i = 0, \dots, K - 1$.

We generalize the approach of the previous chapter and construct a product lattice Λ_π which has N_π central lattice points and N_π/N_i sublattice points from the ith sublattice in each of its Voronoi cells. The Voronoi cells V_π of the product lattice Λ_π are all similar so by concentrating on labeling only central lattice points within one cell, the rest of the central lattice points may be labeled simply by translating this cell throughout $\mathbb{R}^L$. Without loss of generality we let $N_\pi = \prod_{i=0}^{K-1} N_i$, i.e. by construction we let Λ_π be a geometrically-similar and clean sublattice of Λ_i for all i.[44] With this choice of Λ_π, we only label central lattice points within $V_\pi(0)$, which is the Voronoi cell of Λ_π around the origin.

6.1.2   Rate and Distortion Results

The central distortion D_c is identical to that of a symmetric system, which is given by (5.13). It also follows from the symmetric case see (5.14) that the side distortion for the ith description is given by

$$D_i = D_c + \frac{1}{L} \frac{1}{N_\pi} \sum_{\lambda_c \in V_\pi(0)} \|\lambda_c - \alpha_i(\lambda_c)\|^2, \quad i = 0, \dots, K - 1. \tag{6.3}$$

Definition 6.1.1. R_i denotes the entropy of the individual descriptions. The entropy of the ith description is defined as $R_i \triangleq H(\alpha_i(Q(X)))/L$.

The side descriptions are based on a coarser lattice obtained by scaling the Voronoi cells of the central lattice by a factor of N_i. Assuming the pdf of X is roughly constant within a sublattice cell, the entropies of the side descriptions are given by

$$R_i \approx \bar{h}(X) - \frac{1}{L} \log_2(N_i \nu). \tag{6.4}$$

The entropies of the side descriptions are related to the entropy R_c of the central quantizer, given by (5.18), by

$$R_i \approx R_c - \frac{1}{L} \log_2(N_i).$$

---

[44]From Lemma 2.3.1 it follows that the product of admissible index values leads to an admissible index value.

6.2   Construction of Labeling Function

In this section we construct the index-assignment map α, which takes a single vector λ_c and maps it to a set of K vectors $\{\lambda_i\}, i = 0, \ldots, K - 1$, where $\lambda_i \in \Lambda_i$. The mapping is invertible so that we have $\lambda_c = \alpha^{-1}(\lambda_0, \ldots, \lambda_{K-1})$.

In asymmetric MD-LVQ weights are introduced in order to control the amount of asymmetry between the side distortions. We will in the following assume that these weights are based on the packet-loss probabilities of the individual descriptions. However, it should be clear that the weights are not limited to represent packet-loss probabilities but can in fact be almost arbitrarily chosen. We will consider the case where the index-assignment map is constructed such that the expected distortion, given by the sum of the distortions due to all possible description losses weighted by their corresponding loss probabilities, is minimized.

In addition to knowing the weighted distortion over all description losses it is also interesting to know the distortion of any subset of the K descriptions. This issue is considered in Section 6.5.

6.2.1   Expected Distortion

At the receiving side, $X \in \mathbb{R}^L$ is reconstructed to a quality that is determined by the received descriptions. If no descriptions are received we reconstruct using the expected value, EX, and if all K descriptions are received we reconstruct using the inverse map $\alpha^{-1}(\lambda_0, \ldots, \lambda_{K-1})$, hence obtaining the quality of the central quantizer. In all other cases, we reconstruct to the average of the received descriptions as was done in the symmetric case.

There are in general several ways of receiving κ out of K descriptions. Let $\mathscr{L}^{(K,\kappa)}$ denote an index set consisting of all possible κ combinations out of $\{0, \ldots, K - 1\}$ so that $|\mathscr{L}^{(K,\kappa)}| = \binom{K}{\kappa}$. We denote an element of $\mathscr{L}^{(K,\kappa)}$ by $l = \{l_0, \ldots, l_{\kappa-1}\}$. The complement l^c of l denotes the $K - \kappa$ indices not in l, i.e. $l^c = \{0, \ldots, K - 1\} \backslash l$. We will use the notation $\mathscr{L}_i^{(K,\kappa)}$ to indicate the set of all $l \in \mathscr{L}^{(K,\kappa)}$ that contains the index i, i.e., $\mathscr{L}_i^{(K,\kappa)} = \{l : l \in \mathscr{L}^{(K,\kappa)} \text{ and } i \in l\}$ and similarly $\mathscr{L}_{i,j}^{(K,\kappa)} = \{l : l \in \mathscr{L}^{(K,\kappa)} \text{ and } i, j \in l\}$. Furthermore, let p_i be the packet-loss probability for the ith description and let $\mu_i = 1 - p_i$ be the probability that the ith description is received. Finally, let $p(l) = \prod_{i \in l} \mu_i \prod_{j \in l^c} p_j$, $p(\mathscr{L}^{(K,\kappa)}) = \sum_{l \in \mathscr{L}^{(K,\kappa)}} p(l)$, $p(\mathscr{L}_i^{(K,\kappa)}) = \sum_{l \in \mathscr{L}_i^{(K,\kappa)}} p(l)$ and $p(\mathscr{L}_{i,j}^{(K,\kappa)}) = \sum_{l \in \mathscr{L}_{i,j}^{(K,\kappa)}} p(l)$. For example, for $K = 3$ and $\kappa = 2$ we have $\mathscr{L}^{(3,2)} = \{\{0, 1\}, \{0, 2\}, \{1, 2\}\}$ and hence $p(\mathscr{L}^{(3,2)}) = \mu_0\mu_1 p_2 + \mu_0\mu_2 p_1 + \mu_1\mu_2 p_0$. In a similar manner for $K = 6$ and $\kappa = 3$ we have

$$\mathscr{L}_{1,2}^{(6,3)} = \{\{0, 1, 2\}, \{1, 2, 3\}, \{1, 2, 4\}, \{1, 2, 5\}\},$$

and

$$p(\mathscr{L}_{1,2}^{(6,2)}) = \mu_0\mu_1\mu_2 p_3 p_4 p_5 + \mu_1\mu_2\mu_3 p_0 p_4 p_5 + \mu_1\mu_2\mu_4 p_0 p_3 p_5 + \mu_1\mu_2\mu_5 p_0 p_3 p_4.$$

As in the symmetric case, upon reception of any κ out of K descriptions we reconstruct to $\hat{X}$ using

$$\hat{X} = \frac{1}{\kappa} \sum_{j \in l} \lambda_j.$$

The distortion when receiving a set of descriptions can be derived in a similar way as was done in the symmetric case. Thus, by use of (5.14) and (6.3) it can be shown that the norm of (6.3), when receiving descriptions i and j, should read $\|\lambda_c - 0.5(\alpha_i(\lambda_c) + \alpha_j(\lambda_c))\|^2$. It follows that the expected distortion when receiving κ out of K descriptions is given by

$$\begin{aligned}
D_a^{(K,\kappa)} &\approx \sum_{l \in \mathscr{L}^{(K,\kappa)}} p(l) \left(D_c + \frac{1}{L} \frac{1}{N_\pi} \sum_{\lambda_c \in V_\pi(0)} \left\| \lambda_c - \frac{1}{\kappa} \sum_{j=0}^{\kappa-1} \lambda_{l_j} \right\|^2 \right) \\
&= p(\mathscr{L}^{(K,\kappa)}) D_c + \frac{1}{L} \frac{1}{N_\pi} \sum_{\lambda_c \in V_\pi(0)} \sum_{l \in \mathscr{L}^{(K,\kappa)}} p(l) \left\| \lambda_c - \frac{1}{\kappa} \sum_{j=0}^{\kappa-1} \lambda_{l_j} \right\|^2,
\end{aligned}$$

(6.5)

where $\lambda_{l_j} = \alpha_{l_j}(\lambda_c)$ and the two special cases $\kappa \in \{0, K\}$ are given by $D_a^{(K,0)} \approx \frac{1}{L} E\|X\|^2 \prod_{i=0}^{K-1} p_i$ and $D_a^{(K,K)} \approx D_c \prod_{i=0}^{K-1} \mu_i$.

6.2.2   Cost Functional

From (6.5) we see that the distortion $D_a^{(K,\kappa)}$ may be split into two terms, one describing the distortion occurring when the central quantizer is used on the source, and one that describes the distortion due to the index assignment. An optimal index assignment minimizes the second term in (6.5) for all possible combinations of descriptions. The cost functional $J^{(K)}$ to be minimized by the index-assignment algorithm can then be written as

$$J^{(K)} = \sum_{\kappa=1}^{K-1} J^{(K,\kappa)},$$

(6.6)

where

$$J^{(K,\kappa)} = \frac{1}{L} \frac{1}{N_\pi} \sum_{\lambda_c \in V_\pi(0)} \sum_{l \in \mathscr{L}^{(K,\kappa)}} p(l) \left\| \lambda_c - \frac{1}{\kappa} \sum_{j=0}^{\kappa-1} \lambda_{l_j} \right\|^2.$$

(6.7)

The cost functional should be minimized subject to some entropy-constraints on the side descriptions or on e.g. the sum of the side entropies. We remark here that the side entropies depend solely on ν and N_i (see (6.4)) but not on the particular choice of K-tuples. In other words, for fixed N_i's and a fixed ν the index assignment problem is solved if (6.6) is minimized. The problem of choosing ν and N_i such that certain entropy constraints are not violated is independent of the assignment problem and deferred to Section 6.4.

Theorem 6.2.1. For any $1 \leq \kappa \leq K$ we have

$$
\sum_{\lambda_c} \sum_{l \in \mathscr{L}^{(K,\kappa)}} p(l) \left\| \lambda_c - \frac{1}{\kappa} \sum_{j=0}^{\kappa-1} \lambda_{l_j} \right\|^2
$$

$$
= \sum_{\lambda_c} \left(p(\mathscr{L}^{(K,\kappa)}) \left\| \lambda_c - \frac{1}{\kappa p(\mathscr{L}^{(K,\kappa)})} \sum_{i=0}^{K-1} p(\mathscr{L}_i^{(K,\kappa)}) \lambda_i \right\|^2 \right.
$$

$$
\left. + \frac{1}{\kappa^2} \sum_{i=0}^{K-2} \sum_{j=i+1}^{K-1} \left(\frac{p(\mathscr{L}_i^{(K,\kappa)}) p(\mathscr{L}_j^{(K,\kappa)})}{p(\mathscr{L}^{(K,\kappa)})} - p(\mathscr{L}_{i,j}^{(K,\kappa)}) \right) \|\lambda_i - \lambda_j\|^2 \right).
$$

Proof. See Appendix I.1. $\qquad\square$

The cost functional (6.6) can by use of Theorem 6.2.1 be written as

$$
J^{(K,\kappa)} = \frac{1}{L} \frac{1}{N_\pi} \sum_{\lambda_c \in V_\pi(0)} \left(p(\mathscr{L}^{(K,\kappa)}) \left\| \lambda_c - \frac{1}{\kappa p(\mathscr{L}^{(K,\kappa)})} \sum_{i=0}^{K-1} \lambda_i p(\mathscr{L}_i^{(K,\kappa)}) \right\|^2 \right.
$$

$$
\left. + \frac{1}{\kappa^2} \sum_{i=0}^{K-2} \sum_{j=i+1}^{K-1} \|\lambda_i - \lambda_j\|^2 \left(\frac{p(\mathscr{L}_i^{(K,\kappa)}) p(\mathscr{L}_j^{(K,\kappa)})}{p(\mathscr{L}^{(K,\kappa)})} - p(\mathscr{L}_{i,j}^{(K,\kappa)}) \right) \right).
$$
(6.8)

The first term in (6.8) describes the distance from a central lattice point to the weighted centroid of its associated K-tuple. The second term describes the weighted sum of pairwise squared distances (WSPSD) between elements of the K-tuple. In Section 6.3 (Proposition 6.3.2) we show that, under a high-resolution assumption, the second term in (6.8) is dominant, from which we conclude that in order to minimize (6.6) we must use K-tuples with the smallest WSPSD. These K-tuples are then assigned to central lattice points in such a way, that the first term in (6.8) is minimized.

6.2.3 Minimizing Cost Functional

We follow the approach of the symmetric case and center a region $\tilde{V}$ at all sublattice points $\lambda_0 \in \Lambda_0 \cap V_\pi(0)$, and construct K-tuples by combining sublattice points from the other sublattices (i.e. $\Lambda_i, i = 1, \ldots, K - 1$) within $\tilde{V}(\lambda_0)$ in all possible ways and select the ones that minimize (6.6). For each $\lambda_0 \in \Lambda_0 \cap V_\pi(0)$ it is possible to construct $\prod_{i=1}^{K-1} \tilde{N}_i$ K-tuples, where $\tilde{N}_i$ is the number of sublattice points from the ith sublattice within the region $\tilde{V}$. This gives a total of $(N_\pi/N_0) \prod_{i=1}^{K-1} \tilde{N}_i$ K-tuples when all $\lambda_0 \in \Lambda_0 \cap V_\pi(0)$ are used. The number $\tilde{N}_i$ of lattice points within a connected region $\tilde{V}$ of $\mathbb{R}^L$ may be approximated by $\tilde{N}_i \approx \tilde{\nu}/\nu_i$ where $\tilde{\nu}$ is the volume of $\tilde{V}$, which is an approximation that becomes exact as the number of shells of the lattice within $\tilde{V}$ goes to infinity, cf. Section 5.3.3. Therefore, our analysis is only

exact in the asymptotic case of $N_i \to \infty$ and $\nu_i \to 0$. Since $\tilde{N}_i \approx \tilde{\nu}/\nu N_i$ and we need N_0 K-tuples for each $\lambda_0 \in V_\pi(0)$ we see that

$$N_0 = \prod_{i=1}^{K-1} \tilde{N}_i \approx \frac{\tilde{\nu}^{K-1}}{\nu^{K-1}} \prod_{i=1}^{K-1} N_i^{-1},$$

so in order to obtain at least N_0 K-tuples, the volume of $\tilde{V}$ must satisfy

$$\lim_{N_i \to \infty, \forall i} \tilde{\nu} \geq \nu \prod_{i=0}^{K-1} N_i^{1/(K-1)}. \tag{6.9}$$

For the symmetric case, i.e. $N = N_i$, $i = 0, \ldots, K-1$, we have $\tilde{\nu} \geq \nu N^{K/(K-1)}$, which is in agreement with the results obtained in Chapter 5.

Before we outline the design procedure for constructing an optimal index assignment we remark that in order to minimize the WSPSD between a fixed λ_i and the set of points $\{\lambda_j \in \Lambda_j \cap \tilde{V}\}$ it is required that $\tilde{V}$ forms a sphere centered at λ_i. The design procedure can be outlined as follows:

1. Center a sphere $\tilde{V}$ at each $\lambda_0 \in \Lambda_0 \cap V_\pi(0)$ and construct all possible K-tuples $(\lambda_0, \lambda_1, \ldots, \lambda_{K-1})$ where $\lambda_i \in \Lambda_i \cap \tilde{V}(\lambda_0)$ and $i = 1, \ldots, K-1$. This ensures that all K-tuples have their first coordinate (λ_0) inside $V_\pi(0)$ and they are therefore shift-invariant. We will only use K-tuples whose elements satisfy $\|\lambda_i - \lambda_j\| \leq r, \forall i, j \in 0, \ldots K-1$, where r is the radius of $\tilde{V}$. Make $\tilde{V}$ large enough so at least N_0 distinct K-tuples are found for each λ_0.

2. Construct cosets of each K-tuple.

3. The N_π central lattice points in $\Lambda_c \cap V_\pi(0)$ must now be matched to distinct K-tuples. As in the symmetric case, this is a standard linear assignment problem [151] where only one member from each coset is (allowed to be) matched to a central lattice point in $V_\pi(0)$.

The restriction $\|\lambda_i - \lambda_j\| \leq r$ from step 1), which is used to avoid bias towards any of the sublattices, reduces the number of distinct K-tuples that can be constructed within the region $\tilde{V}$. To be able to form N_0 K-tuples it is therefore necessary to use a region $\tilde{V}$ with a volume larger than the lower bound in (6.9). In order to theoretically describe the performance of the quantizers we need to know the optimal $\tilde{\nu}$, i.e. the smallest volume which (asymptotically for large N_i) leads to exactly N_0 K-tuples. In Section 5.3.3 a dimensionless expansion factor ψ_L which only depends on K and L was introduced. ψ_L was used to describe how much $\tilde{V}$ had to be expanded from the theoretical lower bound (6.9), to make sure that N_0 optimal K-tuples could be constructed by combining sublattice points within a region $\tilde{V}$.

Lemma 6.2.1. The dimensionless expansion factor ψ_L for the asymmetric case is identical to the one for the symmetric case.

Proof. Follows by replacing the constant ν_s by ν_i in the proof of Theorem 5.3.2.

□

Adopting this approach leads to

$$\tilde{\nu} = \psi_L^L \nu \prod_{i=0}^{K-1} N_i^{1/(K-1)}.$$

Remark 6.2.1. It might appear that the shift invariance restriction enforced by using only one member from each coset will unfairly penalize Λ_0. However, the next two lemmas prove that, asymptotically as $N_i \to \infty$, there is no bias towards any of the sublattices. We will consider here the case of $K > 2$ (for $K = 2$ we can use similar arguments as given in [28]).

Lemma 6.2.2. For $K > 2$ the number of K-tuples that is affected by the coset restriction is (asymptotically as $N_i \to \infty, \forall i$) neglectable compared to the number of K-tuples which are not affected.

Proof. See Appendix I.4. □

Lemma 6.2.3. The set of N_π K-tuples that is constructed by centering $\tilde{V}$ at each $\lambda_0 \in V_\pi(0) \cap \Lambda_0$ is asymptotically identical to the set constructed by centering $\tilde{V}$ at each $\lambda_i \in V_\pi(0) \cap \Lambda_i$, for any $i \in \{1, \ldots, K-1\}$.

Proof. See Appendix I.4. □

Remark 6.2.2. The K-tuples need to be assigned to central lattice points within $V_\pi(0)$. This is a standard linear assignment problem where a cost measure is minimized. However, solutions to linear assignment problems are generally not unique. Therefore, there might exist several labelings, which all yield the same cost, but exhibit a different amount of asymmetry. To achieve the specified distortions it may then be necessary to e.g. use time sharing through a suitable mixing of labelings.

6.2.4   Comparison to Existing Asymmetric Index Assignments

In this section we have presented a new design for asymmetric MD-LVQ based on the asymmetric design of Diggavi et al. [28]. The main difference between the existing design of Diggavi et al. and the proposed design is that of the shape of the region within which sublattice points are distributed. More specifically, in the design of Diggavi et al., a given sublattice point $\lambda_0 \in \Lambda_0$ is paired with a set of sublattice points of Λ_1 which are all evenly distributed within a Voronoi cell of Λ_π, the product lattice. However, in the proposed design, a sublattice point $\lambda_0 \in \Lambda_0$ is paired with a set of sublattice points of Λ_1 which are all evenly distributed within an L-dimensional hypersphere.

Let us emphasize some of the advantages as well as weaknesses of the proposed design.

- Advantages

    1. The side distortion is reduced (compared to the previous design) when finite dimensional lattice vector quantizers are used (when the dimension is strictly greater than one). To see this, notice that the side distortion is a function of the dimensionless normalized second moment of the region over which the sublattice points are distributed. For $L = 1$ as well as $L \to \infty$ spheres pack space and it is possible to have spherical Voronoi cells of Λ_π by a proper choice of product lattice.

    2. To simplify the design it is often convenient to base the product lattice upon the simple hypercubic Z^L lattice. In this case, the side distortion of the design of Diggavi et al. is independent of the vector dimension of the lattices, whereas with the proposed design the distortion steadily decreases as the dimension increases. The reduction in side distortion is upper bounded by approximately 1.53 dB per description.

    3. The proposed design scales easily to more than two descriptions. It is not clear how to obtain more than two descriptions with the previous designs.

- Weaknesses

    1. The design of Diggavi et al. exploits several geometric properties of the underlying lattices to ensure that any single sublattice point of Λ_0 is paired with exactly N_0 sublattice points of Λ_1. On the other hand, the proposed design guarantees such a symmetry property only in asymptotic cases. Thus, in practice, if such a symmetry property is desired, one might need to search within a set of candidate solutions.

6.3   High-Resolution Analysis

In this section we derive high-resolution approximations for the expected distortion. In line with the high-resolution analysis presented in Chapter 5 we let $N_i \to \infty$ and $\nu_i \to 0$, i.e. for each sublattice the index increase, while the volume of their Voronoi cell shrink.

6.3.1   Total Expected Distortion

Using Theorem 6.2.1, the expected distortion (6.5) when κ out of K descriptions are received can be written as

$$
\begin{aligned}
D_a^{(K,\kappa)} &\approx p(\mathscr{L}^{(K,\kappa)})\, D_c + \frac{1}{L}\frac{1}{N_\pi} \sum_{\lambda_c \in V_\pi(0)} \sum_{l \in \mathscr{L}^{(K,\kappa)}} p(l) \left\| \lambda_c - \frac{1}{\kappa} \sum_{j=0}^{\kappa-1} \lambda_{l_j} \right\|^2 \\
&= p(\mathscr{L}^{(K,\kappa)})\, D_c \\
&\quad + \frac{1}{L}\frac{1}{N_\pi} \sum_{\lambda_c \in V_\pi(0)} \left(p(\mathscr{L}^{(K,\kappa)}) \left\| \lambda_c - \frac{1}{\kappa p(\mathscr{L}^{(K,\kappa)})} \sum_{i=0}^{K-1} p(\mathscr{L}_i^{(K,\kappa)}) \lambda_i \right\|^2 \right. \\
&\quad + \left. \frac{1}{\kappa^2} \sum_{i=0}^{K-2} \sum_{j=i+1}^{K-1} \left(\frac{p(\mathscr{L}_i^{(K,\kappa)}) p(\mathscr{L}_j^{(K,\kappa)})}{p(\mathscr{L}^{(K,\kappa)})} - p(\mathscr{L}_{i,j}^{(K,\kappa)}) \right) \| \lambda_i - \lambda_j \|^2 \right).
\end{aligned}
$$

$$(6.10)$$

Proposition 6.3.1. For $K = 2$ and asymptotically as $N_i \to \infty, \nu_i \to 0$ as well as for $K = 3$ and asymptotically as $N_i, L \to \infty$ and $\nu_i \to 0$, we have for any pair of sublattices, (Λ_i, Λ_j), $i, j = 0, \ldots, K-1$, $i \neq j$,

$$
\frac{1}{L} \sum_{\lambda_c \in V_\pi(0)} \| \alpha_i(\lambda_c) - \alpha_j(\lambda_c) \|^2 = \psi_L^2 \nu^{2/L} G(S_L) N_\pi \prod_{m=0}^{K-1} N_m^{2/L(K-1)}.
$$

Proof. See Appendix I.2.   □

Conjecture 6.3.1. Proposition 6.3.1 is true for any K asymptotically as $L, N_i \to \infty$ and $\nu_i \to 0, \forall i$.

Proposition 6.3.2. For $N_i \to \infty$ we have

$$
\frac{\displaystyle\sum_{\lambda_c \in V_\pi(0)} \left\| \lambda_c - \frac{1}{\kappa p(\mathscr{L})} \sum_{i=0}^{K-1} p(\mathscr{L}_i^{(K,\kappa)}) \lambda_i \right\|^2}{\displaystyle\sum_{\lambda_c \in V_\pi(0)} \sum_{i=0}^{K-2} \sum_{j=i+1}^{K-1} \left(\frac{p(\mathscr{L}_i^{(K,\kappa)}) p(\mathscr{L}_j^{(K,\kappa)})}{p(\mathscr{L}^{(K,\kappa)})} - p(\mathscr{L}_{i,j}^{(K,\kappa)}) \right) \| \lambda_i - \lambda_j \|^2} \to 0.
$$

Proof. See Appendix I.3.   □

By use of Propositions 6.3.1 and 6.3.2 and (5.13) it follows that (6.10) can be

written as

$$D_a^{(K,\kappa)} \approx p(\mathscr{L}^{(K,\kappa)}) D_c$$

$$+ \frac{1}{L} \frac{1}{N_\pi} \sum_{\lambda_c \in V_\pi(0)} \left(\frac{1}{\kappa^2} \sum_{i=0}^{K-2} \sum_{j=i+1}^{K-1} \left(\frac{p(\mathscr{L}_i^{(K,\kappa)}) p(\mathscr{L}_j^{(K,\kappa)})}{p(\mathscr{L}^{(K,\kappa)})} - p(\mathscr{L}_{i,j}^{(K,\kappa)}) \right) \|\lambda_i - \lambda_j\|^2 \right)$$

$$\approx G(\Lambda_c) \nu^{2/L} p(\mathscr{L}^{(K,\kappa)}) + \psi_L^2 \nu^{2/L} G(S_L) \beta^{(K,\kappa)} \prod_{m=0}^{K-1} N_m^{2/L(K-1)},$$

where $\beta^{(K,\kappa)}$ depends on the packet-loss probabilities and is given by

$$\beta^{(K,\kappa)} = \frac{1}{\kappa^2} \sum_{i=0}^{K-2} \sum_{j=i+1}^{K-1} \left(\frac{p(\mathscr{L}_i^{(K,\kappa)}) p(\mathscr{L}_j^{(K,\kappa)})}{p(\mathscr{L}^{(K,\kappa)})} - p(\mathscr{L}_{i,j}^{(K,\kappa)}) \right).$$

The total expected distortion $D_a^{(K)}$ is obtained by summing over κ including the cases where $\kappa = 0$ and $\kappa = K$,

$$D_a^{(K)} \approx G(\Lambda_c) \nu^{2/L} \hat{p}(\mathscr{L}^{(K)}) + \psi_L^2 \nu^{2/L} G(S_L) \prod_{m=0}^{K-1} N_m^{2/L(K-1)} \hat{\beta}^{(K)}$$

$$+ \frac{1}{L} E\|X\|^2 \prod_{i=0}^{K-1} p_i, \tag{6.11}$$

where

$$\hat{p}(\mathscr{L}^{(K)}) = \sum_{\kappa=1}^{K} p(\mathscr{L}^{(K,\kappa)})$$

and

$$\hat{\beta}^{(K)} = \sum_{\kappa=1}^{K} \beta^{(K,\kappa)}.$$

Using (5.18) and (6.4) we can write ν and N_i as a function of differential entropy and side entropies, that is

$$\nu^{2/L} = 2^{2(\bar{h}(X) - R_c)},$$

and

$$\prod_{i=0}^{K-1} N_i^{2/L(K-1)} = 2^{\frac{2K}{K-1} \left(R_c - \frac{1}{K} \sum_{i=0}^{K-1} R_i \right)}.$$

Inserting these results in (6.11) leads to

$$D_a^{(K)} \approx G(\Lambda_c) 2^{2(\bar{h}(X) - R_c)} \hat{p}(\mathscr{L}^{(K)})$$

$$+ \psi_L^2 G(S_L) 2^{2(\bar{h}(X) - R_c)} 2^{\frac{2K}{K-1} \left(R_c - \frac{1}{K} \sum_{i=0}^{K-1} R_i \right)} \hat{\beta}^{(K)} + \frac{1}{L} E\|X\|^2 \prod_{i=0}^{K-1} p_i, \tag{6.12}$$

where we see that the distortion due to the side quantizers is independent of the type of sublattices.

6.4   Optimal Entropy-Constrained Quantizers

In this section we first derive closed-form expressions for the optimal scaling factors ν and N_i subject to entropy constraints on the K side descriptions. With these scaling factors we are able to construct a central lattice and K sublattices. The index assignments are then found using the approach outlined in Section 6.2. The central lattice and the K side lattices combined with their index assignment map completely specify an optimal scheme for asymmetric entropy-constrained MD-LVQ. We then consider the situation where the total bit budget is constrained, i.e. we find the optimal scaling factors subject to entropy constraints on the sum of the side entropies $\sum_i R_i \leq R^*$, where R^* is the target entropy. We also find the optimal bit distribution among the K descriptions.

6.4.1   Entropy Constraints Per Description

We assume K descriptions are to be used. Packet-loss probabilities $p_i, i = 0, \ldots, K-1$, are given as well as entropy-constraints on the side descriptions, i.e. $R_i \leq R_i^*$, where R_i^* are known target entropies. To be optimal, the entropies of the side descriptions must be equal to the target entropies, hence by use of (6.4) we must have that

$$R_i = \bar{h}(X) - \frac{1}{L}\log_2(N_i\nu) = R_i^*,$$

from which we get

$$N_i\nu = 2^{L(\bar{h}(X)-R_i^*)} = \tau_i, \tag{6.13}$$

where τ_i are constants. It follows that $N_i = \tau_i/\nu$ and since $\prod_{i=0}^{K-1} N_i^{2/L(K-1)} = \nu^{-2K/L(K-1)} \prod_{i=0}^{K-1} \tau_i^{2/L(K-1)}$ we can express (6.11) as a function of ν, i.e.

$$D_a^{(K)} \approx G(\Lambda_c)\nu^{2/L}\hat{p}(\mathscr{L}^{(K)})$$

$$+ \psi_L^2\nu^{2/L}G(S_L)\nu^{-2K/L(K-1)}\tau^{2/L(K-1)}\hat{\beta}^{(K)} + \frac{1}{L}E\|X\|^2 \prod_{i=0}^{K-1} p_i$$

$$= G(\Lambda_c)\nu^{2/L}\hat{p}(\mathscr{L}^{(K)}) + \psi_L^2 G(S_L)\nu^{-2/L(K-1)}\tau^{2/L(K-1)}\hat{\beta}^{(K)}$$

$$+ \frac{1}{L}E\|X\|^2 \prod_{i=0}^{K-1} p_i,$$

where $\tau = \prod_{i=0}^{K-1} \tau_i$.

Differentiating w.r.t. ν and equating to zero gives,

$$\frac{\partial D_a^{(K)}}{\partial \nu} = \frac{2}{L}G(\Lambda_c)\nu^{2/L-1}\hat{p}(\mathscr{L}^{(K)})$$

$$- \frac{2}{L(K-1)}\psi_L^2 G(S_L)\nu^{-2/L(K-1)-1}\tau^{2/L(K-1)}\hat{\beta}^{(K)} = 0,$$

from which we obtain the optimal value of ν

$$
\begin{aligned}
\nu &= \tau^{1/K} \left(\psi_L^2 \frac{1}{K-1} \frac{G(S_L)}{G(\Lambda_c)} \frac{\hat{\beta}^{(K)}}{\hat{p}(\mathscr{L}^{(K)})} \right)^{\frac{L(K-1)}{2K}} \\
&= 2^{L(\bar{h}(X) - \frac{1}{K} \sum_i R_i^*)} \left(\psi_L^2 \frac{1}{K-1} \frac{G(S_L)}{G(\Lambda_c)} \frac{\hat{\beta}^{(K)}}{\hat{p}(\mathscr{L}^{(K)})} \right)^{\frac{L(K-1)}{2K}}.
\end{aligned}
\tag{6.14}
$$

The optimal N_i's follow easily by use of (6.13):

$$
N_i = \frac{\tau_i}{\nu} = \tau_i \tau^{-1/K} \left(\frac{1}{\psi_L^2} (K-1) \frac{G(\Lambda_c)}{G(S_L)} \frac{\hat{p}(\mathscr{L}^{(K)})}{\hat{\beta}^{(K)}} \right)^{\frac{L(K-1)}{2K}}.
\tag{6.15}
$$

Eq. (6.15) shows that the optimal redundancies N_i's are, for fixed K, independent of the sublattices. Moreover, since $\tau_i \tau^{-1/K} = 2^{-L(R_i^* - \frac{1}{K} \sum_j R_j^*)}$ the source-dependent term $\bar{h}(X)$ is eliminated and it follows that the redundancies N_i are independent of the source but also of actual values of target entropies (N_i depends only upon the difference between the average target entropy and R_i^*).

6.4.2   Total Entropy Constraint

First we observe from (6.12) that the expected distortion depends upon the *sum* of the side entropies and not the individual side entropies. In order to be optimal it is necessary to achieve equality in the entropy constraint, i.e. $R^* = \sum_i R_i$. From (6.4) we have

$$
R^* = \sum_{i=0}^{K-1} R_i = K\bar{h}(X) - \frac{1}{L} \sum_{i=0}^{K-1} \log_2(N_i \nu).
$$

This equation can be rewritten as

$$
\prod_{i=0}^{K-1} (N_i \nu) = 2^{L(K\bar{h}(X) - R^*)} = \tau_*,
\tag{6.16}
$$

where τ_* is constant for fixed target entropy and differential entropies. Writing (6.16) as

$$
\prod_{i=0}^{K-1} N_i^{2/L(K-1)} = \nu^{-2K/L(K-1)} \tau_*^{2/L(K-1)},
$$

and inserting in (6.11) leads to

$$
\begin{aligned}
D_a^{(K)} &\approx G(\Lambda_c) \nu^{2/L} \hat{p}(\mathscr{L}^{(K)}) + \psi_L^2 \nu^{-2/L(K-1)} \tau_*^{2/L(K-1)} G(S_L) \hat{\beta}^{(K)} \\
&\quad + \frac{1}{L} E\|X\|^2 \prod_{i=0}^{K-1} p_i.
\end{aligned}
$$

Differentiating w.r.t. ν and equating to zero gives

$$\frac{\partial D_a^{(K)}}{\partial \nu} = \frac{2}{L} G(\Lambda_c) \nu^{2/L-1} \hat{p}(\mathscr{L}^{(K)})$$
$$- \frac{2}{L(K-1)} \psi_L^2 G(S_L) \nu^{-2/L(K-1)-1} \tau_*^{2/L(K-1)} \hat{\beta}^{(K)} = 0,$$

from which we obtain the optimal value of ν, that is

$$\nu = 2^{L(\bar{h}(X)-\frac{1}{K}R^*)} \left(\psi_L^2 \frac{1}{K-1} \frac{G(S_L)}{G(\Lambda_c)} \frac{\hat{\beta}^{(K)}}{\hat{p}(\mathscr{L}^{(K)})} \right)^{\frac{L(K-1)}{2K}}. \tag{6.17}$$

We note that this expression is identical to (6.14). The results of this section show that the optimal ν is the same whether we optimize subject to entropy constraints on the individual side entropies or on the sum of the side entropies as long as the total bit budget is the same.

At this point we still need to find expressions for the optimal R_i (or equivalently optimal N_i given ν). Let $R_i = a_i R^*$, where $\sum_i a_i = 1, a_i \geq 0$, hence $R^* = \sum_i R_i$. From (6.4) we have

$$R_i = \bar{h}(X) - \frac{1}{L} \log_2(N_i \nu) = a_i R^*,$$

which can be rewritten as

$$N_i = \nu^{-1} 2^{L(\bar{h}(X)-a_i R^*)}.$$

Inserting (6.17) leads to an expression for the optimal index value N_i, that is

$$N_i = 2^{\frac{L}{K}(1-a_i)R^*} \left(\psi_L^{-2}(K-1) \frac{G(\Lambda_c)}{G(S_L)} \frac{\hat{p}(\mathscr{L}^{(K)})}{\hat{\beta}^{(K)}} \right)^{\frac{L(K-1)}{2K}}. \tag{6.18}$$

It follows from (5.18) and (6.4) that $R_c \geq a_i R^*$ so that $a_i \leq R_c/R^*$. In addition, since the rates must be positive, we obtain the following inequalities:

$$0 < a_i R^* \leq R_c, \quad i = 0, \ldots, K-1. \tag{6.19}$$

Thus, when we only have a constraint R^* on the sum of the side entropies, the individual side entropies $R_i = a_i R^*$ can be arbitrarily chosen (without loss of performance) as long as they satisfy (6.19) and $\sum_i a_i = 1$. We remark that R_i is bounded away from zero by a positive constant, cf. (4.1) and (4.2). For example, for the two-channel case we have $R_0 = a_0 R^*$ and $R_1 = a_1 R^* = (1-a_0)R^*$, so that $R_c \geq (1-a_0)R^*$ which implies that $R^* - R_c \leq R_0 \leq R_c$.[45]

This result leads to an interesting observation. Given a single entropy constraint on the sum of the side entropies, the optimal bit distribution among the two descriptions

---

[45]Recall that R_c is fixed, since it depends on ν which is given by (6.17).

is not unique but contains in fact a set of solutions (i.e. a set of quantizers) which all lead to minimal expected distortion.[46] This allows for additional constraints to be imposed on the quantizers without sacrificing optimality with respect to minimal expected distortion. For example, in some mobile wireless environments, it might be beneficial to use those quantizers from the set of optimal quantizers that require the least amount of power.

6.4.3   Example With Total Entropy Constraint

Let us show by an example some interesting aspects resulting from the fact that we obtain a set of candidate solutions, which all minimize the expected distortion. For example, consider IP-telephony applications, which with the recent spread of broadband networks are being used extensively throughout the world today. More specifically, let us consider a packet-switched network where a user has access to two different channels both based on the unreliable user datagram protocol [133]. Channel 0 is a non priority-based channel whereas channel 1 is a priority-based channel or they are both priority-based channels but of different priorities. Equivalently this network can be thought of as a packet-switched network where the individual packets are given priorities; low or high priority. In any case, we assume that only a single packet is transmitted on each channel for each time instance (this can be justified with e.g. tight delay constraints). The priority-based channel favor packets with higher priority and the packet-loss probability p_1 on channel 1 is therefore lower than that of channel 0, i.e. $p_1 < p_0$. Assume the Internet telephony service provider (ITSP) in question charges a fixed amount of say \$1 (\$2) per bit transmitted via channel 0 (channel 1). If we then use say 6 bits on channel 1 the quality is better than if we use the 6 bits on channel 0. It is therefore tempting to transmit all the bits through channel 1 (or equivalently send both packets with high priority) since it offers better quality than channel 0. However, our results reveal that it is often beneficial to make use of both channels (or equivalently send two packets simultaneously of low and high priority). The importance of exploiting two channels is illustrated in Table 6.1 for the examples given above for a total bit budget of 6 bits and packet-loss probabilities $p_0 = 5\%$ and $p_1 = 2\%$. Notice the peculiarity that since the total bit budget is limited to 6 bits then even if the user is willing to pay more than \$8 the performance would be no better than what can be achieved when paying exactly \$8. The last column of Table 6.1 describes the expected distortion occurring when quantizing a unit-variance Gaussian source which has been scalar quantized at a total entropy of 6 bit/dim. The packet-loss probabilities are $p_0 = 0.05$ and $p_1 = 0.02$. The quantization error (hence not taking

---

[46]In retrospect, this is not a surprising result since, for the two-description case, we already saw that for a fixed distortion tuple (D_c, D_0, D_1) the lower bound of the rate region is piece-wise linear, cf. Fig. 4.5. Furthermore, when the sum rate is minimum, this line segment has a 45 degree (negative) slope. Hence, any choice of rate pairs on this line segment satisfies the sum rate. The new observation here, however, is that now we have a practical scheme, which for any number of descriptions, also satisfies this property.

Network	R_0	R_1	Price	Quality	Expected distortion
Single-channel	6	0	$6	Poor	-12.98 dB
Single-channel	0	6	$12	Good	-16.91 dB
Two-channel	2	4	$10	Optimal	-22.20 dB
Two-channel	**4**	**2**	**$8**	**Optimal**	**-22.20 dB**

Table 6.1: *A total bit budget of 6 bits is spent in four different ways. The bottom row shows the most economical way of spending the bits and still achieve optimal performance. The packet-loss probabilities are $p_0 = 5\%$ and $p_1 = 2\%$.*

packet losses into account) for an optimal entropy-constrained SD system is -34.59 dB but the expected distortion is dominated by the estimation error due to description losses, i.e. $10 \log_{10}(p_0) = -13.01$ dB and $10 \log_{10}(p_1) = -16.99$. It follows that the expected distortion for channel 0 and channel 1 is given by -12.98 dB and -16.91 dB, respectively. For the two-description system the expected distortion is found by use of (6.12) to be -22.20 dB, hence a gain of more than 5 dB is possible when using both channels.

6.5 Distortion of Subsets of Descriptions

We have so far considered the expected distortion occurring when all possible combinations of K descriptions are taken into account. In a sense this corresponds to having only a single receiver. In this section we consider a generalization to multiple receivers that have access to non-identical subsets of the K descriptions and where no packet losses occur. For example one receiver has access to descriptions $\{0, 3\}$ whereas another has access to descriptions $\{0, 1, 2\}$. A total of $2^K - 1$ non-trivial subsets are possible. We note that the design of the index-assignment map is assumed unchanged. We are still minimizing the cost functional given by (6.6). The only difference is that the weights do not necessarily reflect packet-loss probabilities but can be (almost) arbitrarily chosen to trade off distortion among different subsets of descriptions. For example, in a two-description system it is possible to decrease the distortion of description 0 by increasing the distortion of description 1 without affecting the rates.

The main result of this section is given by Theorem 6.5.1.

Theorem 6.5.1. The side distortion $D^{(K,l)}$ due to reception of descriptions $\{l\}$, where $l \in \mathscr{L}^{(K,\kappa)}$ for any $1 \leq \kappa \leq K \leq 3$ is, asymptotically as $L, N_i \to \infty$ and $\nu_i \to 0$, given by

$$D^{(K,l)} = \omega^{(K,l)} \psi_L^2 \nu^{2/L} G(S_L) \prod_{i=0}^{K-1} N_i^{2/L(K-1)},$$

where

$$\omega^{(K,l)} = \frac{1}{p(\mathscr{L}^{(K,\kappa)})^2 \kappa^2} \times \left(p(\mathscr{L}^{(K,\kappa)})^2 \kappa^2 - p(\mathscr{L}^{(K,\kappa)})^2 \binom{\kappa}{2} \right.$$

$$\left. - p(\mathscr{L}^{(K,\kappa)}) \sum_{j \in l} p(\mathscr{L}_j^{(K,\kappa)}) - \sum_{i=0}^{K-2} \sum_{j=i+1}^{K-1} p(\mathscr{L}_i^{(K,\kappa)}) p(\mathscr{L}_j^{(K,\kappa)}) \right)$$

and $\binom{\kappa}{2} = 0$ for $\kappa = 1$.

Proof. See Appendix I.5.   □

Conjecture 6.5.1. Theorem 6.5.1 is true for $K > 3$ as $L, N_i \to \infty$ and $\nu_i \to 0$.

Remark 6.5.1. For $K = 2$ Theorem 6.5.1 is true also for finite L.[47] For $K = 3$ it should be seen as an approximation for finite L.[48]

In Theorem 6.5.1 the term $\omega^{(K,l)}$ is a weight factor that depends on the particular subset of received descriptions. For example for $K = 2$ we let $\gamma_0 = \mu_0 p_1$ and $\gamma_1 = \mu_1 p_0$ then for $\kappa = 1$ the weights for description 0 and 1 are given by

$$\omega^{(2,0)} = \frac{\gamma_1^2}{(\gamma_0 + \gamma_1)^2} \quad \text{and} \quad \omega^{(2,1)} = \frac{\gamma_0^2}{(\gamma_0 + \gamma_1)^2}, \tag{6.20}$$

which are in agreement with the results obtained for the two-channel system in [28].

For $K = 3$ and $\kappa = 1$ we let $\gamma_0 = \mu_0 p_1 p_2$, $\gamma_1 = \mu_1 p_0 p_2$ and $\gamma_2 = \mu_2 p_0 p_1$ and the weight for description 0 is then given by

$$\omega^{(3,0)} = \frac{\gamma_1^2 + \gamma_2^2 + \gamma_1 \gamma_2}{(\gamma_0 + \gamma_1 + \gamma_2)^2},$$

whereas for $\kappa = 2$ we use the notation $\gamma_{01} = \mu_0 \mu_1 p_2$, $\gamma_{02} = \mu_0 \mu_2 p_1$ and $\gamma_{12} = \mu_1 \mu_2 p_0$ from which we find the weight when receiving description 0 and 1 to be

$$\omega^{(3,\{0,1\})} = \frac{\gamma_{02}^2 + \gamma_{12}^2 + \gamma_{02} \gamma_{12}}{4(\gamma_{01} + \gamma_{02} + \gamma_{12})^2}.$$

6.5.1   Asymmetric Assignment Example

In this section we illustrate by an example how one can achieve asymmetric distortions for the case of $K = 2$ and the Z^2 lattices. Let $N_0 = 13$ and $N_1 = 9$ so that $N_\pi = 117$. Thus, within $V_\pi(0)$ we have 117 central lattice points, 9 sublattice points of Λ_0, and 13 sublattice points of Λ_1. This is illustrated in Fig. 6.2. We first let the weight ratio[49] be $\gamma_0 / \gamma_1 = 1$ so that the two side distortions are identical. In this case several sublattice

---

[47]This follows since Proposition 6.3.1 is true for any L for $K = 2$.

[48]It is in fact possible to find an exact expression for finite L. See Remark H.4.1.

[49]The term weight ratio can be related to the ratio of the side distortions by use of (6.22) and (6.23). Specifically, it can be shown that $D_1 / D_0 \approx \gamma_0^2 / \gamma_1^2$.

points of Λ_0 located outside $V_\pi(0)$ will be used when labeling central lattice points inside $V_\pi(0)$. The solid lines in Fig. 6.2 illustrate the 117 edges that are assigned to the 117 central lattice points.

If we let the weight ratio be $\gamma_0/\gamma_1 = 4$ we favor Λ_0 over Λ_1. In this case the edge assignments are chosen such that for a given edge, the sublattice point belonging to Λ_0 is closer to the central lattice point than the sublattice point belonging to Λ_1. This is illustrated in Fig. 6.3. Notice that in this case the sublattice points of Λ_0 used for the edges that labels central lattice points within $V_\pi(0)$ are all located within $V_\pi(0)$. Furthermore, in order to construct the required 117 edges, sublattice points of Λ_1 at greater distance from $V_\pi(0)$ need to be used.

In practice, large index values are required in order to achieve large weight ratios γ_0/γ_1 or γ_1/γ_0. Notice that we can achieve asymmetric side distortions even in the case where the sublattices are identical (so that $N_0 = N_1$ and the rates are therefore identical) simply by letting $\gamma_0 \neq \gamma_1$. Moreover, we can achieve symmetric side distortions by letting $\gamma_0 = \gamma_1$ even when $N_0 \neq N_1$ (i.e. $R_0 \neq R_1$). In the case where either $\gamma_0 = 0$ and $\gamma_1 \neq 0$ or $\gamma_1 = 0$ and $\gamma_0 \neq 0$ the scheme degenerates to a successive refinement scheme, where the side distortion corresponding to the zero weight cannot be controlled. In practice this happens if either $\gamma_0 \gg \gamma_1$ or $\gamma_1 \gg \gamma_0$.
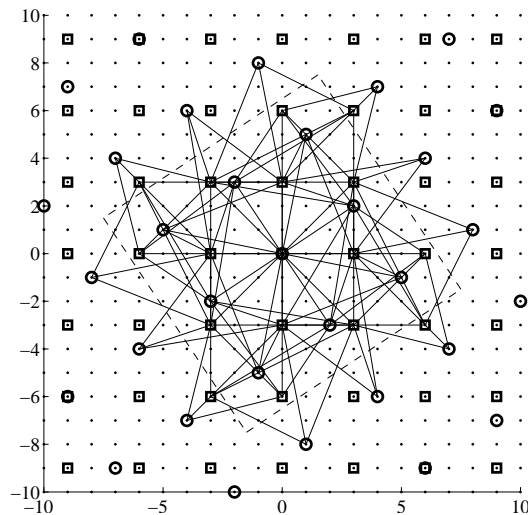
Figure 6.2: *A central lattice based on Z^2 (dots) and two geometrically-similar sublattices of index 13 (circles) and 9 (squares), respectively. The dashed square illustrates the boundary of $V_\pi(0)$. The solid lines illustrate the 117 edges (where some are overlapping). The weight ratio is here set to $\gamma_0/\gamma_1 = 1$.*
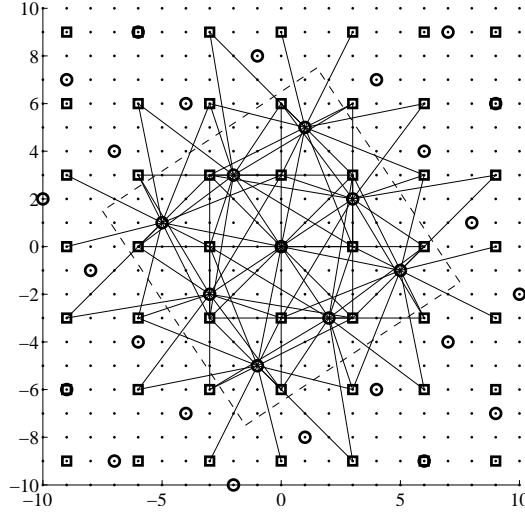
Figure 6.3: *A central lattice based on Z^2 (dots) and two geometrically-similar sublattices of index 13 (circles) and 9 (squares), respectively. The dashed square illustrates the boundary of $V_\pi(0)$. The solid lines illustrate the 117 edges (where some are overlapping). The weight ratio is here set to $\gamma_0/\gamma_1 = 4$.*

6.6   Numerical Results

To verify theoretical results we present in this section experimental results obtained by computer simulations. In all simulations we have used $2 \cdot 10^6$ unit-variance independent Gaussian vectors constructed by blocking an i.i.d. scalar Gaussian process into two-dimensional vectors. We first assess the two-channel performance of our scheme. This is interesting partly because it is the only case where the complete achievable MD rate-distortion region is known and partly because it makes it possible to compare to existing schemes. We end this section by showing the expected distortion (6.12) in an asymmetric setup using three descriptions.

6.6.1   Assessing Two-Channel Performance

The side distortions $\bar{D}_0$ and $\bar{D}_1$ of the two-channel asymmetric MD-LVQ system presented in [27, 28] are given by (4.59) and (4.60) and the central distortion is given by

$$\bar{D}_c \approx G(\Lambda_c)2^{2(\bar{h}(X)-R_c)}. \tag{6.21}$$

The asymmetric scheme presented in this paper satisfies

$$D_0 \approx \frac{\gamma_1^2}{(\gamma_0 + \gamma_1)^2}G(S_L)2^{2\bar{h}(X)}2^{-2(R_0+R_1-R_c)}, \tag{6.22}$$

and

$$D_1 \approx \frac{\gamma_0^2}{(\gamma_0 + \gamma_1)^2} G(S_L) 2^{2\bar{h}(X)} 2^{-2(R_0 + R_1 - R_c)}, \qquad (6.23)$$

and the central distortion is identical to (6.21). It follows that the only difference between the pair of side distortions $(\bar{D}_0, \bar{D}_1)$ and (D_0, D_1) is that the former depends upon $G(\Lambda_\pi)$ and the latter upon $G(S_L)$. In other words, the only difference in distortion between the schemes is the difference between $G(S_L)$ and $G(\Lambda_\pi)$. For the two dimensional case it is known that $G(S_2) = 1/4\pi$ whereas if Λ_π is similar to Z^2 we have $G(\Lambda_\pi) = 1/12$ which is approximately 0.2 dB worse than $G(S_2)$. Fig. 6.4 shows the performance when quantizing a unit-variance Gaussian source using the Z^2 quantizer for the design of [27, 28] as well as for the proposed system. In this setup we have fixed $R_0 = 5$ bit/dim. but R_1 is varied in the range $5 - 5.45$ bit/dim. To do so we fix $N_1 = 101$ and let N_0 step through the following sequence of admissible index values:

$$\{101, 109, 113, 117, 121, 125, 137, 145, 149, 153, 157, 169, 173, 181, 185\},$$

and for each N_0 we scale ν such that R_0 remains constant. When $N_0 = 101$ then $R_0 = R_1 = 5$ bit/dim. whereas when $N_0 > N_1$ then $R_1 > R_0$. We have fixed the ratio $\gamma_0/\gamma_1 = 1.55$ and we keep the side distortions fixed and change the central distortion. Since the central distortion is the same for the two schemes we have not shown it. Notice that D_0 (resp. D_1) is strictly smaller (about 0.2 dB) than $\bar{D}_0$ (resp. $\bar{D}_1$). This is to be expected since $G(S_2)$ is approximately 0.2 dB smaller than $G(\Lambda_\pi)$.

6.6.2 Three Channel Performance

In this setup we let $\psi_L = 1.4808$ and the packet-loss probabilities are fixed at $p_0 = 2.5\%, p_1 = 7.5\%$ except for p_2 which is varied in the range $[1, 10]\%$. As p_2 is varied we update ν according to (6.17) and pick the index values N_i such that $\sum_i R_i \leq R^*$. Since index values are restricted to a certain set of integers, cf. Section 2.3.1, the side entropies might not sum exactly to R^*. To make sure the target entropy is met with equality we then re-scale ν as $\nu = 2^{L(\bar{h}(X) - \frac{1}{K} R^*)} \prod_{i=0}^{K-1} N_i^{-1/K}$. We see from Fig. 6.5 a good correspondence between the theoretically and numerically obtained results.

6.7 Conclusion

We presented a design for high-resolution K-channel asymmetric MD-LVQ. Along the lines of the previous chapter, closed-form expressions for the optimal central and side quantizers based on packet-loss probabilities and subject to target entropy constraints were derived and practical quantizers were constructed to verify theoretical
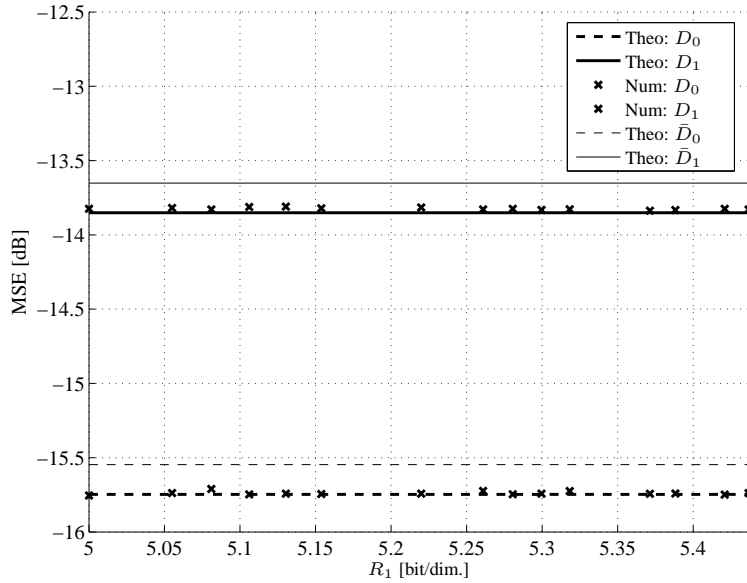
Figure 6.4: *The side distortions are here kept fixed as the rate is increased. Notice that the numerically obtained side distortions D_0 and D_1 (crosses) are strictly smaller than the theoretical $\bar{D}_0$ and $\bar{D}_1$ (thin lines).*

results. For the two-channel case we compared the proposed MD-LVQ scheme to a state-of-the-art two-channel asymmetric scheme and showed that the performance of the central quantizer was equivalent to that of the state-of-the-art scheme whereas the side quantizers were strictly superior in finite dimensions greater than one. The problem of distributing bits among the K descriptions was analyzed and it was shown that the optimal solution was not unique. In fact, it turned out that bits could be almost arbitrarily distributed among the K descriptions without loss of performance. As was the case for the symmetric design, the practical design of asymmetric MD-LVQ allows an arbitrary number of descriptions but the theoretical rate-distortion results were only proven for the case of $K \leq 3$ descriptions and conjectured to be true in the general case of arbitrary K descriptions.
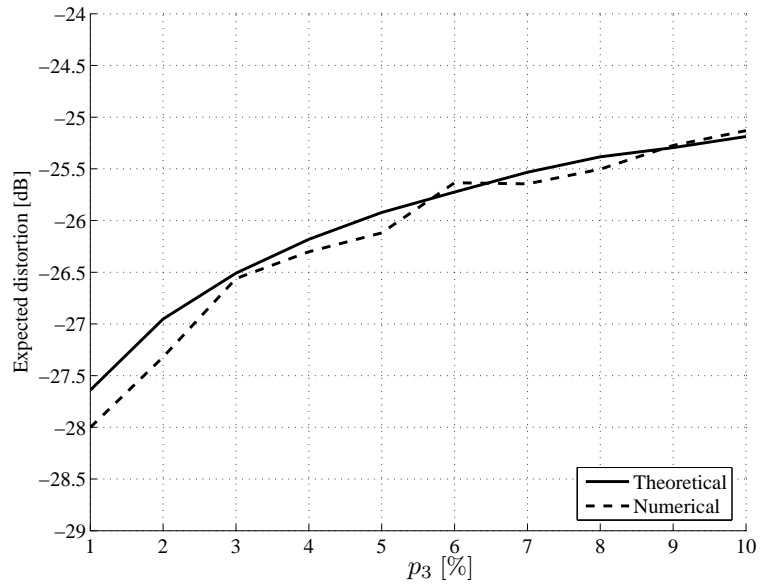
Figure 6.5: *Expected distortion as a function of packet-loss probabilities for $K = 3$ packets and an entropy of 3 bit/dim. per description. The packet-loss probabilities are $p_0 = 2.5\%$, $p_1 = 7.5\%$, $1\% \leq p_2 \leq 10\%$ and $\psi_L = 1.14808$.*

Comparison to Existing High-Resolution MD Results

In this chapter we compare the rate-distortion performance of the proposed MD-LVQ scheme to that of existing state-of-the-art schemes as well as to known information theoretic high-resolution K-channel MD rate-distortion bounds.

7.1 Two-Channel Performance

We will first consider the symmetric case and show that, while the proposed design is different than the design of Vaishampayan et al. [139], the two-channel performance is, in fact, identical to the results of [139]. Then we consider the asymmetric case and show that the asymmetric distortion product given by Lemma 4.1.1 is achievable.

7.1.1 Symmetric Case

Let $K = 2$ so that $\psi_L^2 = 1$. From Theorem 6.5.1 (see also (5.34)) we see that the side distortion (i.e. for $k = 1$) for the symmetric case, i.e. $D_0 = D_1$ and $R_s = R_i, i = 0, 1$, is given by (asymptotically as $N \to \infty$ and $\nu_s \to 0$)

$$D_0 = \frac{1}{4}G(S_L)N^{4/L}\nu^{2/L}. \tag{7.1}$$

In order to trade off the side rate for the central rate we use an idea of [139] and let $2^{-2aR_s} = 4N^{-2/L}$ where $0 < a < 1$, which implies that

$$N = 2^{L(aR_s+1)}. \tag{7.2}$$

Let us insert (7.2) into (5.19) in order to express ν as a function of R_s and a,

$$\nu = 2^{L(h(X)-aR_s-R_s-1)}. \tag{7.3}$$

From (6.21) we know that the two-channel central distortion D_c is given by $D_c = G(\Lambda_c)\nu^{2/L}$ which by use of (7.3) can be rewritten as

$$D_c = G(\Lambda_c)2^{2(h(X)-aR_s-R_s-1)}, \tag{7.4}$$

which leads to

$$\lim_{R_s \to \infty} D_c 2^{2R_s(1+a)} = \frac{1}{4}G(\Lambda_c)2^{2h(X)}. \tag{7.5}$$

By inserting (7.2) and (7.3) in (7.1) we find

$$D_0 = \frac{1}{4}G(S_L)2^{4(aR_s+1)+2(h(X)-aR_s-R_s-1)}, \tag{7.6}$$

which leads to

$$\lim_{R_s \to \infty} D_0 2^{2R_s(1-a)} = G(S_L)2^{2h(X)}. \tag{7.7}$$

Comparing (7.5) and (7.7) with those of Vaishampayan (4.56) and (4.57) reveals that the performance of the proposed two-channel design achieve the same performance as the two-channel design of Vaishampayan et al. [139]. Furthermore, let $b = 1$ and $L \to \infty$ and notice that in the memoryless Gaussian case $G(S_\infty)2^{2h(X)} = \sigma_X^2$ so that, by comparing (7.5) and (7.7) with (4.11) and (4.10), we see that the high-resolution two-channel symmetric rate-distortion function of Ozarow can be achieved.

Remark 7.1.1. It is important to see that a in (7.5) and (7.7) is bounded away from zero and one. In the extreme case where $a = 0$ the ratio of side distortion over central distortion is small and N cannot be made arbitrarily large as is required for the asymptotic expressions to be valid. On the other hand, when $a = 1$ we can no longer force the cells of the side quantizers to be small compared to the variance of the source and the high resolution assumptions are therefore not satisfied. This is also true for the general case of $K > 2$ descriptions.

Remark 7.1.2. We would like to point out an error in [102] where we overlooked the requirement that $a < 1$. In [102] we showed that the high resolution performance of $(3,2)$ SCECs can be achieved by use of lattice codebooks and index assigments (which is true) but we also wrongly claimed that in the extreme case where $a = 1$, lattice codebooks achieve rate-distortion points that cannot be achieved by random codebooks, obviously, this cannot be true since, for $a = 1$, the high resolution assumptions are not satisfied (Remark 7.1.1).

7.1.2 Asymmetric Case

We already showed in Section 6.6 that the performance of the asymmetric two-channel scheme by Diggavi et al. [27, 28] can be achieved. In fact, in finite dimensions greater

than one, the performance of the proposed scheme was strictly superior to that of Diggavi et al. Furthermore, it is easy to show that the high resolution asymmetric distortion product presented by Lemma 4.1.1 can be achieved. To see this note that by use of (6.22), (6.23) and (6.21) we get

$$D_c(D_0 + D_1 + 2\sqrt{D_0 D_1}) = G(\Lambda_c)2^{2(h(X)-R_c)} \tag{7.8}$$
$$\times \left(\frac{\gamma_0^2 + \gamma_1^2}{(\gamma_0 + \gamma_1)^2}G(S_L)2^{2h(X)}2^{-2(R_0+R_1-R_c)} \right.$$
$$\left. + 2\sqrt{\frac{\gamma_0^2\gamma_1^2}{(\gamma_0 + \gamma_1)^4}G(S_L)^2 2^{4h(X)}2^{-4(R_0+R_1-R_c)}} \right)$$
$$= G(\Lambda_c)G(S_L)2^{4h(X)}2^{-2(R_0+R_1)},$$

which, asymptotically as $L \to \infty$, leads to Lemma 4.1.1.

7.2   Achieving Rate-Distortion Region of $(3, 1)$ SCECs

We will now consider the symmetric three-channel case and show that the rate-distortion performance of $(3, 1)$ SCECs can be achieved at high resolution.

We are interested in the three-channel case, i.e. $K = 3$, and in the limit of $L \to \infty$ so that

$$G(S_L) \to \frac{1}{2\pi e} \tag{7.9}$$

and

$$\psi_\infty^2 = \sqrt{\frac{4}{3}}. \tag{7.10}$$

Furthermore, without any loss of generality, we assume that the source has unit variance. Thus, from (5.34) we see that

$$D^{(3,1)} = \frac{1}{3}\psi_\infty^2 N'2^{-2R_s}, \tag{7.11}$$

since $R_c = R_s + \log_2(N')$,

$$D^{(3,2)} = \frac{1}{12}\psi_\infty^2 N'2^{-2R_s}, \tag{7.12}$$

and the central distortion $D_c = D^{(3,3)}$ given by (6.21) can be written as

$$D^{(3,3)} = \left(\frac{1}{N'}\right)^2 2^{-2R_s}. \tag{7.13}$$

The following lemma shows that symmetric three-channel MD-LVQ can achieve the rate-distortion region of $(3, 1)$ SCECs at high resolution.

Lemma 7.2.1. At high resolution, the one, two and three-channel distortions of $(3, 1)$ SCECs are identical to (7.11) – (7.13) in the quadratic Gaussian case.

Proof. See Appendix J.1.   □

Remark 7.2.1. The notion of a large sublattice index N in K-channel MD-LVQ corresponds to a large (negative) codebook correlation ρ_q for $(K, 1)$ SCECs and in the limit of $N \to \infty$ we actually have $\rho_q \to -1/(K-1)$. Thus, for $K = 3$ we have $\rho_q \to -1/2$ as $N \to \infty$.

7.3 Achieving Rate-Distortion Region of $(3, 2)$ SCECs

We will now show that the rate-distortion performance of $(3, 2)$ SCECs can be achieved by extending the proposed design of three-channel MD-LVQ to include random binning on the side codebooks. Specifically, we show that the achievable two-channel versus three-channel distortion region of $(3, 2)$ SCECs for the memoryless Gaussian source and MSE can be achieved under high-resolution assumptions. Since the performance of a $(3, 3)$ SCEC is identical to that of a single description scheme, it is clear that we can also achieve such performance simply by letting $K = 1$ and only use the central quantizer. Explicit bounds for $K > 3$ descriptions were not derived in [111, 114] but we expect that these (non-derived) bounds are also achievable with the proposed K-channel MD-LVQ scheme.

We will begin by considering the general situation where we allow finite dimensional lattice vector quantizers and asymmetric rates and distortions. Then, at the end of the section, we focus on the symmetric case and infinite-dimensional lattice vector quantizers in order to compare the performance to the existing bounds.

Recall that the proposed design of K-channel MD-LVQ is able to vary the redundancy by changing the number of descriptions K as well as the index values N_i. In addition, it is possible to trade off distortion among subsets of descriptions, without affecting the rates, simply by varying the weights. Increasing N_i and at the same time decreasing ν so that $\nu_i = N_i\nu$ remains constant does not affect the rate R_i. However, the distortion due to the ith description is affected (unless counteracted by the weights). For example in the symmetric setup where $N = N_i$ for all i and the weights are also balanced, the side distortion due to reception of only a subset of descriptions is increased as N is increased and νN is kept constant. However, in this case, the central distortion due to reception of all descriptions is decreased. In other words, in the symmetric case, for a given K, the degree of redundancy is controled by the single parameter N.

7.3.1   Random Binning on Side Codebooks of MD-LVQ Schemes

In order to achieve the performance of general (K,k) SCECs we need to introduce more controlling parameters into the design of K-channel MD-LVQ. To do so we follow an idea of Pradhan et al. [111] and exploit recent results on distributed source coding. More specifically, we apply random binning on the side codebooks of the K-channel MD-LVQ scheme. This corresponds in some sense to replacing the random codebooks of (K,k) SCECs with structured lattice codebooks except that we also have a central quantizer and an index assignment map to consider.

Random binning is usually applied on (in principle infinite-dimensional) random codebooks. The idea is to exploit the fact that for a given codevector, say λ_0, of codebook $\mathscr{C}_0$, only a small set of the codevectors in codebook $\mathscr{C}_1$ is jointly typical with λ_0. Then by randomly distributing the codevectors of $\mathscr{C}_1$ over M_1 bins, it is unlikely that two or more codevectors, which are all jointly typical with λ_0, end up in the same bin (at least this is true if M_1 is large enough). Thus, if the binning rate $R_{b,1} = \log_2(M_1)$ is less than the codebook rate R_1 then it is possible to reduce the description rate by sending the bin indices instead of the codevector indices.

The rate and distortion performance of lattice vector quantizers are often described using high-resolution assumptions, i.e. the rate of the quantizer is sufficiently high and the source pdf sufficiently smooth, so that the pdf can be considered constant within Voronoi regions of the code vectors. Under these assumptions the theoretical performance of lattice vector quantizers can be derived for arbitrary vector dimension. This is in contrast to the asymptotics used when deriving theoretical expressions for the performance of random codebooks. For random codebooks the theoretical performance is usually derived based on asymptotically high vector dimension but arbitrary rates. The theory behind random binning relies upon asymptotically high vector dimension and as such when using random binning in K-channel MD-LVQ we make use of both asymptotics, i.e. high vector dimension and high rates. It is also worth mentioning that we consider memoryless sources with infinite alphabets such as e.g. the Gaussian source, whereas the analysis of SCECs relies upon strong typicality and as such only discrete alphabet memoryless sources are valid.[50]

In lattice codebooks, the code vectors are generally not jointly typical and the concept of random binning is therefore not directly applicable. It is, however, possible to simulate joint typicality by for example some distance metric, so that code vectors close together (in e.g. Euclidean sense) are said to be "jointly typical". The index assignments of MD-LVQ is another example of how to simulate joint typicality. We use the term admissible K-tuple for any set of K code vectors $(\lambda_0, \ldots, \lambda_{K-1})$ which is obtained by applying the index-assignment map on a code vector λ_c, i.e. $\alpha(\lambda_c) = (\lambda_0, \ldots, \lambda_{K-1})$ for all $\lambda_c \in \Lambda_c$. So for lattice code vectors we exploit that only a subset of all K-tuples are admissible K-tuples which, in some sense, corresponds to

---

[50]However, in [111] the authors remark that the analysis of SCECs can be generalized to continuous-alphabet memoryless sources by using the techniques of [41, Ch.7].

the fact that only a subset of all K-tuples of random code vectors are jointly typical.

Let $J \subseteq \{0, \ldots, K-1\}$ denote an index set, where $|J| = k$. A k-tuple is a set of k elements $\{\lambda_j\}, j \in J$ where $\lambda_j \in \Lambda_j$. The k-tuple given by $\{\lambda_j\} = \{\alpha_j(\lambda_c)\}, j \in J$ for any $\lambda_c \in \Lambda_c$ is said to be an admissible k-tuple. Each lattice Λ_i contains an infinite number of lattice points (or reproduction vectors) but we show by Lemma 7.3.1 that only finite sets of these points are needed for the codebooks of the side quantizers and we denote these sets by $\mathscr{C}_i \subset \Lambda_i$, where $|\mathscr{C}_i| < \infty$. The set

$$
\begin{aligned}
\{\lambda_2 | \{\lambda_1, \lambda_0\}\} = \\
\{\lambda_2 \in \Lambda_2 : \lambda_2 = \alpha_2(\lambda_c) \text{ and } (\alpha_1(\lambda_c), \alpha_0(\lambda_c)) = (\lambda_1, \lambda_0), \ \forall \lambda_c \in \Lambda_c\},
\end{aligned}
\tag{7.14}
$$

denotes the set of λ_2's which are in admissible k-tuples that also contain the specific elements λ_0 and λ_1.

Since we consider the asymmetric case some ambiguity is present in the term $D^{(K,k)}$, because it is not specified which k out of the K descriptions that are to be considered. To overcome this technicality we introduce the notation $D^{(K,J)}, J \in \mathscr{K}$, where $\mathscr{K}$ denotes the set of combinations of descriptions for which the distortion is specified. For example, if we are only interested in the distortion when receiving descriptions $\{0, 1\}, \{0, 2\}$ or $\{0, 1, 2\}$ out of all subset of $\{0, 1, 2\}$, then $\mathscr{K} = \{\{0, 1\}, \{0, 2\}, \{0, 1, 2\}\}$ and nothing is guaranteed upon reception of either a single description or the pair of descriptions $\{1, 2\}$.

We will now outline the construction of $(K, \mathscr{K})$ MD-LVQ. It can be seen that the construction of $(K, \mathscr{K})$ MD-LVQ resembles the construction of (K, k) SCECs given in [111].

Construction of lattice codebooks   Construct a K-channel MD-LVQ system with one central quantizer and K side quantizers of rate R_i. Let $\mathscr{C}_c$ be the codebook of the central quantizer and let $\lambda_c(j_c) \in \mathscr{C}_c$ denote the j_c^{th} element of $\mathscr{C}_c$. Similarly, let $\mathscr{C}_i$ where $i = 0, \ldots K - 1$ denote the codebook of the ith side quantizer and let $\lambda_i(j_i) \in \mathscr{C}_i$ denote the j_i^{th} codeword of $\mathscr{C}_i$. Finally, let α be the index-assignment function that maps central lattice points to sublattice points.

Random binning   Perform random binning on each of the side codebooks $\mathscr{C}_i$ to reduce the side description rate from R_i to $R_{b,i}$ bit/dim., where we assume $R_i > R_{b,i}$. Let $\xi_i = 2^{L(R_i - R_{b,i} + \gamma_i)}$ where $\gamma_i > 0$. Assign ξ_i codewords to each of the $2^{LR_{b,i}}$ bins of each codebook. The codewords for a given bin of codebook $\mathscr{C}_0$ is found by randomly extracting ξ_0 codewords from $\mathscr{C}_0$ uniformly, independently and with replacement. This procedure is then repeated for all the remaining codebooks $\mathscr{C}_i, i = 1, \ldots, K - 1$.

Encoding   Given a source word $X \in \mathbb{R}^L$, find the closest element $\lambda_c \in \mathscr{C}_c$ and use α to obtain the corresponding K-tuple, i.e. $\alpha(\lambda_c) = (\lambda_0(j_0), \ldots, \lambda_{K-1}(j_{K-1}))$. If

the codeword $\lambda_i \notin \mathscr{C}_i$ then set j_i equal to a fixed special symbol[51], say $j_i = \vartheta$. For $i = 0, \ldots, K - 1$ define the function $f_i(\lambda_i(j_i))$ which indicates the index of a bin containing the codeword $\lambda_i(j_i)$. If $\lambda_i(j_i)$ is found in more than one bin, set $f_i(\lambda_i(j_i))$ equal to the least index of these bins. If $\lambda_i(j_i)$ is not in any bin, set $f_i(\lambda_i(j_i)) = \vartheta$. The bin index $f_i(\lambda_i(j_i))$ is sent over channel i.

Decoding   The decoder receives some m bin indices and searches through the corresponding bins to identify a unique admissible m-tuple.

Remark 7.3.1. For $(K, \mathscr{K})$ MD-LVQ the notion of large block length, i.e. $L \to \infty$, is introduced in order to make sure that standard binning arguments can be applied. However, it should be clear that the quantizer dimension is allowed to be finite. If finite quantizer dimension is used it must be understood that (finite length) codewords from consecutive blocks are concatenated to form an L-sequence of codewords. The dimension of the L-sequence becomes arbitrarily large as $L \to \infty$, but the quantizer dimension remains fixed. As such this will not affect the binning rate but the distortion tuple $\{D^{(K,J)}\}_{J \in \mathscr{K}}$ is affected in an obvious way.

Theorem 7.3.1. Let $X \in \mathbb{R}^L$ be a source vector constructed by blocking an arbitrary i.i.d. source with finite differential entropy into sequences of length L. Let $J \subseteq \{0, \ldots, K - 1\}$ and let λ_J denote the set of codewords indexed by J. The set of decoding functions is denoted $g_J \colon \bigotimes_{j \in J} \Lambda_j \to \mathbb{R}^L$. Then, under high-resolution assumptions, if

$$E[\rho(X, g_J(\lambda_J))] \le D^{(K,J)}, \quad \forall J \in \mathscr{K},$$

where $\rho(\cdot, \cdot)$ is the squared-error distortion measure and for all $S \subseteq J$

$$\sum_{i \in S} R_{b,i} > \sum_{i \in S} \gamma_i + \frac{1}{L} \log_2(|\{\lambda_S | \lambda_{J-S}\}|), \tag{7.15}$$

the rate-distortion tuple $(R_{b,0}, \ldots, R_{b,(K-1)}, \{D^{(K,J)}\}_{J \in \mathscr{K}})$ is achievable.

Proof. See Appendix J.2. $\square$

We have the following corollary for the symmetric case:

Corollary 7.3.1 (Symmetric case)**.** Let $X \in \mathbb{R}^L$ be a source vector constructed by blocking an arbitrary i.i.d. source with finite differential entropy into sequences of length L. For any $J \subseteq \{0, \ldots, K - 1\}$ let λ_J denote the set of received codewords and let $g_J \colon \bigotimes_{j \in J} \Lambda_j \to \mathbb{R}^L$ be the set of decoding functions. Then, under high-resolution assumptions, if

$$E[\rho(X, g_J(\lambda_J))] \le D^{(K,|J|)}, \quad \forall J \subseteq \{0, \ldots, K - 1\}, |J| \ge k,$$

where $\rho(\cdot, \cdot)$ is the squared-error distortion measure and for all $S \subseteq J$

---

[51]The rate increase caused by the introduction of the additional symbol ϑ is vanishing small for large L.

$$R_b > \gamma + \frac{1}{|S|L} \log_2(|\{\lambda_S | \lambda_{J-S}\}|), \tag{7.16}$$

the tuple $(R_b, D^{(K,k)}, D^{(K,k+1)}, \dots, D^{(K,K)})$ is achievable.

Proof. Follows immediately from Theorem 7.3.1. □

7.3.2 Symmetric Case

To actually apply Theorem 7.3.1 we need to find a set of binning rates $\{R_{b,i}\}, i = 0, \dots, K - 1$, such that (7.15) is satisfied for all subsets S of J and for all elements J of $\mathcal{K}$. Let us consider the symmetric case where $K = 3$ and design a $(3, 2)$ MD-LVQ system. We then have $J = \{i_0, i_1\}$ and it suffices to check the two cases where $S = i_0$ and $S = \{i_0, i_1\}$. Without loss of generality we assume that $i_0 = 0$ and $i_1 = 1$. The number of distinct λ_1's that is paired with a given λ_0 can be approximated[52] by $(\psi_L \sqrt{N'})^L$, where $N' = N^{1/L}$ is the dimension normalized index value describing the index (redundancy) per dimension. Let $S = \{0, 1\}$ and notice that $|\{\lambda_S\}| \le |\{\lambda_1 | \lambda_0\}| \cdot |\mathcal{C}_0|$. Then, asymptotically, as $N \to \infty$, it follows that $|\{\lambda_1 | \lambda_0\}| = (\psi_L \sqrt{N'})^L$. Let us now bound the codebook cardinality.

Lemma 7.3.1. $|\mathcal{C}_i| = 2^{LR_i}$. Furthermore, the entropy of the quantizer indices is upper bounded by R_i.[53]

Proof. See Appendix J.1. □

We are now able to find R_b by considering the two cases $|S| = 1, 2$. For $|S| = 1$ we have from (7.16) that

$$R_{b,I} > \gamma + \log_2(\psi_L \sqrt{N'}), \tag{7.17}$$

whereas for $|S| = 2$

$$R_{b,II} > \frac{1}{2}R_s + \gamma + \frac{1}{2}\log_2(\psi_L \sqrt{N'}). \tag{7.18}$$

The dominant R_b is then given by $R_b = \max(R_{b,I}, R_{b,II})$. Since (7.17) and (7.18) depends upon N' the dominating binning rate depends upon N'. To resolve this problem, we form the inequality $R_{b,II} \ge R_{b,I}$ and find that $N' \le 2^{2R_s}/\psi_L^2$. So for $N' \le 2^{2R_s}/\psi_L^2$ we have $R_b = R_{b,II}$. It is interesting to see that when inserting $N' = 2^{2R_s}/\psi_L^2$ in (7.17) we get $R_{b,I} = \gamma + R_s$. Coincidently, $R_{b,I}$ becomes effective when the binning rate R_b is equal to the codebook rate R_s, which violates the assumption that $R_b > R_s$.

It is clear that if we set R_b equal to the lower bound in (7.18) we get

$$R_b = \frac{1}{2}R_s + \frac{1}{4}\log_2(N') + \frac{1}{2}\log_2(\psi_L),$$

---

[52]Recall that this approximation becomes exact as $N \to \infty$.
[53]For large L there is really no loss by assuming that 2^{LR_i} is an integer.

from which we can express N' and R_s as functions of each other and R_b, that is

$$N' = 2^{4R_b - 2R_s} \psi_L^{-2}, \tag{7.19}$$

and

$$R_s = 2R_b - \log_2(\psi_L) - \frac{1}{2} \log_2(N'). \tag{7.20}$$

It follows that when varying the redundancy per dimension N', the binning rate R_b can be kept constant by adjusting R_s according to (7.20).

In order to compare these results to the existing bounds we let $L \to \infty$ so that by inserting (7.20) in (5.34) we get

$$
\begin{aligned}
D^{(3,2)} &= \frac{1}{12} \psi_\infty^2 N' 2^{-2R_s} \\
&= \frac{1}{12} \psi_\infty^4 (N')^2 2^{-4R_b}.
\end{aligned} \tag{7.21}
$$

The central distortion ($D_c = D^{(3,3)}$) in MD-LVQ is given by

$$D^{(3,3)} = 2^{-2R_c}, \tag{7.22}$$

where $R_c = R_s + \log_2(N')$ which leads to

$$R_c = 2R_b - \log_2(\psi_\infty) + \frac{1}{2} \log_2(N'). \tag{7.23}$$

Inserting (7.23) into (7.22) leads to

$$D^{(3,3)} = \frac{\psi_\infty^2}{N'} 2^{-4R_b}. \tag{7.24}$$

Lemma 7.3.2. At high resolution, the two and three-channel distortions of $(3, 2)$ SCECs are identical to (7.21) and (7.24) in the quadratic Gaussian case.

Proof. See Appendix J.1. $\square$

7.3.3 Asymmetric Case

For the asymmetric case, $K = 3$ and where $\mathcal{K} = \{\{0, 1\}, \{0, 2\}, \{1, 2\}, \{0, 1, 2\}\}$, i.e. reconstruction is possible when any two or more descriptions are received, it can be shown (similar to the symmetric case) that the binning rate $R_{b,i}$ is lower bounded by $R_{b,i} = \max(R_{b,i_I}, R_{b,i_{II}})$ where

$$R_{b,i_I} = \log_2(\psi_L) + \frac{1}{2} \log_2(N'_\pi) - \log_2(N'_i) \tag{7.25}$$

and

$$R_{b,i_{II}} = \frac{1}{2} \log_2(\psi_L) + \frac{1}{4} \log_2(N'_\pi) - \frac{1}{2} \log_2(N'_i) + \frac{1}{2} R_i, \tag{7.26}$$

where $N'_\pi = N'_0 N'_1 N'_2$.

To see this note that if λ_i and λ_j both are in the same admissible K-tuple, then λ_i must be within a sphere $\tilde{V}$ centered at λ_j. The volume of $\tilde{V}$ is $\tilde{\nu}$, which implies that the maximum number of distinct λ_i points within $\tilde{V}$ is approximately $\tilde{\nu}/\nu_i$. In other words,

$$
\begin{aligned}
|\{\lambda_i | \lambda_j\}| &\approx \tilde{\nu}/\nu_i \\
&= (\psi_L \sqrt{N'_0 N'_1 N'_2}/N_i)^L,
\end{aligned}
\tag{7.27}
$$

where the approximation becomes exact for large index values. With this it is easy to see that

$$
\begin{aligned}
R_{b,i} &> \frac{1}{L} \log_2(|\{\lambda_i | \lambda_j\}|) \\
&\approx \log_2(\psi_L) + \frac{1}{2} \log_2(N'_0 N'_1 N'_2) - \log_2(N_i),
\end{aligned}
\tag{7.28}
$$

which is identical to (7.25). From Theorem 7.3.1 we can also see that the pair-wise sum rate must satisfy

$$
\begin{aligned}
R_{b,i} + R_{b,j} &> \frac{1}{L} \log_2(|C_i||\{\lambda_j | \lambda_i\}|) \\
&\approx R_i + \log_2(\psi_L) + \frac{1}{2} \log_2(N'_0 N'_1 N'_2) - \log_2(N_j),
\end{aligned}
\tag{7.29}
$$

which can equivalently be expressed as $R_{b,i} + R_{b,j} > \frac{1}{L} \log_2(|C_j||\{\lambda_i | \lambda_j\}|)$ from which the individual rate requirements can be found to be given by (7.26).

7.4   Comparison to K-Channel Schemes

In the asymptotic case of large lattice vector quantizer dimension and under high resolution conditions, we showed in the previous sections that existing MD bounds can be achieved. However, it is also of interest to consider the rate-distortion performance that can be expected in practical situations. Towards that end we presented some numerical results obtained through computer simulations in Sections 5.6 and 6.6.

In this section we will compare the theoretical performance of the proposed MD-LVQ scheme to existing state-of-the-art K-channel MD schemes [18, 127]. While the schemes [18, 127] (as well as the proposed scheme) can be shown to be optimal, under certain asymptotic conditions, they are not without their disadvantages when used in practical situations. We will, however, refrain from comparing implementation specific factors such as computational complexity as well as scalability in dimension, description rate and number of descriptions. Such comparisons, although relevant, are often highly application specific.

The above mentioned schemes are all based on LVQ and it is therefore possible to compare their theoretical rate-distortion performance when finite-dimensional lattice

vector quantizers are used. Recall from Section 4.2.2 that the scheme of Chen et al. [18] has a rate loss of $(2K - 1)$ L-dimensional lattice vector quantizers.[54] The scheme of Østergaard and Zamir [127] was, for the case of $K = 2$, shown to have a rate loss of only two L-dimensional lattice vector quantizers. While this design was shown to permit an arbitrary number of descriptions, the rate loss for $K > 2$ descriptions was not assessed. The rate loss of the proposed scheme, on the other hand, has a somewhat peculiar form. In the case of two descriptions, the rate loss is given by that of two L-dimensional quantizers having spherical Voronoi cells.[55] However, in the case of $K > 2$ descriptions, there is an additional term which influences the rate loss.

7.4.1   Rate Loss of MD-LVQ

To be able to assess the rate loss of MD-LVQ when using finite-dimensional quantizers and more than two descriptions, we let R_f denote the description rate (where the subscript $_f$ indicates that finite-dimensional quantizers are used). Then the distortion when receiving a single description out of $K = 3$ can be found by use of (5.34) to be given by

$$D^{(3,1)} = \frac{1}{3}G(S_L)(2\pi e)\psi_L^2 N' 2^{-2R_f}. \tag{7.30}$$

Equalizing (7.11) and (7.30) reveals that the rate loss $(R_f - R_s)$, for $K = 3$, is given by (at high resolution)

$$R_f - R_s = \frac{1}{2}\log_2(G(S_L)(2\pi e)) + \log_2(\psi_L/\psi_\infty). \tag{7.31}$$

Since $\psi_L \leq \psi_1 = \psi_\infty^2$ (at least for $K = 3$) we can upper bound the second term of (7.31) by

$$\log_2(\psi_L/\psi_\infty) \leq \log_2(\psi_\infty) = 0.1038 \text{ bit/dim.} \tag{7.32}$$

Fig. 7.1 shows $\log_2(\psi_L/\psi_\infty)$ for $1 \leq L \leq 101$ for $K = 3$ using the values of ψ_L from Table 5.1.

Remark 7.4.1. For $K = 2$ we have $\psi_L = 1, \forall L$, and (7.31) is true. Furthermore, if the K-channel MD-LVQ scheme is optimal also for $K > 3$, as we previously conjectured, then (7.31) is true for any $K \geq 2$ (at high resolution).

It is interesting to observe that both terms in (7.31) are independent of the particular type of lattice being used. For example, if the product lattice $\Lambda = Z^\infty$ is used for the side quantizers, then the rate loss vanishes (it becomes identical to

---

[54] In the asymmetric case where corner points of the rate region are desired, the rate loss of [18] is only that of K lattice vector quantizers. However, in the symmetric case, source splitting is necessary and there is an additional rate loss.

[55] This is true in the symmetric case as well as in the asymmetric case.

zero) even though $G(\Lambda) = 1/12$.[56] This is not the case with the other two schemes mentioned above, i.e. [18, 127]. Fig. 7.2 shows the rate loss of the different schemes for $K = 3$ descriptions. The lattices used are those of Table 3.1. Since we do not have ψ_L values for all even L we have in Fig. 7.2 simply used the average of the two neighboring values, that is

$$\psi_L = \begin{cases} \dfrac{\psi_{L-1} + \psi_{L+1}}{2}, & L \text{ even} \\ \psi_L, & L \text{ odd.} \end{cases} \qquad (7.33)$$
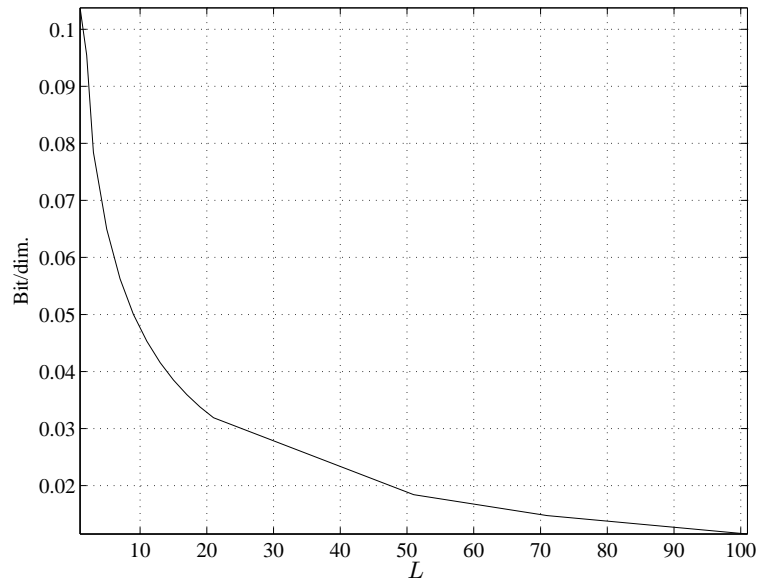
Figure 7.1: *The rate loss due to the term* $\log_2(\psi_L/\psi_\infty)$ *is here expressed in bit/dim. as a function of the dimension L.*

7.5   Conclusion

In the previous two chapters we initially used a single index-assignment map to control the redundancy between descriptions. In this chapter we then showed that by use of random binning on the side codebooks in addition to the index-assignment map it was possible to introduce more rate-distortion controlling parameters into the design. While the use of random binning is standard procedure in distributed source coding

---

[56]Recall that the central distortion depends upon the type of lattice being used. However, at high resolution conditions, the index value is large (i.e. $N \to \infty$) and as such the central distortion is very small compared to the side distortion and can therefore be neglected.
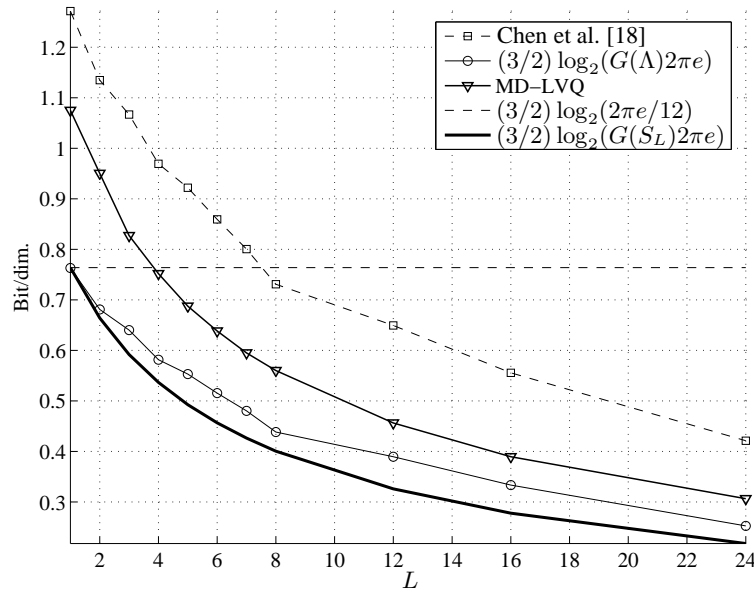
Figure 7.2: *Rate loss of the different three-channel MD schemes. For comparison we have included a lower bound (thick solid curve), which corresponds to the sum rate loss of three L-dimensional quantizers having spherical Voronoi cells. The horizontal dashed line corresponds to the sum rate loss of three lattice vector quantizers with hypercubic cells and the circles illustrate the performance of a scheme having a sum rate loss of three optimal lattice vector quantizers.*

and has previously been applied to MD schemes based on random codebooks as well, it appears to be the first time it is used in connection with index-assignment based MD schemes.

We showed that the proposed design of MD-LVQ, asymptotically in rate and lattice vector quantizer dimension, achieves existing rate-distortion MD bounds in the quadratic Gaussian case for two and three descriptions.

In finite lattice vector quantizer dimensions, we showed that the rate-loss of the proposed design is superior to existing state-of-the-art schemes.

Chapter 8

Network Audio Coding

In this chapter we apply the developed MD coding scheme to the practical problem of network audio coding. Specifically, we consider the problem of reliable distribution of audio over packet-switched networks such as the Internet or general ad hoc networks.[57] Thus, in order to combat (excessive) audio packet losses we choose to transmit multiple audio packets.

Many state-of-the-art audio coding schemes perform time-frequency analysis of the source signal, which makes it possible to exploit perceptual models in both the time and the frequency domain in order to discard perceptually-irrelevant information. This is done in e.g. MPEG-1 (MP3) [93], MPEG-2 advanced audio coding (AAC) [94], Lucent PAC [123] and Ogg Vorbis [134]. The time-frequency analysis is often done by a transform coder which is applied to blocks of the input signal. A common approach is to use the modified discrete cosine transform (MDCT) [90] as was done in e.g. MPEG-2 AAC [94], Lucent PAC [123] and Ogg Vorbis [134]. In this chapter we combine the MDCT with K-channel MD-LVQ in order to obtain a perceptual transform coder, which is robust to packet losses.

MD coding of audio has to the best of the author's knowledge so far only been considered for two descriptions [3, 119]. However, here we propose a scheme that is able to use an arbitrary number of descriptions without violating the target entropy. We show how to distribute the bit budget among the MDCT coefficients and present closed-form expressions for the rate and distortion performance of the K-channel MD-LVQ system which minimize the expected distortion based on the packet-loss probabilities. Theoretical results are verified with numerical computer simulations and it is shown that in environments with excessive packet losses it is advantageous to use more than two descriptions. We verify the findings that more than two descriptions are needed by subjective listening tests, which further proves that acceptable audio

---

[57]Part of the research presented in this chapter represents joint work with O. Niamut.

quality can be obtained even when the packet-loss rate is as high as 30%.

8.1 Transform Coding

In this section we describe the MDCT and we define a perceptual distortion measure in the MDCT domain.

8.1.1 Modified Discrete Cosine Transform

The MDCT is a modulated lapped transform [90] which is applied on overlapping blocks of the input signal. A window of $2M$ time-domain samples is transformed into M MDCT coefficients, whereafter the window is shifted M samples for the next M MDCT coefficients to be calculated.

Given a block $s \in \mathbb{R}^{2M}$, the set of M MDCT coefficients is given by [90]

$$x_k = \frac{1}{\sqrt{2M}} \sum_{n=0}^{2M-1} h_n s_n \cos\left(\frac{(2n+M+1)(2k+1)\pi}{4M}\right), \quad k = 0, \ldots, M-1,$$
(8.1)

where $x_k, h_n \in \mathbb{R}$ and h is an appropriate analysis window, e.g. the symmetric sine window [90]

$$h_n = \sin\left(\left(n + \frac{1}{2}\right)\left(\frac{\pi}{2M}\right)\right), \quad n = 0, \ldots, 2M-1.$$
(8.2)

The inverse MDCT is given by [90][58]

$$\tilde{s}_n = h_n \frac{1}{\sqrt{2M}} \sum_{k=0}^{M-1} x_k \cos\left(\frac{(2n+M+1)(2k+1)\pi}{4M}\right), \quad n = 0, \ldots, 2M-1.$$
(8.3)

8.1.2 Perceptual Weighting Function

On each block a psycho-acoustic analysis is performed which leads to a masking curve that describes thresholds in the frequency domain below which distortions are inaudible. In our work the masking curve is based on a $2nM$-point DFT where $n \in \mathbb{N}$ and the computation of the masking curve is described in detail in [140]. Let us denote the masking curve by Σ. We then define a perceptual weight μ as the inverse of the masking threshold Σ evaluated at the center frequencies of the MDCT basis functions, that is

$$\mu_k = \Sigma_{2nk+1}^{-1}, \quad k = 0, \ldots, M-1.$$
(8.4)

---

[58]Notice that the MDCT is not an invertible transform on a block-by-block basis since $2M$ samples are transformed into only M samples. We therefore use the tilde notation to indicate that, at this point, the reconstructed samples $\tilde{s}_n$ are not identical to the original samples s_n. In order to achieve perfect reconstruction we need to perform overlap-add of consecutive reconstructed blocks [90].

We require μ to be a multiplicative weight but otherwise arbitrary. We will not go into more details about μ except mentioning that we assume it can be efficiently encoded at e.g. 4 kpbs as was done in [96].

8.1.3   Distortion Measure

Let $X \in \mathbb{R}^M$ denote a random vector process[59] and let $x \in \mathbb{R}^M$ be a realization of X. By X_k and x_k we denote the kth components of X and x, respectively, and we will use $\mathscr{X}_k$ to denote the alphabet of X_k. The pdf of X is denoted f_X with marginals f_{X_k}.

We define a perceptual distortion measure in the MDCT domain between x and a quantized version $\hat{x}$ of x to be the single-letter distortion measure given by[60]

$$\rho(x, \hat{x}) \triangleq \frac{1}{M} \sum_{k=0}^{M-1} \mu_k |x_k - \hat{x}_k|^2, \tag{8.5}$$

where μ_k is given by (8.4). The expected perceptual distortion follows from (8.5) simply by taking the expectation over x, that is

$$D(x, \hat{x}) = \frac{1}{M} \sum_{k=0}^{M-1} \int_{\mathscr{X}_k} \mu_k |x_k - \hat{x}_k|^2 f_{X_k}(x_k) dx_k, \tag{8.6}$$

where we remark that μ depends on s through x.

8.1.4   Transforming Perceptual Distortion Measure to ℓ_2

For the traditional MSE distortion measure which is also known as the ℓ_2 distortion measure, it is known that, under high-resolution assumptions, a lattice vector quantizer is good (even optimal as $L \to \infty$) for smooth sources, see Chapter 3. The MSE distortion measure is used mainly due its mathematical tractability. However, in applications involving a human observer it has been noted that distortion measures which include some aspects of human auditory perception generally perform better than the MSE. A great number of perceptual distortion measures are non-difference distortion measures and unfortunately even for simple sources their corresponding rate-distortion functions are not known. For example, the perceptual distortion measure given by (8.6) is an input-weighted MSE (because μ is a function of s), hence it is a non-difference distortion measure.

In certain cases it is possible to derive the rate-distortion functions for general sources under non-difference distortion measures. For example, for the Gaussian process with a weighted squared error criterion, where the weights are restricted to

---

[59]In fact it is the output of the MDCT of a random vector process $S \in \mathbb{R}^{2M}$.

[60]Strictly speaking this is not a single-letter distortion measure since the perceptual weight depends upon the entire vector.

be linear time-invariant operators, the complete rate-distortion function was found in [118]. Other examples include the special case of locally quadratic distortion measures for fixed rate vector quantizers and under high-resolution assumptions [43], results which are extended to variable-rate vector quantizers in [80, 83]. With regards to the MD problem, [84] presents a high-resolution rate-distortion region for smooth sources and locally quadratic distortion measures for the case of two descriptions. The case of vector sources and more than two descriptions remains unsolved.

Remark 8.1.1. In the SD case it has been shown that it is sometimes possible to apply a function (called a multidimensional compressor) on the source signal in order to transform it into a domain where a lattice vector quantizer is good. This approach was first considered by Bennett in [7] for the case of a scalar compressor followed by uniform scalar quantization. The general case of a multidimensional compressor followed by lattice vector quantization was considered in [85]. In general an L-dimensional source vector X is "compressed" by an invertible mapping F.[61] Hereafter $F(X)$ is quantized by a lattice vector quantizer. To obtain the reconstructed signal $\hat{X}$, the inverse mapping F^{-1} (the expander) is applied, that is

$$X \to F(\cdot) \to Q(\cdot) \to F^{-1}(\cdot) \to \hat{X}, \tag{8.7}$$

where Q denotes a lattice vector quantizer. It was shown in [85] that an optimal compressor F is independent of the source distribution and only depends upon the distortion measure. However, it was also shown that an optimal compressor does not always exists.[62] In the MD case, results on optimal compressors are very limited. However, it was suggested in [84], that a compressor obtained in a similar way as for the SD case, might perform well also in the two-description case for smooth scalar processes. Unfortunately, we have been unsuccessful in finding an analytical expression for such a vector compressor for our distortion measure (8.5).

In this chapter we will assume that the decoder has access to the perceptual weight μ, which makes it possible to exploit μ also at the encoder when quantizing the MDCT coefficients. This has been done before by e.g. Edler et al. [31]. In addition, in the perceptual MD low delay audio coder presented in [119] a post filter, which resembles the auditory masking curve, was transmitted as side information. The input signal was first pre filtered by a perceptual filter which transforms the input signal into a perceptual domain that approximates an ℓ_2 domain. A lattice vector quantizer is used in this domain and at the decoder the signal is reconstructed by applying the post filter.

We adopt the approach of normalizing the input signal by the perceptual weight. First we show that, under a mild assumption on the masking curve, this procedure transforms the perceptual distortion measure into an ℓ_2 distortion measure. From (8.6)

---

[61]The invertible mapping F is for historically reasons called a compressor and said to compress the signal. However, F is allowed to be any invertible mapping (also an expander) but we will use the term compressor to be consistent with earlier literature.

[62]In the scalar case an optimal compressor always exists for a wide range of distortion measures.

we have that

$$D(x, \hat{x}) = \frac{1}{M} \sum_{k=0}^{M-1} \int_{\mathscr{X}_k} \mu_k |x_k - \hat{x}_k|^2 f_{X_k}(x_k) dx_k \tag{8.8}$$

$$\overset{(a)}{=} \frac{1}{M} \sum_{k=0}^{M-1} \sum_{j} \int_{\mathscr{X}_k \cap V_j'} \mu_k |x_k - \hat{x}_k|^2 f_{X_k}(x_k) dx_k$$

$$= \frac{1}{M} \sum_{k=0}^{M-1} \sum_{j} \int_{\mathscr{X}_k \cap V_j'} |y_k - \hat{y}_k|^2 f_{X_k}(x_k) dx_k, \tag{8.9}$$

where $y_k = x_k \sqrt{\mu_k}, \hat{y}_k = \hat{x}_k \sqrt{\mu_k}$ and (a) follows by breaking up the integral into disjoint partial integrals over each Voronoi cell V_j' of the quantizer. In order to perform the necessary variable substitution in the integral given by (8.9) we write

$$\frac{dy_k}{dx_k} = x_k \frac{d}{dx_k}(\sqrt{\mu_k}) + \sqrt{\mu_k}. \tag{8.10}$$

At this point we enforce the following condition on the masking curve. Within each quantization cell, the first derivative of the masking curve with respect to the source signal is assumed approximately zero so that from (8.10) $dx_k \approx \sqrt{1/\mu_k} dy_k$.[63] Inserting this in (8.9) leads to

$$D(x, \hat{x}) \approx \frac{1}{M} \sum_{k=0}^{M-1} \sum_{j} \int_{\mathscr{Y}_k \cap V_j} |y_k - \hat{y}_k|^2 f_{X_k}(x_k) \sqrt{1/\mu_k} dy_k$$

$$= \frac{1}{M} \sum_{k=0}^{M-1} \sum_{j} \int_{\mathscr{Y}_k \cap V_j} |y_k - \hat{y}_k|^2 f_{Y_k}(y_k) dy_k, \tag{8.11}$$

$$= \frac{1}{M} E \sum_{k=0}^{M-1} |y_k - \hat{y}_k|^2,$$

since it can be shown that $f_{Y_k}(y_k) = f_{X_k}(x_k) \sqrt{1/\mu_k}$ cf. [126, p.100]. In other words, simply by normalizing the input signal x by the root of the input-dependent weight μ, the perceptual distortion measure for x is transformed into an ℓ_2 distortion measure for y. Therefore, when quantizing y, the distortion is approximately the same when measuring the ℓ_2-distortion i.e. $E\|y - \hat{y}\|^2/M$ or transforming y and $\hat{y}$ back into x and $\hat{x}$, respectively, and measuring the perceptual distortion given by (8.6).

8.1.5   Optimal Bit Distribution

Each block s leads to M MDCT coefficients, which we first normalize by $\sqrt{\mu}$ and then vector quantize using K-channel MD-LVQ. Since, the number of coefficients in the

---

[63]To justify this assumption notice that we can approximate the masking curve by piece-wise flat regions (since the masking curve also needs to be coded), which means that small deviations of the source will not affect the masking curve.

MDCT is quite large, e.g. $M = 1024$ in our case, it is necessary to split the sequence of M coefficients into smaller vectors to make the quantization problem practically feasible. Any small number of coefficients can be combined and jointly quantized. For example, if the set of M coefficients is split into M' bands (vectors) of length L_k where $k = 0, \ldots, M' - 1$ it can be deduced from (5.40) that the total distortion is given by[64]

$$
\begin{aligned}
D_a = \frac{1}{M'} \sum_{k=0}^{M'-1} & \hat{K}_{1,k} G(\Lambda_k) 2^{2(\bar{h}(Y_k) - R_{c_k})} \\
& + \hat{K}_{2,k} \psi_{L_k}^2 G(S_k) 2^{2(\bar{h}(Y_k) - R_{c_k})} 2^{\frac{2K_k}{K_k-1}(R_{c_k} - R_k)} + \frac{p^{K_k}}{L_k} E\|Y_k\|^2,
\end{aligned}
\tag{8.12}
$$

where we allow the quantizers Λ_k and the number of packets K_k to vary among the M' bands as well as from block to block. For a given target entropy R^* we need to find the individual entropies R_k for the M' bands, such that $\sum R_k = R^*/K$ and in addition we need to find the entropies R_{c_k} of the central quantizers. For simplicity we assume in the following that the M' bands are of equal dimension L', that similar central lattices Λ_c are used, and that the number of packets K is fixed for all k.

We now use the fact that (5.44) and (5.45) hold for any bit distribution, hence we may insert (5.44) and (5.45) into (8.12) which leads to individual distortions given by

$$
\begin{aligned}
D_k = {} & \hat{K}_1 G(\Lambda_c) 2^{2(\bar{h}(Y_k) - R_k)} \left(\frac{1}{K-1} \frac{\hat{K}_2}{\hat{K}_1} \frac{G(S_{L'})}{G(\Lambda_c)} \psi_{L'}^2 \right)^{\frac{K-1}{K}} \\
& + \hat{K}_2 G(S_{L'}) 2^{2(\bar{h}(Y_k) - R_k)} \left((K-1) \frac{\hat{K}_1}{\hat{K}_2} \frac{G(\Lambda_c)}{G(S_{L'})} \right) \left(\frac{1}{K-1} \frac{\hat{K}_2}{\hat{K}_1} \frac{G(S_{L'})}{G(\Lambda_c)} \psi_{L'}^2 \right)^{\frac{K-1}{K}} \\
& + \frac{p^K}{L'} E\|Y_k\|^2 \\
= {} & a_0 2^{2(\bar{h}(Y_k) - R_k)} + \frac{p^K}{L'} E\|Y_k\|^2,
\end{aligned}
\tag{8.13}
$$

where a_0 is independent of k and given by

$$
a_0 = \hat{K}_1 G(\Lambda_c) \left(\frac{1}{K-1} \frac{\hat{K}_2}{\hat{K}_1} \frac{G(S_{L'})}{G(\Lambda_c)} \psi_{L'}^2 \right)^{\frac{K-1}{K}}.
\tag{8.14}
$$

---

[64]The distortion over individual normalized MDCT coefficients is additive in the MDCT domain (recall that we are using a single-letter distortion measure). However, adding the entropies of a set of MDCT coefficients is suboptimal unless the coefficients are independent. Futhermore, the individual MDCT coefficients will generally be correlated over consecutive blocks. For example, overlapping blocks of an i.i.d. process yields a Markov process. For simplicity, we do not exploit any correlation across blocks nor between the vectors of MDCT coeffficients (but only within the vectors).

In order to find the optimal bit distribution among the M' bands subject to the entropy constraint $\sum_{k=0}^{M'-1} R_k = R^*/K$ we take the common approach of turning the constrained optimization problem into an unconstrained problem by introducing a Lagrangian cost functional of the form

$$J = \sum_{k=0}^{M'-1} D_k + \lambda \sum_{k=0}^{M'-1} R_k. \tag{8.15}$$

Differentiating (8.15) w.r.t. R_k leads to

$$\frac{\partial J}{\partial R_k} = -2\ln(2)a_0 2^{2(\bar{h}(Y_k)-R_k)} + \lambda. \tag{8.16}$$

After equating (8.16) to zero and solving for R_k we get

$$R_k = -\frac{1}{2}\log_2\left(\frac{\lambda}{2\ln(2)a_0}\right) + \bar{h}(Y_k). \tag{8.17}$$

In order to eliminate λ we invoke the sum-rate constraint $\sum_{k=0}^{M'-1} R_k = R^*/K$ and get

$$\sum_{k=0}^{M-1} R_k = -\frac{M'}{2}\log_2\left(\frac{\lambda}{2\ln(2)a_0}\right) + \sum_{k=0}^{M'-1} \bar{h}(Y_k) = R^*/K, \tag{8.18}$$

from which we obtain

$$\lambda = 2\ln(2)a_0 2^{-\frac{2}{M'}\left(R^*/K-\sum_{k=0}^{M'-1}\bar{h}(Y_k)\right)}. \tag{8.19}$$

We can now eliminate λ by inserting (8.19) into (8.17), that is

$$R_k = \frac{R^*/K - \sum_{k=0}^{M'-1}\bar{h}(Y_k)}{M'} + \bar{h}(Y_k). \tag{8.20}$$

With the simple Lagrangian approach taken here there is no guarantee that the entropies R_k given by (8.20) are all non-negative. It might be possible to extend the Lagrangian cost functional (8.15) by M' additional Lagrangian weights (also called "complementary slackness" variables [128]) in order to obtain M' inequality constraints making sure that $R_k \geq 0$ in addition to the single equality constraint $\sum R_k = R^*/K$. While the resulting problem can be solved using numerical techniques, it does not appear to lead to a closed-form expression for the individual entropies R_k. It is not possible either to simply set negative entropies equal to zero since this will most likely violate the constraint $\sum R_k = R^*/K$. Instead we propose a sequential procedure where we begin by considering all M' bands and then one-by-one eliminate bands having negative entropies. We assign entropies to each band using (8.20) and then find the one having the largest negative entropy and exclude that one from the optimization process. This procedure continues until all entropies are positive or zero as shown in Table 8.1.

1. $\mathscr{I} = \{0, \ldots, M' - 1\}$

2. $h = \sum_{k \in \mathscr{I}} \bar{h}(Y_k)$

3. $c = \frac{R^*/K - h}{|\mathscr{I}|}$

4. $\mathscr{R} = \{R_k : R_k = c + \bar{h}(Y_k) \text{ and } R_k < 0, k \in \mathscr{I}\}$

5. If $|\mathscr{R}| > 0$ then goto 2 and set $\mathscr{I} := \mathscr{I} \backslash j$, where $R_j \leq R_k, \forall k \in \mathscr{I}$

6. $R_k = \begin{cases} c + \bar{h}(Y_k), & k \in \mathscr{I} \\ 0, & \text{otherwise} \end{cases}$

Table 8.1: *Bit-allocation algorithm.*

The motivation for this approach is that ultimately we would like the contribution of each band to the total distortion to be equal, since they are all approximately equally sensitive to distortion after being flattened by the masking curve. However, the normalized MDCT coefficients in some bands have variances which are smaller than the average distortion, hence assigning zero bits to these bands leads to distortions which are lower than the average distortion over all bands. Therefore, the bit budget should only be distributed among the higher variance components.

8.2 Robust Transform Coding

In this work we apply MD-LVQ on the normalized coefficients of an MDCT to obtain a desired degree of robustness when transmitting encoded audio over a lossy network. The encoder and decoder of the complete scheme are shown in Figs. 8.1(a) and 8.1(b), respectively. In the following we describe how the encoding and decoding is performed.

8.2.1 Encoder

By s we denote the current block, which has been obtained by blocking the input signal into overlapping blocks each containing $2M$ samples. The M MDCT coefficients are obtained by applying an M-channel MDCT on s and is represented by the vector x. It is worth mentioning that we allow for the possibility to use a flexible time segmentation in order to better match the time-varying nature of typical audio signals, cf. [95]. Each block is encoded into K descriptions independent of previous blocks in order to avoid that the decoder is unable to successfully reconstruct due to previous description losses.
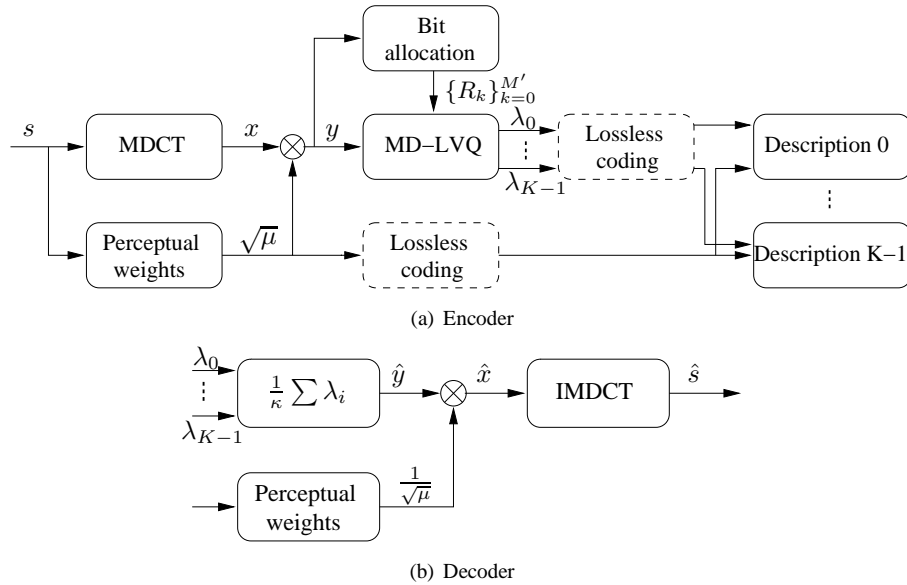
(a) Encoder

(b) Decoder

Figure 8.1: *Encoder and decoder.*

As discussed in Section 8.1.5 it is infeasible to jointly encode the entire set of M MDCT coefficients and instead we split x into M' disjoint subsets. The MDCT coefficients are then normalized by the perceptual weights μ in order to make sure that they are approximately equally sensitive to distortion and moreover to make sure that we operate in an ℓ_2 domain where it is known that lattice vector quantizers are among the set of good quantizers. Based on the differential entropies of the normalized MDCT coefficients y and the target entropy R^* we find the individual entropies $R_k, k = 0, \ldots, M' - 1$ by using the algorithm described in Table 8.1. Fig. 8.2(a) shows an example of the distribution of differential entropies $\bar{h}(Y)$ in a 1024-channel MDCT. In this example a 10 sec. audio signal (jazz music) sampled at 48 kHz was input to the MDCT. Fig. 8.2(b) shows the corresponding discrete entropies assigned to each of the 1024 bands when the target entropy is set to $R^* = 88$ kbps.

It may be noticed from Fig. 8.2(b) that the bit budget is mainly spent on the lower part of the normalized MDCT spectrum. This behavior is typical for the audio signals we have encountered. The reason is partly that the audio signals have most of their energy concentrated in the low frequency region but also that the high frequency part is deemphasized by the perceptual weight. The perceptual weight is approximately proportional to the inverse of the masking curve and at the high frequency region the steep positive slope of the threshold in quiet dominates the masking curve. We remark that the bit allocation effectively limits the band width of the source signal since high frequency bands are simply discarded and it might therefore prove beneficial

(a) Differential entropies

(b) Discrete entropies
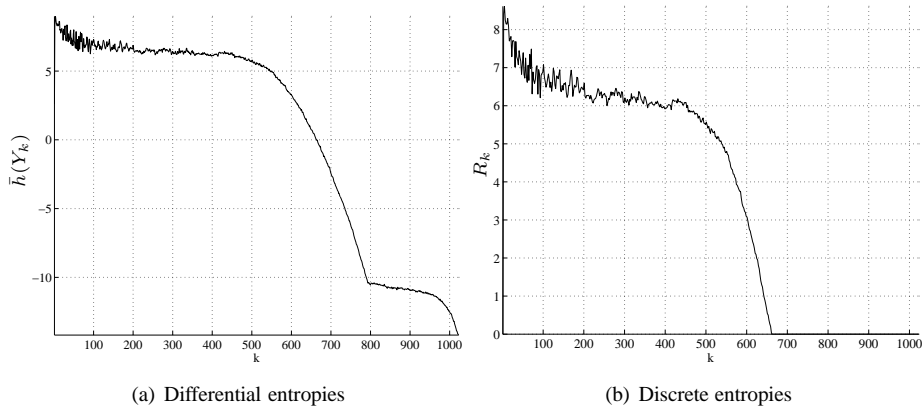
Figure 8.2: *Differential and discrete entropies for the normalized MDCT coefficients (expressed in bit/dim.).*

(perceptually) to use some kind of spectral band replication at the decoder in order to recover some of the lost high frequency components.

The entropy R_k describes the total entropy assigned to the kth band (or the kth subset of bands if vector quantization is applied). If the number of descriptions is K then each side description operates at an entropy of R_k/K bit/dim. Knowledge of R_k, the differential entropy $\bar{h}(Y_k)$, the number of descriptions K and the packet-loss probability p makes it possible to find the scaling factors ν_k and N_k of the central and side quantizers, respectively by use of (5.44) and (5.45). This in turn completely specify a MD-LVQ scheme having K descriptions. Each normalized MDCT coefficient or vector of coefficients y_k is then first quantized with the central quantizer $Q_k(y_k) = \lambda_{c_k}$ after which index assignments $\alpha(\lambda_{c_k}) = \{\lambda_{0_k}, \ldots, \lambda_{K_k-1}\}$ are performed in order to find the codewords of the side quantizers. The codewords of the side quantizers are losslessly coded and put into K individual packets. Each packet then contains M' encoded codewords.

It is required that the perceptual weight μ is somehow transmitted to the decoder in order to be able to reconstruct. Since the K packets have an equal chance of getting lost we need the perceptual weight in all packets, which leads to a certain degree of overhead. In the case where more than one packet is received we therefore waste bits. It might be possible to apply some sort of MD coding on the perceptual weight in order to decrease the amount of side information which needs to be duplicated in all packets. However, it is outside the scope of this chapter to investigate the many aspects of perceptual lossless coding of μ and we refer the readers to the work of [96] for more details. In the following we will simply assume that the perceptual weight can be perceptually lossless coded at 4 kbps, hence if the target entropy is $R^* = 96$ kpbs and two packets are to be used, the entropy we can actually use for MD-LVQ is

then only 88 kbps, since 8 kbps (4 kbps in each packet) are used for the weight. If a greater number of packets is desired the overhead for transmitting μ increases even further.

8.2.2   Decoder

At the receiving side an estimate $\hat{y}$ of the normalized MDCT spectrum is first obtained by simply taking the average of the received descriptions, i.e. $\hat{y}_k = \frac{1}{\kappa'} \sum_{i \in l'} \lambda_{i_k}$, where l' denotes the indices of the received descriptions and $\kappa' = |l'|$. This estimate is then denormalized in order to obtain $\hat{x}$, i.e. $\hat{x}_k = \hat{y}_k / \sqrt{\mu_k}$. Finally the inverse MDCT (including overlap-add) is applied in order to obtain an approximation $\hat{s}$ of the time domain signal s. The decoding procedure is shown in Fig. 8.1(b).

8.3   Results

In this section we compare numerical simulations with theoretical results and in addition we show the results of a subjective listening test. We first show results related to the expected distortion based on the packet-loss probabilities and then we show results for the case of scalable coding. In both cases we assume a symmetric setup.

8.3.1   Expected Distortion Results

For the objective test we use four short audio clips of different genres (classical jazz music, German male speech, pop music, rock music) each having a duration between 10 and 15 sec. and a sampling frequency of 48 kHz. We refer to these fragments as "jazz", "speech" , "pop" and "rock". We set the target entropy to 96 kbps (as was done in [119]) which corresponds to 2 bit/dim. since the sampling frequency is 48 kHz. We do not encode the perceptual weight but simply assume that it can be transmitted to the receiver at an entropy of 4 kbps. Since the weight must be included in all of the K descriptions we deduct $4K$ kbps from the total entropy, hence the effective target entropy R_e^* is given by $R_e^* = R^* - 4K$ so that a single description system has $R_e^* = 92$ kbps whereas a four description system has $R_e^* = 80$ kbps (i.e. 20 kbps for each side description). For simplicity we furthermore assume that the sources are stationary processes so that we can measure the statistics for each vector of MDCT coefficients upfront. However, since audio signals in general have time varying statistics we expect that it will be possible to reduce the bit rate by proper adaptation to the source. Since for this particular test we are merely interested in the performance of the proposed audio coder with a varying number of descriptions we will not address the issue of efficient entropy coding but simply assume that the quantized variables can be losslessly coded arbitrarily close to their discrete entropies.

Table 8.2 shows the discrete entropies of the quantized normalized MDCT coefficients for the four test fragments.

	$K = 2$ kbps	$K = 2$ bit/dim.	$K = 3$ kbps	$K = 3$ bit/dim.	$K = 4$ kbps	$K = 4$ bit/dim.
jazz	96.22	1.00	97.09	0.67	96.87	0.51
speech	93.48	0.98	96.00	0.67	96.47	0.50
pop	93.35	0.98	95.25	0.66	95.57	0.50
rock	93.76	0.98	95.38	0.66	95.60	0.50

Table 8.2: *Numerical measured output entropies in kilobits per second (kbps) and bit/dim. per description. The target entropy is $R^* = 96$ kbps or 2 bit/dim.*

We block the normalized MDCT spectrum into vectors of length two and use the Z^2 lattice vector quantizer. Because of the short duration of the test fragments the resulting expected distortions depend upon the realizations of the packet loss patterns. This phenomena has been noted by other authors, cf. [3]. We therefore decided to average the distortion results over three different loss patterns obtained by using different seeds to the random number generator. The numerically obtained expected distortions are shown in Tables 8.3–8.6 and Figs. 8.3(a) and 8.3(b).

$K = 1$	$p = 10\%$	$p = 30\%$	$p = 50\%$
jazz	18.17 (18.15)	22.94 (23.12)	25.16 (25.23)
speech	17.84 (17.79)	22.61 (22.82)	24.83 (24.86)
pop	17.89 (17.83)	22.66 (22.83)	24.88 (24.91)
rock	18.20 (18.20)	22.97 (23.12)	25.18 (25.23)

Table 8.3: *Theoretical (numerical) expected distortions expressed in dB for $K = 1$ and $p = 10, 30$ and 50%. The target entropy is $R^* = 96$ kbps or 2 bit/dim.*

$K = 2$	$p = 10\%$	$p = 30\%$	$p = 50\%$
jazz	9.44 (10.42)	17.96 (18.33)	22.24 (22.38)
speech	8.80 (9.94)	17.55 (18.04)	21.88 (21.80)
pop	9.04 (10.32)	17.62 (18.22)	21.94 (22.11)
rock	9.70 (10.66)	18.00 (18.36)	22.27 (22.39)

Table 8.4: *Theoretical (numerical) expected distortions expressed in dB for $K = 2$ and $p = 10, 30$ and 50%. The target entropy is $R^* = 96$ kbps or 2 bit/dim.*

As can be seen in Figs. 8.3(a) and 8.3(b) the expected distortions depend not only on the packet-loss rate but also upon the number of descriptions. At high packet-loss

$K = 3$	$p = 10\%$	$p = 30\%$	$p = 50\%$
jazz	17.54 (17.49)	18.80 (18.76)	21.39 (21.34)
speech	15.62 (15.50)	17.34 (17.29)	20.51 (20.56)
pop	16.38 (16.28)	17.85 (17.75)	20.76 (20.66)
rock	17.44 (17.33)	18.75 (18.63)	21.38 (21.29)

Table 8.5: *Theoretical (numerical) expected distortions expressed in dB for $K = 3$ and $p =$ $10, 30$ and 50%. The target entropy is $R^* = 96$ kbps or 2 bit/dim.*

$K = 4$	$p = 10\%$	$p = 30\%$	$p = 50\%$
jazz	20.39 (20.35)	20.61 (20.59)	21.65 (21.59)
speech	18.88 (18.75)	19.17 (19.18)	20.52 (20.42)
pop	19.14 (19.08)	19.41 (19.46)	20.70 (20.71)
rock	20.27 (20.18)	20.50 (20.44)	21.58 (21.50)

Table 8.6: *Theoretical (numerical) expected distortions expressed in dB for $K = 4$ and $p =$ $10, 30$ and 50%. The target entropy is $R^* = 96$ kbps or 2 bit/dim.*

rates it is advantageous to use a higher number of packets. To verify these findings we performed an additional subjective comparison test. We chose three different fragments (jazz, speech and rock) and three different packet-loss rates ($p = 0.1$, $p = 0.3$ and $p = 0.5$). We then performed a standard MUSHRA test [66]. At each packet-loss rate the original signals were encoded using $K = 1, 2, 3$ and 4 descriptions. Also included in each test were the hidden reference and two anchor signals (3.5 kHz and 7 kHz lowpass filtered signals). We used nine (non-experts) listeners in the listening test and the results are shown in Figs. K.2–K.4 in Appendix K for the individual fragments averaged over the nine participants. The circles in the figures denote mean values and the bars describe 95% confidence intervals. Fig. 8.4 shows the result when averaging over participants and fragments. Notice that for $p = 0.3$ and $p = 0.5$ there is a significant preference for using more than two descriptions.

The results of the subjective listening tests show generally no significant difference between the two and three packet versions for a packet-loss rate of $p = 0.1$, cf. Figs. K.2(a)– K.4(a). However, the results based on the perceptual distortion measure reveals that at $p = 0.1$ it is beneficial to use two packets instead of three, cf. Figs. 8.3(a) and 8.3(b). In fact, a reduction in distortion of about 7 dB can be achieved. This discrepancy can be partly explained by our implementation of the the bit-allocation strategy outlined in Section 8.1.5. To avoid assigning a too small rate to a given frequency band (which then would violate the high-resolution assumptions) we have, in the experiments described above, excluded MDCT bands which were
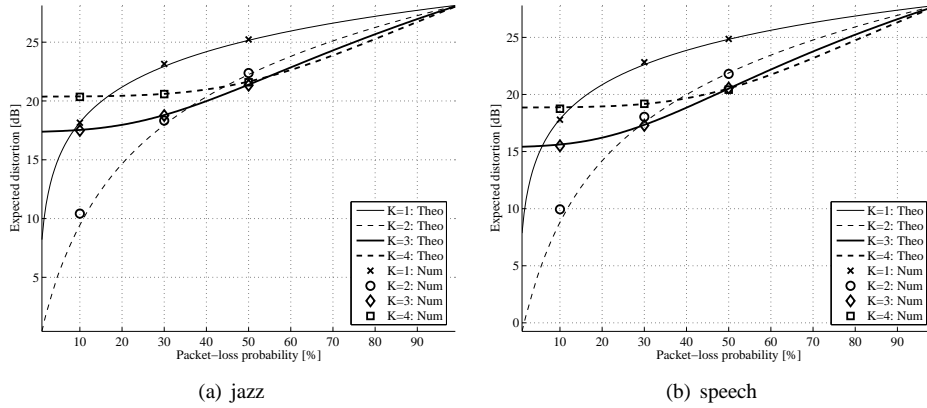
Figure 8.3: *The expected distortion as a function of packet-loss probabilities for MD-LVQ when operating at a target entropy of 96 kbps.*

assigned a rate lower than 3 bit/dim. per description.[65] The effect of this is that the high-resolution approximations are good so that theoretical and numerical results agree but the downside is that the input signal is severely lowpass filtered. The contribution of the high frequency bands to the total distortion is therefore high, hence, the reception of more than two descriptions does not improve the quality of the reconstructed signal much. In addition we would like to emphasize two important factors which might also contribute to the inconsistency between subjective listening tests and the perceptual distortion measure. First of all, the perceptual distortion measure is based upon a single block at a time and therefore the continuity of the signal over time is not addressed.[66] Secondly, the distortion measure is defined in the MDCT domain and since the MDCT is not an orthogonal transform the distortion in the MDCT domain is not equivalent to the distortion in the time domain.

As previously mentioned we have in these tests excluded MDCT bands where the rate assignment is less than 3 bit/dim. per description to make sure that the high-resolution assumptions are valid. Such an approach excludes a great amount of MDCT bands (especially those representing the high frequency contents of the signal) and the coded signal sounds muffled (lowpass filtered). The reasoning behind this

---

[65]If the numerically measured discrete entropy is, for example, 0.1 bit/dim. greater than the specified theoretical entropy, then, since the sampling frequency is 48 kHz, the resulting bit rate is 4.8 kbps above the target entropy. Furthermore, if this 0.1 bit/dim. gap is per description, then, in a three-description setup, the resulting rate would exceed the target rate by 14.4 kbps. Practical experiments have shown that at 3 bit/dim. per description, the numerically measured discrete entropy is off by less than 0.03 bit/dim. per description for a range of index values.

[66]The listeners agreed that the "hick-ups" resulting from time gaps due to packet losses were the most annoying artifacts present in the coded signals. The overlapping nature of the MDCT is, however, able to reduce the impact of isolated packet losses.
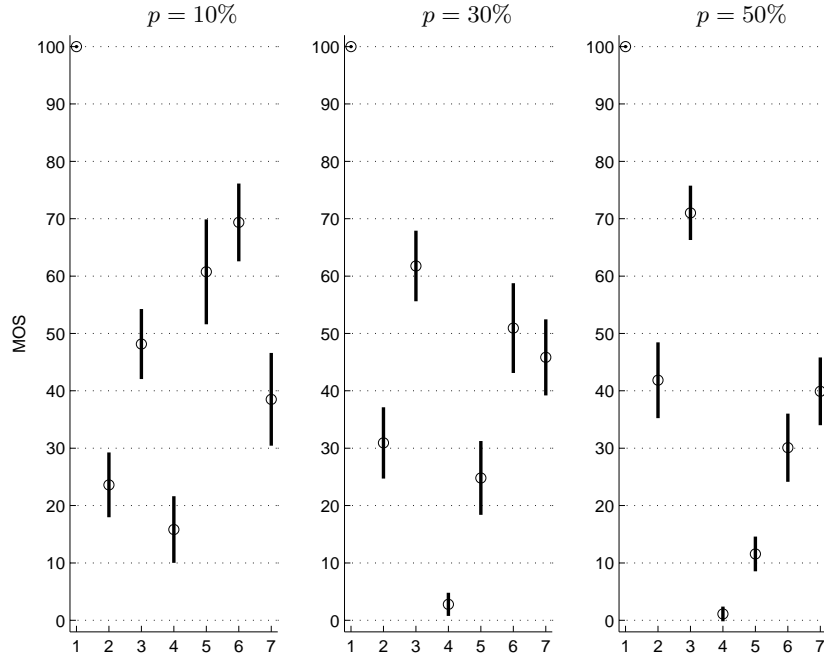
Figure 8.4: *MUSHRA test results averaged over all three audio clips for $p = 0.1, 0.3$ and $p = 0.5$. The seven signals appear in the following order: Hidden ref., 3.5 kHz, 7 kHz, $K = 1, K = 2, K = 3$ and $K = 4$.*

choice is that a "lowpass" filtered version of the signal (without time gaps) is often preferable over a full bandwidth signal (with time gaps). Alternatively, we may take into account that the practical rate becomes too high for the bands that are assigned a too low theoretical rate. Thus, we can heuristically assign a lower target rate for the MDCT coefficients representing the higher frequency bands. Since we encode two-dimensional vectors there are 512 bands in total but only about the first 300 of these are assigned a positive rate. We then modify the scale factor ν_k for the kth band by the following rule

$$\nu_k = \begin{cases} 1.0 \cdot \nu_k, & 0 \leq k \leq 50, \\ 1.3 \cdot \nu_k, & 51 \leq k \leq 100, \\ 1.4 \cdot \nu_k, & 101 \leq k \leq 200, \\ 1.5 \cdot \nu_k, & 201 \leq k \leq 250, \\ 2.0 \cdot \nu_k, & 251 \leq k \leq 300. \end{cases} \tag{8.21}$$

For each different fragment we set the target R^* such that the practical rate is very close to 96 kbit/sec. (incl. 4 kbit/sec. per packet for the masking curve). These rates

Fragment	R^* [kbit/sec.]	$H(Y)$ [kbit/sec.]
jazz	92.16	95.92
harpsi	86.40	96.34
speech	91.92	96.03
pop	89.76	96.29
rock	94.08	96.09

Table 8.7: *The target rate R^* is set lower than 96 kbit/sec. which leads to a practical rate $H(Y)$ close to 96 kbit/sec.*

are shown in Table 8.7.[67]

The numerically measured expected distortions based on the packet-loss probabilities are shown in Fig. 8.5(a) for the jazz fragment. We have swept the packet-loss probability between 1% and 50% in steps of 1%. Each test is repeated 10 times to reduce the influence of a particular loss pattern. Notice that already at packet-loss probabilities as low as one percent it becomes advantageous to use three descriptions instead of two descriptions. Fig. 8.5(b) shows the results of a similar experiment for the speech fragment.

(a) jazz fragment   (b) speech fragment
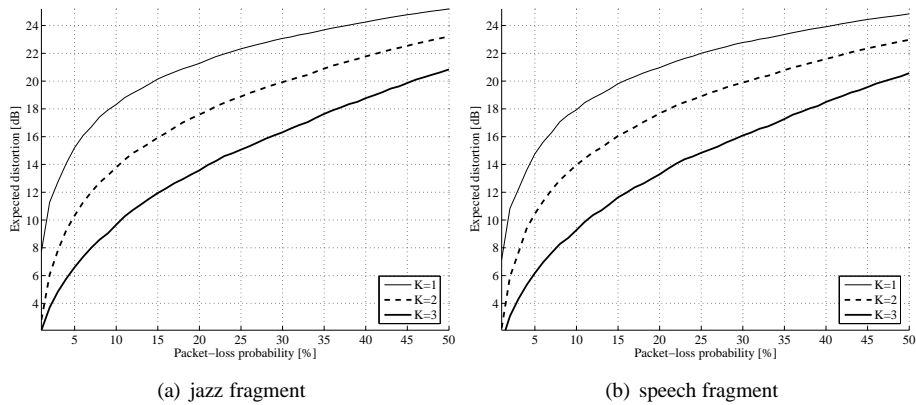
Figure 8.5: *Expected distortion as a function of packet-loss probabilities.*

8.3.2 Scalable Coding Results

We now assess the improvement of audio quality as more packets are received. This is a form of scalable coding, where some receivers have access to more information

---

[67]In this experiment we have included an additional audio fragment "harpsi", which consists of "music" from a Harpsichord.

Impairment	ITU-R Grade	ODG
Imperceptible	5.0	0.0
Perceptiple, but not annoying	4.0	-1.0
Slightly annoying	3.0	-2.0
Annoying	2.0	-3.0
Very annoying	1.0	-4.0

Table 8.8: *Relationship between the ITU-R 5-grade impairment scale and the ODGs [12].*

Fragment	(λ_0)	(λ_1)	(λ_2)	Avg.
jazz	-2.652	-2.571	-2.720	-2.647
harpsi	-1.976	-1.757	-2.606	-2.113
speech	-2.649	-2.492	-2.961	-2.701
pop	-3.328	-3.375	-3.445	-3.383
rock	-2.699	-2.556	-2.787	-2.681

Table 8.9: *ODGs when receiving a single description out of three.*

(descriptions) than others. In this case no description losses occur. Instead of using the expected distortion we will use the Objective Difference Grade (ODG) based on the Matlab implementation by Kabal et al. [70] of the PEAQ standard [108]. The ODGs are related to the standard ITU-R 5-grade impairment scale as shown in Table 8.8. Tables 8.9–8.11 show the ODGs for the five different test fragments. The last column of Tables 8.9 and 8.10 show the mean ODGs when averaged over the three different combinations of descriptions. These average ODGs as well as the results of Table 8.11 are also shown in the bar diagram in Fig. 8.6.

From the tables it may be observed that the perceptual distortion is approximately symmetric, i.e. the ODG is essentially independent of which packet is received. In addition, it can be seen that as more packets are received a substantial improvement in quality can be expected.

Fragment	(λ_0, λ_1)	(λ_0, λ_2)	(λ_1, λ_2)	Avg.
jazz	-1.033	-1.162	-1.021	-1.072
harpsi	-0.729	-0.993	-0.893	-0.872
speech	-0.994	-1.171	-1.040	-1.068
pop	-1.897	-2.401	-2.082	-2.127
rock	-1.125	-1.284	-1.128	-1.179

Table 8.10: *ODGs when receiving two descriptions out of three.*

Fragment	$(\lambda_0, \lambda_1, \lambda_2)$
jazz	-0.104
harpsi	-0.166
speech	-0.189
pop	-0.171
rock	-0.184

Table 8.11: *ODGs when receiving all three descriptions.*
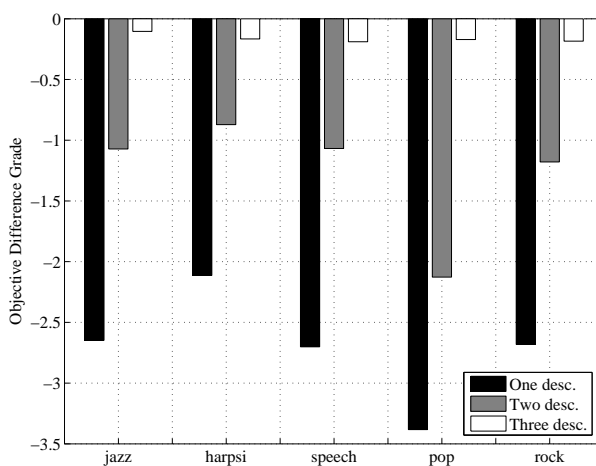
Figure 8.6: *ODGs for the reception of one to three packets out of three for different test fragments.*

8.4 Conclusion

We combined MD-LVQ with transform coding in order to obtain a perceptually robust audio coder. Previous approaches to this problem were restricted to the case of only two descriptions. In this work we used K-Channel MD-LVQ, which allowed for the possibility of using more than two descriptions. For a given packet-loss probability we found the number of descriptions and the bit allocation between transform coefficients, which minimizes a perceptual distortion measure subject to an entropy constraint. The optimal MD lattice vector quantizers were presented in closed form, thus avoiding any iterative quantizer design procedures. The theoretical results were verified with numerical computer simulations using audio signals and it was shown that in environments with excessive packet losses it is advantageous to use more than two descriptions. We verified in subjective listening tests that using more than two descriptions lead to signals of perceptually higher quality.

Chapter 9

Conclusions and Discussion

9.1 Summary of Results

We presented an index-assignment based design of K-channel MD-LVQ. Where previous designs have been limited to two descriptions we considered the general case of K descriptions. Exact rate-distortion results were derived for the case of $K \leq 3$ descriptions and high resolution conditions for smooth stationary sources and the squared error distortion measure. In the asymptotic case of large lattice vector quantizer dimension and high resolution conditions, it was shown that existing rate-distortion MD bounds can be achieved in the quadratic Gaussian case. These results were conjectured to hold also for $K > 3$ descriptions.

In the two-description asymmetric case it was shown that the performance was superior to existing state-of-the-art asymmetric schemes in finite lattice vector quantizer dimensions greater than one. In one and infinite dimensions as well as in the symmetric case (for all dimensions), the performance is identical to existing state-of-the-art schemes.

In the three-description symmetric and asymmetric cases for finite lattice vector quantizer dimensions, the rate loss of the proposed design is superior to that of existing schemes.

The optimal amount of redundancy in the system was shown to be independent of the source distribution, target rate and type of lattices used for the side quantizers. Basically, the channel conditions (expressed through a set of packet-loss probabilities) describe the required amount of redundancy in the system. Thus, for given channel conditions, the optimal index-assignment map can be found and adapting to time-varying source distributions or bit rate requirements amounts to a simple scaling of the central and side lattice vector quantizers.

We proposed an entropy-constrained design where either the side description rates

147

or their sum rate are subject to entropy contraints. In the case of a single sum rate entropy contraint, we showed that the optimal bit allocation across descriptions is not unique, but in fact consists of a set of solutions, which all lead to minimal expected distortion.

On the practical side it was shown that the optimal K-channel MD lattice vector quantizers can be found in closed-form, hence avoiding any iterative (e.g. generalized Lloyd-like) design algorithms. Furthermore, we combined MD-LVQ with transform coding in order to obtain a perceptually robust audio coder. Previous approaches to this problem were restricted to the case of only two descriptions. For a given packet-loss probability we found the number of descriptions and the bit allocation between transform coefficients, which minimizes a perceptual distortion measure subject to an entropy constraint. The theoretical results were verified with numerical computer simulations using audio signals and it was shown that in environments with excessive packet losses it is advantageous to use more than two descriptions. We verified in subjective listening tests that using more than two descriptions leads to signals of perceptually higher quality.

9.2 Future Research Directions

In this thesis we considered index-assignment based MD schemes at high resolution conditions, which provide a partial solution to the K-channel MD problem. However, more work is needed before the general MD problem is solved. Besides the information theoretic open problems discussed in Chapter 4 there are many unsolved problems related to MD-LVQ. Below we list a few of these.

- Proving the conjectures of this thesis, i.e. proving the rate-distortion results for $K > 3$ descriptions.

- Extending the results to general resolution. To the best of the authors knowledge, the only case where exact rate-distortion expressions (in non high-resolution cases) have been presented for index-assignment based MD schemes, is the two-channel scalar scheme by Frank-Dayan and Zamir [39].

- It is an open problem of how to construct practical MD-LVQ schemes that comes arbitrarily close to the known MD bounds. Such schemes require high-dimensional lattice vector quantizers and large index values. However, solving the linear assignment problem can become computationally infeasible for large index values. For the symmetric case and certain low dimensional lattices, some progress have been made in reducing this complexity by the design of Huang and Wu [65]. A construction for high-dimensional nested lattice codes was recently presented by Zamir et al. [162]. No index-assignment methods have, however, been presented for the nested lattice code design and the problem is therefore not solved.

- Constructing functional MD schemes for existing applications in real environments and assessing their performance. For example for real-time application, even if the packet-loss rate of a network is very low, the delay might occasionally be high, which then means that (at least for real-time applications) a delayed packet is considered lost (at least for the current frame) and the use of MD coding might become beneficial.

Appendix A

Quaternions

We will here briefly define the Quaternions and describe a few important properties that we will use in this work. For a comprehensive treatment of the Quaternions we refer the reader to [23, 71, 150].

The Quaternions, which were discovered in the middle of the 19th century by Hamilton [71], is in some sense a generalization of the complex numbers. Just as 1 and i denote unit vectors of the complex space $\mathbb{C}$ we define $1, i, j$ and k to be unit vectors in Quaternion space $\mathbb{H}$. The set of numbers defined as $\{a + bi + cj + dk : a, b, c, d \in \mathbb{R}\}$ are then called Quaternion numbers or simply Quaternions. Addition of two Quaternions $q = a + bi + cj + dk$ and $q' = a' + b'i + c'j + d'k$ is defined as

$$q + q' = (a + a') + (b + b')i + (c + c')j + (d + d')k, \tag{A.1}$$

and multiplication follows by first defining a multiplication rule for pairs of Quaternion units, that is

$$
\begin{aligned}
i^2 = j^2 &= k^2 = -1, \\
ij &= k, \quad ji = -k, \\
jk &= i, \quad kj = -1, \\
ki &= j, \quad ik = -j,
\end{aligned}
\tag{A.2}
$$

which leads to

$$
\begin{aligned}
qq' = (aa' - bb' - cc' - dd') + (ab' + ba' + cd' - dc')i \\
+ (ac' + ca' + db' - bd')j + (ad' + da' + bc' - cb')k.
\end{aligned}
\tag{A.3}
$$

Definition A.1.1. The skew field $\mathbb{H}$ of Quaternions is defined as the set $\{z = a + bi + cj + dk : a, b, c, d \in \mathbb{R}\}$ combined with two maps (addition and multiplication) given by (A.1) and (A.3), respectively, that satisfies field properties except that multiplication is non commutative.

Definition A.1.2. Quaternionic conjugation of $q = a + bi + cj + dk \in \mathbb{H}$ is given by $q^* = a - bj - cj - dk$ and we denote by $\boldsymbol{q}^\dagger$ Quaternionic conjugation and vector transposition where $\boldsymbol{q} \in \mathbb{H}^L$.

Definition A.1.3. The real part of a Quaternion $q = a + bi + cj + dk$ is given by $\Re(q) = a$ and the complex part (also called the vector part) is given by $\Im(q) = bi + cj + dk$.

Lemma A.1.1 ([6]). Two Quaternions q_0 and q_1 commute, i.e. $q_0 q_1 = q_1 q_0$ if their vector parts are proportional (i.e. linear dependent) or, in other words, if the cross product $\Im(q_0) \times \Im(q_1) = 0$.

Lemma A.1.2 ([22]). The norm $\|q\|$ of a Quaternion $q \in \mathbb{H}$ is given by $\|q\| = \sqrt{q^* q}$ and satisfies the usual vector norm, i.e. $\|q\| = \sqrt{a^2 + b^2 + c^2 + d^2}$.

Definition A.1.4 ([14]). The Quaternions can be represented in terms of matrices. The isomorphic map $\phi_L \colon (\mathbb{H}, +, \cdot) \rightarrow (H_{4 \times 4}, \oplus, \otimes)$ between the space $\mathbb{H}$ of Quaternions and the space $H_{4 \times 4}$ of 4×4 matrices over the real numbers $\mathbb{R}$ defined by

$$\phi_L(a + bi + cj + dk) \mapsto \begin{bmatrix} a & -b & -c & -d \\ b & a & -d & c \\ c & d & a & -b \\ d & -c & b & a \end{bmatrix}, \tag{A.4}$$

describes left multiplication by the Quaternion q. Similar we define right multiplication by the map $\phi_R \colon (\mathbb{H}, +, \cdot) \rightarrow (H_{4 \times 4}, \oplus, \otimes)$ given by

$$\phi_R(a + bi + cj + dk) \mapsto \begin{bmatrix} a & -b & -c & -d \\ b & a & d & -c \\ c & -d & a & b \\ d & c & -b & a \end{bmatrix}. \tag{A.5}$$

It follows from Definition A.1.4 that addition and multiplication of two Quaternions can be done by use of the usual matrix addition $\oplus$ and matrix multiplication $\otimes$. Furthermore, Quaternionic conjugation can easily be done in $H_{4 \times 4}$ space where it is simply the matrix transpose.

Appendix B

Modules

In this appendix we give a brief introduction to the theory of algebraic modules. For more information we refer the reader to the following textbooks [1, 22, 61, 72].

B.1 General Definitions

Definition B.1.1. Let $\mathscr{J}$ be a ring which is not necessarily commutative with respect to multiplication. Then an Abelian (commutative) group S is called a left $\mathscr{J}$-module or a left module over $\mathscr{J}$ with respect to a mapping (scalar multiplication on the left which is simply denoted by juxtaposition) $\mathscr{J} \times S \to S$ such that for all $a, b \in \mathscr{J}$ and $g, h \in S$,

1) $a(g + h) = ag + ah$,

2) $(a + b)g = ag + bg$,

3) $(ab)g = a(bg)$.

Remark B.1.1. For simplicity we have used the same notations for addition/multiplication in the group as well as in the ring.

Remark B.1.2. A right module is defined in a similar way but with multiplication on the right. In fact if the ring $\mathscr{J}$ is commutative then every left $\mathscr{J}$-module is also a right $\mathscr{J}$-module [61].

Definition B.1.2. If $\mathscr{J}$ has identity 1 and if $1a = a$ for all $a \in S$, then S is called a unitary or unital $\mathscr{J}$-module.

Remark B.1.3. In this work all modules have an identity.

Definition B.1.3 ([72])**.** A subset $S' = \{m_1, \ldots, m_n\} \subset S$ of the $\mathscr{J}$-module S is linearly independent over $\mathscr{J}$ if, for $x_i \in \mathscr{J}$, $x_1 m_1 + \cdots + x_n m_n = 0$ only if $x_1 = \cdots = x_n = 0$. If in addition S' generates S then S' is a basis for S.

Example B.1.1. The set $S = \{2, 3\}$ is finite and generates $\mathbb{Z}$, considered as a $\mathbb{Z}$-module over itself [72]. However, S is not a linearly independent set. Further, neither element of S can be omitted to give a generating set with one member. Hence, S is not a basis of $\mathbb{Z}$.

Definition B.1.4 ([72])**.** A $\mathscr{J}$-module that has a basis is called a free $\mathscr{J}$-module.

Definition B.1.5 ([72])**.** The number of elements in a basis of a $\mathscr{J}$-module S is called the rank or dimension of S.

Remark B.1.4. Not all modules have a basis [72]. Let $\mathbb{Z}_m = \mathbb{Z}/m\mathbb{Z}$ be the residue ring of integers, i.e. $\mathbb{Z}_m = \{[0], \ldots, [m-1]\}$, where $[s] = [r]$ in $\mathbb{Z}_m$ implies $s \equiv r \pmod{m}$. Notice that $\mathbb{Z}_m$ contains no linear independent subsets, since $mx = 0$ for any $x \in \mathbb{Z}$, hence $\mathbb{Z}_m$ has no basis and is therefore not a free module.

Definition B.1.6 ([1])**.** Let $\mathscr{J}$ be a ring and let S, S' be left $\mathscr{J}$-modules. A function $f : S \to S'$ is a $\mathscr{J}$-module homomorphism if

1. $f(m_1 + m_2) = f(m_1) + f(m_2)$ for all $m_1, m_2 \in S$, and

2. $f(am) = af(m)$ for all $a \in \mathscr{J}$ and $m \in S$.

Definition B.1.7 ([1])**.** The set of all $\mathscr{J}$-module homomorphisms from S to S' is denoted $\mathrm{Hom}(S, S')$. If $S = S'$ then we write $\mathrm{End}(S)$ where elements of $\mathrm{End}(S)$ are called endomorphisms. If $f \in \mathrm{End}(S)$ is invertible, then it is called an automorphism. The group of all automorphisms is denoted $\mathrm{Aut}(S)$.

Definition B.1.8 ([72])**.** Let $\mathscr{J}$ be a ring and S a $\mathscr{J}$-module. Then an annihilator of an element $g \in S$ is the set

$$\mathrm{Ann}(g) = \{h \in \mathscr{J} : hg = 0\}. \tag{B.1}$$

An element $g \in S$ is said to be a torsion element of S if $\mathrm{Ann}(g) \neq 0$, that is, there is some non-zero element $a \in \mathscr{J}$ with $ag = 0$.

Definition B.1.9 ([72])**.** A $\mathscr{J}$-module S is said to be torsion-free if the only torsion element in S is 0.

Definition B.1.10. Let S' be a finite group and let S be a left $\mathscr{J}$-module. The orbit under the action of $m \in S$ is obtained by left multiplication, i.e. $S'm = \{gm : g \in S'\}$.

B.2   Submodule Related Definitions

Definition B.2.1. Let S be a $\mathscr{J}$-module and S' a nonempty subset of S. Then S' is called a submodule of S if S' is a subgroup of S and for all $g \in S, h \in S'$, we have $gh \in S'$.

Definition B.2.2 ([61])**.** A cyclic submodule is a submodule which is generated by a single element. For example in a left $\mathscr{J}$-module S, a cyclic submodule can be generated by $m \in S$ in the following ways $\mathscr{J}m = \{xm : x \in \mathscr{J}\}$ or $m\mathscr{J} = \{mx : x \in \mathscr{J}\}$.

Definition B.2.3 ([61])**.** In general the submodule S' of the $\mathscr{J}$-module S generated by a finite subset $\{m_1, \ldots, m_n\} \subset S$ is the set

$$\mathscr{J}m_1 + \cdots + \mathscr{J}m_n = \{x_1 m_1 + \cdots + x_n m_n : x_1, \ldots, x_i \in \mathscr{J}\} \qquad \text{(B.2)}$$

of all linear combinations of $m_1, \ldots, m_n$. Such submodules are called finitely generated. If $S' = S$ then $\{m_1, \ldots, m_n\}$ is a set of generators for S.

Lemma B.2.1 ([72])**.** Let S and S' be submodules of a $\mathscr{J}$-module S. Then their sum

$$S + S' = \{l + n : l \in S, n \in S'\}, \qquad \text{(B.3)}$$

is also a submodule. Moreover, $S + S' = S \iff S' \subseteq S$.

Lemma B.2.2 ([72])**.** Let S and S' be submodules of a $\mathscr{J}$-module S. Then their intersection

$$S \cap S' = \{x : x \in S \text{ and } x \in S'\}, \qquad \text{(B.4)}$$

is also a submodule. Moreover, $S \cap S' = S \iff S \subseteq S'$.

Remark B.2.1. Submodules of a vector space are its subspaces.

Proposition B.2.1 ([72])**.** Let S' be a submodule of the $\mathscr{J}$-module S. Let $m, n \in S$ and define a relation on S by the rule that $m \equiv n \iff m - n \in S'$. The equivalence class of an element $m \in S$ is given by the set

$$[m] = m + S' = \{m + l : l \in S'\}. \qquad \text{(B.5)}$$

The quotient module (or factor module) S/S' is defined to be the set of all such equivalence classes, with addition given by

$$[m] + [n] = [m + n], [m], [n] \in S/S', \qquad \text{(B.6)}$$

and multiplication by $r \in \mathscr{J}$ is given by

$$r[m] = [rm], [m] \in S/S'. \qquad \text{(B.7)}$$

Definition B.2.4 ([72])**.** The module homomorphism $\pi : S \to S/S'$ defined by $\pi(m) = [m]$ is called the natural map (or canonical homomorphism) from S to S/S'.

Definition B.2.5. Let S' and S'' be arbitrary submodules of the $\mathscr{J}$-module S. If $S' + S'' \neq S$ and $S' \cap S'' \neq 0$ their configuration or relationship is often expressed in the diagram shown in Fig. B.1(a). If S is the direct sum of S' and S'' we have $S' \cap S'' = 0$ and $S' + S'' = S$ which lead to the simpler diagram shown in Fig. B.1(b).
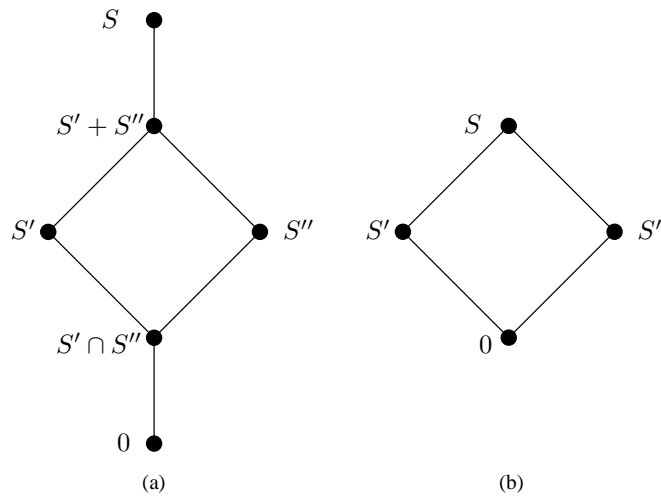
Figure B.1: *(a) The module S is not a direct sum of the submodules S' and S''. (b) The module S is a direct sum of S' and S'' and therefore $S' \cap S'' = 0$ and $S' + S'' = S$.*

B.3   Quadratic Forms

Definition B.3.1 ([1])**.** A conjugation on $\mathscr{J}$ is a function $c : \mathscr{J} \to \mathscr{J}$ satisfying

1. $c(c(\xi)) = \xi, \quad \forall \xi \in \mathscr{J}$

2. $c(\xi_1 + \xi_2) = c(\xi_1) + c(\xi_2), \quad \forall \xi_1, \xi_2 \in \mathscr{J}$

3. $c(\xi_1\xi_2) = c(\xi_1)c(\xi_2), \quad \forall \xi_1, \xi_2 \in \mathscr{J}$

Definition B.3.2 ([1])**.** Let S be a free $\mathscr{J}$-module. A bilinear form on S is a function $\phi : S \times S \to \mathscr{J}$ satisfying

1. $\phi(\xi_1 x_1 + \xi_2 x_2, y) = \xi_1 \phi(x_1, y) + \xi_2 \phi(x_2, y)$

2. $\phi(x, \xi_1 y_1 + \xi_2 y_2) = \xi_1 \phi(x, y_1) + \xi_2 \phi(x, y_2)$

for all $x_1, x_2, y_1, y_2 \in S$ and $\xi_1, \xi_2 \in \mathscr{J}$.

Definition B.3.3 ([1])**.** Let S be a free $\mathscr{J}$-module. A sesquilinear form on S is a function $\phi : S \times S \to \mathscr{J}$ satisfying

1. $\phi(\xi_1 x_1 + \xi_2 x_2, y) = \xi_1 \phi(x_1, y) + \xi_2 \phi(x_2, y)$

2. $\phi(x, \xi_1 y_1 + \xi_2 y_2) = c(\xi_1)\phi(x, y_1) + c(\xi_2)\phi(x, y_2)$

for all $x_1, x_2, y_1, y_2 \in S$ and $\xi_1, \xi_2 \in \mathscr{J}$ for a non-trivial conjugation $\xi \mapsto c(\xi)$ on $\mathscr{J}$.

Definition B.3.4 ([22])**.** Let Λ be a $\mathscr{J}$-lattice in $\mathbb{R}^L$ having basis vectors $\zeta_1, \ldots, \zeta_L \in \mathbb{R}^L$ whose transposes form the rows of the generator matrix M. Then any lattice point $\lambda \in \Lambda$ may be written on generic form as $\lambda = \xi^T M$ where $\xi = (\xi_1, \ldots, \xi_L)^T$ and where $\xi_i \in \mathscr{J}$. Let us define the following function of λ (i.e. a squared norm)

$$\begin{aligned}
\tau(\lambda) &= \sum_{i=1}^{L} \sum_{j=1}^{L} (\xi_i \zeta_i)^T \xi_j \zeta_j \\
&= \xi^T M M^T \xi.
\end{aligned} \tag{B.8}$$

The function τ in (B.8) is referred to as the quadratic form associated with the lattice Λ. If Λ has full rank, then MM^T is a positive definite matrix and the associated quadratic form is called a positive definite form. If we extend τ to $\tau(\lambda_1, \lambda_2) = \xi_1^T M M^T \xi_2$ we obtain the bilinear form of Definition B.3.2 and if the underlying field is non real we get the sesquilinear form of Definition B.3.3 where the conjugation function c depends on the field.

Remark B.3.1. In this work we will not make explicitly use of quadratic forms. Instead we equip the underlying field with an inner product $\langle \cdot, \cdot \rangle$ which satisfies Definition B.3.2 and is therefore a bilinear form.

Example B.3.1. Let $\Lambda \subset \mathbb{R}^L$, i.e. Λ is a lattice embedded in the field $\mathbb{R}^L$. Then we can define the usual vector norm $\|\lambda\|^2 \triangleq \langle \lambda, \lambda \rangle$, where $\lambda \in \Lambda$. Notice that here the conjugation is simply the identity. See Appendix C for more examples.

Lattice Definitions

In this appendix we present a number of lattice-related definitions and properties which are used throughout the thesis.

Let $\mathbb{V}$ be a vector space over the field $\mathbb{K}$ and let $\mathbb{V}$ be equipped with an inner product $\langle \cdot, \cdot \rangle$. If $\mathbb{K}^L = \mathbb{R}^L$ then $\mathbb{V}$ is the traditional vector space over the Cartesian product of the reals.[68] As such, $(\mathbb{V}, \langle \cdot, \cdot \rangle)$ is an inner-product space. An inner-product space induces a norm $\| \cdot \|$ defined as $\| \cdot \|^2 \triangleq \langle \cdot, \cdot \rangle$. If $\mathbb{K}^L = \mathbb{R}^L$ we use the ℓ_2-norm defined as $\|x\|^2 \triangleq x^T x$ whereas if $\mathbb{K}^L = \mathbb{C}^L$ we have $\|x\|^2 \triangleq x^H x$ where ^{H} denotes Hermitian transposition (i.e. the conjugate transpose). If $\mathbb{K}^L = \mathbb{H}^L$ then $\|x\|^2 \triangleq x^\dagger x$ where † denotes Quaternionic conjugation and transposition. For more information about inner-product spaces we refer the reader to the widely used textbook by Luenberger [89].

C.1 General Definitions

Definition C.1.1 ([22]). A lattice $\Lambda \subset \mathbb{K}^L$ consists of all possible integral linear combinations of a set of basis vectors, or, more formally

$$\Lambda = \left\{ \lambda \in \mathbb{K}^L : \lambda = \sum_{i=1}^{L} \xi_i \zeta_i, \ \forall \xi_i \in \mathscr{J} \right\}, \tag{C.1}$$

where $\zeta_i \in \mathbb{K}^L$ are the basis vectors also known as generator vectors of the lattice and $\mathscr{J} \subset \mathbb{K}$ is a well defined ring of integers.

Remark C.1.1. It should be noted that it is often convenient to use $L' > L$ basis vectors to form an L-dimensional lattice embedded in $\mathbb{K}^{L'}$.

---

[68]Recall that, in a vector space over $\mathbb{R}^L$, addition and subtraction is with respect to vectors of $\mathbb{R}^L$ whereas multiplication is defined as multiplications of vectors in $\mathbb{R}^L$ with scalar elements of $\mathbb{R}$. Thus, a vector space is a $\mathscr{J}$-module where $\mathscr{J}$ is a field, i.e. a ring where all elements (except 0) have inverses.

Definition C.1.2. Let M be a generator matrix of the lattice Λ. Then the rows of M are given by the tranposes of the column vectors $\zeta_i^T, i = 1, \ldots, L$, where we actually do not require that M is square.

Definition C.1.3. The square matrix $A = MM^T$ is called the Gram matrix.

Definition C.1.4. A fundamental region of a lattice is a closed region which contains a single lattice points and tessellate the underlying space.

Lemma C.1.1 ([22]). All fundamental regions have the same volume.

Lemma C.1.2 ([22]). The fundamental volume ν of Λ is given by $\nu = \sqrt{\det(A)}$, sometimes written as $\nu = \det(\Lambda)$. If M is a square generator matrix then $\nu = |\det(M)|$.

Definition C.1.5 ([25]). An L-dimensional polytope is a finite convex region in $\mathbb{K}^L$ enclosed by a finite number of hyperplanes.

Definition C.1.6 ([30]). The quotient $\mathbb{K}^L/\Lambda$ is the L-dimensional torus obtained by combining opposite faces of the fundamental parallelotope $\{a_1\zeta_1 + \ldots + a_L\zeta_L | 0 \leq a_i \leq 1\}$.

Definition C.1.7. The Cartesian product $\otimes$ of two lattices Λ_1 and Λ_2 is obtained by pairing all points in Λ_1 with every point in Λ_2, i.e.

$$\Lambda_1 \otimes \Lambda_2 = \{(\lambda_1, \lambda_2) | \lambda_1 \in \Lambda_1, \lambda_2 \in \Lambda_2\}. \tag{C.2}$$

It follows that the dimension of $\Lambda = \Lambda_1 \otimes \Lambda_2$ is equal to the sum of the dimensions of the two lattices Λ_1 and Λ_2.

Definition C.1.8 ([22]). The automorphism group $\text{Aut}(\Lambda)$ of a lattice Λ is the set of distance-preserving transformations (or isometries) of the space that fix the origin and takes the lattice to itself.

Theorem C.1.1 ([22]). For a lattice in ordinary Euclidean space $\mathbb{R}^L$, $\text{Aut}(\Lambda)$ is finite and the transformations in $\text{Aut}(\Lambda)$ may be represented by orthogonal matrices. Let Λ have generator matrix M. Then an orthogonal matrix B is in $\text{Aut}(\Lambda)$ if and only if there is an integral matrix U with determinant ± 1 such that

$$UM = MB. \tag{C.3}$$

This implies $U = MBM^TA^{-1}$, where A^{-1} is the Gram matrix of Λ.

Remark C.1.2. $\text{Aut}(\Lambda = Z^L)$ consists of all sign changes of the L coordinates $(= 2^L)$ and all permutations $(= L!)$. Hence, $|\text{Aut}(Z^L)| = 2^L L!$ [22].

Definition C.1.9 ([22])**.** The dual lattice $\tilde{\Lambda}$ of the lattice Λ is given by

$$\tilde{\Lambda} = \{x \in \mathbb{R}^L | x^T \lambda \in \mathbb{Z} \text{ for all } \lambda \in \Lambda\}. \tag{C.4}$$

Alternatively, if M is a square generator matrix of Λ then $\tilde{\Lambda}$ can be constructed by use of the generator matrix $\tilde{M} = (M^{-1})^T$.

Theorem C.1.2 ([30])**.** If $\Lambda \subset \mathbb{R}^L$ is a discrete subgroup with compact quotient $\mathbb{R}^L/\Lambda$ then Λ is a lattice.

Definition C.1.10 ([22])**.** The coefficients B_i of the Theta series $\Theta_\Lambda(z) \triangleq \sum_i B_i q^i$ of a lattice Λ describe the number of points at squared distance i from an arbitrary point in space (which is usually taken to be the origin). The indeterminate q is sometimes set to $q = \exp(i\pi z)$, where $z \in \mathbb{C}$ and $\Im(z) > 0$.

C.2   Norm Related Definitions

Definition C.2.1 ([22])**.** Let $\Lambda \subset \mathbb{K}^L$ be a lattice. The nearest neighbor region of $\lambda \in \Lambda$ is defined as

$$V(\lambda) \triangleq \{x \in \mathbb{K}^L : \|x - \lambda\|^2 \leq \|x - \lambda'\|^2, \, \forall \, \lambda' \in \Lambda\}. \tag{C.5}$$

Definition C.2.2. The nearest neighbor regions of a lattice are also called Voronoi cells, Voronoi regions or Dirichlet regions. In this work we will use the name Voronoi cells.

Definition C.2.3. Voronoi cells of a lattice are congruent polytopes, hence they are similar in size and shape and may be seen as translated versions of a fundamental region, e.g. $V_0 = V(0)$, i.e. the Voronoi cell around the origin.

Definition C.2.4 ([22])**.** The dimensionless normalized second moment of inertia $G(\Lambda)$ of a lattice Λ is defined by

$$G(\Lambda) \triangleq \frac{1}{L\nu^{1+2/L}} \int_{V_0} \|x\|^2 dx. \tag{C.6}$$

Remark C.2.1. Applying any scaling or orthogonal transform, e.g. rotation or reflection on Λ will not change $G(\Lambda)$, which makes it a good figure of merit when comparing different lattices (quantizers). In other words, $G(\Lambda)$ depends only upon the shape of the fundamental region, and in general, the more sphere-like shape, the smaller normalized second-moment [22].

Definition C.2.5 ([38])**.** The minimum squared distance $d^2_{\min}(\Lambda)$ between lattice points is the minimum non-zero norm of any lattice point $\lambda \in \Lambda$, i.e.

$$d^2_{\min}(\Lambda) \triangleq \min_{\substack{\lambda \in \Lambda \\ \lambda \neq 0}} \|\lambda\|^2. \tag{C.7}$$

Definition C.2.6 ([38])**.** The packing radius $\rho_p(\Lambda)$ of the lattice $\Lambda \subset \mathbb{R}^L$ is the radius of the greatest L-dimensional sphere that can be inscribed within V_0. We then have

$$\rho_p(\Lambda) \triangleq d_{\min}(\Lambda)/2. \tag{C.8}$$

Definition C.2.7 ([38])**.** The covering radius $\rho_c(\Lambda)$ of the lattice $\Lambda \subset \mathbb{R}^L$ is the radius of the least L-dimensional sphere that contains V_0, i.e.

$$\rho_c(\Lambda) \triangleq \max_{x \in V_0} \|x\|. \tag{C.9}$$

Definition C.2.8 ([38])**.** The kissing[69] number $\mathfrak{K}(\Lambda)$ is the number of nearest neighbors to any lattice point, which is also equal to the number of lattice points of squared norm $d_{\min}^2(\Lambda)$, i.e.

$$\mathfrak{K}(\Lambda) \triangleq |\{\lambda \in \Lambda : \|\lambda\|^2 = d_{\min}^2(\Lambda)\}|. \tag{C.10}$$

Definition C.2.9. The space-filling loss of a lattice Λ with dimensionless normalized second moment $G(\Lambda)$ is given by

$$D_{\text{Loss}} = 10 \log_{10} \left(2\pi e G(\Lambda)\right) \text{dB}. \tag{C.11}$$

C.3 Sublattice Related Definitions

Definition C.3.1. A sublattice $\Lambda' \subseteq \Lambda$ is a subset of the elements of Λ that is itself a lattice.

Definition C.3.2 ([28])**.** A sublattice $\Lambda' \subset \Lambda$ is called clean if no point of Λ lies on the boundary of the Voronoi cells of Λ'.

Definition C.3.3. If Λ' is a sublattice of Λ then $N = |\Lambda/\Lambda'|$ denotes the index or order of the quotient Λ/Λ'.

Definition C.3.4. If Λ' is a clean sublattice of Λ then the index value $N = |\Lambda/\Lambda'|$ is called an admissible index value.

Definition C.3.5. The Lth root of the index N is called the nesting ratio N', i.e. $N' = N^{1/L}$.

Definition C.3.6 ([28])**.** Let Λ be an L dimensional lattice with square generator matrix M. A sublattice $\Lambda' \subseteq \Lambda$ is geometrically strictly similar to Λ if and only if the following holds

  1. There is an invertible $L \times L$ matrix U_1 with integer entries

---

[69]The terminology kissing number was introduced by N. J. A. Sloane who drew an analogy to billiards, where two balls are said to kiss if they touch each other, see for example the interview with N. J. A. Sloane by R. Calderbank, which can be found online at http://www.research.att.com/˜njas/doc/interview.html.

2. a non-zero scalar $c_1 \in \mathbb{R}$

3. an orthogonal $L \times L$ matrix K_1 with determinant 1,

such that a generator matrix M_1 for Λ_1 can be written as

$$M_1 = U_1 M = c_1 M K_1. \qquad (C.12)$$

If (C.12) holds then the index N_1 of Λ' is equal to

$$N_1 = |\Lambda/\Lambda'| = \frac{\det(\Lambda')}{\det(\Lambda)} = \left| \frac{\det(M_1)}{\det(M)} \right| = \det(U_1) = c_1^L. \qquad (C.13)$$

Furthermore, Λ' has Gram matrix

$$A_1 = M_1 M_1^T = U_1 M M^T U_1^T = U_1 A U_1^T = c_1^2 A, \qquad (C.14)$$

where $A = MM^T$ is a Gram matrix for Λ.

Definition C.3.7. If in Definition C.3.6 the determinant of K_1 is allowed to be ± 1, i.e. K_1 can be either a rotation or a reflection operator, then the sublattice Λ' is said to be geometrically similar to Λ.

Appendix D

Root Lattices

This appendix describes some properties of the root[70] lattices considered in this thesis.

D.1 Z^1

The scalar uniform lattice also called Z^1 partitions the real line into intervals of equal lengths. Table D.1 outlines important constants related to the Z^1 lattice.

Description	Notation	Value
Dimension	L	1
Fundamental volume	ν	1
Packing radius	ρ_p	1/2
Covering radius	ρ_c	1/2
Space-filling loss	D_{loss}	1.5329 dB
Space-filling gain over Z^1	D_{gain}	0 dB
Kissing-number	$\mathfrak{K}$	2
Minimal squared distance	d_{min}^2	1
Dimensionless normalized second moment	$G(\Lambda)$	1/12

Table D.1: *Relevant constants for the Z^1 lattice.*

The set of admissible index values for Z^1 is the set of all odd integers [28] and the coefficients of the Theta series are given by $B_0 = 1$ and $B_i = 2, i > 0$.

---

[70]The term root lattice refers to a lattice which can be generated by the roots of specific reflection groups [22, 34].

D.2 Z^2

A generator matrix for Z^2 (also known as the square lattice) is given by

$$M = \begin{bmatrix} 1 & 0 \\ 0 & 1 \end{bmatrix}. \tag{D.1}$$

The Gram matrix A is identical to the generator matrix, i.e. $A = M$. Table D.2 gives an overview of important constants related to the Z^2 lattice.

Description	Notation	Value
Dimension	L	2
Fundamental volume	ν	1
Packing radius	ρ_p	1/2
Covering radius	ρ_c	$\rho_p\sqrt{2}$
Space-filling loss	D_{loss}	1.5329 dB
Space-filling gain over Z^1	D_{gain}	0 dB
Kissing-number	$\mathfrak{K}$	4
Minimal squared distance	d^2_{min}	1
Dimensionless normalized second moment	$G(\Lambda)$	1/12

Table D.2: *Relevant constants for the Z^2 lattice.*

The first 50 coefficients of the Theta series, i.e. the number of points in each of the 50 first shells of Λ are shown in Table D.3 and the first seven shells are shown in Fig. D.1.

1,4,4,0,4,8,0,0,4,4,8,0,0,8,0,0,4,8,4,0,8,0,0,0,0,12, 8,0,0,8,0,0,4,0,8,0,4,8,0,0,8,8,0,0,0,8,0,0,0,4

Table D.3: *The first 50 coefficients of the Theta series with starting point at zero for the Z^2 lattice.*

Let Λ be the square lattice represented in the scalar complex domain, i.e. $\Lambda = \mathscr{G}$. Then a sublattice $\Lambda' = \xi\Lambda$, where $\xi = a + ib$ and $\xi \in \mathscr{G}$ is clean if and only if $N = a^2 + b^2$ is odd [28]. Equivalently an integer N is an admissible index value if it can be written as a product of primes congruent to $1 \pmod 4$ and/or a product of primes congruent to $3 \pmod 4$ [21, 28]. This set is given by integer sequence A057653 [125], see also Table D.4.

A subgroup $\Gamma_4 \subset \text{Aut}(\Lambda = \mathbb{Z}^2)$ of order 4 is given by (2.9).
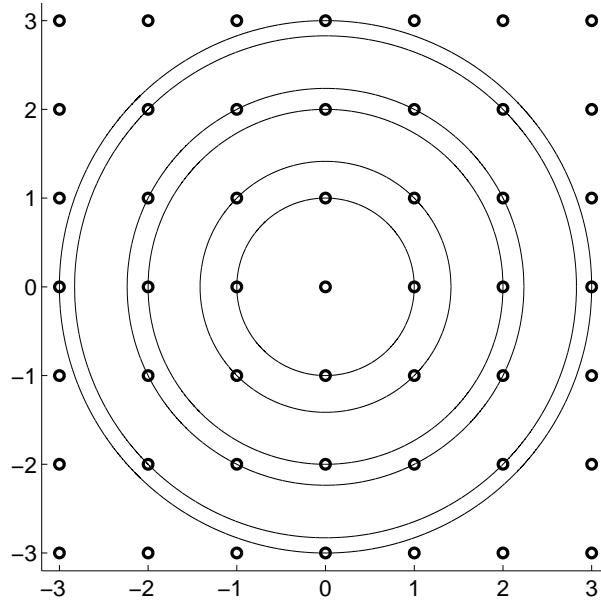
Figure D.1: *The first 7 non-zero shells of Z^2 is here shown as large circles (incl. the one at the origin). Notice that the number of points lying on each circle agrees with the corresponding coefficient of its Theta series.*

D.3 A_2

The hexagonal lattice (also known as A_2) can be represented in the complex field where it is identical to $\mathscr{E}$. When represented in $\mathbb{R}^2$ a possible generator matrix is

$$M = \begin{bmatrix} 1 & 0 \\ -1/2 & \sqrt{3}/2 \end{bmatrix}. \tag{D.2}$$

Its Gram matrix is given by

$$A = \begin{bmatrix} 1 & -1/2 \\ -1/2 & 1 \end{bmatrix}. \tag{D.3}$$

Table D.5 summarizes important constants related to the A_2 lattice.

Let Λ be the hexagonal lattice represented in the scalar complex domain, i.e. $\Lambda = \mathscr{E}$. Then a sublattice $\Lambda' = \xi\Lambda$, where $\xi = a + \omega b$ and $\xi \in \mathscr{E}$ is clean if and only if a and b are relative prime or equivalently if and only if N is a product of primes congruent to $1 \pmod{6}$ [28]. This set is given by integer sequence A004611 [125], see also Table D.6.

A subgroup $\Gamma_6 \subset \mathrm{Aut}(\Lambda = \mathscr{E})$ of order 6 is given by the rotational group

$$\Gamma_6 = \{\exp(ik\pi/6), k = 0, \ldots, 5\}. \tag{D.4}$$

1,5,9,13,17,25,29,37,41,45,49,53,61,65,73,81,85,89,97,101,109,113,
117,121,125,137,145,149,153,157,169,173,181,185,197,205,221,225,
229,233,241,245,257,261,265,269,277,281,289,293,305,313,317,325
333,337,...

Table D.4: *Admissible index values for* Z^2.

Description	Notation	Value
Dimension	L	2
Fundamental volume	ν	$\sqrt{3}/2$
Packing radius	ρ_p	1/2
Covering radius	ρ_c	$2\rho_p\sqrt{3}$
Space-filling loss	D_{loss}	1.3658 dB
Space-filling gain over Z^1	D_{gain}	0.1671 dB
Kissing-number	$\mathfrak{K}$	6
Minimal squared distance	d^2_{min}	1
Dimensionless normalized second moment	$G(\Lambda)$	$5/(36\sqrt{3})$

Table D.5: *Relevant constants for the* A_2 *lattice.*

The first 50 coefficients of the Theta series for A_2 are shown in Table D.7 and Fig. D.2

D.4 $\quad Z^4$

The hypercubic lattice Z^4 is generated by

$$M = \begin{bmatrix} 1 & 0 & 0 & 0 \\ 0 & 1 & 0 & 0 \\ 0 & 0 & 1 & 0 \\ 0 & 0 & 0 & 1 \end{bmatrix}. \tag{D.5}$$

The Gram matrix A is identical to the generator matrix, i.e. $A = M$. Table D.8 gives an overview of important constants related to the Z^4 lattice.

Z^4 has a geometrically-similar and clean sublattice of index N if and only if N is odd and of the form a^2 for some integer a [28]. The set of admissible index values is given by integer sequence A016754 [125], see also Table D.9.

The first 50 coefficients of the Theta series for Z^4 are given in Table D.10.

1,7,13,19,31,37,43,49,61,67,73,79,91,97,103,109,127,133,139,
151,157,163,169,181,193,199,211,217,223,229,241,247,259,271,
277,283,301,307,313,331,337,343,349,361,367,373,379,397,403,
409,421,427,433,439,457,...

Table D.6: *Admissible index values for A_2.*

1,6,0,6,6,0,0,12,0,6,0,0,6,12,0,0,6,0,0,12,0,12,0,0,0,6,0,6,
12,0,0,12,0,0,0,0,6,12,0,12,0,0,0,12,0,0,0,0,6,18

Table D.7: *The first 50 coefficients of the Theta series with starting point at zero for the A_2 lattice.*

A subgroup $\Gamma_8 \subset \mathrm{Aut}(\Lambda = \mathbb{Z}^4)$ of order 8 is given by [139]

$$\Gamma_8 = \left\{ \pm I_4, \pm \begin{pmatrix} 0 & -1 & 0 & 0 \\ 1 & 0 & 0 & 0 \\ 0 & 0 & 0 & 1 \\ 0 & 0 & -1 & 0 \end{pmatrix}, \pm \begin{pmatrix} 0 & 0 & -1 & 0 \\ 0 & 0 & 0 & -1 \\ 1 & 0 & 0 & 0 \\ 0 & 1 & 0 & 0 \end{pmatrix}, \pm \begin{pmatrix} 0 & 0 & 0 & -1 \\ 0 & 0 & 1 & 0 \\ 0 & -1 & 0 & 0 \\ 1 & 0 & 0 & 0 \end{pmatrix} \right\}. \quad \text{(D.6)}$$

D.5 D_4

The D_4 lattice (also known as the Schläfli lattice or checkerboard lattice) consists of all points of Z^4 that have even squared norms [22]. A possible generator matrix is given by

$$M = \begin{bmatrix} 1 & 1 & 0 & 0 \\ -1 & 0 & 1 & 0 \\ 0 & -1 & 0 & 1 \\ 0 & -1 & 0 & -1 \end{bmatrix}. \quad \text{(D.7)}$$

The Gram matrix is given by

$$A = \begin{bmatrix} 2 & -1 & -1 & -1 \\ -1 & 2 & 0 & 0 \\ -1 & 0 & 2 & 0 \\ -1 & 0 & 0 & 2 \end{bmatrix}, \quad \text{(D.8)}$$

and a subgroup $\Gamma_8 \subset \mathrm{Aut}(\Lambda = D_4)$ of order 8 is given by (D.6). See Table D.11 for a an overview of important constants related to the D_4 lattice.

If a is 7 or a product of primes congruent to $1 \pmod 4$ then D_4 has a geometrically-similar and clean sublattice of index $N = a^2$ [28]. This is the set 7 and integer sequence A004613 [125], see also Table D.12.

The first 50 coefficients of the Theta series for D_4 are shown in Table D.13.
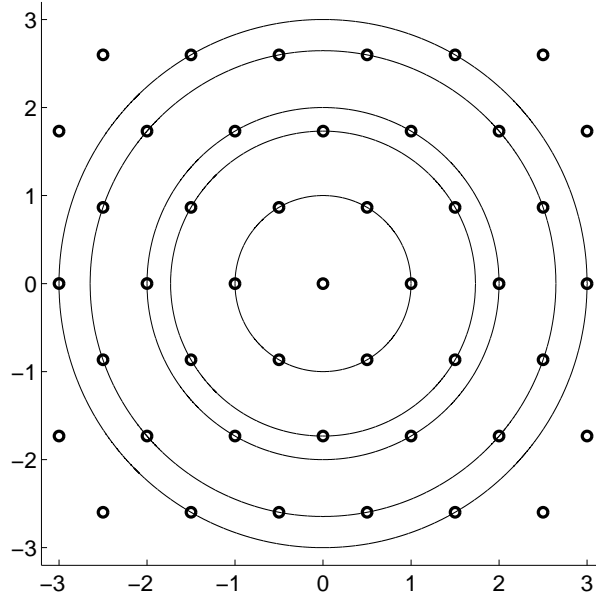
Figure D.2: *The first 6 non-zero shells of A_2 is here shown as large circles (incl. the one at the origin). Notice that the number of points lying on each circle agrees with the corresponding coefficient of the Theta series.*

Description	Notation	Value
Dimension	L	4
Fundamental volume	ν	1
Packing radius	ρ_p	1/2
Covering radius	ρ_c	1
Space-filling loss	D_{loss}	1.5329 dB
Space-filling gain over Z^1	D_{gain}	0 dB
Kissing-number	$\mathfrak{K}$	8
Minimal squared distance	d^2_{min}	1
Dimensionless normalized second moment	$G(\Lambda)$	1/12

Table D.8: *Relevant constants for the Z^4 lattice.*

1,9,25,49,81,121,169,225,289,361,441,529,625,729,841,961,
1089,1225,1369,1521,1681,1849,2025,2209,2401,2601,2809,
3025,3249,3481,3721,3969,4225,4489,4761,5041,5329,5625,
5929,6241,6561,...

Table D.9: *Admissible index values for Z^4.*

1,8,24,32,24,48,96,64,24,104,144,96,96,112,192,192,24,144,
312,160,144, 256,288,192,96,248,336,320,192,240,576,256,24,
384,432,384,312,304,480,448,144,336,768,352,288,624,576,
384,96,456

Table D.10: *The first 50 coefficients of the Theta series with starting point at zero for the Z^4 lattice.*

Description	Notation	Value
Dimension	L	4
Fundamental volume	ν	2
Packing radius	ρ_p	$1/\sqrt{2}$
Covering radius	ρ_c	$\rho_p\sqrt{2}$
Space-filling loss	D_{loss}	1.1672 dB
Space-filling gain over Z^1	D_{gain}	0.3657 dB
Kissing-number	$\mathfrak{K}$	24
Minimal squared distance	d^2_{min}	2
Dimensionless normalized second moment	$G(\Lambda)$	0.076603

Table D.11: *Relevant constants for the D_4 lattice.*

1,5,7,13,17,25,29,37,41,53,61,65,73,85,89,97,101,109,
113,125,137,145,149,157,169,173,181,185,193,197,205,
221,229,233,241,257,265,269,277,281,289,293,305,313,
317,325,337,349,353,365,373,377,389,397,401,409,421,...

Table D.12: *Admissible index values for D_4.*

1,0,24,0,24,0,96,0,24,0,144,0,96,0,192,0,24,0,312,0,144,
0,288,0,96,0,336,0,192,0,576,0,24,0,432,0,312,0,480,0,
144,0,768,0,288,0,576,0,96,0

Table D.13: *The first 50 coefficients of the Theta series with starting point at zero for the D_4 lattice.*

Proofs for Chapter 2

Proof of Lemma 2.3.1. Most of the work towards proving the lemma has already been done in [21] and [28] and we only need some simple extensions of their results. For Z^1 the proof is trivial, since any odd integer is an admissible index value [28] and the product of odd integers yields odd integers. Now let $a, b \in \mathbb{Z}^+$ be odd integers that can be written as the product of primes from a certain set s. It is clear that the product ab is also odd an can be written as the product of primes of s. For Z^2 an integer is an admissible index value if it can be written as a product of a set of primes which are congruent to $1 \pmod 4$ and/or congruent to $3 \pmod 4$ [21, 28]. For A_2 an integer is an admissible index value if and only if it is a product of primes which are congruent to $1 \pmod 6$ [21, 28] and if m is a product of primes which are congruent to $1 \pmod 4$ then m^2 is an an admissible integer for D_4 [28].[71] It follows that the lemma holds for the lattices mentioned above. Finally, for Z^L and $L = 4k$, where $k \geq 1$, an integer is an admissible index value if it is odd and can be written on the form $m^{L/2}$ for some integer m [28]. Let $a = m^{L/2}$ and $b = (m')^{L/2}$ we then have that $ab = m^{L/2}(m')^{L/2} = (m'')^{L/2}$, where $m'' = mm'$ is odd and therefore an admissible index value for Z^L. □

Proof of Lemma 2.3.2. The cyclic submodule $\Lambda_0 = \xi_0 \Lambda$ is closed under multiplication by elements of Λ so for any $\xi' = \xi_1 \xi_2 \cdots \xi_{K-1} \in \Lambda$ and any $\lambda_0 \in \Lambda_0$ it is true that $\xi' \lambda_0 \in \Lambda_0$ which further implies that $\Lambda_\pi \subseteq \Lambda_0$ since $\xi' \lambda_0 \in \Lambda_\pi$. Moreover, multiplication is commutative in $\mathbb{Z}, \mathscr{G}$ and $\mathscr{E}$ so the order of the set of elements $\xi_0, \ldots, \xi_{K-1}$ when forming Λ_π is irrelevant. Thus, $\Lambda_\pi \subseteq \Lambda_i$ and it is therefore a product lattice. □

Proof of Lemma 2.3.3. Since the rings considered are unique factorization rings there

---

[71] We have excluded the index value obtained for $m = 7$, since this particular index value cannot be written as a product of primes mod 4 but is a special case found in [28].

must be an element $\xi' \in \Lambda$ such that $\xi_0 \xi' = \xi_\cap$, where ξ' is unique up to multiplication by units of the respective rings. However, a unit $u \in \Lambda$ belongs to $\mathrm{Aut}(\Lambda)$ and multiplication by u is therefore an isometric operation which takes a lattice to itself. It follows that $\xi_0 \xi' \in \Lambda_0$ for any $\xi_0 \in \Lambda_0$ which implies that $\Lambda'_\pi \subseteq \Lambda_0 = \xi_0 \Lambda$. Once again we invoke the fact that $\mathbb{Z}, \mathscr{G}$ and $\mathscr{E}$ are multiplicative commutative rings from which it is clear that $\Lambda'_\pi \subseteq \Lambda_i = \xi_i \Lambda, \ i = 0, \ldots, K-1$. $\qquad \square$

Proof of Lemma 2.3.4. Follows trivially from the fact that Gaussian integers commute and Lipschitz integers include Gaussian integers as a special case where the jth and k^{th} elements are both zero. $\qquad \square$

Appendix F

Estimating ψ_L

In this appendix we present a method to numerically estimate ψ_L for any L and K.

F.1   Algorithm

In Chapter 5 we presented closed-form expressions for ψ_L for the case of $K = 3$ and $L = 2$ or odd as well as for the asymptotic case of $L \to \infty$. In order to extend these results to $K > 3$ it follows from the proof of Theorem 5.3.2 that we need closed-form expressions for the volumes of all the different convex regions that can be obtained by $K - 1$ overlapping spheres. With such expressions it should be straightforward to find ψ_L for any K. However, we will take a different approach here.

Let $\tilde{\nu}$ be the volume of the sphere $\tilde{V}$, which contains the exact number of sublattice points required to construct N distinct K-tuples, where the elements of each K-tuple satisfy $\|\lambda_i - \lambda_j\| \le r$, where r is the radius of $\tilde{V}$. Notice that $\tilde{V}$ is the expanded sphere. Thus, the volume $\tilde{\nu}$ of $\tilde{V}$ is ψ_L^L times larger than the lower bound of (5.26). Now let $\tilde{\nu}' = \tilde{\nu}/\psi_L^L$ denote the volume of a sphere that achieves the lower bound (5.26) so that $N = (\tilde{\nu}'/\nu_s)^{K-1}$ (at least this is true for large N). But this implies that asymptotically as the number of lattice points in $\tilde{V}$ goes to infinity we have

$$N = \left(\frac{\tilde{\nu}/\psi_L^L}{\nu_s} \right)^{K-1}, \tag{F.1}$$

which leads to

$$\psi_L = \left(\frac{\omega_L r^L}{\nu_s N^{1/K-1}} \right)^{1/L}, \tag{F.2}$$

where, without loss of generality, we can assume that $\nu_s = 1$ (simply a matter of scaling). For a given r in (F.2) we can numerically estimate N, which then leads to an estimate of ψ_L. To numerically estimate N it follows that we need to find the set

175

of lattice points within a sphere $\tilde{V}$ of radius r. For each of these lattice points we center another sphere of radius r and find the set of lattice points which are within the intersection of the two spheres. This procedure continues $K-1$ times. In the end we find N by adding the number of lattice points within each intersection, i.e.

$$N = \sum_{\tilde{\Lambda}_1} \sum_{\tilde{\Lambda}_2} \cdots \sum_{\tilde{\Lambda}_{K-2}} |\Lambda_s \cap \tilde{V}(\lambda_{K-2}) \cap \cdots \cap \tilde{V}(\lambda_0)|, \tag{F.3}$$

where

$$\begin{aligned}
\tilde{\Lambda}_1 &= \{\lambda_1 : \lambda_1 \in \Lambda_s \cap \tilde{V}(\lambda_0)\}, \\
\tilde{\Lambda}_2 &= \{\lambda_2 : \lambda_2 \in \Lambda_s \cap \tilde{V}(\lambda_1) \cap \tilde{V}(\lambda_0)\}, \\
&\vdots \\
\tilde{\Lambda}_{K-2} &= \{\lambda_{K-2} : \lambda_{K-2} \in \Lambda_s \cap \tilde{V}(\lambda_{K-3}) \cap \cdots \cap \tilde{V}(\lambda_0)\}.
\end{aligned} \tag{F.4}$$

As r gets large the estimate gets better. For example for $K = 4, \Lambda = Z^2$ and $r = 10, 20, 50$ and 70 then using the algorithm outlined above we find $\psi_2 \approx 1.1672, 1.1736, 1.1757$ and 1.1762, respectively.

Assignment Example

In this appendix we give an example of part of a complete assignment. We let $\Lambda = Z^2, K = 2$ and $N = 101$ and construct 2-tuples as outlined in Sections 5.3.3 and 5.5.2. These 2-tuples are then assigned to central lattice points in $V_\pi(0)$. Since $N = 101$ then (at least theoretically) each sublattice points will be used 101 times. Furthermore, for a given sublattice point, say $\lambda_0 \in \Lambda_s$, the N associated sublattice points, i.e. the set of sublattice points representing the second coordinate of the 2-tuples having λ_0 as first coordinate, will be approximately spherically distributed around λ_0 (since $\tilde{V}$ forms a sphere). Fig. G.1(a) shows the set of N sublattice points given by

$$\{\lambda_1 \in \Lambda_s : \lambda_1 = \alpha_1(\lambda_c) \text{ and } \alpha_0(\lambda_c) = (1, -10), \lambda_c \in \Lambda_c\}, \qquad \text{(G.1)}$$

which represent the set of second coordinates of the N 2-tuples all having $\lambda_0 = (1, -10)$ as first coordinate. Each 2-tuple is assigned to a central lattice point. This assignment is illustrated in Fig. G.1(b). Here a dashed line connects a given 2-tuple (represented by its second coordinate λ_1) with a central lattice point. These N assignments are also shown in Table G.1.

(a)

(b)
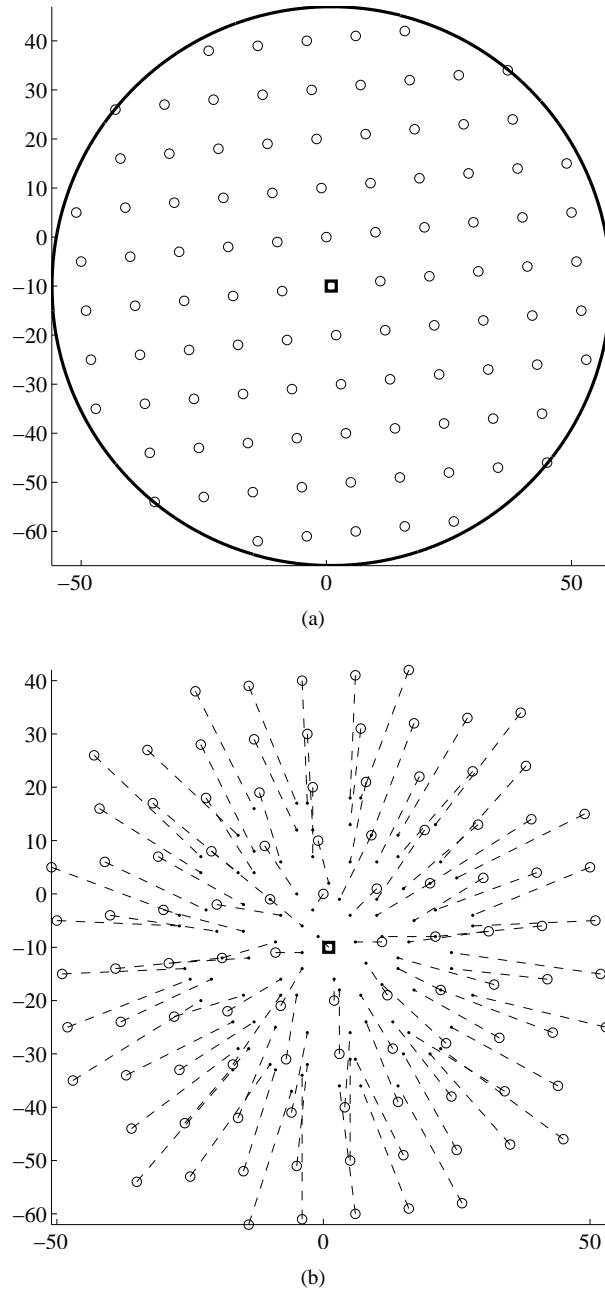
Figure G.1: *The square marks the sublattice point $\lambda_0 = (1, -10)$ and the small circles illustrate the 101 sublattice points which are associated with λ_0. (a) The large circle emphasize that the sublattice points are approximately spherically distributed around λ_0. (b) The assignments are illustrated with dashed lines and the small dots represent central lattice points.*

$\lambda_c \in \Lambda$	$\alpha_1(\lambda_c) \in \Lambda_s$	$\lambda_c \in \Lambda$	$\alpha_1(\lambda_c) \in \Lambda_s$	$\lambda_c \in \Lambda$	$\alpha_1(\lambda_c) \in \Lambda_s$
(-27,-6)	(-50,-5)	(21,-8)	(41,-6)	(-3,-32)	(-5,-51)
(-27,-4)	(-51,5)	(20,2)	(39,14)	(-10,-32)	(-25,-53)
(-26,-14)	(-49,-15)	(17,-5)	(30,3)	(6,-31)	(15,-49)
(-25,-16)	(-48,-25)	(16,-9)	(31,-7)	(5,-31)	(5,-50)
(-23,-20)	(-47,-35)	(15,1)	(29,13)	(20,-30)	(35,-47)
(-23,4)	(-42,16)	(14,11)	(27,33)	(15,-30)	(25,-48)
(-23,7)	(-43,26)	(14,7)	(28,23)	(22,-29)	(45,-46)
(-22,-3)	(-41,6)	(14,-12)	(32,-17)	(-14,-29)	(-26,-43)
(-21,-16)	(-38,-24)	(11,-8)	(21,-8)	(-16,-29)	(-36,-44)
(-20,-7)	(-40,-4)	(10,6)	(18,22)	(16,-26)	(34,-37)
(-19,-12)	(-39,-14)	(10,-1)	(19,12)	(5,-26)	(4,-40)
(-16,4)	(-32,17)	(10,-4)	(20,2)	(-3,-26)	(-6,-41)
(-16,11)	(-33,27)	(5,-4)	(10,1)	(24,-25)	(44,-36)
(-15,-7)	(-30,-3)	(3,-1)	(9,11)	(-9,-25)	(-16,-42)
(-15,-2)	(-31,7)	(5,18)	(6,41)	(13,-24)	(24,-38)
(-14,-12)	(-29,-13)	(7,18)	(16,42)	(8,-24)	(14,-39)
(-13,4)	(-22,18)	(-5,17)	(-14,39)	(-13,-24)	(-27,-33)
(-13,8)	(-23,28)	(-3,17)	(-4,40)	(-17,-24)	(-37,-34)
(-10,-1)	(-21,8)	(-13,16)	(-24,38)	(7,-19)	(13,-29)
(-9,-9)	(-19,-12)	(5,13)	(7,31)	(-5,-19)	(-7,-31)
(-8,-4)	(-20,-2)	(-5,12)	(-13,29)	(-8,-19)	(-17,-32)
(-8,6)	(-12,19)	(-2,12)	(-3,30)	(-15,-19)	(-28,-23)
(-5,0)	(-11,9)	(9,11)	(17,32)	(17,-18)	(33,-27)
(28,-4)	(50,5)	(-2,7)	(-2,20)	(3,-18)	(3,-30)
(28,-6)	(51,-5)	(5,6)	(8,21)	(11,-17)	(23,-28)
(28,-19)	(53,-25)	(1,2)	(-1,10)	(2,-16)	(2,-20)
(25,3)	(49,15)	(-6,-37)	(-14,-62)	(-8,-16)	(-18,-22)
(24,-11)	(52,-15)	(14,-36)	(26,-58)	(14,-14)	(22,-18)
(24,-14)	(42,-16)	(7,-36)	(16,59)	(-4,-14)	(-8,-21)
(22,6)	(38,24)	(3,-36)	(6,-60)	(8,-13)	(12,-19)
(22,-18)	(43,-26)	(-4,-34)	(-4,-61)	(-4,-11)	(-9,-11)
(21,13)	(37,34)	(-9,-33)	(-15,-52)	(6,-9)	(11,-9)
(21,-3)	(40,4)	(-17,-33)	(-35,-54)	(-1,-8)	(1,-10)
(-4,-6)	(-10,-1)	(-2,-3)	(0,0)		

Table G.1: *The assignments of the $N = 101$ 2-tuples which all have $\lambda_0 = (1, -10)$ as first coordinate, i.e. $\alpha_0(\lambda_c) = (1, -10)$.*

Proofs for Chapter 5

For notational convenience we will in this appendix use the shorter notation $\mathscr{L}$ instead of $\mathscr{L}^{(K,\kappa)}$.

H.1 Proof of Theorem 5.3.1

In order to prove Theorem 5.3.1, we need the following results.

Lemma H.1.1. For $1 \leq \kappa \leq K$ we have

$$\sum_{l \in \mathscr{L}} \left\langle \lambda_c, \sum_{j=0}^{\kappa-1} \lambda_{l_j} \right\rangle = \frac{\kappa}{K} \binom{K}{\kappa} \left\langle \lambda_c, \sum_{i=0}^{K-1} \lambda_i \right\rangle.$$

Proof. Expanding the sum on the left-hand-side leads to $\binom{K}{\kappa}\kappa$ different terms of the form $\langle \lambda_c, \lambda_i \rangle$, where $i \in \{0, \ldots, K-1\}$. There are K distinct λ_i's so the number of times each λ_i occur is $\binom{K}{\kappa}\kappa/K$. □

Lemma H.1.2. For $1 \leq \kappa \leq K$ we have

$$\sum_{l \in \mathscr{L}} \left\| \sum_{j=0}^{\kappa-1} \lambda_{l_j} \right\|^2 = \frac{\kappa}{K}\binom{K}{\kappa} \sum_{i=0}^{K-1} \|\lambda_i\|^2 + \frac{2\kappa(\kappa-1)}{K(K-1)}\binom{K}{\kappa} \sum_{i=0}^{K-2} \sum_{j=i+1}^{K-1} \langle \lambda_i, \lambda_j \rangle.$$

Proof. There are $\binom{K}{\kappa}$ distinct ways of adding κ out of K elements. Squaring a sum of κ elements leads to κ squared elements and $2\binom{\kappa}{2}$ cross products (product of two different elements). This gives a total of $\binom{K}{\kappa}\kappa$ squared elements, and $2\binom{K}{\kappa}\binom{\kappa}{2}$ cross products. Now since there are K distinct elements, the number of times each squared element occurs is given by

$$\#_{\|\lambda_i\|^2} = \binom{K}{k}\frac{\kappa}{K}. \tag{H.1}$$

There are $\binom{K}{2}$ distinct cross products, so the number of times each cross product occurs is given by

$$\#_{\langle\lambda_i,\lambda_j\rangle} = \binom{K}{\kappa}\frac{2\binom{\kappa}{2}}{\binom{K}{2}} = \frac{2\kappa(\kappa-1)}{K(K-1)}\binom{K}{\kappa}. \tag{H.2}$$

$\square$

Lemma H.1.3. For $K \geq 1$ we have

$$(K-1)\sum_{i=0}^{K-1}\|\lambda_i\|^2 - 2\sum_{i=0}^{K-2}\sum_{j=i+1}^{K-1}\langle\lambda_i,\lambda_j\rangle = \sum_{i=0}^{K-2}\sum_{j=i+1}^{K-1}\|\lambda_i-\lambda_j\|^2. \tag{H.3}$$

Proof. Expanding the right-hand-side of (H.3) yields

$$\sum_{i=0}^{K-2}\sum_{j=i+1}^{K-1}\|\lambda_i-\lambda_j\|^2 = \sum_{i=0}^{K-2}\sum_{j=i+1}^{K-1}\left(\|\lambda_i\|^2 + \|\lambda_j\|^2 - 2\langle\lambda_i,\lambda_j\rangle\right). \tag{H.4}$$

We also have

$$\begin{aligned}
\sum_{i=0}^{K-2}\sum_{j=i+1}^{K-1}\left(\|\lambda_i\|^2 + \|\lambda_j\|^2\right) &= \sum_{i=0}^{K-2}(K-1-i)\|\lambda_i\|^2 + \sum_{i=0}^{K-2}\sum_{j=i+1}^{K-1}\|\lambda_j\|^2 \\
&= \sum_{i=0}^{K-2}(K-1-i)\|\lambda_i\|^2 + \sum_{j=1}^{K-1}j\|\lambda_j\|^2 \\
&= \sum_{i=0}^{K-1}(K-1-i)\|\lambda_i\|^2 + \sum_{j=0}^{K-1}j\|\lambda_j\|^2 \\
&= \sum_{i=0}^{K-1}(K-1)\|\lambda_i\|^2 - \sum_{i=0}^{K-1}i\|\lambda_i\|^2 + \sum_{j=0}^{K-1}j\|\lambda_j\|^2 \\
&= (K-1)\sum_{i=0}^{K-1}\|\lambda_i\|^2,
\end{aligned} \tag{H.5}$$

which completes the proof. $\square$

We are now in a position to prove the following result.

Proposition H.1.1. For $1 \leq \kappa \leq K$ we have

$$\begin{aligned}
\sum_{l\in\mathscr{L}}\left\|\lambda_c - \frac{1}{\kappa}\sum_{j=0}^{\kappa-1}\lambda_{l_j}\right\|^2 &= \binom{K}{\kappa}\Bigg(\left\|\lambda_c - \frac{1}{K}\sum_{i=0}^{K-1}\lambda_i\right\|^2 \\
&\quad + \left(\frac{K-\kappa}{K^2\kappa(K-1)}\right)\sum_{i=0}^{K-2}\sum_{j=i+1}^{K-1}\|\lambda_i-\lambda_j\|^2\Bigg).
\end{aligned}$$

Proof. We have

$$\left\| \lambda_c - \frac{1}{\kappa} \sum_{j=0}^{\kappa-1} \lambda_{l_j} \right\|^2 = \|\lambda_c\|^2 - 2 \left\langle \lambda_c, \frac{1}{\kappa} \sum_{j=0}^{\kappa-1} \lambda_{l_j} \right\rangle + \frac{1}{\kappa^2} \left\| \sum_{j=0}^{\kappa-1} \lambda_{l_j} \right\|^2 .$$

Hence, by use of Lemmas H.1.1 and H.1.2, we have that

$$\sum_{l \in \mathscr{L}} \left\| \lambda_c - \frac{1}{\kappa} \sum_{j=0}^{\kappa-1} \lambda_{l_j} \right\|^2 = \binom{K}{\kappa} \left(\|\lambda_c\|^2 - \frac{2}{K} \left\langle \lambda_c, \sum_{i=0}^{K-1} \lambda_i \right\rangle + \frac{1}{K\kappa} \sum_{i=0}^{K-1} \|\lambda_i\|^2 \right.$$

$$\left. + \frac{2(\kappa-1)}{K(K-1)\kappa} \sum_{i=0}^{K-2} \sum_{j=i+1}^{K-1} \langle \lambda_i, \lambda_j \rangle \right)$$

$$= \binom{K}{\kappa} \left(\left\| \lambda_c - \frac{1}{K} \sum_{i=0}^{K-1} \lambda_i \right\|^2 - \frac{1}{K^2} \left\| \sum_{i=0}^{K-1} \lambda_i \right\|^2 \right.$$

$$\left. + \frac{1}{K\kappa} \sum_{i=0}^{K-1} \|\lambda_i\|^2 + \frac{2(\kappa-1)}{K(K-1)\kappa} \sum_{i=0}^{K-2} \sum_{j=i+1}^{K-1} \langle \lambda_i, \lambda_j \rangle \right)$$

$$= \binom{K}{\kappa} \left(\left\| \lambda_c - \frac{1}{K} \sum_{i=0}^{K-1} \lambda_i \right\|^2 + \left(\frac{1}{K\kappa} - \frac{1}{K^2} \right) \sum_{i=0}^{K-1} \|\lambda_i\|^2 \right.$$

$$\left. + \left(\frac{2(\kappa-1)}{K(K-1)\kappa} - \frac{2}{K^2} \right) \sum_{i=0}^{K-2} \sum_{j=i+1}^{K-1} \langle \lambda_i, \lambda_j \rangle \right)$$

$$= \binom{K}{\kappa} \left(\left\| \lambda_c - \frac{1}{K} \sum_{i=0}^{K-1} \lambda_i \right\|^2 + \left(\frac{K-\kappa}{K^2 \kappa} \right) \sum_{i=0}^{K-1} \|\lambda_i\|^2 \right.$$

$$\left. - \left(\frac{K-\kappa}{K^2 \kappa (K-1)} \right) 2 \sum_{i=0}^{K-2} \sum_{j=i+1}^{K-1} \langle \lambda_i, \lambda_j \rangle \right)$$

so that, by Lemma H.1.3, we finally have that

$$= \binom{K}{\kappa} \left(\left\| \lambda_c - \frac{1}{K} \sum_{i=0}^{K-1} \lambda_i \right\|^2 \right.$$

$$\left. + \left(\frac{K-\kappa}{K^2 \kappa (K-1)} \right) \sum_{i=0}^{K-2} \sum_{j=i+1}^{K-1} \|\lambda_i - \lambda_j\|^2 \right),$$

which completes the proof.   □

Theorem 5.3.1. *For $1 \leq \kappa \leq K$ we have*

$$
\sum_{\lambda_c} \sum_{l \in \mathscr{L}} \left\| \lambda_c - \frac{1}{\kappa} \sum_{j=0}^{\kappa-1} \lambda_{l_j} \right\|^2 = \sum_{\lambda_c} \binom{K}{\kappa} \left(\left\| \lambda_c - \frac{1}{K} \sum_{i=0}^{K-1} \lambda_i \right\|^2 \right.
$$
$$
\left. + \left(\frac{K-\kappa}{K^2 \kappa (K-1)} \right) \sum_{i=0}^{K-2} \sum_{j=i+1}^{K-1} \| \lambda_i - \lambda_j \|^2 \right).
$$

Proof. Follows trivially from Proposition H.1.1. $\qquad\square$

H.2   Proof of Theorem 5.3.2

Theorem 5.3.2. *For the case of $K = 3$ and any odd L, the dimensionless expansion factor is given by*

$$
\psi_L = \left(\frac{\omega_L}{\omega_{L-1}} \right)^{1/2L} \left(\frac{L+1}{2L} \right)^{1/2L} \beta_L^{-1/2L}, \tag{H.6}
$$

where β_L is given by

$$
\beta_L = \sum_{n=0}^{\frac{L+1}{2}} \binom{\frac{L+1}{2}}{n} 2^{\frac{L+1}{2}-n} (-1)^n \sum_{k=0}^{\frac{L-1}{2}} \frac{\left(\frac{L+1}{2} \right)_k \left(\frac{1-L}{2} \right)_k}{\left(\frac{L+3}{2} \right)_k k!}
$$
$$
\times \sum_{j=0}^{k} \binom{k}{j} \left(\frac{1}{2} \right)^{k-j} (-1)^j \left(\frac{1}{4} \right)^j \frac{1}{L+n+j}. \tag{H.7}
$$

Proof. In the following we consider the case of $K = 3$. For a specific $\lambda_0 \in \Lambda_s$ we need to construct N 3-tuples all having λ_0 as the first coordinate. To do this we first center a sphere $\tilde{V}$ of radius r at λ_0, see Fig. 5.2. For large N and small ν_s this sphere contains approximately $\tilde{\nu}/\nu_s$ lattice points from Λ_s. Hence, it is possible to construct $(\tilde{\nu}/\nu_s)^2$ distinct 3-tuples using lattice points inside $\tilde{V}$. However, the maximum distance between λ_1 and λ_2 points is greater than the maximum distance between λ_0 and λ_1 points and also between λ_0 and λ_2 points. To avoid this bias towards λ_0 points we only use 3-tuples that satisfy $\| \lambda_i - \lambda_j \| \leq r$ for $i, j = 0, 1, 2$. However, with this restriction we can no longer form N 3-tuples. In order to make sure that exactly N 3-tuples can be made we expand $\tilde{V}$ by the factor ψ_L. It is well known that the number of lattice points at exactly squared distance l from c, for any $c \in \mathbb{R}^L$ is given by the coefficients of the Theta series of the lattice Λ [22]. Theta series depend on the lattices and also on c [22]. Instead of working directly with Theta series we will, in order to be lattice and displacement independent, consider the L-dimensional *hollow* sphere $\bar{\mathscr{C}}$ obtained as $\bar{\mathscr{C}} = S(c, m) - S(c, m-1)$ and shown in Fig. H.1(a).
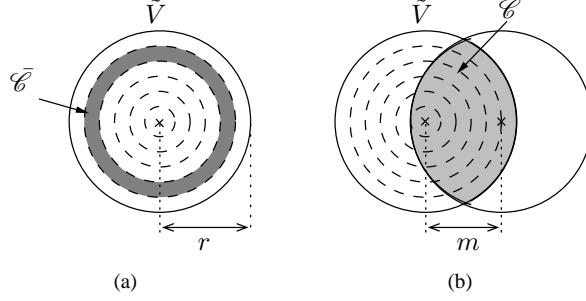
Figure H.1: *The number of lattice points in the shaded region in (a) given by $a_m = \text{Vol}(\bar{\mathscr{C}})/\nu_s$ and in (b) it is given by $b_m = \text{Vol}(\mathscr{C})/\nu_s$.*

The number of lattice points a_m in $\bar{\mathscr{C}}$ is given by $|\bar{\mathscr{C}} \cap \Lambda|$ and asymptotically as $\nu_s \to 0$ (and independent of c)

$$a_m = \text{Vol}(\bar{\mathscr{C}})/\nu_s = \frac{\omega_L}{\nu_s}\left(m^L - (m-1)^L\right). \tag{H.8}$$

The following construction makes sure that we have $\|\lambda_1 - \lambda_2\| \leq r$. For a specific $\lambda_1 \in \tilde{V}(\lambda_0) \cap \Lambda_s$ we center a sphere $\tilde{V}$ at λ_1 and use only λ_2 points from $\tilde{V}(\lambda_0) \cap \tilde{V}(\lambda_1) \cap \Lambda_s$. In Fig. H.1(b) we have shown two overlapping spheres where the first one is centered at some λ_0 and the second one is centered at some $\lambda_1 \in \tilde{V}(\lambda_0)$ which is at distance m from λ_0, i.e. $\|\lambda_0 - \lambda_1\| = m$. Let us by $\mathscr{C}$ denote the convex region obtained as the intersection of the two spheres, i.e. $\mathscr{C} = \tilde{V}(\lambda_0) \cap \tilde{V}(\lambda_1)$. Now let b_m denote the number of lattice points in $\mathscr{C} \cap \Lambda_s$. With this we have, asymptotically as $\nu_s \to 0$, that b_m is given by

$$b_m = \text{Vol}(\mathscr{C})/\nu_s. \tag{H.9}$$

It follows that the number T of distinct 3-tuples which satisfy $\|\lambda_i - \lambda_j\| \leq r$ is given by

$$\lim_{\nu_s \to 0} T = \sum_{m=1}^{r} a_m b_m. \tag{H.10}$$

We now proceed to find a closed-form expression for the volume of $\mathscr{C}$, which eventually will lead to a simple expression for b_m. Let $_2\mathscr{F}_1(\cdot)$ denote the Hypergeometric function defined by [115]

$$_2\mathscr{F}_1(a, b; c; z) = \sum_{k=0}^{\infty} \frac{(a)_k (b)_k}{(c)_k \, k!} z^k, \tag{H.11}$$

where $(\cdot)_k$ is the Pochhammer symbol defined as

$$(a)_k = \begin{cases} 1 & k = 0 \\ a(a+1)\cdots(a+k-1) & k \geq 1. \end{cases} \tag{H.12}$$

Lemma H.2.1. The volume of an L-dimensional (L odd) spherical cap V_{cap} is given by

$$
\begin{aligned}
\text{Vol}(V_{\text{cap}}) = {} & \frac{2\omega_{L-1}}{L+1} r^{(L-1)/2} (2r-m)^{(L+1)/2} \\
& \times {}_2\mathscr{F}_1\left(\frac{L+1}{2}, \frac{1-L}{2}; \frac{L+3}{2}; \frac{2r-m}{4r}\right),
\end{aligned}
\tag{H.13}
$$

Proof. This is a special case of what was proven in [143] and we can therefore use the same technique with only minor modifications. Let $h = m/2$ and let u be a unit vector of $\mathbb{R}^L$. Furthermore, let $H_{h,u}$ be the affine hyperplane $\{z + hu | z \in \mathbb{R}^L, z \cdot u = 0\}$ of $\mathbb{R}^L$ which contains the intersection of two spheres of equal radii r and with centers at distance $m \leq r$ apart, see Fig. H.2.
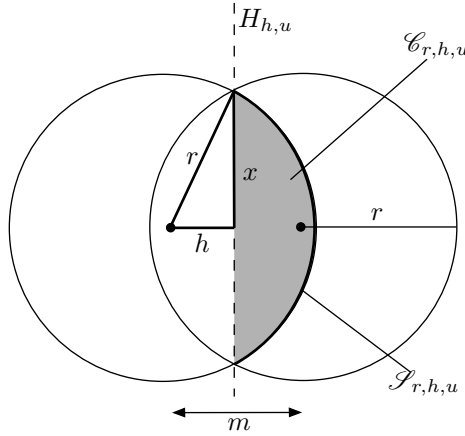
Figure H.2: *Two balls in $\mathbb{R}^2$ of equal radii r and distance m apart.*

We define the spherical cap as

$$
\mathscr{C}_{r,h,u} = \{z \in B(0,r) | z \cdot u \geq h\},
\tag{H.14}
$$

and its surface is described by

$$
\mathscr{S}_{r,h,u} = \{z \in S(0,r) | z \cdot u \geq h\},
\tag{H.15}
$$

where $B(0,r) \in \mathbb{R}^L$ and $S(0,r) \in \mathbb{R}^L$ denote the ball[72] respectively the sphere of radius r and centered at the origin.

---

[72]In this proof we redefine the concept of a sphere to be in line with [143]. As such, the term sphere denotes the surface of a ball, hence, a sphere has no interior. This terminology is only needed in this proof. Elsewhere we define the sphere to be a solid sphere (i.e. a ball and its surface) as is customary in the lattice literature.

The sphere $H_{h,u} \cap \mathscr{S}_{r,h,u}$ has radius $x = \sqrt{r^2 - h^2}$ and it is clear that $h = \sqrt{r^2 - x^2}$. Moreover, any point of $\mathscr{S}_{r,h,u}$ which is at distance[73] t from $H_{h,u}$ is at distance $(x^2 - t^2 - 2th)^{1/2}$ from the real line $\mathbb{R}u$ (i.e. the span of u). Hence, the volume $\mathrm{Vol}(\mathscr{C}_{r,h,u})$ of $\mathscr{C}_{r,h,u}$ is given by

$$
\begin{aligned}
\mathrm{Vol}(\mathscr{C}_{r,h,u}) &= \int_0^{r-h} \omega_{L-1}(x^2 - t^2 - 2th)^{(L-1)/2}\, dt \\
&= \omega_{L-1} \int_0^{r-h} ((r - h - t)(r + h + t))^{(L-1)/2}\, dt \qquad \text{(H.16)} \\
&= \omega_{L-1} \int_0^{\alpha} (\alpha - t)^{\gamma}(t - \beta)^{\gamma}\, dt,
\end{aligned}
$$

where $\alpha = r - h, \beta = -r - h$ and $\gamma = (L-1)/2$. The last integral in (H.16) can be shown to be equal to [69, Eq. 3.196.1]

$$
\int_0^{\alpha} (\alpha - t)^{\gamma}(t - \beta)^{\gamma}\, dt = \frac{\alpha^{\gamma+1}(-\beta)^{\gamma}}{\gamma + 1}\,{}_2\mathscr{F}_1\left(1, -\gamma; \gamma + 2; \frac{\alpha}{\beta}\right), \qquad \text{(H.17)}
$$

which by use of (H.35) can be written as

$$
\begin{aligned}
\frac{\alpha^{\gamma+1}(-\beta)^{\gamma}}{\gamma + 1}\,{}_2\mathscr{F}_1\left(1, -\gamma; \gamma + 2; \frac{\alpha}{\beta}\right) = \\
\left(1 - \frac{\alpha}{\beta}\right)^{\gamma} \frac{\alpha^{\gamma+1}(-\beta)^{\gamma}}{\gamma + 1}\,{}_2\mathscr{F}_1\left(\gamma + 1, -\gamma; \gamma + 2; \frac{\alpha}{\alpha - \beta}\right).
\end{aligned} \qquad \text{(H.18)}
$$

The volume $\mathrm{Vol}(\mathscr{C}_{r,h,u})$ follows by inserting (H.18) in (H.16), that is

$$
\begin{aligned}
\mathrm{Vol}(\mathscr{C}_{r,h,u}) &= \omega_{L-1}\left(1 - \frac{\alpha}{\beta}\right)^{\gamma} \frac{\alpha^{\gamma+1}(-\beta)^{\gamma}}{\gamma + 1}\,{}_2\mathscr{F}_1\left(\gamma + 1, -\gamma; \gamma + 2; \frac{\alpha}{\alpha - \beta}\right) \\
&= \frac{\omega_{L-1}}{L + 1} r^{(L-1)/2}(2r - m)^{(L+1)/2} \\
&\quad \times {}_2\mathscr{F}_1\left(L/2 + 1/2, 1/2 - L/2; L/2 + 3/2; \frac{2r - m}{4r}\right),
\end{aligned}
$$

$$\text{(H.19)}$$

which completes the proof. $\square$

The region $\mathscr{C}$ consists of two equally sized spherical caps. Inserting (H.8)

---

[73]By distance we mean the length of the shortest straight line that can be drawn between $H_{h,u}$ and $\mathscr{S}_{r,h,u}$. It is clear that this line is perpendicular to $H_{h,u}$.

and (H.9) into (H.10) leads to[74] (asymptotically as $\nu_s \to 0$)

$$
\begin{aligned}
T &= \sum_{m=1}^{r} a_m b_m \\
&= \frac{2\omega_L \omega_{L-1}}{\nu_s^2 (L+1)} \sum_{m=1}^{r} (m^L - (m-1)^L) r^{(L-1)/2} \\
&\quad \times (2r-m)^{(L+1)/2} {}_2\mathscr{F}_1\left(\frac{L+1}{2}, \frac{1-L}{2}; \frac{L+3}{2}; \frac{2r-m}{4r}\right) \\
&\stackrel{(a)}{=} \frac{2\omega_L \omega_{L-1}}{\nu_s^2 (L+1)} r^{\frac{L-1}{2}} \sum_{n=0}^{\frac{L+1}{2}} \binom{\frac{L+1}{2}}{n} (2r)^{\frac{L+1}{2}-n} (-1)^n \\
&\quad \times \sum_{k=0}^{\frac{L-1}{2}} \frac{\left(\frac{L+1}{2}\right)_k \left(\frac{1-L}{2}\right)_k}{\left(\frac{L+3}{2}\right)_k k!} \sum_{j=0}^{k} \binom{k}{j} \left(\frac{1}{2}\right)^{k-j} (-1)^j \left(\frac{1}{4r}\right)^j \\
&\quad \times \sum_{m=1}^{r} (m^L - (m-1)^L) m^n m^j \\
&\stackrel{(b)}{=} \frac{2\omega_L \omega_{L-1}}{\nu_s^2 (L+1)} r^{\frac{L-1}{2}} \sum_{n=0}^{\frac{L+1}{2}} \binom{\frac{L+1}{2}}{n} (2r)^{\frac{L+1}{2}-n} (-1)^n \\
&\quad \times \sum_{k=0}^{\frac{L-1}{2}} \frac{\left(\frac{L+1}{2}\right)_k \left(\frac{1-L}{2}\right)_k}{\left(\frac{L+3}{2}\right)_k k!} \sum_{j=0}^{k} \binom{k}{j} \left(\frac{1}{2}\right)^{k-j} (-1)^j \left(\frac{1}{4r}\right)^j \\
&\quad \times \left(L \sum_{m=1}^{r} m^{L-1+n+j} + \mathscr{O}(m^{L-2+n+j})\right). \\
&\stackrel{(c)}{=} \frac{2\omega_L \omega_{L-1}}{\nu_s^2 (L+1)} r^{\frac{L-1}{2}} \sum_{n=0}^{\frac{L+1}{2}} \binom{\frac{L+1}{2}}{n} (2r)^{\frac{L+1}{2}-n} (-1)^n \\
&\quad \times \sum_{k=0}^{\frac{L-1}{2}} \frac{\left(\frac{L+1}{2}\right)_k \left(\frac{1-L}{2}\right)_k}{\left(\frac{L+3}{2}\right)_k k!} \sum_{j=0}^{k} \binom{k}{j} \left(\frac{1}{2}\right)^{k-j} (-1)^j \left(\frac{1}{4r}\right)^j \\
&\quad \times \left(\frac{L}{L+n+j} r^{L+n+j} + \mathscr{O}\left(r^{L-1+n+j}\right)\right),
\end{aligned}
\tag{H.20}
$$

where (a) follows by use of the binomial series expansion [56, p.162], i.e. $(x+y)^k = \sum_{n=0}^{k} \binom{k}{n} x^{k-n} y^n$, which in our case leads to

$$
(2r-m)^{\frac{L+1}{2}} = \sum_{n=0}^{\frac{L+1}{2}} \binom{\frac{L+1}{2}}{n} (2r)^{\frac{L+1}{2}-n} (-1)^n m^n
\tag{H.21}
$$

---

[74] In this asymptotic analysis we assume that all λ_1 points within a given $\mathscr{C}$ is at exact same distance from the center of $\tilde{V}$ (i.e. from λ_0). The error due to this assumption is neglectable, since any constant offset from m will appear inside $\mathscr{O}(\cdot)$.

and

$$\left(\frac{2r-m}{4r}\right)^k = \sum_{j=0}^{k} \binom{k}{j}\left(\frac{1}{2}\right)^{k-j}(-1)^j\left(\frac{m}{4r}\right)^j. \tag{H.22}$$

(b) is obtained by once again applying the binomial series expansion, that is

$$(m-1)^L = m^L - Lm^{L-1} + \mathcal{O}(m^{L-2}), \tag{H.23}$$

and (c) follows from the fact that $\sum_{m=1}^{r} m^L = \frac{1}{L+1}r^{L+1} + \mathcal{O}(r^L)$.

Next we let $r \to \infty$ so that the number of *hollow* spheres inside $\tilde{V}$ goes to infinity.[75] From (H.20) we see that, asymptotically as $\nu_s \to 0$ and $r \to \infty$, we have

$$T = 2\frac{\omega_L\omega_{L-1}}{\nu_s^2}\frac{L}{L+1}\beta_L r^{2L}, \tag{H.25}$$

where β_L is constant for fixed L and given by (H.7).

We are now in a position to find an expression for ψ_L. Let $\bar{\nu}$ be equal to the lower bound (5.26), i.e. $\bar{\nu} = \nu_s\sqrt{N}$ and let $\bar{r}$ be the radius of the sphere having volume $\bar{\nu}$. Then ψ_L is given by the ratio of r and $\bar{r}$, i.e. $\psi_L = r/\bar{r}$, where r is the radius of $\tilde{V}$. Using this in (H.25) leads to

$$r = \left(\frac{T\nu_s(L+1)}{2\omega_L\omega_{L-1}L\beta_L}\right)^{1/2L}. \tag{H.26}$$

Since the radius $\bar{r}$ of an L-dimensional sphere of volume $\bar{\nu}$ is given by

$$\bar{r} = \left(\frac{\bar{\nu}}{\omega_L}\right)^{1/L}, \tag{H.27}$$

we can find ψ_L by dividing (H.26) by (H.27), that is

$$\psi_L = \frac{r}{\bar{r}} = \left(\frac{T\nu_s^2(L+1)}{2\omega_L\omega_{L-1}L\beta_L}\right)^{1/2L}\left(\frac{\bar{\nu}}{\omega_L}\right)^{-1/L}. \tag{H.28}$$

Since we need to obtain N 3-tuples we let $T = N$ so that with $\bar{\nu} = \sqrt{N}\nu_s$ we can rewrite (H.28) as

$$\psi_L = \left(\frac{\omega_L}{\omega_{L-1}}\right)^{1/2L}\left(\frac{L+1}{2L}\right)^{1/2L}\beta_L^{-1/2L}. \tag{H.29}$$

This completes the proof. $\square$

---

[75]We would like to emphasize that this is equivalent to keeping r fixed, say $r = 1$, and then let the number of *hollow* spheres inside $\tilde{V}$ go to infinity. To see this let $M \to \infty$ and then rewrite (H.8) as

$$a_{m/M} = \text{Vol}(\bar{\mathscr{C}})/\nu_s = \frac{\omega_L}{\nu_s}\left(\left(\frac{m}{M}\right)^L - \left(\frac{m-1}{M}\right)^L\right), \quad 1 \le m \le M. \tag{H.24}$$

A similar change applies to (H.9). Hence, the asymptotic expression for T is also valid within a localized region of $\mathbb{R}^L$ which is a useful property we exploit when proving Proposition 5.4.1.

H.3   Proof of Theorem 5.3.3

Lemma H.3.1. For $L \to \infty$ we have

$$\left(\frac{\omega_L}{\omega_{L-1}}\right)^{1/2L} = 1. \tag{H.30}$$

Proof. The volume ω_L of an L-dimensional unit hypersphere is given by $\omega_L = \pi^{L/2}/(L/2)!$ so we have that

$$
\begin{aligned}
\lim_{L \to \infty} & \left(\frac{\pi^{L/2}}{(L/2)!} \frac{(L/2 - 1/2)!}{\pi^{L/2 - 1/2}}\right)^{1/2L} \\
&= \lim_{L \to \infty} \pi^{1/4L} \left(\mathcal{O}(L^{-1})\right)^{1/2L} \\
&= 1. \qquad \qquad \square
\end{aligned}
\tag{H.31}
$$

Lemma H.3.2. For $L \to \infty$ we have

$$\frac{1}{\beta_L^{1/2L}} = \left(\frac{4}{3}\right)^{1/4}. \tag{H.32}$$

Proof. The inner sum in (5.28) may be well approximated by using that $\frac{1}{L+c} \approx \frac{1}{L}$ for $L \gg c$, which leads to

$$
\begin{aligned}
\sum_{j=0}^{k} & \binom{k}{j} \left(\frac{1}{2}\right)^{k-j} (-1)^j \left(\frac{1}{4}\right)^j \frac{1}{L+n+j} \\
&\approx \sum_{j=0}^{k} \binom{k}{j} \left(\frac{1}{2}\right)^{k-j} (-1)^j \left(\frac{1}{4}\right)^j \frac{1}{L} \\
&= \frac{1}{L} \left(\frac{1}{4}\right)^k.
\end{aligned}
\tag{H.33}
$$

We also have that

$$
\begin{aligned}
\sum_{k=0}^{\frac{L-1}{2}} & \frac{\left(\frac{L+1}{2}\right)_k \left(\frac{1-L}{2}\right)_k}{\left(\frac{L+3}{2}\right)_k k!} \left(\frac{1}{4}\right)^k = {}_2\mathscr{F}_1 \left(\frac{L+1}{2}, \frac{1-L}{2}; \frac{L+3}{2}; \frac{1}{4}\right) \\
& \overset{(a)}{=} (1 - 1/4)^{(-1+L)/2} {}_2\mathscr{F}_1 \left(1, \frac{1-L}{2}; \frac{L+3}{2}; -\frac{1}{3}\right) \\
& = (3/4)^{(-1+L)/2} \sum_{k=0}^{L/2-1/2} \frac{k!\,(1/2 - L/2)_k}{k!\,(3/2 + L/2)_k} (-1/3)^k \\
& = (3/4)^{(-1+L)/2} \\
& \quad \times \sum_{k=0}^{L/2-1/2} \left(\frac{(-L/2)^k}{(L/2)^k + \mathcal{O}(L^{k-1})} + \mathcal{O}(L^{-1})\right) (-1/3)^k
\end{aligned}
$$

$$\approx (3/4)^{(-1+L)/2} \sum_{k=0}^{L/2-1/2} (1/3)^k, \tag{H.34}$$

where (a) follows from the following hypergeometric transformation [115]

$$_2\mathscr{F}_1\left(a,b;c;z\right) = (1-z)^{-b}{}_2\mathscr{F}_1\left(c-a,b;c;\xi\right), \tag{H.35}$$

where $\xi = \frac{z}{z-1}$. Finally, it is true that

$$\sum_{n=0}^{L/2+1/2} \binom{L/2+1/2}{n} 2^{L/2+1/2-n}(-1)^n = 1. \tag{H.36}$$

Inserting (H.33), (H.34) and (H.36) into (H.7) leads to

$$\beta_L \approx (3/4)^{(-1+L)/2}\frac{1}{L} \sum_{k=0}^{L/2-1/2} (1/3)^k, \tag{H.37}$$

where since $\sum_{k=0}^{\infty}(1/3)^k = 3/2$, we get

$$\begin{aligned}
\lim_{L\to\infty} \frac{1}{\beta_L^{1/2L}} &= \lim_{L\to\infty} (4/3)^{1/4}(4/3)^{-1/4L}L^{1/2L}(2/3)^{1/2L} \\
&= (4/3)^{1/4},
\end{aligned} \tag{H.38}$$

which proves the Lemma. $\qquad\square$

We are now in a position to prove the following theorem.

Theorem 5.3.3. *For $K = 3$ and $L \to \infty$ the dimensionless expansion factor ψ_L is given by*

$$\psi_\infty = \left(\frac{4}{3}\right)^{1/4}. \tag{H.39}$$

Proof. The proof follows trivially by use of Lemma H.3.1 and Lemma H.3.2 in (H.29).
$\qquad\square$

H.4   Proof of Proposition 5.4.1

Let $T_i = \{\lambda_i : \lambda_i = \alpha_i(\lambda_c),\ \lambda_c \in V_\pi(0)\}$, i.e. the set of N^2 sublattice points $\lambda_i \in \Lambda_s$ associated with the N^2 central lattice points within $V_\pi(0)$. Furthermore, let $T_i' \subseteq T_i$ be the set of unique elements of T_i, where $|T_i'| \approx N$. Finally, let

$$T_j(\lambda_i) = \{\lambda_j : \lambda_j = \alpha_j(\lambda_c) \text{ and } \lambda_i = \alpha_i(\lambda_c),\ \lambda_c \in V_\pi(0)\}, \tag{H.40}$$

and let $T_j'(\lambda_i) \subseteq T_j(\lambda_i)$ be the set of unique elements. That is, $T_j(\lambda_i)$ contains all the elements $\lambda_j \in \Lambda_s$ which are in the K-tuples that also contains a specific λ_i. We will

also make use of the notation $\#_{\lambda_j}$ to indicate the number of occurrences of a specific λ_j in $T_j(\lambda_i)$.

For the pair (i, j) we have

$$\sum_{\lambda_c \in V_\pi(0)} \|\alpha_i(\lambda_c) - \alpha_j(\lambda_c)\|^2 = \sum_{\lambda_i \in T_i'} \sum_{\lambda_j \in T_j(\lambda_i)} \|\lambda_i - \lambda_j\|^2.$$

Given $\lambda_i \in T_i'$, we have

$$
\begin{aligned}
\sum_{\lambda_j \in T_j(\lambda_i)} \|\lambda_i - \lambda_j\|^2 \nu_s &= \sum_{\lambda_j \in T_j'(\lambda_i)} \#_{\lambda_j} \|\lambda_i - \lambda_j\|^2 \nu_s \\
&\stackrel{(a)}{\approx} \frac{N}{\tilde{N}} \sum_{\lambda_j \in T_j'(\lambda_i)} \|\lambda_i - \lambda_j\|^2 \nu_s \\
&\approx \frac{N}{\tilde{N}} \int_{\tilde{V}(\lambda_i)} \|\lambda_i - x\|^2 \, dx \\
&\approx \frac{N}{\tilde{N}} \tilde{\nu}^{1+2/L} L G(S_L) \\
&\stackrel{(b)}{=} N \nu_s \tilde{\nu}^{2/L} L G(S_L),
\end{aligned}
\tag{H.41}
$$

where (a) follows by assuming (see the discussion below for the case of $K = 3$) that $\#_{\lambda_j} = N/\tilde{N}$ for all $\lambda_j \in T_j(\lambda_i)$ and (b) follows since $\tilde{\nu} = \tilde{N} \nu_s$. Hence, with $\tilde{\nu} = \tilde{N} \nu_s = \psi N^{1/(K-1)} \nu_s$ and $\nu_s = N\nu$, we have

$$
\begin{aligned}
\frac{1}{L} \sum_{\lambda_j \in T_j(\lambda_i)} \|\lambda_i - \lambda_j\|^2 \nu_s &\approx N \nu_s \psi_L^2 \nu^{2/L} N^{2/L} N^{2/L(K-1)} G(S_L) \\
&= \nu_s \psi_L^2 N^{1+2K/L(K-1)} \nu^{2/L} G(S_L),
\end{aligned}
$$

which is independent of λ_i, so that

$$
\begin{aligned}
\frac{1}{L} \sum_{\lambda_i \in T_i'} \sum_{\lambda_j \in T_j(\lambda_i)} \|\lambda_i - \lambda_j\|^2 &\approx \frac{N}{L} \sum_{\lambda_j \in T_j(\lambda_i)} \|\lambda_i - \lambda_j\|^2 \\
&\approx \psi_L^2 N^{2+2K/L(K-1)} \nu^{2/L} G(S_L).
\end{aligned}
$$

In (H.41) we used the approximation $\#_{\lambda_j} \approx N/\tilde{N}$ without any explanation. For the case of $K = 2$ and as $N \to \infty$ we have that $T_i' = T_i$ and $N = \tilde{N}$, hence the approximation becomes exact, i.e. $\#_{\lambda_j} = 1$. This proves the Proposition for $K = 2$. We will now consider the case of $K = 3$ and show that asymptotically, as $L \to \infty$, the following approximation becomes exact.

$$\frac{1}{L} \sum_{\lambda_j \in T_j(\lambda_i)} \|\lambda_i - \lambda_j\|^2 \approx N \tilde{\nu}^{2/L} G(S_L). \tag{H.42}$$

To prove this we use the same procedure as when deriving closed-form expressions for ψ_L leads to the following asymptotic expression

$$\sum_{\lambda_j \in T_j(\lambda_i)} \|\lambda_i - \lambda_j\|^2 = \sum_{m=1}^{r} a_m b_m m^2, \tag{H.43}$$

where we without loss of generality assumed that $\lambda_i = 0$ and used the fact that we can replace $\|\lambda_j\|^2$ by m^2 for the λ_j points which are at distance m from $\lambda_i = 0$. It follows that we have

$$\frac{1}{L} \sum_{\lambda_j \in T_j(\lambda_i)} \|\lambda_i - \lambda_j\|^2 = 2\frac{\omega_L \omega_{L-1}}{\nu_s^2} \frac{1}{L+1} \beta'_L r^{2L+2}, \tag{H.44}$$

where

$$\beta'_L = \sum_{n=0}^{\frac{L+1}{2}} \binom{\frac{L+1}{2}}{n} 2^{\frac{L+1}{2}-n} (-1)^n \sum_{k=0}^{\frac{L-1}{2}} \frac{\left(\frac{L+1}{2}\right)_k \left(\frac{1-L}{2}\right)_k}{\left(\frac{L+3}{2}\right)_k k!}$$
$$\times \sum_{j=0}^{k} \binom{k}{j} \left(\frac{1}{2}\right)^{k-j} (-1)^j \left(\frac{1}{4}\right)^j \frac{1}{L+n+j+2}. \tag{H.45}$$

Since $\tilde{\nu} = \omega_L r^L = \psi_L^L \sqrt{N} \nu_s$ we can rewrite (H.44) as

$$\sum_{\lambda_j \in T_j(\lambda_i)} \|\lambda_i - \lambda_j\|^2 = 2\frac{\omega_L \omega_{L-1}}{\nu_s^2} \frac{1}{L+1} \beta'_L \tilde{\nu}^{2+2/L} \frac{1}{\omega_L^{2+2/L}}$$
$$= 2\frac{\omega_{L-1}}{\omega_L^{1+2/L}} \frac{1}{L+1} \beta'_L \tilde{\nu}^{2/L} \psi_L^{2L} N$$
$$\stackrel{(a)}{=} 2\frac{\omega_{L-1}}{\omega_L^{1+2/L}} \frac{1}{L+1} \beta'_L \tilde{\nu}^{2/L} N \left(\frac{\omega_L}{\omega_{L-1}}\right) \left(\frac{L+1}{2L}\right) \frac{1}{\beta_L}$$
$$= \frac{1}{\omega_L^{2/L}} \frac{1}{L} \tilde{\nu}^{2/L} N \frac{\beta'_L}{\beta_L}, \tag{H.46}$$

where (a) follows by inserting (H.29). Dividing (H.46) by (H.42) leads to

$$\frac{1}{\omega_L^{2/L}} \frac{1}{L} \frac{1}{G(S_L)} \frac{\beta'_L}{\beta_L} = \frac{L+2}{L} \frac{\beta'_L}{\beta_L}. \tag{H.47}$$

Hence, asymptotically as $L \to \infty$ we have that

$$\lim_{L \to \infty} \frac{L+2}{L} \frac{\beta'_L}{\beta_L} = 1, \tag{H.48}$$

which proves the Proposition.

Remark H.4.1. Proposition 5.4.1 considered the asymptotic case of $L \to \infty$. Exact distortion expressions for the case of $K = 3$ and finite L follow by replacing (H.41) with (H.43).

Remark H.4.2. For $K > 3$ it is very likely that similar equations can be found for ψ_L which can then be used to verify the goodness of the approximations for any K. Moreover, in Appendix H.5 we show that the rate of growth of (H.41) is unaffected if we replace $\#_{\lambda_j}$ by either $\min_{\lambda_j}\{\#_{\lambda_j}\}$ or $\max_{\lambda_j}\{\#_{\lambda_j}\}$ which means that the error by using the approximation $N/\tilde{N}$ instead of the true $\#_{\lambda_j}$ is constant (i.e. it does not depend on N) for fixed K and L. It remains to be shown whether this error term tends to zero as $L \rightarrow \infty$ for $K > 3$. However, based on the discussion above we conjecture that Proposition 5.4.1 is true for any K asymptotically as $N, L \rightarrow \infty$ and $\nu_s \rightarrow 0$. In other words, the side distortion of a K-channel MD-LVQ system can be expressed through the normalized second moment of a sphere as the dimension goes to infinity.

H.5   Proof of Proposition 5.4.2

Before proving Proposition 5.4.2 we need to lower and upper bound $\#_{\lambda_j}$ (see Appendix H.4 for an introduction to this notation). As previously mentioned the λ_j points which are close (in Euclidean sense) to λ_i occur more frequently than λ_j points farther away. To see this observe that the construction of K-tuples can be seen as an iterative procedure that first picks a $\lambda_0 \in \Lambda_s \cap V_\pi(0)$ and then any $\lambda_1 \in \Lambda_s$ is picked such that $\|\lambda_0 - \lambda_1\| \leq r$, hence $\lambda_1 \in \Lambda_s \cap \tilde{V}(\lambda_0)$. The set of λ_{K-1} points that can be picked for a particular $(K-1)$-tuple e.g. $(\lambda_0, \ldots, \lambda_{K-2})$ is then given by $\{\lambda_{K-1} : \lambda_{K-1} \in \Lambda_s \cap \tilde{V}(\lambda_{K-2}) \cap \cdots \cap \tilde{V}(\lambda_0)\}$. It is clear that $\|\lambda_i - \lambda_j\| \leq r$ where $(\lambda_i, \lambda_j) = (\alpha_i(\lambda_c), \alpha_j(\lambda_c)), \forall \lambda_c \in \Lambda_c$ and any $i, j \in \{0, \ldots, K-1\}$.

Let $T_{\min}(\lambda_i, \lambda_j)$ denote the minimum number of times the pair (λ_i, λ_j) is used. The minimum $T_{\min}$ of $T_{\min}(\lambda_i, \lambda_j)$ over all pairs (λ_i, λ_j) lower bounds $N/\tilde{N}$. We will now show that $T_{\min}$ is always bounded away from zero. To see this notice that the minimum overlap between two spheres of radius r centered at λ_0 and λ_1, respectively, is obtained when λ_0 and λ_1 are are maximally separated, i.e. when $\|\lambda_0 - \lambda_1\| = r$. This is shown by the shaded area in Fig. H.3 for $L = 2$. For three spheres the minimum overlap is again obtained when all pairwise distances are maximized, i.e. when $\|\lambda_i - \lambda_j\| = r$ for $i, j \in \{0, 1, 2\}$ and $i \neq j$. It is clear that the volume of the intersection of three spheres is less than that of two spheres, hence the minimum number of λ_2 points is greater than the minimum number of λ_3 points. However, by construction it follows that when centering K spheres at the set of points $s = \{\lambda_0, \ldots, \lambda_{K-1}\} = \{\alpha_0(\lambda_c), \ldots, \alpha_{K-1}(\lambda_c)\}$ each of the points in s will be in the intersection $\cap_s$ of the K spheres. Since the intersection of an arbitrary collection of convex sets leads to a convex set [117], the convex hull $\mathscr{C}(s)$ of s will also be in $\cap_s$. Furthermore, for the example in Fig. H.3, it can be seen that $\mathscr{C}(s)$ (indicated by the equilateral triangle) will not get smaller for $K \geq 3$ and this is true in general since points are never removed from s as K grows. For $L = 3$ the regular tetrahedron [25] consisting of four points with a pairwise distance of r describes a regular convex polytope which lies in $\cap_s$. In general the regular L-simplex [25] lies in $\cap_s$ and the
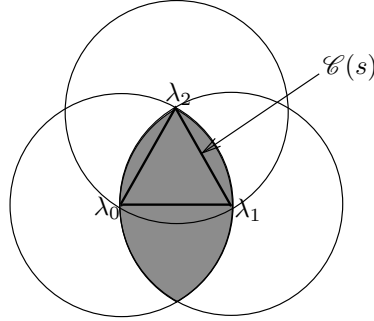
Figure H.3: *Three spheres of equal radius are here centered at the set of points* $s = \{\lambda_0, \lambda_1, \lambda_2\}$. *The shaded area describes the intersection of two spheres. The equilateral triangle describes the convex hull* $\mathscr{C}(s)$ *of s.*

volume $\text{Vol}(L)$ of a regular L-simplex with side length r is given by [13]

$$\text{Vol}(L) = \frac{r^L}{L!} \sqrt{\frac{L+1}{2^L}} = c_L r^L, \tag{H.49}$$

where c_L depends only on L. It follows that the minimum number of K-tuples that contains a specific (λ_i, λ_j) pair is lower bounded by $\text{Vol}(L)^{K-2}/\nu_s^{K-2}$. Since the volume $\tilde{\nu}$ of $\tilde{V}$ is given by $\tilde{\nu} = \omega_L r^L$ we get

$$\left(\frac{\text{Vol}(L)}{\nu_s} \right)^{K-2} = \left(\frac{c_L}{\omega_L} \right)^{K-2} \left(\frac{\tilde{\nu}}{\nu_s} \right)^{K-2}. \tag{H.50}$$

Also, by construction we have that $N \leq (\tilde{\nu}/\nu_s)^{K-1}$ and that $\tilde{N} = \tilde{\nu}/\nu_s$ so an upper bound on $N/\tilde{N}$ is given by

$$\frac{N}{\tilde{N}} \leq \left(\frac{\tilde{\nu}}{\nu_s} \right)^{K-2}, \tag{H.51}$$

which differs from the lower bound in (H.50) by a multiplicative constant.

   We are now in a position to prove Proposition 5.4.2.

Proposition 5.4.2 For $N \to \infty$ and $2 \leq K < \infty$ we have

$$\frac{\sum_{\lambda_c \in V_\pi(0)} \left\| \lambda_c - \frac{1}{K} \sum_{i=0}^{K-1} \lambda_i \right\|^2}{\sum_{\lambda_c \in V_\pi(0)} \sum_{i=0}^{K-2} \sum_{j=i+1}^{K-1} \| \lambda_i - \lambda_j \|^2} \to 0. \tag{H.52}$$

Proof. The numerator describes the distance from a central lattice point to the mean vector of its associated K-tuple. This distance is upper bounded by the covering radius of the sublattice Λ_s. The rate of growth of the covering radius is proportional

to $\nu_s^{1/L} = (N\nu)^{1/L}$, hence

$$\sum_{\lambda_c \in V_\pi(0)} \left\| \lambda_c - \frac{1}{K} \sum_{i=0}^{K-1} \lambda_i \right\|^2 = \mathscr{O}\left(N^2 N^{2/L} \nu^{2/L}\right). \tag{H.53}$$

Since the approximation $N/\tilde{N}$ used in Proposition 5.4.1 is sandwiched between the lower and upper bounds (i.e. Eqs. (H.50) and (H.51)) we can write

$$\begin{aligned}
&\sum_{\lambda_c \in V_\pi(0)} \sum_{i=0}^{K-2} \sum_{j=i+1}^{K-1} \|\alpha_i(\lambda_c) - \alpha_j(\lambda_c)\|^2 \\
&= \sum_{i=0}^{K-2} \sum_{j=i+1}^{K-1} \sum_{\lambda_c \in V_\pi(0)} \|\alpha_i(\lambda_c) - \alpha_j(\lambda_c)\|^2 \\
&\approx \frac{L}{2} K(K-1) G(S_L) \psi_L^2 N^2 N^{2K/L(K-1)} \nu^{2/L},
\end{aligned} \tag{H.54}$$

so that, since $\lambda_i = \alpha_i(\lambda_c)$,

$$\sum_{\lambda_c \in V_\pi(0)} \sum_{i=0}^{K-2} \sum_{j=i+1}^{K-1} \|\lambda_i - \lambda_j\|^2 = \mathscr{O}\left(N^2 N^{2K/L(K-1)} \nu^{2/L}\right). \tag{H.55}$$

Comparing (H.53) to (H.55) we see that (H.52) grows as $\mathscr{O}\left(N^{-K/(K-1)}\right) \to 0$ for $N \to \infty$ and $K < \infty$. $\qquad\square$

Proofs for Chapter 6

For notational convenience we will in this appendix use the shorter notations $\mathscr{L}, \mathscr{L}_i$ and $\mathscr{L}_{i,j}$ instead of $\mathscr{L}^{(K,\kappa)}, \mathscr{L}_i^{(K,\kappa)}$ and $\mathscr{L}_{i,j}^{(K,\kappa)}$.

I.1 Proof of Theorem 6.2.1

To prove Theorem 6.2.1 we need the following results.

Lemma I.1.1. For $1 \le \kappa \le K$ and any $i \in \{0, \dots, K-1\}$ we have

$$\sum_{\substack{j=0 \\ j \ne i}}^{K-1} p(\mathscr{L}_j) = \kappa p(\mathscr{L}) - p(\mathscr{L}_i).$$

Proof. Since $|\mathscr{L}_j| = \binom{K-1}{\kappa-1}$ the sum $\sum_{j=0}^{K-1} p(\mathscr{L}_j)$ contains $K\binom{K-1}{\kappa-1}$ terms. However, the number of distinct terms is $|\mathscr{L}| = \binom{K}{\kappa}$ and each individual term occurs κ times in the sum, since

$$\frac{K\binom{K-1}{\kappa-1}}{\binom{K}{\kappa}} = \kappa.$$

Subtracting the terms for $j = i$ proves the lemma. $\qquad\square$

Lemma I.1.2. For $1 \le \kappa \le K$ and any $i, j \in \{0, \dots, K-1\}$ we have

$$\sum_{j=0}^{K-1} p(\mathscr{L}_{i,j}) = \kappa p(\mathscr{L}_i).$$

197

Proof. It is true that $\mathscr{L}_{i,i} = \mathscr{L}_i$ and since $|\mathscr{L}_i| = \binom{K-1}{\kappa-1}$ and $|\mathscr{L}_{i,j}| = \binom{K-2}{\kappa-2}$ the sum $\sum_{j=0}^{K-1} p(\mathscr{L}_{i,j})$ contains $(K-1)\binom{K-2}{\kappa-2} + \binom{K-1}{\kappa-1}$ terms. However, the number of distinct $l \in \mathscr{L}_i$ terms is $|\mathscr{L}_i| = \binom{K-1}{\kappa-1}$ and each term occurs κ times in the sum, since

$$\frac{(K-1)\binom{K-2}{\kappa-2} + \binom{K-1}{\kappa-1}}{\binom{K-1}{\kappa-1}} = \kappa.$$

$\square$

Lemma I.1.3. For $1 \le \kappa \le K$ we have

$$\sum_{l \in \mathscr{L}} p(\mathscr{L}) \left\langle \lambda_c, \frac{1}{\kappa} \sum_{i \in l} \lambda_i \right\rangle = \left\langle \lambda_c, \frac{1}{\kappa} \sum_{i=0}^{K-1} \lambda_i p(\mathscr{L}_i) \right\rangle.$$

Proof. We have that

$$\sum_{l \in \mathscr{L}} p(\mathscr{L}) \left\langle \lambda_c, \frac{1}{\kappa} \sum_{i \in l} \lambda_i \right\rangle = \left\langle \lambda_c, \frac{1}{\kappa} \sum_{l \in \mathscr{L}} p(l) \sum_{i \in l} \lambda_i \right\rangle$$

$$= \left\langle \lambda_c, \frac{1}{\kappa} \sum_{i=0}^{K-1} \lambda_i p(\mathscr{L}_i) \right\rangle,$$

where the last equality follows since $\mathscr{L}_i$ denotes the set of all l-terms that contains the index i. $\square$

Lemma I.1.4. For $1 \le \kappa \le K$ we have

$$\sum_{i=0}^{K-2} \sum_{j=i+1}^{K-1} p(\mathscr{L}_i)p(\mathscr{L}_j)\|\lambda_i - \lambda_j\|^2 = \sum_{i=0}^{K-1} p(\mathscr{L}_i)\left(\kappa p(\mathscr{L}) - p(\mathscr{L}_i)\right)\|\lambda_i\|^2$$

$$- 2\sum_{i=0}^{K-2} \sum_{j=i+1}^{K-1} p(\mathscr{L}_i)p(\mathscr{L}_j)\langle\lambda_i, \lambda_j\rangle.$$

Proof. We have that

$$\sum_{i=0}^{K-2} \sum_{j=i+1}^{K-1} p(\mathscr{L}_i)p(\mathscr{L}_j)\|\lambda_i - \lambda_j\|^2 = \sum_{i=0}^{K-2} \sum_{j=i+1}^{K-1} p(\mathscr{L}_i)p(\mathscr{L}_j)(\|\lambda_i\|^2 + \|\lambda_j\|^2)$$

$$- 2\sum_{i=0}^{K-2} \sum_{j=i+1}^{K-1} p(\mathscr{L}_i)p(\mathscr{L}_j)\langle\lambda_i, \lambda_j\rangle.$$

Furthermore, it follows that

$$\sum_{i=0}^{K-2} \sum_{j=i+1}^{K-1} p(\mathscr{L}_i)p(\mathscr{L}_j)(\|\lambda_i\|^2 + \|\lambda_j\|^2)$$

$$
= \sum_{i=0}^{K-2} p(\mathscr{L}_i)\|\lambda_i\|^2 \sum_{j=i+1}^{K-1} p(\mathscr{L}_j) + \sum_{j=1}^{K-1} p(\mathscr{L}_j)\|\lambda_j\|^2 \sum_{i=0}^{j-1} p(\mathscr{L}_i)
$$

$$
= \sum_{i=0}^{K-1} p(\mathscr{L}_i)\|\lambda_i\|^2 \underbrace{\sum_{j=i+1}^{K-1} p(\mathscr{L}_j)}_{0 \text{ for } i=K-1} + \sum_{j=0}^{K-1} p(\mathscr{L}_j)\|\lambda_j\|^2 \underbrace{\sum_{i=0}^{j-1} p(\mathscr{L}_i)}_{0 \text{ for } j=0}
$$

$$
= \sum_{i=0}^{K-1} p(\mathscr{L}_i)\|\lambda_i\|^2 \left(\sum_{j=0}^{i-1} p(\mathscr{L}_j) + \sum_{j=i+1}^{K-1} p(\mathscr{L}_j) \right)
$$

$$
= \sum_{i=0}^{K-1} p(\mathscr{L}_i)\|\lambda_i\|^2 \sum_{\substack{j=0 \\ j\neq i}}^{K-1} p(\mathscr{L}_j)
$$

$$
= \sum_{i=0}^{K-1} p(\mathscr{L}_i)\|\lambda_i\|^2 \left(\kappa p(\mathscr{L}) - p(\mathscr{L}_i) \right),
$$

where the last equality follows by use of Lemma I.1.1. $\qquad\square$

Lemma I.1.5. For $1 \leq \kappa \leq K$ we have

$$
\sum_{i=0}^{K-2} \sum_{j=i+1}^{K-1} p(\mathscr{L}_{i,j})\|\lambda_i - \lambda_j\|^2 = (\kappa - 1) \sum_{i=0}^{K-1} p(\mathscr{L}_i)\|\lambda_i\|^2
$$

$$
- 2 \sum_{i=0}^{K-2} \sum_{j=i+1}^{K-1} p(\mathscr{L}_{i,j})\langle \lambda_i, \lambda_j \rangle.
$$

Proof. We have that

$$
\sum_{i=0}^{K-2} \sum_{j=i+1}^{K-1} p(\mathscr{L}_{i,j})\|\lambda_i - \lambda_j\|^2 = \sum_{i=0}^{K-2} \sum_{j=i+1}^{K-1} p(\mathscr{L}_{i,j})(\|\lambda_i\|^2
$$

$$
+ \|\lambda_j\|^2) - 2 \sum_{i=0}^{K-2} \sum_{j=i+1}^{K-1} p(\mathscr{L}_{i,j})\langle \lambda_i, \lambda_j \rangle.
$$

Furthermore, it follows that

$$
\sum_{i=0}^{K-2} \sum_{j=i+1}^{K-1} p(\mathscr{L}_{i,j})(\|\lambda_i\|^2 + \|\lambda_j\|^2)
$$

$$
= \sum_{i=0}^{K-2} \sum_{j=i+1}^{K-1} p(\mathscr{L}_{i,j})\|\lambda_i\|^2 + \sum_{i=0}^{K-2} \sum_{j=i+1}^{K-1} p(\mathscr{L}_{i,j})\|\lambda_j\|^2
$$

$$
= \sum_{i=0}^{K-2} \|\lambda_i\|^2 \sum_{j=i+1}^{K-1} p(\mathscr{L}_{i,j}) + \sum_{j=1}^{K-1} \sum_{i=0}^{j-1} p(\mathscr{L}_{i,j})\|\lambda_j\|^2
$$

$$
= \sum_{i=0}^{K-1} \|\lambda_i\|^2 \underbrace{\sum_{j=i+1}^{K-1} p(\mathscr{L}_{i,j})}_{0 \text{ for } i=K-1} + \sum_{j=0}^{K-1} \|\lambda_j\|^2 \underbrace{\sum_{i=0}^{j-1} p(\mathscr{L}_{i,j})}_{0 \text{ for } j=0}
$$

$$
= \sum_{i=0}^{K-1} \|\lambda_i\|^2 \left(\sum_{j=0}^{i-1} p(\mathscr{L}_{i,j}) + \sum_{j=i+1}^{K-1} p(\mathscr{L}_{i,j}) \right)
$$

$$
= \sum_{i=0}^{K-1} \|\lambda_i\|^2 \left(\sum_{j=0}^{K-1} p(\mathscr{L}_{i,j}) - p(\mathscr{L}_i) \right)
$$

$$
\stackrel{(a)}{=} \sum_{i=0}^{K-1} \|\lambda_i\|^2 \left(\kappa p(\mathscr{L}_i) - p(\mathscr{L}_i) \right)
$$

$$
= (\kappa - 1) \sum_{i=0}^{K-1} \|\lambda_i\|^2 p(\mathscr{L}_i),
$$

where (a) follows by use of Lemma I.1.2. $\qquad\square$

Lemma I.1.6. For $1 \le \kappa \le K$ we have

$$
\sum_{l \in \mathscr{L}} p(l) \left\| \sum_{i \in l} \lambda_i \right\|^2 = \kappa \sum_{i=0}^{K-1} p(\mathscr{L}_i) \|\lambda_i\|^2 - \sum_{i=0}^{K-2} \sum_{j=i+1}^{K-1} p(\mathscr{L}_{i,j}) \|\lambda_i - \lambda_j\|^2.
$$

Proof. The set of all elements l of $\mathscr{L}$ that contains the index i is denoted by $\mathscr{L}_i$. Similarly the set of all elements that contains the indices i and j is denoted by $\mathscr{L}_{i,j}$. From this we see that

$$
\sum_{l \in \mathscr{L}} p(l) \left\| \sum_{i \in l} \lambda_i \right\|^2 = \sum_{l \in \mathscr{L}} p(l) \left(\sum_{i \in l} \|\lambda_i\|^2 + 2 \sum_{i=0}^{\kappa-2} \sum_{j=i+1}^{\kappa-1} \langle \lambda_{l_i}, \lambda_{l_j} \rangle \right)
$$

$$
= \sum_{i=0}^{K-1} p(\mathscr{L}_i) \|\lambda_i\|^2 + 2 \sum_{i=0}^{K-2} \sum_{j=i+1}^{K-1} p(\mathscr{L}_{i,j}) \langle \lambda_i, \lambda_j \rangle.
$$

By use of Lemma I.1.5 it follows that

$$
\sum_{l \in \mathscr{L}} p(l) \left\| \sum_{i \in l} \lambda_i \right\|^2 = \sum_{i=0}^{K-1} p(\mathscr{L}_i) \|\lambda_i\|^2 + (\kappa - 1) \sum_{i=0}^{K-1} p(\mathscr{L}_i) \|\lambda_i\|^2
$$

$$
- \sum_{i=0}^{K-2} \sum_{j=i+1}^{K-1} p(\mathscr{L}_{i,j}) \|\lambda_i - \lambda_j\|^2
$$

$$
= \kappa \sum_{i=0}^{K-1} p(\mathscr{L}_i) \|\lambda_i\|^2 - \sum_{i=0}^{K-2} \sum_{j=i+1}^{K-1} p(\mathscr{L}_{i,j}) \|\lambda_i - \lambda_j\|^2
$$

$\qquad\square$

We are now in a position to prove the following result.

Proposition I.1.1. For $1 \leq \kappa \leq K$ we have

$$
\sum_{l \in \mathscr{L}} p(l) \left\| \lambda_c - \frac{1}{\kappa} \sum_{i \in l} \lambda_i \right\|^2 = p(\mathscr{L}) \left\| \lambda_c - \frac{1}{\kappa p(\mathscr{L})} \sum_{i=0}^{K-1} p(\mathscr{L}_i) \lambda_i \right\|^2
$$
$$
+ \frac{1}{\kappa^2} \sum_{i=0}^{K-2} \sum_{j=i+1}^{K-1} \left(\frac{p(\mathscr{L}_i) p(\mathscr{L}_j)}{p(\mathscr{L})} - p(\mathscr{L}_{i,j}) \right) \| \lambda_i - \lambda_j \|^2.
$$

$$(\text{I.1})$$

Proof. Expansion of the norm on the left-hand-side in (I.1) leads to

$$
\sum_{l \in \mathscr{L}} p(l) \left\| \lambda_c - \frac{1}{\kappa} \sum_{i \in l} \lambda_i \right\|^2 = \sum_{l \in \mathscr{L}} p(l) \left(\| \lambda_c \|^2 - 2 \left\langle \lambda_c, \frac{1}{\kappa} \sum_{i \in l} \lambda_i \right\rangle + \frac{1}{\kappa^2} \left\| \sum_{i \in l} \lambda_i \right\|^2 \right)
$$

$$
\overset{(a)}{=} p(\mathscr{L}) \| \lambda_c \|^2 - 2 \left\langle \lambda_c, \frac{1}{\kappa} \sum_{i=0}^{K-1} p(\mathscr{L}_i) \lambda_i \right\rangle + \frac{1}{\kappa^2} \sum_{l \in \mathscr{L}} p(l) \left\| \sum_{i \in l} \lambda_i \right\|^2
$$

$$
= p(\mathscr{L}) \left\| \lambda_c - \frac{1}{\kappa p(\mathscr{L})} \sum_{i=0}^{K-1} p(\mathscr{L}_i) \lambda_i \right\|^2 - \frac{1}{\kappa^2 p(\mathscr{L})} \left\| \sum_{i=0}^{K-1} p(\mathscr{L}_i) \lambda_i \right\|^2
$$

$$
+ \frac{1}{\kappa^2} \sum_{l \in \mathscr{L}} p(l) \left\| \sum_{i \in l} \lambda_i \right\|^2
$$

$$
= p(\mathscr{L}) \left\| \lambda_c - \frac{1}{\kappa p(\mathscr{L})} \sum_{i=0}^{K-1} p(\mathscr{L}_i) \lambda_i \right\|^2 + \frac{1}{\kappa^2} \sum_{l \in \mathscr{L}} p(l) \left\| \sum_{i \in l} \lambda_i \right\|^2
$$

$$
- \frac{1}{\kappa^2 p(\mathscr{L})} \left(\sum_{i=0}^{K-1} p(\mathscr{L}_i)^2 \| \lambda_i \|^2 + 2 \sum_{i=0}^{K-2} \sum_{j=i+1}^{K-1} p(\mathscr{L}_i) p(\mathscr{L}_j) \langle \lambda_i, \lambda_j \rangle \right)
$$

$$
\overset{(b)}{=} p(\mathscr{L}) \left\| \lambda_c - \frac{1}{\kappa p(\mathscr{L})} \sum_{i=0}^{K-1} p(\mathscr{L}_i) \lambda_i \right\|^2 + \frac{1}{\kappa} \sum_{i=0}^{K-1} p(\mathscr{L}_i) \| \lambda_i \|^2
$$

$$
- \frac{1}{\kappa^2} \sum_{i=0}^{K-2} \sum_{j=i+1}^{K-1} p(\mathscr{L}_{i,j}) \| \lambda_i - \lambda_j \|^2 - \frac{1}{\kappa^2 p(\mathscr{L})} \sum_{i=0}^{K-1} p(\mathscr{L}_i)^2 \| \lambda_i \|^2
$$

$$
+ \frac{1}{\kappa^2 p(\mathscr{L})} \left(\sum_{i=0}^{K-2} \sum_{j=i+1}^{K-1} p(\mathscr{L}_i) p(\mathscr{L}_j) \| \lambda_i - \lambda_j \|^2 \right.
$$

$$
\left. - \sum_{i=0}^{K-1} p(\mathscr{L}_i)(\kappa p(\mathscr{L}) - p(\mathscr{L}_i)) \| \lambda_i \|^2 \right)
$$

$$
= p(\mathscr{L}) \left\| \lambda_c - \frac{1}{\kappa p(\mathscr{L})} \sum_{i=0}^{K-1} p(\mathscr{L}_i) \lambda_i \right\|^2
$$

$$+ \frac{1}{\kappa^2} \sum_{i=0}^{K-2} \sum_{j=i+1}^{K-1} \left(\frac{p(\mathscr{L}_i)p(\mathscr{L}_j)}{p(\mathscr{L})} - p(\mathscr{L}_{i,j}) \right) \|\lambda_i - \lambda_j\|^2,$$

where (a) follows by use of Lemma I.1.3 and (b) by use of Lemmas I.1.4 and I.1.6.
□

Theorem I.1.1. For $1 \leq \kappa \leq K$ we have

$$\sum_{\lambda_c} \sum_{l \in \mathscr{L}} p(l) \left\| \lambda_c - \frac{1}{\kappa} \sum_{i \in l} \lambda_i \right\|^2 = \sum_{\lambda_c} \left(p(\mathscr{L}) \left\| \lambda_c - \frac{1}{\kappa p(\mathscr{L})} \sum_{i=0}^{K-1} p(\mathscr{L}_i)\lambda_i \right\|^2 \right. \tag{I.2}$$
$$\left. + \frac{1}{\kappa^2} \sum_{i=0}^{K-2} \sum_{j=i+1}^{K-1} \left(\frac{p(\mathscr{L}_i)p(\mathscr{L}_j)}{p(\mathscr{L})} - p(\mathscr{L}_{i,j}) \right) \|\lambda_i - \lambda_j\|^2 \right).$$

Proof. Follows trivially from Proposition I.1.1.
□

I.2 Proof of Proposition 6.3.1

Proposition 6.3.1 For $K = 2$ and asymptotically as $N_i \to \infty, \nu_i \to 0$ as well as for $K = 3$ and asymptotically as $N_i, L \to \infty$ and $\nu_i \to 0$, we have for any pair of sublattices, (Λ_i, Λ_j), $i, j = 0, \ldots, K-1$, $i \neq j$,

$$\frac{1}{L} \sum_{\lambda_c \in V_\pi(0)} \|\alpha_i(\lambda_c) - \alpha_j(\lambda_c)\|^2 = \psi_L^2 \nu^{2/L} G(S_L) N_\pi \prod_{m=0}^{K-1} N_m^{2/L(K-1)}.$$

Proof. Let $T_i = \{\lambda_i : \lambda_i = \alpha_i(\lambda_c), \ \lambda_c \in V_\pi(0)\}$, i.e. the set of N_π sublattice points $\lambda_i \in \Lambda_i$ associated with the N_π central lattice points within $V_\pi(0)$. Furthermore, let $T_i' \subseteq T_i$ be the set of unique elements of T_i. Since (for large N_i) all the lattice points of Λ_i which are contained within $V_\pi(0)$ are used in some K-tuples, it follows that $|T_i'| \approx \tilde{\nu}/\nu_i = N_\pi/N_i$. Finally, let $T_j(\lambda_i) = \{\lambda_j : \lambda_j = \alpha_j(\lambda_c)$ and $\lambda_i = \alpha_i(\lambda_c), \ \lambda_c \in V_\pi(0)\}$ and let $T_j'(\lambda_i) \subseteq T_j(\lambda_i)$ be the set of unique elements. That is, $T_j(\lambda_i)$ contains all the elements $\lambda_j \in \Lambda_j$ which are in the K-tuples that also contains a specific $\lambda_i \in \Lambda_i$. We will also make use of the notation $\#_{\lambda_j}$ to indicate the number of occurrences of a specific λ_j in $T_j(\lambda_i)$. For example for $K = 2$ we have $\#_{\lambda_j} = 1, \forall \lambda_j$ whereas for $K > 2$ we have $\#_{\lambda_j} \geq 1$. We will show later that using the approximation $\#_{\lambda_j} \approx N_i/\tilde{N}_j$ is asymptotically good for $K = 3, L \to \infty$ and $N_n \to \infty, \forall n$. Furthermore, we conjecture this to be the case for $K > 3$ as well.

For sublattice Λ_i and Λ_j we have

$$\sum_{\lambda_c \in V_\pi(0)} \|\alpha_i(\lambda_c) - \alpha_j(\lambda_c)\|^2 = \sum_{\lambda_i \in T_i'} \sum_{\lambda_j \in T_j(\lambda_i)} \|\lambda_i - \lambda_j\|^2.$$

Given $\lambda_i \in T_i'$, we have

$$\sum_{\lambda_j \in T_j(\lambda_i)} \|\lambda_i - \lambda_j\|^2 \nu_j = \sum_{\lambda_j \in T_j'(\lambda_i)} \#_{\lambda_j} \|\lambda_i - \lambda_j\|^2 \nu_j$$

$$\approx \frac{N_i}{\tilde{N}_j} \sum_{\lambda_j \in T_j'(\lambda_i)} \|\lambda_i - \lambda_j\|^2 \nu_j$$

$$\approx \frac{N_i}{\tilde{N}_j} \int_{\tilde{V}(\lambda_i)} \|\lambda_i - x\|^2 \, dx \qquad \text{(I.3)}$$

$$= \frac{N_i}{\tilde{N}_j} \tilde{\nu}^{1+2/L} L G(S_L)$$

$$= N_i \nu_j \tilde{\nu}^{2/L} L G(S_L)$$

since $\tilde{N}_j = \tilde{\nu}/\nu_j$. Hence, with $\tilde{\nu} = \psi_L^L \nu \prod_{m=0}^{K-1} N_m^{1/(K-1)}$, we have

$$\frac{1}{L} \sum_{\lambda_j \in T_j(\lambda_i)} \|\lambda_i - \lambda_j\|^2 \nu_j \approx N_i \nu_j \psi_L^2 \nu^{2/L} G(S_L) \prod_{m=0}^{K-1} N_m^{2/L(K-1)},$$

which is independent of λ_i, so that

$$\frac{1}{L} \sum_{\lambda_i \in T_i'} \sum_{\lambda_j \in T_j(\lambda_i)} \|\lambda_i - \lambda_j\|^2 \approx \frac{1}{L} \frac{N_\pi}{N_i} \sum_{\lambda_j \in T_j(\lambda_i)} \|\lambda_i - \lambda_j\|^2$$

$$\approx \psi_L^2 \nu^{2/L} G(S_L) N_\pi \prod_{m=0}^{K-1} N_m^{2/L(K-1)},$$

which completes the first part of the proof. We still need to show that for $K = 3$ and $L \to \infty$ as well as $N_m \to \infty, \forall m$ the approximation $\#_{\lambda_j} \approx N_i/\tilde{N}_j$ is good. That this is so can be deduced from the proof of Proposition 5.4.1 (the last part where $K = 3$) by using the fact that $\tilde{\nu} = \psi_L^L \nu \prod N_m^{1/(K-1)}$ in order to prove that

$$\frac{1}{L} \sum_{\lambda_j \in T_j(\lambda_i)} \|\lambda_i - \lambda_j\|^2 = N_i \tilde{\nu}^{2/L} G(S_L), \qquad \text{(I.4)}$$

which shows that (I.3) is asymptotically true for $K = 3, L \to \infty$ and $N_n \to \infty, \forall n$.

$\square$

I.3   Proof of Proposition 6.3.2

Proposition 6.3.2 For $N_i \to \infty$ we have

$$\frac{\sum_{\lambda_c \in V_\pi(0)} \left\| \lambda_c - \frac{1}{\kappa p(\mathscr{L})} \sum_{i=0}^{K-1} p(\mathscr{L}_i) \lambda_i \right\|^2}{\sum_{\lambda_c \in V_\pi(0)} \sum_{i=0}^{K-2} \sum_{j=i+1}^{K-1} \left(\frac{p(\mathscr{L}_i) p(\mathscr{L}_j)}{p(\mathscr{L})} - p(\mathscr{L}_{i,j}) \right) \|\lambda_i - \lambda_j\|^2} \to 0. \qquad \text{(I.5)}$$

Proof. The numerator describes the distance from a central lattice point to the weighted centroid of its associated K-tuple. Let us choose Λ_0 such that $N_0 \leq N_i, \forall i$. Then, since by construction there is no bias towards any of the sublattices, the weighted centroids will be evenly distributed around λ_0 points. Hence, the distance from central lattice points to the centroids can be upper bounded by the covering radius of Λ_0. This is a conservative[76] upper bound but will suffice for the proof. The rate of growth of the covering radius is proportional to $\nu_0^{1/L} = (N_0\nu)^{1/L}$, hence

$$\sum_{\lambda_c \in V_\pi(0)} \left\| \lambda_c - \frac{1}{\kappa p(\mathscr{L})} \sum_{i=0}^{K-1} p(\mathscr{L}_i)\lambda_i \right\|^2 = \mathscr{O}\left(N_\pi N_0^{2/L}\nu^{2/L}\right). \quad \text{(I.6)}$$

By use of Proposition 6.3.1 we have[77]

$$\frac{1}{L} \sum_{\lambda_c \in V_\pi(0)} \sum_{i=0}^{K-2} \sum_{j=i+1}^{K-1} \left(\frac{p(\mathscr{L}_i)p(\mathscr{L}_j)}{p(\mathscr{L})} - p(\mathscr{L}_{i,j}) \right) \|\alpha_i(\lambda_c) - \alpha_j(\lambda_c)\|^2$$

$$= \frac{1}{L} \sum_{i=0}^{K-2} \sum_{j=i+1}^{K-1} \left(\frac{p(\mathscr{L}_i)p(\mathscr{L}_j)}{p(\mathscr{L})} - p(\mathscr{L}_{i,j}) \right) \sum_{\lambda_c \in V_\pi(0)} \|\alpha_i(\lambda_c) - \alpha_j(\lambda_c)\|^2$$

$$\approx \psi_L^2 \nu^{2/L} G(S_L) N_\pi \prod_{m=0}^{K-1} N_m^{2/L(K-1)} \sum_{i=0}^{K-2} \sum_{j=i+1}^{K-1} \left(\frac{p(\mathscr{L}_i)p(\mathscr{L}_j)}{p(\mathscr{L})} - p(\mathscr{L}_{i,j}) \right),$$

so that, since $\lambda_i = \alpha_i(\lambda_c)$, we get by use of Proposition 6.3.1[78]

$$\sum_{\lambda_c \in V_\pi(0)} \sum_{i=0}^{K-2} \sum_{j=i+1}^{K-1} \left(\frac{p(\mathscr{L}_i)p(\mathscr{L}_j)}{p(\mathscr{L})} - p(\mathscr{L}_{i,j}) \right) \|\lambda_i - \lambda_j\|^2$$

$$= \Omega\left(N_\pi \nu^{2/L} \prod_{m=0}^{K-1} N_m^{2/L(K-1)} \right). \quad \text{(I.7)}$$

Comparing (I.6) to (I.7) we see that (I.5) grows as $\Theta\left(N_0^{2/L}/N_\pi^{2/L(K-1)}\right) \to 0$ for $N_i \to \infty$. $\square$

---

[76]The number of distinct centroids per unit volume is larger than the number of points of Λ_0 per unit volume.

[77]The approximation of $\#_{\lambda_j}$ in Proposition 6.3.1 does not influence this analysis. To see this we refer the reader to Appendix H.5.

[78]In this case we actually lower bound the expression and as such the order operator $\mathscr{O}$ is in fact Ω. Recall that we say that $f(n) = \mathscr{O}(g(n))$ if $0 < f(n) \leq c_1 g(n)$ and $f(n) = \Omega(g(n))$ if $f(n) \geq c_0 g(n)$, for $c_0, c_1 > 0$ and some large n. Furthermore, $f(n) = \Theta(g(n))$ if $c_0 g(n) \leq f(n) \leq c_1 g(n)$, cf. [56].
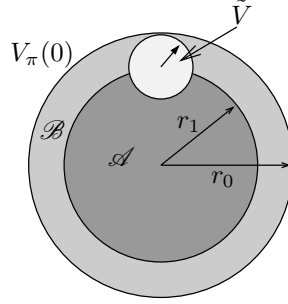
Figure I.1: *The complete sphere consisting of the regions $\mathscr{A}$ and $\mathscr{B}$ describe $V_\pi(0)$. The radius of $V_\pi(0)$ is r_0. The small bright sphere describe $\tilde{V}$. When $\tilde{V}$ is centered at λ_0 points within the sphere $\mathscr{A}$ of radius r_1 it will be completely contained within $V_\pi(0)$.*

I.4   Proof of Lemmas

Proof of Lemma 6.2.2. For simplicity (and without any loss of generality) we assume that $V_\pi(0)$ forms the shape of a sphere, see Fig. I.1. The K-tuples are constructed by centering a sphere $\tilde{V}$ of volume $\tilde{\nu}$ around each $\lambda_0 \in V_\pi(0)$ and taking all combinations of lattice points within this region (keeping λ_0 as first coordinate). From Fig. I.1 it may be seen that any λ_0 which is contained in the region denoted $\mathscr{A}$ will always be combined with sublattice points that are also contained in $V_\pi(0)$. On the other hand, any λ_0 which is contained in region $\mathscr{B}$ will occasionally be combined with points outside $V_\pi(0)$. Therefore, we need to show that the volume $V_\mathscr{A}$ of $\mathscr{A}$ approaches the volume of $V_\pi(0)$ as $N_i \to \infty$ or equivalently that the ratio of $V_\mathscr{B}/V_\mathscr{A} \to 0$ as $N_i \to \infty$, where $V_\mathscr{B}$ denotes the volume of the region $\mathscr{B}$.

Let ω_L denote the volume of an L-dimensional unit sphere. Then $V_\mathscr{A} = \omega_L r_1^L$ and $V_\mathscr{B} = \nu_\pi - V_\mathscr{A}$, where ν_π is the volume of $V_\pi(0)$. The radius r_1 of $\mathscr{A}$ can be expressed as the difference between the radius r_0 of $V_\pi(0)$ and the radius of $\tilde{V}$, that is

$$r_1 = (\nu_\pi/\omega_L)^{1/L} - (\tilde{\nu}/\omega_L)^{1/L}. \tag{I.8}$$

Since, $\nu_\pi = \nu \prod N_i = \nu N_\pi$ and $\tilde{\nu} = \psi_L^L \nu \prod N_i^{1/(K-1)} = \psi_L^L \nu N_\pi^{1/(K-1)}$ we can write $V_\mathscr{A}$ as

$$V_\mathscr{A} = \omega_L r_1^L$$

$$= \omega_L \left(\left(\frac{\nu N_\pi}{\omega_L} \right)^{1/L} - \left(\frac{\psi_L^L \nu N_\pi^{1/(K-1)}}{\omega_L} \right)^{1/L} \right)^L \tag{I.9}$$

$$= \nu \left(N_\pi^{1/L} - \psi_L N_\pi^{1/L(K-1)} \right)^L.$$

The volume of $\mathscr{B}$ can be expressed through the volume of $\mathscr{A}$ as

$$V_\mathscr{B} = \nu_\pi - V_\mathscr{A}, \tag{I.10}$$

so that their ratio is given by

$$\frac{V_{\mathscr{B}}}{V_{\mathscr{A}}} = \frac{N_\pi}{\left(N_\pi^{1/L} - N_\pi^{1/L(K-1)}\right)^L} - 1. \tag{I.11}$$

Clearly, for $K > 2$ we have

$$\lim_{N_\pi \to \infty} \frac{N_\pi}{\left(N_\pi^{1/L} - N_\pi^{1/L(K-1)}\right)^L} = 1, \tag{I.12}$$

which proves the claim. $\qquad\square$

Proof of Lemma 6.2.3. We only need to prove Lemma 6.2.3 for Λ_0 and Λ_1. Then by symmetry it must hold for any pair. Let $\mathscr{S}_{\lambda_0}$ denote the set of K-tuples constructed by centering $\tilde{V}$ at some $\lambda_0 \in V_\pi(0) \cap \Lambda_0$. Hence, $s \in \mathscr{S}_{\lambda_0}$ has λ_0 as first coordinate and the distance between any two elements of s is less than r, the radius of $\tilde{V}$. We will assume[79] that $S_{\lambda_0} \neq \emptyset, \forall \lambda_0$.

Similarly, define the set $\mathscr{S}_{\lambda_1} \neq \emptyset$ by centering $\tilde{V}$ at some $\lambda_1 \in V_\pi(0) \cap \Lambda_1$. Assume[80] all elements of the K-tuples are in $V_\pi(0)$. Then it must hold that for any $s \in \mathscr{S}_{\lambda_1}$ we have $s \in \bigcup_{\lambda_0 \in V_\pi \cap \Lambda_0} \mathscr{S}_{\lambda_0}$. But it is also true that for any $s' \in \mathscr{S}_{\lambda_0}$ we have $s' \in \bigcup_{\lambda_1 \in V_\pi \cap \Lambda_1} \mathscr{S}_{\lambda_1}$. Hence, we deduce that $\bigcup_{\lambda_0 \in V_\pi \cap \Lambda_0} \mathscr{S}_{\lambda_0} \equiv \bigcup_{\lambda_1 \in V_\pi \cap \Lambda_1} \mathscr{S}_{\lambda_1}$. Furthermore, $|V_\pi(0) \cap \Lambda_0| = N_\pi/N_0, |\mathscr{S}_{\lambda_0}| = N_0, \forall \lambda_0 \in V_\pi(0) \cap \Lambda_0$ and $\mathscr{S}_{\lambda_0'} \cap \mathscr{S}_{\lambda_0''} = \emptyset, \lambda_0' \neq \lambda_0''$, which implies that $|\bigcup_{\lambda_0 \in V_\pi \cap \Lambda_0} \mathscr{S}_{\lambda_0}| = N_\pi$. $\qquad\square$

I.5 Proof of Theorem 6.5.1

Before proving Theorem 6.5.1 we need the following results.

Lemma I.5.1. For $1 \leq \kappa \leq K$ and any $l \in \mathscr{L}$ we have

$$\left\|\sum_{j \in l} \lambda_j\right\|^2 = \kappa \sum_{j \in l} \|\lambda_j\|^2 - \sum_{i=0}^{\kappa-2} \sum_{j=i+1}^{\kappa-1} \|\lambda_{l_j} - \lambda_{l_i}\|^2.$$

---

[79]This is always the case if $r \geq \max_i r(\Lambda_i)$ where $r(\Lambda_i)$ is the covering radius of the ith sublattice. The covering radius depends on the lattice and is maximized if Λ_i is geometrically similar to Z^L, in which case we have [22]

$$r(\Lambda_i) = \frac{1}{2}\sqrt{2}\nu^{1/L} N_i^{1/L}.$$

Since $r = \psi_L \nu^{1/L} N_\pi^{1/L(K-1)}/\omega_L^{1/L}$ it follows that in order to make sure that $\mathscr{S}_{\lambda_0} \neq \emptyset$ the index values must satisfy

$$N_i \leq (\sqrt{2}\psi_L)^L \omega_L N_\pi^{1/(K-1)}, \quad i = 0, \ldots, K-1. \tag{*}$$

Throughout this work we therefore require (and implicitly assume) that (*) is satisfied.

[80]This is asymptotically true according to Lemma 6.2.2 since we at this point do not consider the cosets of the K-tuples. Furthermore, the cosets are invariant to which lattice is used for the construction of K-tuples as long as all elements of the K-tuples are within $V_\pi(0)$.

Proof. We can write

$$\left\| \sum_{j \in l} \lambda_j \right\|^2 = \sum_{j \in l} \|\lambda_j\|^2 + 2 \sum_{i=0}^{\kappa-2} \sum_{j=i+1}^{\kappa-1} \langle \lambda_{l_j}, \lambda_{l_i} \rangle,$$

which by use of Lemma H.1.3 leads to

$$\left\| \sum_{j \in l} \lambda_j \right\|^2 = \sum_{j \in l} \|\lambda_j\|^2 + (\kappa - 1) \sum_{j \in l} \|\lambda_j\|^2 - \sum_{i=0}^{\kappa-2} \sum_{j=i+1}^{\kappa-1} \|\lambda_{l_j} - \lambda_{l_i}\|^2$$

$$= \kappa \sum_{j \in l} \|\lambda_j\|^2 - \sum_{i=0}^{\kappa-2} \sum_{j=i+1}^{\kappa-1} \|\lambda_{l_j} - \lambda_{l_i}\|^2.$$

□

Lemma I.5.2. For $1 \leq \kappa \leq K$ and any $l \in \mathscr{L}$ we have

$$2 \left\langle \sum_{j \in l} \lambda_j, \sum_{i=0}^{K-1} p(\mathscr{L}_i) \lambda_i \right\rangle = p(\mathscr{L}) \kappa \sum_{j \in l} \|\lambda_j\|^2$$

$$+ \kappa \sum_{i=0}^{K-1} p(\mathscr{L}_i) \|\lambda_i\|^2 - \sum_{j \in l} \sum_{i=0}^{K-1} p(\mathscr{L}_i) \|\lambda_j - \lambda_i\|^2.$$

Proof.

$$2 \left\langle \sum_{j \in l} \lambda_j, \sum_{i=0}^{K-1} p(\mathscr{L}_i) \lambda_i \right\rangle = 2 \sum_{j \in l} \sum_{i=0}^{K-1} p(\mathscr{L}_i) \langle \lambda_j, \lambda_i \rangle$$

$$= - \sum_{j \in l} \sum_{i=0}^{K-1} p(\mathscr{L}_i) \|\lambda_j - \lambda_i\|^2$$

$$+ \sum_{j \in l} \sum_{i=0}^{K-1} p(\mathscr{L}_i) \left(\|\lambda_j\|^2 + \|\lambda_i\|^2 \right)$$

where by use of Lemma I.1.1 we obtain

$$2 \left\langle \sum_{j \in l} \lambda_j, \sum_{i=0}^{K-1} p(\mathscr{L}_i) \lambda_i \right\rangle = - \sum_{j \in l} \sum_{i=0}^{K-1} p(\mathscr{L}_i) \|\lambda_j - \lambda_i\|^2$$

$$+ \kappa p(\mathscr{L}) \sum_{j \in l} \|\lambda_j\|^2 + \kappa \sum_{i=0}^{K-1} p(\mathscr{L}_i) \|\lambda_i\|^2.$$

□

Proposition I.5.1. For $0 < \kappa \le K \le 3$, $N_i \to \infty$, $\nu_i \to 0$ and any $l \in \mathscr{L}$ we have

$$\frac{1}{L} \sum_{\lambda_c \in V_\pi(0)} \left\| \frac{1}{\kappa} \sum_{j \in l} \lambda_j - \frac{1}{\kappa p(\mathscr{L})} \sum_{i=0}^{K-1} p(\mathscr{L}_i)\lambda_i \right\|^2$$

$$= \omega^{(K,l)} \psi_L^2 \nu^{2/L} G(S_L) N_\pi \prod_{m=0}^{K-1} N_m^{2/L(K-1)},$$

where

$$\omega^{(K,l)} = \frac{1}{p(\mathscr{L})^2 \kappa^2} \left(p(\mathscr{L})^2 \kappa^2 - p(\mathscr{L})^2 \binom{\kappa}{2} - p(\mathscr{L}) \sum_{j \in l} p(\mathscr{L}_j) \right.$$

$$\left. - \sum_{i=0}^{K-2} \sum_{j=i+1}^{K-1} p(\mathscr{L}_i) p(\mathscr{L}_j) \right),$$

where $\binom{\kappa}{2} = 0$ for $\kappa = 1$.

Proof. We have that

$$\left\| \frac{1}{\kappa} \sum_{j \in l} \lambda_j - \frac{1}{\kappa p(\mathscr{L})} \sum_{i=0}^{K-1} p(\mathscr{L}_i)\lambda_i \right\|^2$$

$$= \frac{1}{p(\mathscr{L})^2 \kappa^2} \left(p(\mathscr{L})^2 \left\| \sum_{j \in l} \lambda_j \right\|^2 + \left\| \sum_{i=0}^{K-1} p(\mathscr{L}_i)\lambda_i \right\|^2 \right.$$

$$\left. - 2p(\mathscr{L}) \left\langle \sum_{j \in l} \lambda_j, \sum_{i=0}^{K-1} p(\mathscr{L}_i)\lambda_i \right\rangle \right),$$

which by use of Lemmas I.5.1 and I.5.2 leads to

$$\left\| \frac{1}{\kappa} \sum_{j \in l} \lambda_j - \frac{1}{p(\mathscr{L})\kappa} \sum_{i=0}^{K-1} p(\mathscr{L}_i)\lambda_i \right\|^2$$

$$= \frac{1}{p(\mathscr{L})^2 \kappa^2} \left(p(\mathscr{L})^2 \kappa \sum_{j \in l} \|\lambda_j\|^2 - p(\mathscr{L})^2 \sum_{i=0}^{\kappa-2} \sum_{j=i+1}^{\kappa-1} \|\lambda_{l_i} - \lambda_{l_j}\|^2 \right.$$

$$+ p(\mathscr{L})\kappa \sum_{i=0}^{K-1} p(\mathscr{L}_i)\|\lambda_i\|^2 - \sum_{i=0}^{K-2} \sum_{j=i+1}^{K-1} p(\mathscr{L}_i)p(\mathscr{L}_j)\|\lambda_i - \lambda_j\|^2$$

$$- p(\mathscr{L})^2 \kappa \sum_{j \in l} \|\lambda_j\|^2 - p(\mathscr{L})\kappa \sum_{i=0}^{K-1} p(\mathscr{L}_i)\|\lambda_i\|^2$$

$$\left. + p(\mathscr{L}) \sum_{j \in l} \sum_{i=0}^{K-1} p(\mathscr{L}_i)\|\lambda_j - \lambda_i\|^2 \right)$$

$$
= \frac{1}{p(\mathscr{L})^2 \kappa^2} \left(p(\mathscr{L}) \sum_{j \in l} \sum_{i=0}^{K-1} p(\mathscr{L}_i) \|\lambda_j - \lambda_i\|^2 \right.
$$

$$
- p(\mathscr{L})^2 \sum_{i=0}^{\kappa-2} \sum_{j=i+1}^{\kappa-1} \|\lambda_{l_i} - \lambda_{l_j}\|^2
$$

$$
\left. - \sum_{i=0}^{K-2} \sum_{j=i+1}^{K-1} p(\mathscr{L}_i) p(\mathscr{L}_j) \|\lambda_i - \lambda_j\|^2 \right). \tag{I.13}
$$

It follows from Proposition 6.3.1, (I.13) and Lemma I.1.1 that we can write

$$
\frac{1}{L} \sum_{\lambda_c \in V_\pi(0)} \left\| \frac{1}{\kappa} \sum_{j \in l} \lambda_j - \frac{1}{p(\mathscr{L})\kappa} \sum_{i=0}^{K-1} p(\mathscr{L}_i)\lambda_i \right\|^2
$$

$$
\approx \frac{1}{p(\mathscr{L})^2 \kappa^2} \left(p(\mathscr{L}) \sum_{j \in l} \sum_{\substack{i=0 \\ i \neq j}}^{K-1} p(\mathscr{L}_i) - p(\mathscr{L})^2 \sum_{i=0}^{\kappa-2} \sum_{j=i+1}^{\kappa-1} - \sum_{i=0}^{K-2} \sum_{j=i+1}^{K-1} p(\mathscr{L}_i) p(\mathscr{L}_j) \right)
$$

$$
\times \psi_L^2 \nu^{2/L} G(S_L) N_\pi \prod_{m=0}^{K-1} N_m^{2/L(K-1)}
$$

$$
= \frac{1}{p(\mathscr{L})^2 \kappa^2} \left(p(\mathscr{L})^2 \kappa^2 - p(\mathscr{L}) \sum_{j \in l} p(\mathscr{L}_j) - p(\mathscr{L})^2 \binom{\kappa}{2} \right.
$$

$$
\left. - \sum_{i=0}^{K-2} \sum_{j=i+1}^{K-1} p(\mathscr{L}_i) p(\mathscr{L}_j) \right) \psi_L^2 \nu^{2/L} G(S_L) N_\pi \prod_{m=0}^{K-1} N_m^{2/L(K-1)}.
$$

This completes the proof. $\qquad\qquad\square$

Proposition I.5.2. For any $1 \leq \kappa \leq K$ and $l \in \mathscr{L}$ we have

$$
\sum_{\lambda_c \in V_\pi(0)} \left\| \frac{1}{\kappa} \sum_{j \in l} \lambda_j - \frac{1}{p(\mathscr{L})\kappa} \sum_{i=0}^{K-1} p(\mathscr{L}_i)\lambda_i \right\| = \mathscr{O} \left(\nu^{1/L} N_\pi \prod_{m=0}^{K-1} N_m^{1/L(K-1)} \right)
$$

Proof. Recall that the sublattice points λ_i and λ_j satisfy $\|\lambda_i - \lambda_j\| \leq r$, where $r = (\tilde{\nu}/\omega_L)^{1/L}$ is the radius of $\tilde{V}$. Hence, without loss of generality, we let $\lambda_j = r$ and $\lambda_i = 0$, which leads to

$$
\sum_{\lambda_c \in V_\pi(0)} \left\| \frac{1}{\kappa} \sum_{j \in l} \lambda_j - \frac{1}{p(\mathscr{L})\kappa} \sum_{i=0}^{K-1} p(\mathscr{L}_i)\lambda_i \right\| \leq r N_\pi
$$

$$
= \mathscr{O} \left(\nu^{1/L} N_\pi \prod_{m=0}^{K-1} N_m^{1/L(K-1)} \right),
$$

since $\tilde{\nu} = \psi_L^L \nu \prod_{m=0}^{K-1} N_m^{1/(K-1)}$. $\qquad\qquad\square$

Proposition I.5.3. For $1 \leq \kappa \leq K \leq 3$, $l \in \mathscr{L}$, $N_i \to \infty$ and $\nu_i \to 0$ we have

$$\sum_{\lambda_c \in V_\pi(0)} \left\| \frac{1}{\kappa} \sum_{j \in l} \lambda_j - \lambda_c \right\|^2 = \sum_{\lambda_c \in V_\pi(0)} \left\| \frac{1}{\kappa} \sum_{j \in l} \lambda_j - \frac{1}{p(\mathscr{L})\kappa} \sum_{i=0}^{K-1} p(\mathscr{L}_i)\lambda_i \right\|^2.$$

Proof. Let $\bar{\lambda} = \frac{1}{p(\mathscr{L})\kappa} \sum_{i=0}^{K-1} p(\mathscr{L}_i)\lambda_i$ and $\lambda' = \frac{1}{\kappa} \sum_{j \in l} \lambda_j$. We now follow [28, Eqs. (67) – (72)] and obtain the following inequalities:

$$\|\lambda' - \lambda_c\|^2 = \|\lambda' - \bar{\lambda} + \bar{\lambda} - \lambda_c\|^2$$
$$= \|\lambda' - \bar{\lambda}\|^2 + \|\bar{\lambda} - \lambda_c\|^2 + 2\langle(\lambda' - \bar{\lambda}), (\bar{\lambda} - \lambda_c)\rangle,$$

from which we can establish the inequality

$$\|\lambda' - \bar{\lambda}\|^2 + \|\bar{\lambda} - \lambda_c\|^2 - 2|\langle(\lambda' - \bar{\lambda}), (\bar{\lambda} - \lambda_c)\rangle| \leq \|\lambda' - \lambda_c\|^2$$
$$\leq \|\lambda' - \bar{\lambda}\|^2 + \|\bar{\lambda} - \lambda_c\|^2 + 2|\langle(\lambda' - \bar{\lambda}), (\bar{\lambda} - \lambda_c)\rangle|.$$

Using the Cauchy-Schwartz inequality we get

$$\|\lambda' - \bar{\lambda}\|^2 + \|\bar{\lambda} - \lambda_c\|^2 - 2\|(\lambda' - \bar{\lambda})\|\|(\bar{\lambda} - \lambda_c)\| \leq \|\lambda' - \lambda_c\|^2$$
$$\leq \|\lambda' - \bar{\lambda}\|^2 + \|\bar{\lambda} - \lambda_c\|^2 + 2\|(\lambda' - \bar{\lambda})\|\|(\bar{\lambda} - \lambda_c)\|.$$

which can be rewritten as

$$\|\lambda' - \bar{\lambda}\|^2 \left(1 - \frac{\|\bar{\lambda} - \lambda_c\|}{\|\lambda' - \bar{\lambda}\|}\right)^2 \leq \|\lambda' - \lambda_c\|^2$$
$$\leq \|\lambda' - \bar{\lambda}\|^2 \left(1 + \frac{\|\bar{\lambda} - \lambda_c\|}{\|\lambda' - \bar{\lambda}\|}\right)^2$$

Summing over $\lambda_c \in V_\pi(0)$ and observing that $\|\bar{\lambda} - \lambda_c\|^2 \geq 0$, we get

$$\sum_{\lambda_c \in V_\pi(0)} \left(\|\lambda' - \bar{\lambda}\|^2 - 2\|\lambda' - \bar{\lambda}\|\|\bar{\lambda} - \lambda_c\|\right) \leq \sum_{\lambda_c \in V_\pi(0)} \|\lambda_c - \lambda'\|^2$$
$$\leq \sum_{\lambda_c \in V_\pi(0)} \left(\|\lambda' - \bar{\lambda}\|^2 + \|\bar{\lambda} - \lambda_c\|^2 + 2\|\lambda' - \bar{\lambda}\|\|\bar{\lambda} - \lambda_c\|\right),$$

which can be rewritten as

$$\left(\sum_{\lambda_c \in V_\pi(0)} \|\lambda' - \bar{\lambda}\|^2\right) \left(1 - 2\frac{\sum_{\lambda_c \in V_\pi(0)} \|\lambda' - \bar{\lambda}\|\|\bar{\lambda} - \lambda_c\|}{\sum_{\lambda_c \in V_\pi(0)} \|\lambda' - \bar{\lambda}\|^2}\right) \tag{I.14}$$

$$\leq \sum_{\lambda_c \in V_\pi(0)} \|\lambda_c - \lambda'\|^2 \tag{I.15}$$

$$\leq \left(\sum_{\lambda_c \in V_\pi(0)} \|\lambda' - \bar{\lambda}\|^2\right)$$
$$\times \left(1 + \frac{\sum_{\lambda_c \in V_\pi(0)} \|\bar{\lambda} - \lambda_c\|^2}{\sum_{\lambda_c \in V_\pi(0)} \|\lambda' - \bar{\lambda}\|^2} + 2\frac{\sum_{\lambda_c \in V_\pi(0)} \|\lambda' - \bar{\lambda}\|\|\bar{\lambda} - \lambda_c\|}{\sum_{\lambda_c \in V_\pi(0)} \|\lambda' - \bar{\lambda}\|^2}\right). \tag{I.16}$$

By use of (I.6) and Proposition I.5.2 it is possible to upper bound the numerator of the fraction in (I.14) by

$$\sum_{\lambda_c \in V_\pi(0)} \|\lambda' - \bar{\lambda}\|\|\bar{\lambda} - \lambda_c\| = \mathscr{O}\left((N_k\nu)^{1/L}N_\pi\nu^{1/L}\prod_{m=0}^{K-1}N_m^{1/L(K-1)}\right),$$

since the covering radius of the kth sublattice is proportional to $(N_k\nu)^{1/L}$, where N_k is the minimum of $N_i, i = 0, \ldots, K-1$.

By use of Proposition I.5.1 it is easily seen that the denominator in (I.14) grows as

$$\sum_{\lambda_c \in V_\pi(0)} \|\lambda' - \bar{\lambda}\|^2 = \mathscr{O}\left(\nu^{2/L}N_\pi\prod_{m=0}^{K-1}N_m^{2/L(K-1)}\right),$$

hence the fraction in (I.14) go to zero for $N_i \to \infty$. By a similar analysis it is easily seen that the fractions in (I.16) also go to zero as $N_i \to \infty$.

Based on the asymptotic behavior of the fractions in (I.14) and (I.16) we see that (asymptotically as $N_i \to \infty$)

$$\sum_{\lambda_c \in V_\pi(0)} \|\lambda' - \bar{\lambda}\|^2 \leq \sum_{\lambda_c \in V_\pi(0)} \|\lambda_c - \lambda'\|^2 \leq \sum_{\lambda_c \in V_\pi(0)} \|\lambda' - \bar{\lambda}\|^2,$$

hence

$$\sum_{\lambda_c \in V_\pi(0)} \|\lambda_c - \lambda'\|^2 \approx \sum_{\lambda_c \in V_\pi(0)} \|\lambda' - \bar{\lambda}\|^2,$$

which completes the proof. $\square$

We are now in a position to prove Theorem 6.5.1.

Theorem 6.5.1 *The side distortion $D^{(K,l)}$ due to reception of descriptions $\{l\}$, where $l \in \mathscr{L}$ for any $1 \leq \kappa \leq K \leq 3$ is, asymptotically as $L, N_i \to \infty$ and $\nu_i \to 0$, given by*

$$D^{(K,l)} = \omega^{(K,l)}\psi_L^2\nu^{2/L}G(S_L)\prod_{i=0}^{K-1}N_i^{2/L(K-1)},$$

where

$$\omega^{(K,l)} = \frac{1}{p(\mathscr{L})^2\kappa^2}\left(p(\mathscr{L})^2\kappa^2 - p(\mathscr{L})^2\binom{\kappa}{2} - p(\mathscr{L})\sum_{j\in l}p(\mathscr{L}_j)\right.$$

$$\left. - \sum_{i=0}^{K-2}\sum_{j=i+1}^{K-1}p(\mathscr{L}_i)p(\mathscr{L}_j)\right),$$

where $\binom{\kappa}{2} = 0$ for $\kappa = 1$.

Proof. By use of (5.16) we can write the distortion as

$$
\begin{aligned}
D^{(K,l)} &= \frac{1}{L} E \left\| \frac{1}{\kappa} \sum_{j \in l} \lambda_j - X \right\|^2 \\
&\approx D_c + \frac{1}{L} \frac{1}{N_\pi} \sum_{\lambda_c \in V_\pi(0)} \left\| \frac{1}{\kappa} \sum_{j \in l} \lambda_j - \lambda_c \right\|^2 \qquad \text{(I.17)} \\
&\approx \frac{1}{L} \frac{1}{N_\pi} \sum_{\lambda_c \in V_\pi(0)} \left\| \frac{1}{\kappa} \sum_{j \in l} \lambda_j - \lambda_c \right\|^2,
\end{aligned}
$$

where the second approximation follows from that fact that as $N_i \to \infty$, the distortion due to the index assignment is dominating. Furthermore, by use of Propositions I.5.3 and I.5.1 in (I.17) we are able to write

$$
\begin{aligned}
D^{(K,l)} &\approx \frac{1}{L} \frac{1}{N_\pi} \sum_{\lambda_c \in V_\pi(0)} \left\| \frac{1}{\kappa} \sum_{j \in l} \lambda_j - \frac{1}{p(\mathscr{L})\kappa} \sum_{i=0}^{K-1} p(\mathscr{L}_i)\lambda_i \right\|^2 \\
&\approx \omega^{(K,l)} \psi_L^2 \nu^{2/L} G(S_L) \prod_{m=0}^{K-1} N_m^{2/L(K-1)},
\end{aligned}
$$

which completes the proof. $\qquad \square$

Proofs for Chapter 7

This appendix contains proofs of the Lemmas and Theorems presented in Chapter 7.

J.1 Proofs of Lemmas

Proof of Lemma 7.2.1. For $K = 3, k = 1$ and $R_s \rightarrow \infty$ we see from (4.39) that

$$
\begin{aligned}
\sigma_q^2 &= \left((1 - \rho_q) 2^{2R_s} \left(\frac{1 + 2\rho_q}{1 - \rho_q} \right)^{1/3} - 1 \right)^{-1} \\
&\approx (1 - \rho_q)^{-2/3} (1 + 2\rho_q)^{-1/3} 2^{-2R_s},
\end{aligned}
\tag{J.1}
$$

where the approximation follows from the high resolution assumption which implies that $2^{2R_s} \gg 1$. With this, we can write the optimal single-channel distortion of a $(3, 1)$ SCEC, which is given by (4.37), as

$$
\begin{aligned}
D^{(3,1)} &= \frac{\sigma_q^2}{\sigma_q^2 + 1} \\
&\approx \sigma_q^2,
\end{aligned}
\tag{J.2}
$$

where the approximation follows since $\sigma_q^2 \ll 1$. We now equalize the single-channel distortion of three-channel MD-LVQ (or (3,1) MD-LVQ) and (3,1) SCECs (i.e. we set (7.11) equal to (J.2)) so that we can express ρ_q as a function of N'. This leads to

$$
1 + 2\rho_q = \left(\frac{3}{\psi_\infty^2 N'} \right)^3 (1 - \rho_q)^{-2}.
\tag{J.3}
$$

Using (4.37) we rewrite the two-channel distortion of (3,1) SCECs as

$$
D^{(3,2)} = \frac{\sigma_q^2 (1 + \rho_q)}{\sigma_q^2 (1 + \rho_q) + 2}
$$

$$\overset{(a)}{\approx} \frac{1}{2}\sigma_q^2(1+\rho_q)$$

$$\overset{(b)}{=} \frac{1+\rho_q}{6}\psi_\infty^2 N' 2^{-2R_s}$$

$$\overset{(c)}{\approx} \frac{1}{12}\psi_\infty^2 N' 2^{-2R_s} \tag{J.4}$$

where (a) is true at high resolution since $\sigma_q^2 \ll 1$, (b) follows by replacing σ_q^2 with (J.1) and inserting (J.3) and (c) is valid for large N' since $N' \gg 1$ implies that $\rho_q \approx -1/2$. Similarly, by using (J.3) in (4.37) the optimal three-channel distortion can be written as

$$\begin{aligned}
D^{(3,3)} &= \frac{\sigma_q^2(1+2\rho_q)}{\sigma_q^2(1+2\rho_q)+3} \\
&\approx \frac{1}{3}\sigma_q^2(1+2\rho_q) \\
&= 3\psi_\infty^{-4}(1-\rho_q)^{-2}\left(\frac{1}{N'}\right)^2 2^{-2R_s} \\
&\approx \left(\frac{1}{N'}\right)^2 2^{-2R_s},
\end{aligned} \tag{J.5}$$

where the first approximation is valid when $\sigma_q^2 \ll 1$ and the second follows since $\rho_q \approx -1/2$. Comparing (J.4) and (J.5) to (7.12) and (7.13) shows that three-channel MD-LVQ reach the achievable rate-distortion region of a $(3,1)$ SCEC in the quadratic Gaussian case at high resolution. $\qquad\square$

Proof of Lemma 7.3.1. Let $A_\epsilon^{(L)}$ denote the set of epsilon-typical sequences [24] and note that $A_\epsilon^{(L)}$ must have bounded support since, for any L, $f_X(x_0,\ldots,x_{L-1}) > 2^{-L(h(X)+\epsilon)}$ for $x \in A_\epsilon^{(L)}$ and

$$\int_{A_\epsilon^{(L)}} f_X(x_0,\ldots,x_{L-1})dx \le 1.$$

Let the side quantizers of an MD-LVQ system be SD entropy-constrained lattice vector quantizers. An SD lattice vector quantizer designed for an output entropy of, say R_i, for the L-dimensional uniform source with bounded support (in fact matched to the support of $A_\epsilon^{(L)}$) has a finite number of codewords given by 2^{LR_i}. The distortion performance of a lattice vector quantizer is, under high-resolution assumptions, independent of the source pdf [22, 86]. Therefore, using this quantizer for $A_\epsilon^{(L)}$ instead of a truly uniformly distributed source will not affect the distortion performance but it might affect the rate. However, since the bounded uniform distribution is entropy maximizing it follows that R_i upper bounds the rate of the quantizer. $\qquad\square$

Proof of Lemma 7.3.2. The two-channel distortion of a $(3,2)$ SCEC is given by

$$D^{(3,2)} \approx \frac{1}{2}\sigma_q^2(1+\rho_q), \tag{J.6}$$

where from (4.39) we see that

$$\sigma_q^2 = 2(1 - \rho_q)^{-1/3}(1 + 2\rho_q)^{-2/3}2^{-4R_b}. \tag{J.7}$$

Inserting (J.7) into (J.6) and setting the result equal to (7.21), i.e. we normalize such that the two-channel distortion of (3,2) SCECs is equal to that of (3,2) MD-LVQ. This leads to

$$(1 + \rho_q)(1 - \rho_q)^{-1/3}(1 + 2\rho_q)^{-2/3} = \frac{1}{12}\psi_\infty^4(N')^2, \tag{J.8}$$

from which we find that

$$(1 + 2\rho_q)^{1/3} = \left(\frac{1}{12}\psi_\infty^4(N')^2\right)^{-1/2}(1 + \rho_q)^{1/2}(1 - \rho_q)^{-1/6}. \tag{J.9}$$

It follows that we can write $D^{(3,3)}$ as

$$\begin{aligned}
D^{(3,3)} &= \frac{1}{3}\sigma_q^2(1 + 2\rho_q) \\
&= \frac{2}{3}(1 - \rho_q)^{-1/3}(1 + 2\rho_q)^{1/3}2^{-4R_b} \\
&= \frac{2}{3}(1 - \rho_q)^{-1/3}\sqrt{12}(1 + \rho_q)^{1/2}(1 - \rho_q)^{-1/6}\psi_\infty^{-2}(N')^{-1}2^{-4R_b} \\
&\approx \frac{\psi_\infty^2}{N'}2^{-4R_b}, \tag{J.10}
\end{aligned}$$

where the approximation follows by inserting $\rho \approx -1/2$. The proof is now complete since (J.10) is identical to (7.24). □

J.2   Proof of Theorem 7.3.1

Since $(3,2)$ MD-LVQ is closely related to $(3,2)$ SCECs we can to some extent use the proof techniques of [111]. However, there are some important differences. We cannot rely on random coding arguments since we are not using random codebooks. For example where [111] exploit properties of the entropy of subsets, we need to show that certain properties hold for all subsets and not just on average. Furthermore, we consider the asymmetric case where the individual codebook rates R_i and binning rates $R_{b,i}$ are allowed to be unequal whereas in [111] the symmetric case was considered, i.e. only a single codebook rate R_s and a single binning rate R_b was taken into account.

Theorem 7.3.1 *Let $X \in \mathbb{R}^L$ be a source vector constructed by blocking an arbitrary i.i.d. source with finite differential entropy into sequences of length L. Let $J \subseteq \{0, \ldots, K - 1\}$ and let λ_J denote the set of codewords indexed by J. The set of decoding functions is denoted $g_J \colon \bigotimes_{j \in J} \Lambda_j \to \mathbb{R}^L$. Then, under high-resolution assumptions, if*

$$E[\rho(X, g_J(\lambda_J))] \leq D^{(K,J)}, \quad \forall J \in \mathscr{K},$$

where $\rho(\cdot, \cdot)$ is the squared-error distortion measure and for all $S \subseteq J$

$$\sum_{i \in S} R_{b,i} > \sum_{i \in S} \gamma_i + \frac{1}{L} \log_2(|\{\lambda_S | \lambda_{J-S}\}|), \tag{J.11}$$

the rate-distortion tuple $(R_{b,0}, \ldots, R_{b,(K-1)}, \{D^{(K,J)}\}_{J \in \mathscr{K}})$ is achievable.

Proof of Theorem 7.3.1. Define the following error events.

1. $\mathscr{E}_0 : X$ does not belong to $A_\epsilon^{(L)}(X)$.

2. $\mathscr{E}_1 :$ There exists no indices $(j_0, \ldots, j_{K-1})$ such that $(\lambda_0(j_0), \ldots, \lambda_{K-1}(j_{K-1})) = \alpha(\lambda_c)$ for $\lambda_c = Q(X)$.

3. $\mathscr{E}_2 :$ Not all channel indices are valid.

4. $\mathscr{E}_3 :$ For some k received bin indices there exists another admissible k-tuple in the same bins.

As usual we have $\mathscr{E} = \bigcup_{i=0}^{K-1} \mathscr{E}_i$ and the probability of error is bounded from above by the union bound, i.e. $P(\mathscr{E}) \leq \sum_{i=0}^{K-1} P(\mathscr{E}_i)$.

Bounding $P(\mathscr{E}_0)$: Applying standard arguments for typical sequences it can be shown that $P(\mathscr{E}_0) \to 0$ for L sufficiently large [24]. We may now assume the event $\mathscr{E}_0^c$, i.e. all source vectors belong to the set of typical sequences and hence they are approximately uniformly distributed.

Bounding $P(\mathscr{E}_1)$: The source vector X is encoded by the central quantizer using a nearest neighbor rule. Since any source vector will have a closest element (which might not be unique) in $\mathscr{C}_c$ and by construction all $\lambda_c \in \mathscr{C}_c$ have an associated K-tuple of sublattice points, it follows that $P(\mathscr{E}_1) = 0$ for all L.

Bounding $P(\mathscr{E}_2)$: We only have to prove this for one of the channels. Then by symmetry it holds for all of them. Furthermore, since the intersection of a finite number of sets of probability 1 is 1 it follows that with probability 1 a codeword λ_i given λ_c can be found in some bin. In the following we assume $K < \infty$. Let λ_c be the codeword associated with X (i.e. X is quantized to λ_c), where $X \in A_\epsilon^{(L)}(X)$. Let A denote the event that $\lambda_0(j_0)$ exists in the codebook $\mathscr{C}_0$, i.e. the event $[\lambda_0(j_0) \in \mathscr{C}_0, \lambda_0(j_0) = \alpha_0(\lambda_c)]$. We then have that

$$\begin{aligned} P(f_0(\lambda_0(j_0)) \neq \vartheta) = &P(f_0(\lambda_0(j_0)) \neq \vartheta | A^c)P(A^c) \\ &+ P(f_0(\lambda_0(j_0)) \neq \vartheta | A)P(A), \end{aligned}$$

where the first term on the right hand side is zero if we make sure that all λ_c's are assigned a (unique) K-tuple. Therefore, we only have to look at the second term as was the case in [111]. We must show that $G = P[f_0(\lambda_0(j_0)) \neq \vartheta | A] \to 1$, i.e.

$$1 - G = P[\lambda_{0_j} \neq \lambda_0(j_0), 0 \leq j \leq M_0 - 1 | A], \tag{J.12}$$

where $M_0 = \xi_0 2^{LR_{b,0}} = 2^{L(R_0+\gamma_0)}$ is the total number of codewords selected for all bins from $\mathscr{C}_0$ and λ_{0_j} indicates the jth such selected codeword. Since the codewords λ_{0_j} are chosen independently (uniformly) and with replacement they all have the same probability of being equal to $\lambda_0(j_0)$, so we let $j = 0$ and rewrite (J.12) as

$$1 - G = [P(\lambda_{0_0} \neq \lambda_0(j_0)|A)]^{M_0}.$$

The size of $\mathscr{C}_0$ is $|\mathscr{C}_0|$ and all codewords of $\mathscr{C}_0$ are equally probable so

$$1 - G = \left(1 - \frac{1}{|\mathscr{C}_0|}\right)^{M_0}. \tag{J.13}$$

Taking logs and invoking the log-inequality[81], Eq. (J.13) can be rewritten as

$$\log(1 - G) \leq -\frac{M_0}{|\mathscr{C}_0|} = -\frac{2^{L(R_0+\gamma_0)}}{|\mathscr{C}_0|},$$

which goes to $-\infty$ for $L \to \infty$ if $R_0 + \gamma_0 > \frac{1}{L}\log_2(|\mathscr{C}_0|)$. By use of Lemma 7.3.1 we have $|C_0| = 2^{LR_0}$ so that $1 - G \to 0$ for $L \to \infty$ if $\gamma_0 > 0$.

Bounding $P(\mathscr{E}_3)$: Assume we receive k bin indices from the encoder. We then need to show that there is a unique set of codewords (one from each bin) which form an admissible k-tuple. Let $J = \{i_0, \ldots, i_{k-1}\}$. Along the lines of [111] we define the following error event for any $S \subseteq J$:

$$\mathscr{E}'_S : \exists j'_i \neq j_i, \forall i \in S, f_S(\lambda_S(j'_S)) = f_S(\lambda_S(j_S)),$$
$$(\lambda_S(j'_S), \lambda_{J-S}(j_{J-S})) = \alpha_J(\lambda_c), \quad \lambda_c \in C_c,$$

i.e. that there exist more than one admissible k-tuple in the given k bins. The event $\mathscr{E}_3$ can be expressed as $\mathscr{E}_3 = \bigcup_{S \subseteq J} \mathscr{E}'_S$. The probability of the error event $\mathscr{E}'_S$ can be upper bounded by

$$P(\mathscr{E}'_S) \leq \prod_{i \in S}(\xi_i - 1)P[(\lambda^*_S, \lambda_{J-S}(j_{J-S})) = \alpha_J(\lambda_c)],$$

for some λ_c, where λ^*_i is a randomly chosen vector from $\mathscr{C}_i$ for $i \in S$. Let $\{\lambda_S|\lambda_{J-S}\}$ denote the set of admissible k-tuples that contains λ_{J-S} so that

$$P[(\lambda^*_S, \lambda_{J-S}(j_{J-S})) = \alpha_J(\lambda_c)] < \frac{|\{\lambda_S|\lambda_{J-S}\}|}{\prod_{i \in S}|\mathscr{C}_i|}.$$

We are then able to bound $P(\mathscr{E}'_s)$ by

$$P(\mathscr{E}'_S) < \prod_{i \in S}\xi_i \frac{|\{\lambda_S|\lambda_{J-S}\}|}{\prod_{i \in S}|\mathscr{C}_i|}$$
$$= \prod_{i \in S}2^{L(\gamma_i - R_{b,i})}|\{\lambda_S|\lambda_{J-S}\}|,$$

---

[81]The log-inequality is given by $\log(z) \leq z - 1, z > 0$, where log denotes the natural logarithm.

which goes to zero if

$$\sum_{i \in S} R_{b,i} > \sum_{i \in S} \gamma_i + \frac{1}{L} \log_2(|\{\lambda_S|\lambda_{J-S}\}|). \tag{J.14}$$

Finally, the expected distortion is bounded by $P(\mathscr{E}^c)D_J + P(\mathscr{E})d_{\max}, \forall J \in \mathscr{K}$ where $P(\mathscr{E}) \to 0$ for $L \to \infty$ and assuming that the distortion measure is bounded, i.e. $d_{\max} < \infty$, proves the theorem.[82] $\qquad\square$

---

[82]We here make the assumption, as appears to be customary, that the distortion measure is bounded also for sources with unbounded support.

Appendix K

Results of Listening Test

In this appendix we present the results of the MUSHRA listening test described in Chapter 8.
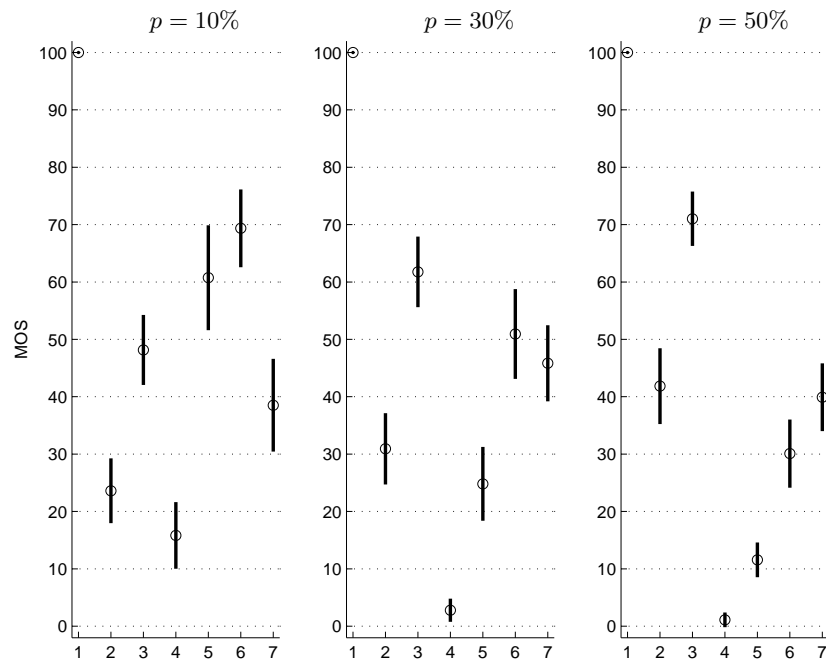
Figure K.1: *MUSHRA test results averaged over all three audio clips for $p = 0.1, 0.3$ and $p = 0.5$. The seven signals appear in the following order: Hidden ref., 3.5 kHz, 7 kHz, $K = 1, K = 2, K = 3$ and $K = 4$.*
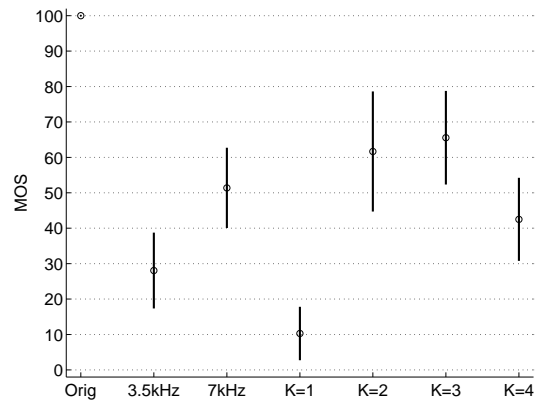
(a) $p = 0.1$
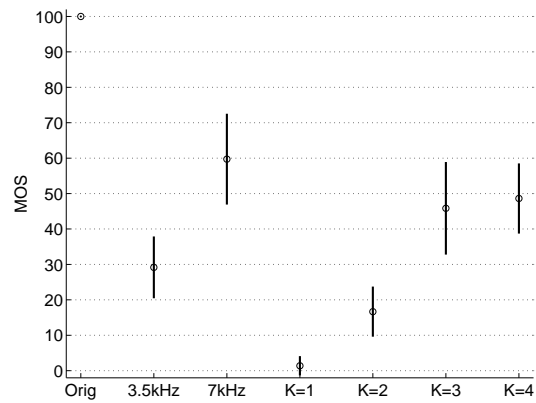
(b) $p = 0.3$
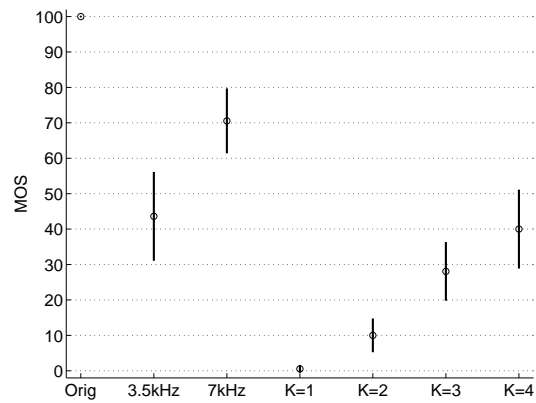
(c) $p = 0.5$

Figure K.2: *MUSHRA test results for the jazz fragment and $p = 0.1, 0.3$ and $p = 0.5$.*
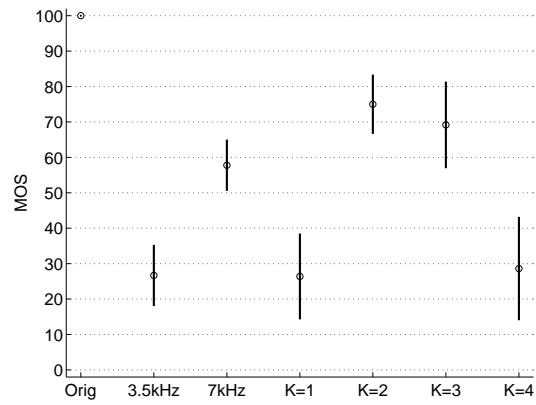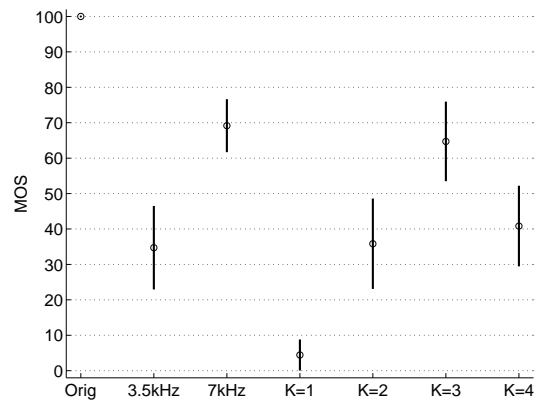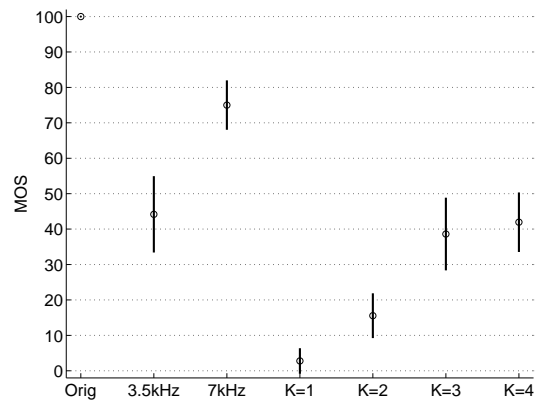
(a) $p = 0.1$

(b) $p = 0.3$

(c) $p = 0.5$

Figure K.3: *MUSHRA test results for the speech fragment and $p = 0.1, 0.3$ and $p = 0.5$.*
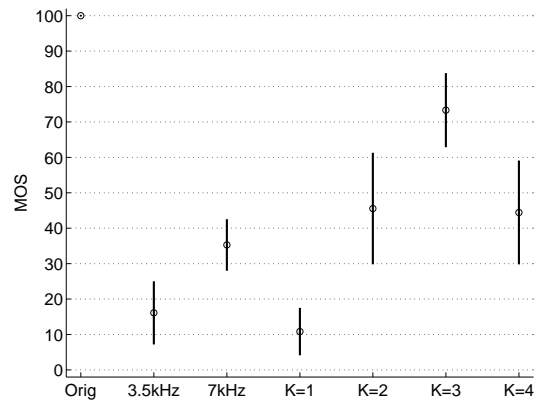
(a) $p = 0.1$
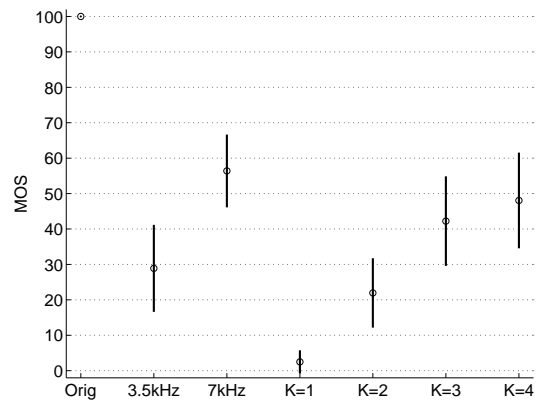
(b) $p = 0.3$
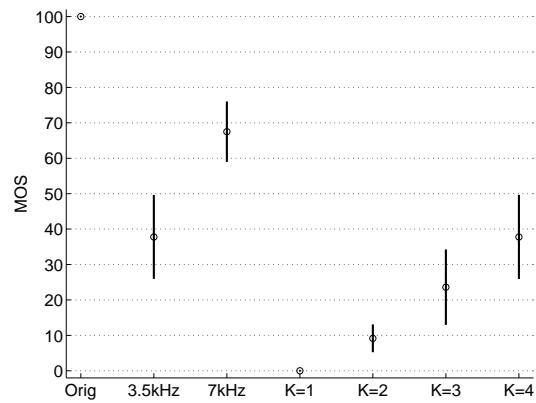
(c) $p = 0.5$

Figure K.4: *MUSHRA test results for the rock fragment and $p = 0.1, 0.3$ and $p = 0.5$.*

Samenvatting

Internetdiensten zoals het voice over Internet-protocol (VoIP) en audio/video streaming (b.v. video op verzoek en video vergaderen) worden steeds populairder door de recente groei van breedbandnetwerken. Dit soort "real-time" diensten vereisen vaak een lage verzendtijd, een hoge bandbreedte en een lage pakket-verlies kans om acceptabele kwaliteit voor de eindgebruikers te leveren. De heterogene communicatie infrastructuur van de huidige pakketgeschakelde netwerken verschaffen echter geen gegarandeerde prestaties met betrekking tot bandbreedte of verzendtijd en daarom wordt de gewenste kwaliteit over het algemeen niet bereikt.

Om een bepaalde mate van robuustheid te bereiken op kanalen waarop fouten kunnen voorkomen, kan multiple-description (MD) coding toegepast worden. Dit is een methode waar de laatste tijd erg veel aandacht aan is besteed. Het MD probleem is in wezen een gecombineerd bron-kanaal coderingsprobleem dat gaat over (het met verlies) coderen van informatie voor transmissie over een onbetrouwbaar K-kanalen communicatie systeem. De kanalen kunnen falen, met als resultaat het verlies van een pakket en daardoor een verlies van informatie aan de ontvangende kant. Welke van de $2^K - 1$ niet-triviale deelverzamelingen van de K kanalen falen, wordt bekend verondersteld aan de ontvangende kant, maar niet bij de encoder. Het probleem is dan een MD schema te ontwerpen dat, voor gegeven kanaal rate (of een gegeven som rate), de distorsies minimaliseert die een gevolg zijn van reconstruering van de bron, gebruik makend van informatie van willekeurige deelverzamelingen van de kanalen.

Hoewel wij ons in dit proefschrift hoofdzakelijk richten op de informatie theoretische aspecten van MD codering, zullen we voor de volledigheid ook laten zien hoe het voorgestelde MD coderingsschema kan worden gebruikt om een perceptueel robuuste audio coder te construeren, die geschikt is voor b.v. audio-streaming op pakketgeschakelde netwerken.

We richten ons op het MD probleem vanuit een bron-codering standpunt en bekijken het algemene geval van K pakketten. We maken uitgebreid gebruik van

223

lattice vector kwantisatie (LVQ) theorie, hetgeen een goed instrument blijkt, in de zin dat het voorgestelde MD-LVQ schema als brug tussen theorie en praktijk dient. Voor asymptotische gevallen van hoge resolutie en grote lattice vector kwantisator dimensie, tonen wij aan dat de beste bekende informatie theoretische rate-distorsie MD grenzen kunnen worden bereikt, terwijl we, in niet asymptotische gevallen van eindig-dimensionale lattice vector kwantisators (maar nog onder hoge resolutie veronderstelling), praktische MD-LVQ schemas construeren, die vergelijkbaar met en vaak superieur zijn aan bestaande state-of-the-art schemas.

In het twee-kanaal symmetrische geval is eerder aangetoond dat de zij-representaties van een MD-LVQ schema zij-distorsies toelaten, die (bij hoge resolutie voorwaarden) identiek zijn aan die van L-dimensionale kwantisators met bolvormige Voronoi cellen. In dit geval zeggen wij dat de zij-kwantisators de L-bol grens bereikt. Een dergelijk resultaat is niet eerder aangetoond voor het twee-kanaal asymmetrische geval. Het voorgestelde MD-LVQ schema is echter in staat de L-bol grens te bereiken, bij hoge resolutie voorwaarden, voor zowel het symmetrische geval als het asymmetrische geval.

Het voorgestelde MD-LVQ schema schijnt een van de eerste schemas in de literatuur te zijn die het grootst bekende hoge resolutie drie-kanaal MD gebied in het kwadratische Gaussische geval bereikt. Hoewel de optimaliteit alleen voor $K \leq 3$ wordt bewezen, nemen we aan dat het optimaal is voor willekeurige K representaties.

We laten gesloten-vorm uitdrukkingen zien voor de rate en distorsie prestaties voor algemene gladde stationaire bronnen en een kwadratische-fout distorsie criterium en voor hoge resolutie voorwaarden (ook voor eindig-dimensionale lattice vector kwantisators). Er wordt aangetoond dat de zij-distorsies in het drie-kanaal geval kan worden uitgedrukt in het dimensieloze, genormaliseerde, tweede moment van een L-bol, onafhankelijk van het type lattice dat wordt gebruikt voor de zij-kwantisators. Dit komt overeen met eerdere resultaten voor het geval van twee representaties.

Het rate verlies wanneer eindig-dimensionale lattice vector kwantisators gebruikt worden is onafhankelijk van het lattice en wordt gegeven door het rate verlies van een L-bol en een bijkomende term die de ratio van twee dimensieloze expansie factoren beschrijft. Er wordt aangetoond dat het totale rate verlies superieur is aan bestaande drie-kanaal schemas. Dit resultaat lijkt te gelden voor elk aantal representaties.

Curriculum Vitae

Jan Østergaard was born in Frederikshavn, Denmark, in 1974. He obtained his high school diploma at Frederikshavns Tekniske Skole (HTX) in Frederikshavn in 1994. In 1999 he received the M.Sc. degree in Electrical Engineering at Aalborg University, Denmark. From 1999 to 2002 he worked as a researcher in the area of signal analysis and classification at ETI A/S in Aalborg, Denmark. From 2002 to 2003 he worked as a researcher at ETI US in Virginia, United States. In February 2003, he started as a Ph.D. student in the Information and Communication Theory group at Delft University of Technology, Delft, The Netherlands. During the period June 2006 – September 2006 he was a visiting researcher in the department of Electrical Engineering-Systems at Tel Aviv University, Tel Aviv, Israel.

Glossary of Symbols and Terms

Symbol	Description
$\mathbb{R}^L$	L-dimensional Euclidean space (real field)
$\mathbb{C}^L$	L-dimensional complex field
$\mathbb{Z}^L$	L-dimensional set of all rational integers
$\mathscr{G}$	Gaussian integers
$\mathscr{Q}$	Algebraic integers
$\mathscr{E}$	Eisenstein integers
$\mathscr{H}_0$	Lipschitz integers
$\mathscr{H}_1$	Hurwitzian integers
x^H	Hermitian transposition (conjugate transposition)
$x^\dagger$	Quaternionic transposition (Quaternionic conjugate transposition)
$\mathscr{J}$	$\mathscr{J}$-module ($\mathscr{J}$-lattice)
$\|X\|$	Vector norm with respect to underlying field
$\langle X, X \rangle$	Inner product

Table K.1: *Algebra-related symbols.*

Symbol	Description
X	Scalar random process or L-dimensional random vector ($X \in \mathbb{R}^L$)
x	L-dimensional vector (realization of X)
f_X	Distribution of X
$\hat{X}$	Reconstruction of X
$\mathscr{X}$	Alphabet of X (usually $\mathscr{X} = \mathbb{R}^L$)
$\hat{\mathscr{X}}$	Alphabet of $\hat{X}$ (usually $\hat{\mathscr{X}} \subset \mathbb{R}^L$)
ρ	Fidelity criterion (usually squared-error)
$R(D)$	Rate-distortion function
$D(R)$	Distortion-rate function
$I(\cdot;\cdot)$	Mutual information
$h(\cdot)$	Differential entropy
$\bar{h}(\cdot)$	Differential entropy rate
$H(\cdot)$	Discrete entropy
E	Statistical expectation operator
R_{SLB}	Shannon lower bound
R_{Loss}	Rate loss
R^*_{red}	Rate redundancy
D_{Loss}	Space-filling loss
σ^2_X	Variance of X
P_X	Entropy power
$Q(X)$	Quantization of X

Table K.2: *Source-coding related symbols.*

Symbol	Description
Λ_c	Central lattice (central quantizer)
Λ_s	Sublattice $\Lambda_s \subseteq \Lambda_c$ (side quantizer in symmetric case)
Λ_i	Sublattice $\Lambda_i \subseteq \Lambda_c$ (side quantizer in asymmetric case)
Λ_π	Product lattice $\Lambda_\pi \subset \Lambda_i$ or $\Lambda_\pi \subset \Lambda_s$
Λ_c/Λ_π	Quotient lattice
V_c	Voronoi cell of Λ_c
V	Voronoi cell of Λ_s or Λ_i
ν	Volume of Voronoi cell of Λ_c
ν_s	Volume of Voronoi cell of Λ_s
ν_i	Volume of Voronoi cell of Λ_i
ν_π	Volume of Voronoi cell of Λ_π
N	Index value of sublattice Λ_s ($N = |\Lambda_c/\Lambda_s|$)
N_i	Index value of sublattice Λ_s ($N_i = |\Lambda_c/\Lambda_i|$)
N_π	Index value of product lattice Λ_π ($N_\pi = |\Lambda_c/\Lambda_\pi|$)
N'	Nesting ratio of Λ_s (index per dimension)
$G(\Lambda)$	Dimensionless normalized second moment of Λ
$G(S_L)$	Dimensionless normalized second moment of L-sphere
ζ_i	Basis vector (lattice generator vector)
M	Lattice generator matrix
A	Gram matrix
Γ_m	Multiplicative group of automorphisms of order m
$\Lambda_c/\Lambda_\pi/\Gamma_m$	Set of orbit representatives
Z^1	Scalar lattice (uniform lattice)
Z^2	Square lattice
Z^L	Hypercubic lattice
A_2	Hexagonal two-dimensional lattice
D_4	Four dimensional (checker board) lattice
$\xi\Lambda_c$	Sublattice of Λ_c (cyclic right submodule)
$\Lambda_c\xi$	Sublattice of Λ_c (cyclic left submodule)
$\mathfrak{K}(\Lambda)$	Kissing number of Λ

Table K.3: *Lattice-related symbols.*

Symbol	Description
α	Index assignment map ($\alpha(\lambda_c) = (\lambda_0, \ldots, \lambda_{K-1})$)
α^{-1}	Inverse index assignment map
α_i	Component function ($\lambda_i = \alpha_i(\lambda_c)$)
K	Number of descriptions
κ	Number of received descriptions
$\tilde{V}$	L-dimensional sphere
$\tilde{\nu}$	Volume of $\tilde{V}$
$\tilde{N}_i$	Number of lattice points of Λ_i within $\tilde{V}$
ψ_L	Dimensionless expansion factor
ω_L	Volume of unit L-sphere
R_s	Description rate [bit/dim.] in symmetric setup
R_i	Description rate [bit/dim.] of ith description
R_c	Rate of central quantizer
R_T	Sum rate ($R_T = \sum R_i$)
D_i	Side distortion of ith description
D_c	Central distortion
$D^{(K,\kappa)}$	Distortion due to reconstructing using κ descriptions out of K
$J^{(K)}$	Cost functional
p	Packet-loss probability
$\mathscr{L}^{(K,\kappa)}$	Index set describing all distinct κ-tuples out of the set $\{0, \ldots, K-1\}$
$\mathscr{L}_i^{(K,\kappa)}$	Index set describing all distinct κ-tuples out of the set $\{0, \ldots, K-1\}$, which contains the index i
$\mathscr{L}_{i,j}^{(K,\kappa)}$	Index set describing all distinct κ-tuples out of the set $\{0, \ldots, K-1\}$, which contains the pair of indices (i,j)
$p(\mathscr{L}_{i,j}^{(K,\kappa)})$	Probability of the set $\mathscr{L}_{i,j}^{(K,\kappa)}$
$D_a^{(K,\kappa)}$	Expected distortion when receiving κ out of K descriptions based on the packet-loss probability
$D^{(K,l)}$	Distortion due to reconstructing using the subset of descriptions $l \subseteq \{0, \ldots, K-1\}$
MD-LVQ	Multiple-description lattice vector quantization
SCEC	Source-channel erasure code
SPSD	Sum of pairwise squared distances
WSPSD	Weighted sum of pairwise squared distances

Table K.4: *MD-LVQ related symbols and terms.*

Bibliography

[1] W. A. Adkins and S. H. Weintraub. *Algebra an Approach via Module Theory*. Springer-Verlag, 1992.

[2] R. Ahlswede. The rate-distortion region for multiple-descriptions without excess rate. *IEEE Trans. Inf. Theory*, IT-31:721 – 726, November 1985.

[3] R. Arean, J. Kovačević, and V. K. Goyal. Multiple description perceptual audio coding with correlating transform. *IEEE Trans. Speech Audio Processing*, 8(2):140 – 145, March 2000.

[4] R. Balan, I. Daubechies, and V. Vaishampayan. The analysis and design of windowed fourier frame based multiple description source coding schemes. *IEEE Trans. Inf. Theory*, 46(7):2491 – 2536, November 2000.

[5] J.-C. Batllo and V. A. Vaishampayan. Asymptotic performance of multiple description transform codes. *IEEE Trans. Inf. Theory*, 43(2):703 – 707, March 1997.

[6] W. E. Baylis and G. Jones. The Pauli algebra approach to special relativity. *J. Phys. A: Math. Gen.*, 22:1 – 15, January 1989.

[7] W. R. Bennett. Spectra of quantized signals. *Bell System Technical Journal*, 27:446 – 472, July 1948.

[8] T. Berger. *Rate distortion theory, a mathematical basis for data compression*. Prentice-Hall, 1971.

[9] T. Berger and J. D. Gibson. Lossy source coding. *IEEE Trans. Inf. Theory*, 44(6):2693 – 2723, October 1998.

[10] T. Y. Berger-Wolf and E. M. Reingold. Index assignment for multichannel communication under failure. *IEEE Trans. Inf. Theory*, 48(10):2656 – 2668, October 2002.

[11] J. Bokowski and A. M. Odlyzko. Lattice points and the volume/area ratio of convex bodies. *Geometriae Dedicata*, 2:249 – 254, 1973.

[12] M. Bosi and R. E. Goldberg. *Introduction to digital audio coding and standards*. Kluwer Academic Publishers, 2003.

[13] R. H. Buchholz. Perfect pyramids. *Bulletin Australian Mathematical Society*, 45(3), 1992.

[14] A R. Calderbank, S. Das, N. Al-Dhahir, and S N. Diggavi. Construction and analysis of a new quaternionic space-time code for 4 transmit antennas. *Communications in Information and Systems*, 2005.

[15] J. Cardinal. Entropy-constrained index assignments for multiple description quantizers. *IEEE Trans. Signal Proc.*, 52(1):265 – 270, January 2004.

[16] J. Chen, C. Tian, T. Berger, and S. Hemami. Achieving the multiple description rate-distortion region with lattice quantization. In *Proc. Conf. Information Sciences and Systems*, 2005.

[17] J. Chen, C. Tian, T. Berger, and S. S. Hemami. A new class of universal multiple description lattice quantizers. In *Proc. IEEE Int. Symp. Information Theory*, pages 1803 – 1807, Adelaide, Australia, September 2005.

[18] J. Chen, C. Tian, T. Berger, and S. S. Hemami. Multiple description quantization via Gram-Schmidt orthogonalization. *IEEE Trans. Inf. Theory*, 52(12):5197 – 5217, December 2006.

[19] P. A. Chou, T. Lookabaugh, and R. M. Gray. Entropy-constrained vector quantization. *IEEE Trans. Acoust., Speech, and Signal Proc.*, 37(1):31 – 42, January 1989.

[20] P. A. Chou, S. Mehrotra, and A. Wang. Multiple description decoding of overcomplete expansions using projections onto convex sets. In *Proc. Data Compression Conf.*, pages 72 – 81, March 1999.

[21] J. H. Conway, E. M. Rains, and N. J. A. Sloane. On the existence of similar sublattices. *Canadian Jnl. Math.*, 51:1300 – 1306, 1999.

[22] J. H. Conway and N. J. A. Sloane. *Sphere packings, Lattices and Groups*. Springer, 3rd edition, 1999.

[23] J. H. Conway and D. A. Smith. *On Quaternions and Octonions*. AK Peters, 2003.

[24] T. M. Cover and J. A. Thomas. *Elements of information theory*. Wiley, 1991.

[25] H. S. M. Coxeter. *Regular polytopes*. Dover, 1973.

[26] I. Csiszár and J. Körner. *Information Theory: Coding Theorems for Discrete Memoryless Systems*. Academic Press, New York, 1981.

[27] S. N. Diggavi, N. J. A. Sloane, and V. A. Vaishampayan. Design of asymmetric multiple description lattice vector quantizers. In *Proc. Data Compression Conf.*, pages 490 – 499, March 2000.

[28] S. N. Diggavi, N. J. A. Sloane, and V. A. Vaishampayan. Asymmetric multiple description lattice vector quantizers. *IEEE Trans. Inf. Theory*, 48(1):174 – 191, January 2002.

[29] P. L. Dragotti, J. Kovačević, and V. K. Goyal. Quantized oversampled filter banks with erasures. In *Proc. Data Compression Conf.*, pages 173 – 182, March 2001.

[30] W. Ebeling. *Lattices and Codes*. Friedr. Vieweg & Sohn, 1994.

[31] B. Edler and G. Schuller. Audio coding using a psychoacoustic pre- and post-filter. In *Proc. IEEE Int. Conf. Acoustics, Speech, and Signal Processing*, volume II, pages 881 – 884, 2000.

[32] W. H. R. Equitz and T. M. Cover. Successive refinement of information. *IEEE Trans. Inf. Theory*, 37(2):269 – 275, March 1991.

[33] P. Erdös, P. M. Gruber, and J. Hammer. *Lattice points*, volume 39 of *Pitman Monographs and Surveys in Pure and Applied Mathematics*. John Wiley & Sons, New York, 1989.

[34] T. Ericson and V. Zinoviev. *Codes on Euclidean Spheres*. North-Holland, May 2001.

[35] H. Feng and M. Effros. On the rate loss of multiple description source codes. *IEEE Trans. Inf. Theory*, 51(2):671 – 683, February 2005.

[36] M. Fleming and M. Effros. Generalized multiple description vector quantization. In *Proc. Data Compression Conf.*, March 1999.

[37] M. Fleming, Q. Zhao, and M. Effros. Network vector quantization. *IEEE Trans. Inf. Theory*, 50(8):1584 – 1604, August 2004.

[38] G. David Forney. On the duality of coding and quantization. In R. Calderbank, G. D. Forney Jr., and N. Moayeri, editors, *DIMACS*, volume 14 of *Series in Discrete Mathematics and Theoretical Computer Science*, pages 1 – 14. American Mathematical Society, 1993.

[39] Y. Frank-Dayan and R. Zamir. Dithered lattice-based quantizers for multiple descriptions. *IEEE Trans. Inf. Theory*, 48(1):192 – 204, January 2002.

[40] F. Fricker. *Einführung in die gitterpunktlehre*. Birkhäuser, 1982.

[41] R. G. Gallager. *Information Theory and Reliable Communication*. New-York: Wiley, 1968.

[42] A. A. El Gamal and T. M. Cover. Achievable rates for multiple descriptions. *IEEE Trans. Inf. Theory*, IT-28(6):851 – 857, November 1982.

[43] W. R. Gardner and B. D. Rao. Theoretical analysis of the high-rate vector quantization of LPC parameters. *IEEE Trans. Speech Audio Processing*, pages 367 – 381, September 1995.

[44] A. Gersho. Asymptotically optimal block quantization. *IEEE Trans. Inf. Theory*, IT-25:373 – 380, July 1979.

[45] A. Gersho and R. M. Gray. *Vector Quantization and Signal Compression*. Kluwer Academic Publishers, 1992.

[46] J. D. Gibson and K. Sayood. Lattice quantization. *Advances in Electronics and Electron Physics*, 72:259 – 330, 1988.

[47] H. Gish and J. Pierce. Asymptotically efficient quantizing. *IEEE Trans. Inf. Theory*, 14(5):676 – 683, September 1968.

[48] N. Görtz and P. Leelapornchai. Optimization of the index assignments for multiple description vector quantizers. *IEEE Trans. Commun.*, 51(3):336 – 340, March 2003.

[49] V. Goyal, J. Kovačević, and J. Kelner. Quantized frame expansions with erasures. *Journal of Appl. and Comput. Harmonic Analysis*, 10(3):203–233, May 2001.

[50] V. K. Goyal. Multiple description coding: Compression meets the network. *IEEE Signal Processing Mag.*, 18(5):74 – 93, September 2001.

[51] V. K. Goyal, J. A. Kelner, and J. Kovačević. Multiple description vector quantization with a coarse lattice. *IEEE Trans. Inf. Theory*, 48(3):781 – 788, March 2002.

[52] V. K. Goyal and J. Kovačević. Generalized multiple descriptions coding with correlating transforms. *IEEE Trans. Inf. Theory*, 47(6):2199 – 2224, September 2001.

[53] V. K. Goyal, J. Kovačević, and M. Vetterli. Multiple description transform coding: Robustness to erasures using tight frame expansions. In *Proc. IEEE Int. Symp. Information Theory*, page 408, August 1998.

[54] V. K. Goyal, J. Kovačević, and M. Vetterli. Quantized frame expansions as source channel codes for erasure channels. In *Proc. Data Compression Conf.*, pages 326 – 335, March 1999.

[55] V. K. Goyal, M. Vetterli, and N. T. Thao. Quantized overcomplete expansions in R^N: analysis, synthesis, and algorithms. *IEEE Trans. Inf. Theory*, 44(1):16 – 31, January 1998.

[56] R. L. Graham, D. E. Knuth, and O. Patashnik. *Concrete mathematics*. Addison-Wesley, 2nd edition, 1994.

[57] R. M. Gray. *Source Coding Theory*. Kluwer Academic Publishers, 1990.

[58] R. M. Gray and T. Linder. Results and conjectures on high rate quantization. In *Proc. Data Compression Conf.*, pages 3 – 12, March 2004.

[59] R. M. Gray, T. Linder, and J. Li. A Lagrangian formulation of zador's entropy-constrained quantization theorem. *IEEE Trans. Inf. Theory*, 48(3):695 – 707, March 2002.

[60] R. M. Gray and D. Neuhoff. Quantization. *IEEE Trans. Inf. Theory*, 44(6):2325 – 2383, 1998.

[61] Pierre Grillet. *Algebra*. John Wiley & Sons, 1999.

[62] P. M. Gruber and C. G. Lekkerkerker. *Geometry of numbers*. North-Holland, 2nd edition, 1987.

[63] A. György and T. Linder. A note on the existence of optimal entropy-constrained vector quantizers. In *Proc. IEEE Int. Symp. Information Theory*, page 37, June 2002.

[64] A. György, T. Linder, P. A. Chou, and B. J. Betts. Do optimal entropy-constrained quantizers have a finite or infinite number of codewords? *IEEE Trans. Inf. Theory*, 49(11):3031 – 3037, November 2003.

[65] X. Huang and X. Wu. Optimal index assignment for multiple description lattice vector quantization. In *Proc. Data Compression Conf.*, Snowbird, Utah, March 2006.

[66] Radiocommunication Sector BS.1534-1 International Telecommunications Union. Method for the subjective assessment of intermediate quality level coding systems (MUSHRA), January 2003.

[67] H. Jafarkhani and V. Tarokh. Multiple description trellis-coded quantization. *IEEE Trans. Commun.*, 47(6):799 – 803, June 1999.

[68] N. S. Jayant. Subsampling of a DPCM speech channel to provide two self-contained, half-rate channels. *Bell Syst. Tech. Jour.*, 60:501 – 509, April 1981.

[69] Alan Jeffrey and Daniel Zwillinger, editors. *Table of integrals, series, and products*. Academic Press, 6th edition, July 2000.

[70] P. Kabel. An examination and interpretation of ITU-R BS.1387: Perceptual evaluation of audio quality. TSP Lab Technical Report, Dept. Electrical & Computer Engineering, McGill University, May 2002.

[71] I. L. Kantor and A.S. Solodovnikov. *Hypercomplex numbers; an elementary introduction to algebras*. Springer-verlag, 1989.

[72] M. E. Keating. *A first course in module theory*. Imperial College Press, 1998.

[73] J. A. Kelner, V. K. Goyal, and J. Kovačević. Multiple description lattice vector quantization: Variations and extensions. In *Proc. Data Compression Conf.*, pages 480 – 489, March 2000.

[74] J. C. Kieffer. A survey of the theory of source coding with a fidelity criterion. *IEEE Trans. Inf. Theory*, 39(5):1473 – 1490, September 1993.

[75] P. Koulgi, S. L. Regunathan, and K. Rose. Multiple description quantization by deterministic annealing. *IEEE Trans. Inf. Theory*, 49(8):2067 – 2075, August 2003.

[76] J. Kovačević, P. L. Dragotti, and V. K. Goyal. Filter bank frame expansions with erasures. *IEEE Trans. Inf. Theory*, 48(6):1439 – 1450, June 2002.

[77] E. Krätzel. *Lattice points*. Kluwer Academic Publisher, 1988.

[78] H. W. Kuhn. The Hungarian method for the assignment problem. In *Naval Research Logistics Quaterly*, volume 2, pages 83 – 97, 1955.

[79] L. A. Lastras-Montaño and V. Castelli. Near sufficiency of random coding for two descriptions. *IEEE Trans. Inf. Theory*, 52(2):681 – 695, February 2006.

[80] J. Li, N. Chaddha, and R. M. Gray. Asymptotic performance of vector quantizers with a perceptual distortion measure. *IEEE Trans. Inf. Theory*, 45(4):1082 – 1091, May 1999.

[81] Y. Linde, A. Buzo, and R. M. Gray. An algorithm for vector quantizer design. *IEEE Trans. Commun.*, 28(1):84 – 95, January 1980.

[82] T. Linder and R. Zamir. On the asymptotic tightness of the Shannon lower bound. *IEEE Trans. Inf. Theory*, 40(6):2026 – 2031, November 1994.

[83] T. Linder and R. Zamir. High-resolution source coding for non-difference distortion measures: the rate-distortion function. *IEEE Trans. Inf. Theory*, 45(2):533 – 547, march 1999.

[84] T. Linder, R. Zamir, and K. Zeger. The multiple description rate region for high resolution source coding. In *Proc. Data Compression Conf.*, pages 149 – 158, March 1998.

[85] T. Linder, R. Zamir, and K. Zeger. High-resolution source coding for non-difference distortion measures: multidimensional companding. *IEEE Trans. Inf. Theory*, 45(2):548 – 561, march 1999.

[86] T. Linder and K. Zeger. Asymptotic entropy-constrained performance of tesselating and universal randomized lattice quantization. *IEEE Trans. Inf. Theory*, 40(2):575 – 579, March 1994.

[87] S. P. Lloyd. Least squares quantization in PCM. Unpublished Bell Laboratories technical note, 1957.

[88] S. P. Lloyd. Least squares quantization in PCM. *IEEE Trans. Inf. Theory*, IT-28(2):127 – 135, March 1982.

[89] D. G. Luenberger. *Optimization by vector space methods*. John Wiley and Sons, Inc., 1 edition, 1997.

[90] H. S. Malvar. *Signal processing with lapped transforms*. Artech House, 1992.

[91] D. Marco and D. L. Neuhoff. Low-resolution scalar quantization for Gaussian sources and squared error. *IEEE Trans. Inf. Theory*, 52(4):1689 – 1697, April 2006.

[92] J. E. Mazo and A. M. Odlyzko. Lattice points in high-dimensional spheres. *Monatsh. Math.*, 110:47 – 61, 1990.

[93] International Standard ISO/IEC 11172-3 (MPEG). Information technology - coding of moving pictures and associated audio for digital storage media at up to about 1.5 mbit/s. part 3: Audio, 1993.

[94] International Standard ISO/IEC 13818-7 (MPEG). Information technology - generic coding of moving pictures and associated audio, part 7: Advanced audio coding, 1997.

[95] O. A. Niamut. *Rate-distortion optimal time-frequency decompositions for MDCT-based audio coding*. PhD thesis, Delft University of Technology, November 2006.

[96] O. Niemeyer and B. Edler. Efficient coding of excitation patterns combined with a transform audio coder. In *Proc. of the 118th AES Conv.*, Barcelona, Spain, May 2005.

[97] M. T. Orchard, Y. Wang, V. Vaishampayan, and A. R. Reibman. Redundancy rate-distortion analysis of multiple description coding using pairwise correlating transforms. In *Proc. IEEE Conf. on Image Proc.*, volume 1, pages 608 – 611, 1997.

[98] J. Østergaard, R. Heusdens, and J. Jensen. n-channel asymmetric entropy-constrained multiple-description lattice vector quantization. *IEEE Trans. Inf. Theory*, 2005. Submitted.

[99] J. Østergaard, R. Heusdens, and J. Jensen. n-channel asymmetric multiple-description lattice vector quantization. In *Proc. IEEE Int. Symp. Information Theory*, pages 1793 – 1797, September 2005.

[100] J. Østergaard, R. Heusdens, and J. Jensen. On the bit distribution in asymmetric multiple-description coding. In *26th Symposium on Information Theory in the Benelux*, pages 81 – 88, May 2005.

[101] J. Østergaard, R. Heusdens, and J. Jensen. On the rate loss in perceptual audio coding. In *Proc. of IEEE BENELUX/DSP Valley Signal Processing Symposium*, pages 27 – 30, Antwerpen, Belgium, 2006.

[102] J. Østergaard, R. Heusdens, and J. Jensen. Source-channel erasure codes with lattice codebooks for multiple description coding. In *Proc. IEEE Int. Symp. Information Theory*, pages 2324 – 2328, July 2006.

[103] J. Østergaard, J. Jensen, and R. Heusdens. Entropy constrained multiple description lattice vector quantization. In *Proc. IEEE Int. Conf. Acoustics, Speech, and Signal Processing*, volume 4, pages 601 – 604, May 2004.

[104] J. Østergaard, J. Jensen, and R. Heusdens. n-channel symmetric multiple-description lattice vector quantization. In *Proc. Data Compression Conf.*, pages 378 – 387, March 2005.

[105] J. Østergaard, J. Jensen, and R. Heusdens. n-channel entropy-constrained multiple-description lattice vector quantization. *IEEE Trans. Inf. Theory*, 52(5):1956 – 1973, May 2006.

[106] J. Østergaard, O. A. Niamut, J. Jensen, and R. Heusdens. Perceptual audio coding using n-channel lattice vector quantization. In *Proc. IEEE Int. Conf. Acoustics, Speech, and Signal Processing*, volume 5, pages 197 – 200, May 2006.

[107] L. Ozarow. On a source-coding problem with two channels and three receivers. *Bell System Technical Journal*, 59:1909 – 1921, December 1980.

[108] Method for the objective measurements of perceived audio quality. ITU-R BS. 1387, 1998.

[109] S. S. Pradhan, R. Puri, and K. Ramchandran. MDS source-channel erasure codes. In *Proc. IEEE Int. Symp. Information Theory*, June 2001. Special session on new results.

[110] S. S. Pradhan, R. Puri, and K. Ramchandran. (n, k) source-channel erasure codes: Can parity bits also refine quality? In *Conference on Information Sciences and Systems*, March 2001.

[111] S. S. Pradhan, R. Puri, and K. Ramchandran. n-channel symmetric multiple descriptions–part I: (n, k) source-channel erasure codes. *IEEE Trans. Inf. Theory*, 50(1):47 – 61, January 2004.

[112] R. Puri, S. S. Pradhan, and K. Ramchandran. n-channel multiple descriptions: Theory and constructions. In *Proc. Data Compression Conf.*, pages 262 – 271, March 2002.

[113] R. Puri, S. S. Pradhan, and K. Ramchandran. n-channel symmetric multiple descriptions: New rate regions. In *Proc. IEEE Int. Symp. Information Theory*, page 93, June 2002.

[114] R. Puri, S. S. Pradhan, and K. Ramchandran. n-channel symmetric multiple descriptions- part II: An achievable rate-distortion region. *IEEE Trans. Inf. Theory*, 51(4):1377 – 1392, April 2005.

[115] E. D. Rainville. *Special functions*. The Macmillan company, 1960.

[116] D. O. Reudink. The channel splitting problem with interpolative coders. Technical Report TM80-134-1, Bell Labs, October 1980.

[117] R. T. Rockafellar. *Convex analysis*. Princeton University Press, 1970.

[118] D. J. Sakrison. The rate distortion function of a Gaussian process with a weighted square error criterion. *IEEE Trans. Inf. Theory*, IT-14:506 – 508, May 1968.

[119] G. Schuller, J. Kovačević, F. Masson, and V. K. Goyal. Robust low-delay audio coding using multiple descriptions. *IEEE Trans. Speech Audio Processing*, 13(5), September 2005.

[120] S. D. Servetto, V. A. Vaishampayan, and N. J. A. Sloane. Multiple description lattice vector quantization. In *Proc. Data Compression Conf.*, pages 13 – 22, March 1999.

[121] C. E. Shannon. A mathematical theory of communication. *Bell Syst. Tech. Journal*, 27:379 – 423; 623 – 656, July and October 1948.

[122] C. E. Shannon. Coding theorems for a discrete source with a fidelity criterion. In *IRE Conv. Rec.*, volume 7, pages 142 – 163, 1959.

[123] D. Sinha, J. D. Johnston, S. Dorward, and S. Quackenbush. The perceptual audio coder (PAC). In *The digital signal processing handbook*. New York: IEEE Press, 1998.

[124] D. Slepian and J. K. Wolf. Noiseless coding of correlated information sources. *IEEE Trans. Inf. Theory*, IT-19:471 – 480, 1973.

[125] N. J. A. Sloane. On-line encyclopedia of integer sequences. Published electronically at http://www.research.att.com/˜njas/sequences, 2006.

[126] H. Stark and J. W. Woods. *Probability, random processes, and estimation theory for engineers*. Prentice-Hall, 1986.

[127] J. Østergaard and R. Zamir. Multiple-description coding by dithered delta-sigma quantization. In *Proc. Data Compression Conf.*, pages 63 – 72, March 2007.

[128] R. K. Sundaram. *A first course in optimization theory*. Cambridge university press, 1999.

[129] C. Tian and S. S. Hemami. Optimality and suboptimality of multiple-description vector quantization with a lattice codebook. *IEEE Trans. Inf. Theory*, 50(10):2458 – 2470, October 2004.

[130] C. Tian and S. S. Hemami. Sequential design of multiple description scalar quantizers. In *Proc. Data Compression Conf.*, pages 32 – 41, March 2004.

[131] C. Tian and S. S. Hemami. Universal multiple description scalar quantization: analysis and design. *IEEE Trans. Inf. Theory*, 50(9):2089 – 2102, September 2004.

[132] C. Tian and S. S. Hemami. Staggered lattices in multiple description quantization. In *Proc. Data Compression Conf.*, pages 398 – 407, March 2005.

[133] User datagram protocol: RFC-768. http://www.rfc-editor.org.

[134] Ogg Vorbis open-source audio codec. Published electronically at: http://www.vorbis.com.

[135] V. A. Vaishampayan. Design of multiple description scalar quantizers. *IEEE Trans. Inf. Theory*, 39(3):821 – 834, May 1993.

[136] V. A. Vaishampayan and J.-C. Batllo. Asymptotic analysis of multiple description quantizers. *IEEE Trans. Inf. Theory*, 44(1):278 – 284, January 1998.

[137] V. A. Vaishampayan, J.-C. Batllo, and A.R. Calderbank. On reducing granular distortion in multiple description quantization. In *Proc. IEEE Int. Symp. Information Theory*, page 98, August 1998.

[138] V. A. Vaishampayan and J. Domaszewicz. Design of entropy-constrained multiple-description scalar quantizers. *IEEE Trans. Inf. Theory*, 40(1):245 – 250, January 1994.

[139] V. A. Vaishampayan, N. J. A. Sloane, and S. D. Servetto. Multiple-description vector quantization with lattice codebooks: Design and analysis. *IEEE Trans. Inf. Theory*, 47(5):1718 – 1734, July 2001.

[140] S. van de Par, A. Kohlrausch, G. Charestan, and R. Heusdens. A new psychoacoustical masking model for audio coding applications. In *Proc. of the 2002 Int. Conf. on Acoustics, Speech and Signal Processing*, pages 1805–1808, Orlando, USA, May 2002.

[141] R. Venkataramani, G. Kramer, and V. K. Goyal. Bounds on the achievable region for certain multiple description coding problems. In *Proc. IEEE Int. Symp. Information Theory*, page 148, June 2001.

[142] R. Venkataramani, G. Kramer, and V. K. Goyal. Multiple description coding with many channels. *IEEE Trans. Inf. Theory*, 49(9):2106 – 2114, September 2003.

[143] J. L. Verger-Gaugry. Covering a ball with smaller equal balls in $\mathbb{R}^n$. *Discrete and Computational Geometry*, 33:143 – 155, 2005.

[144] I. M. Vinograd. On the number of integer points in a sphere. *Izv. Akad. Nauk SSSR Ser. Math.*, 27, 1963.

[145] H. Viswanathan and R. Zamir. On the whiteness of high-resolution quantization errors. *IEEE Trans. Inf. Theory*, 47(5):2029 – 2038, July 2001.

[146] H. Wang and P. Viswanath. Vector gaussian multiple description with individual and central receivers. In *Proc. IEEE Int. Symp. Information Theory*, 2006.

[147] X. Wang and M. T. Orchard. Multiple description coding using trellis coded quantization. In *IEEE Int. Conf. Image Processing*, volume 1, pages 391 – 394, September 2000.

[148] Y. Wang, M. T. Orchard, and A. R. Reibman. Multiple description image coding for noisy channels by pairing transform coefficients. In *Proc. IEEE Workshop Multimedia Signal Processing*, pages 419 – 424, 1997.

[149] Y. Wang, A. R. Reibman, M. T. Orchard, and H. Jafarkhani. An improvement to multiple description transform coding. *IEEE Trans. Signal Proc.*, 50(11):2843 – 2854, November 2002.

[150] J. P. Ward. *Quaternions and Cayley numbers; algebra and applications.* Kluwer, 1997.

[151] D. B. West. *Introduction to graph theory.* Prentice Hall, 2001.

[152] H. Witsenhausen. On source networks with minimal breakdown degradation. *Bell System Technical Journal*, 59(6):1083 – 1087, July-August 1980.

[153] J. Wolf, A. Wyner, and J. Ziv. Source coding for multiple descriptions. *Bell System Technical Journal*, 59(8):1417 – 1426, October 1980.

[154] A. Wyner and J. Ziv. The rate-distortion function for source coding with side information at the receiver. *IEEE Trans. Inf. Theory*, 22:1 – 11, January 1976.

[155] P. Yahampath. On index assignment and the design of multiple description quantizers. In *Proc. IEEE Int. Conf. Acoustics, Speech, and Signal Processing*, May 2004.

[156] P. L. Zador. Asymptotic quantization error of continuous signals and their quantization dimension. *IEEE Trans. Inf. Theory*, IT-28(2), 1982.

[157] R. Zamir. Gaussian codes and shannon bounds for multiple descriptions. *IEEE Trans. Inf. Theory*, 45(7):2629 – 2636, November 1999.

[158] R. Zamir. Shannon type bounds for multiple descriptions of a stationary source. *Journal of Combinatorics, Information and System Sciences*, pages 1 – 15, December 2000.

[159] R. Zamir and M. Feder. On universal quantization by randomized uniform/lattice quantizer. *IEEE Trans. Inf. Theory*, 38(2):428 – 436, March 1992.

[160] R. Zamir and M. Feder. Information rates of pre/post-filtered dithered quantizers. *IEEE Trans. Inf. Theory*, 42(5):1340 – 1353, September 1996.

[161] R. Zamir and M. Feder. On lattice quantization noise. *IEEE Trans. Inf. Theory*, 42(4):1152 – 1159, July 1996.

[162] R. Zamir, S. Shamai, and U. Erez. Nested linear/lattice codes for structured multiterminal binning. *IEEE Trans. Inf. Theory*, Special A.D. Wyner issue:1250 – 1276, June 2002.

[163] Z. Zhang and T. Berger. New results in binary multiple descriptions. *IEEE Trans. Inf. Theory*, 33(4):502 – 521, July 1987.

[164] Z. Zhang and T. Berger. Multiple description source coding with no excess marginal rate. *IEEE Trans. Inf. Theory*, 41(2):349 – 357, March 1995.

[165] J. Ziv. On universal quantization. *IEEE Trans. Inf. Theory*, IT-31:344 – 347, May 1985.

Index